Politecnico di Milano

SCUOLA DI INGEGNERIA INDUSTRIALE E DELL'INFORMAZIONE
Corso di Laurea Magistrale in Computer Science and Engineering
Sound and Music Engineering

Tesi di Laurea Magistrale

FEEDBACK CONTROL OF A DYNAMIC LOUDSPEAKER WITH EMBEDDED SENSOR COIL

Relatore
Prof. Luigi Piroddi

Correlatore
Prof. Luca Larcher

Candidato
Paolo La Torraca
Matr.787280

Anno Accademico 2014–2015

Contents

List of Figures

List of Tables

Abstract

Il comportamento non lineare dell'altoparlante dinamico è un fenomeno indesiderato che causa livelli di distorsione percepibili dall'orecchio umano ed impedisce l'applicazione di tecniche di controllo lineare della dinamica.

Questo lavoro propone un approccio per risolvere questo problema, utilizzando tecniche di elaborazione del segnale digitale per imporre una relazione di input-output lineare e per controllare la dinamica così linearizzata.

L'altoparlante dinamico considerato è dotato di una bobina secondaria, utilizzata come sensore integrato nell'altoparlante dal controllore progettato. Il controllore si basa su modelli a spazio di stati dell'altoparlante considerato sia lineari che non lineari, derivati rispettivamente dal modello di Beranek e dal modello di Klippel. I modelli sono caratterizzati e validati utilizzando i parametri estratti con il Klippel Distortion Analyzer.

La compensazione delle non linearità è implementata in retroazione, utilizzando un osservatore non lineare, capace di stimare lo stato dell'altoparlante non lineare attraverso la misura della bobina sensore, ed un modello interno dell'altoparlante non lineare controllato.

Il controllo della dinamica linearizzata è implementato attraverso un posizionamento dei poli mediante retroazione dello stato (pole placement), stimando lo stato dell'altoparlante lineare equivalente attraverso un osservatore ad anello aperto.

L'osservatore non lineare, la compensazione delle non linearità ed il controllore completo sono simulati in Simulink MATLAB e le rispettive performance sono valutate nel dominio dei tempi, nel dominio delle frequenze ed anche in termini di distorsione armonica totale (THD) residua. I risultati delle simulazioni dimostrano che l'altoparlante è efficacemente linearizzato e la relativa dinamica è controllata in modo soddisfacente.

Gli effetti introdotti dai ritardi nell'anello di retroazione sono discussi e simulati, mostrando i limiti implementativi del controllo proposto. I risultati forniscono informazioni utili per la selezione di un'architettura hardware adatta per l'implementazione del controllo.

Abstract

The nonlinear behavior of a dynamic loudspeaker is an undesired phenomenon which produces audible distortion and prevents the successful application of linear dynamic control.

This work proposes an approach to address this issue, that employs digital signal processing to enforce a linear input-output relation and to control the linearized dynamics.

The considered dynamic loudspeaker is customized with a secondary coil, used as embedded sensor by the developed controller. The controller is based on linear and nonlinear state-space models of the custom loudspeaker, derived from the Beranek model and the Klippel model, respectively. The models are characterized and validated extracting the required parameters with the Klippel Distortion Analyzer.

The compensation of the nonlinearities is implemented in feedback form, exploiting a nonlinear observer that estimates the state of the nonlinear loudspeaker from the sensor coil measurements, and an internal model of the controlled, nonlinear loudspeaker.

The control of the linearized dynamics is implemented as a full-state feedback pole placement, estimating the equivalent linear loudspeaker state by means of an open-loop observer.

The nonlinear observer, the nonlinearity compensator and the full controller are simulated in Simulink MATLAB, and their performance is evaluated both in the time and frequency domain and also in terms of residual Total Harmonic Distortion (THD). The simulation results show that the controlled loudspeaker is well linearized and its dynamics are quite satisfactorily controlled.

The effects of time delays in the feedback loop is discussed and simulated, showing the implementation limitations of the proposed control scheme. The results provide useful information for the selection of a suitable hardware architecture for the implementation of the controller.

Introduzione

Questa tesi è stata sviluppata durante un tirocinio svoltosi presso l'azienda RCF e in collaborazione con l'Università degli studi di Modena e Reggio Emilia.

RCF è una azienda italiana con sede a Reggio Emilia, leader mondiale nella progettazione e produzione di prodotti audio ad alta tecnologia, sia in ambito professionale che consumer. L'azienda è particolarmente rinomata per la progettazione di altoparlanti all'avanguardia e sistemi audio professionali, richiesti in tutto il mondo per la diffusione audio in cinema, teatri, auditorium, etc.

La configurazione standard di un sistema audio professionale è composto da tre elementi fondamentali: il processore digitale (DSP, acronimo derivato dall'inglese: Digital Signal Processor), l'amplificatore di potenza e l'altoparlante.

Il DSP è un componente di elettronica digitale in grado di elaborare un segnale proveniente da una sorgente audio.

Per essere elaborato, il segnale audio deve essere convertito in un segnale digitale mediante un convertitore analogico-digitale (ADC), e quindi essere riconvertito in un segnale analogico dopo l'elaborazione, tramite un convertitore digitale-analogico (DAC).

Oggigiorno, tutti i sistemi audio professionali attivi sono dotati di un DSP, che viene utilizzato per diversi scopi: regolare il volume di uscita, applicare filtri digitali, sia per la messa a punto del sistema audio, sia per filtrare il segnale audio in ingresso, ed attuare la logica di protezione del sistema audio, che permette di evitare danni agli altri componenti del sistema audio causati da un uso scorretto o da guasti.

La capacità computazionale di questi componenti è costantemente aumentata nel corso degli anni, permettendo l'implementazione di algoritmi di elaborazione del segnale sempre più complessi. Conversamente, il loro costo è in costante declino.

La potenza di calcolo a disposizione di un DSP è raramente sfruttata appieno, permettendo l'introduzione di tecniche di ottimizzazione del sistema più specifiche e raffinate.

L'amplificatore di potenza è un componente di elettronica analogica di potenza, il cui scopo è quello di convertire il segnale a bassa potenza prodotto da una sorgente audio o dal DSP, in un segnale ad alta potenza, adatto a pilotare l'altoparlante e produrre così livelli sonori significativi.

A seconda della specifica applicazione del sistema audio, l'architettura dell'amplificatore utilizzato può essere molto diversa: sistemi audio ad alta potenza, utilizzati per la diffusione audio in concerti o teatri, sono progettati principalmente con architetture a commutazione (classe D), al fine di erogare la massima potenza acustica con

la massima efficienza possibile, eventualmente sacrificando la qualità del suono riprodotto fino a livelli tollerabili.

Al contrario, i sistemi a bassa potenza, utilizzati negli studi di registrazione, sono principalmente progettati con architetture lineari (classe A, classe AB) al fine di ottenere una migliore qualità del suono, sacrificando l'efficienza energetica.

Tutte le architetture sono soggette alle tipiche non linearità degli amplificatori, come il clipping di tensione, introducendo distorsione. A causa dell'intrinseca non linearità della tecnologia, le architetture a commutazione possono introdurre ulteriori distorsioni. Tuttavia, le tipologie più recenti sono in grado di competere con livelli di distorsione introdotti dagli amplificatori di classe AB.

Ai fini di questa tesi, l'amplificatore sarà considerato un componente ideale, caratterizzato da un guadagno di tensione costante ed in grado di fornire all'altoparlante un qualsiasi valore di corrente, senza introdurre alcuna distorsione.

L'altoparlante è un trasduttore elettroacustico, cioè un dispositivo capace di convertire un segnale elettrico in un segnale acustico con sufficiente energia per essere percepito dall'orecchio umano.

A seconda della specifica applicazione del sistema audio, l'altoparlante è realizzato con diverse tecnologie ed in diversi fattori di forma. I Subwoofer, raggiungendo i $55cm$ di diametro, sono i dispositivi più grandi impiegati nei sistemi audio e permettono di trasmettere il moto una grande quantità d'aria. Essi sono utilizzati per la riproduzione della gamma di frequenze basse ($20Hz$ - $200Hz$). I Woofer sono dispositivi più piccoli, utilizzati per riprodurre la gamma delle frequenze medie ($100Hz$ - $5000Hz$). I Tweeter sono i dispositivi più piccoli impiegati nei sistemi audio, utilizzati per riprodurre la gamma delle frequenze alte ($5000Hz$ - $20000Hz$). Esistono e vengono utilizzati anche dispositivi di dimensioni intermedie (midbass, midrange, etc.), e non è raro lo sviluppo di trasduttori special-purpose.

La tecnologia di altoparlante più comune nei sistemi audio professionali è l'altoparlante dinamico, grazie alla sua versatilità ed alla qualità del suono riprodotto.

Un problema comune a tutte le tecnologie di trasduzione è l'introduzione di distorsione, che determina una degradazione della qualità del suono riprodotto. Ciò può essere attribuito al fatto che il segnale di ingresso influenza la struttura stessa dell'altoparlante. A causa dei significativi cambiamenti a cui l'altoparlante è sottoposto nel processo di trasduzione, esso non si comporta come un sistema ideale e lineare, introducendo distorsione.

E' importante puntualizzare che, nei sistemi audio professionali, l'altoparlante è la principale fonte di distorsione del suono.

Oggigiorno, l'approccio tipico per alleviare l'effetto della distorsione è quello di sovradimensionare le parti critiche dell'altoparlante. In questo modo è possibile estendere l'intervallo di tensione del segnale di ingresso per cui l'altoparlante si comporta come un sistema lineare ideale, con lo svantaggio di un maggior costo ed un maggior peso del dispositivo.

Questo è attualmente il compromesso più importante nella progettazione di altoparlanti professionali, poiché esso influenza profondamente le caratteristiche e le prestazioni complessive del sistema audio.

I componenti fin qui descritti sono sempre montati su una cassa, le cui caratteristiche sono molto importanti ai fini dell'efficienza e della qualità complessiva del sistema audio. Nei sistemi audio professionali la cassa è progettata su misura per una specifica combinazione di altoparlanti (e viceversa), al fine di migliorare le prestazioni globali del sistema.

Due sono le tipologie di casse tipicamente utilizzate: la cassa chiusa, una struttura molto semplice che impedisce ogni passaggio di aria tra l'interno e l'esterno della cassa stessa, e la cassa accordata, una struttura più complessa che permette il passaggio dell'aria attraverso un condotto accordato, consentendo di ottenere una maggiore efficienza e un miglior comportamento dell'altoparlante. Il volume della cassa, la sua forma e (se presente) le dimensioni del condotto accordato sono tutti fattori cruciali per realizzare un buon accoppiamento tra l'altoparlante e la cassa stessa.

Dato che l'altoparlante è l'elemento più critico per quanto riguarda la qualità del suono riprodotto da un sistema audio professionale, molte tecniche di controllo sono state sviluppate per consentire il superamento dei suoi limiti fisici.

Le prime tecniche sperimentate includono retroazioni nel dominio elettrico, l'uso di regolatori PID sviluppati ad hoc per lo specifico dispositivo e l'introduzione di più di un ingresso di pilotaggio. Tali approcci furono perlopiù empirici ed ottennero scarsi risultati.

Un interessante passo in avanti è stato fatto con l'introduzione dei primi modelli fisici dell'altoparlante (Beranek [Ber86], Thiele [Thi71a, Thi71b] and Small [Sma72, Sma73a, Sma73b, Sma73c]).Questi sono dei semplici modelli lineari che però fornirono una prima base teorica per studiare ed affrontare il problema.

I successivi tentativi di progettazione di sistemi di controllo furono orientati al modello (model-based), sfruttando i nuovi modelli lineari per sviluppare un controllo lineare dell'altoparlante tramite elaborazione del segnale in ingresso [Cat85]. Queste tecniche erano focalizzate sull'estensione della banda di lavoro dei trasduttori, cercando di ottenere una riproduzione soddisfacente delle basse frequenze utilizzando dispositivi più piccoli, più leggeri e meno costosi di quelli normalmente impiegati per tale scopo.

Queste tecniche diedero risultati promettenti per piccoli segnali, condizione in cui l'altoparlante si comporta come un sistema ideale e lineare, effettivamente migliorando la larghezza di banda dell'altoparlante.

Sfortunatamente, gli stessi risultati non furono raggiunti per segnali relativamente grandi, condizione in cui i fenomeni non lineari dell'altoparlante ne dominano la dinamica: in quanto i modelli utilizzati a tale regime non sono più validi, il controllore non è più in grado di sintetizzare un segnale di controllo corretto, spesso causando instabilità.

Lo stesso comportamento non lineare dell'altoparlante venne anche riconosciuto come fattore cruciale per la qualità del suono riprodotto, provocandone il degrado soprattutto alle basse frequenze. Questo ha portato ai primi tentativi di compensazione delle non linearità tramite il pilotaggio in corrente [MH89].

Un approccio più recente, che è ancora oggetto di ricerca, è la compensazione attiva della distorsione dell'altoparlante effettuata attraverso tecniche di elaborazione del segnale digitale, che consentirebbe di migliorare la qualità del sistema audio senza modificare i dispositivi fisici.

Ciò avrebbe il vantaggio di essere applicabile a dispositivi già esistenti e di poter migliorare la qualità del suono di dispositivi sub-ottimali senza un significativo aumento del peso e dei costi. La compensazione della parte non lineare della dinamica degli altoparlanti permetterebbe, inoltre, di utilizzare tecniche di controllo lineare precedentemente sviluppate senza inconvenienti.

I primi tentativi di compensazione della distorsione tramite elaborazione del segnale cercarono di utilizzare la teoria del controllo non lineare in combinazione con tecniche di identificazione dei sistemi non lineari, principalmente attraverso le Serie di Volterra [Kai87, BDNR05]. Sfortunatamente tale approccio, essendo estremamente generale, non riesce catturare le caratteristiche comuni dei diversi altoparlanti: il sistema fisico è modellato attraverso una complessa combinazione di parametri privi di significato fisico, rendendo anche il controllore estremamente complesso ed oneroso dal punto di vista computazionale. A causa di ciò, questo approccio è stato messo da parte.

Gli approcci orientati ai modelli costituiscono una migliore alternativa per affrontare il problema. La ricerca in questa direzione iniziò con l'introduzione di un modello non lineare e sufficientemente completo dell'altoparlante [Kli05] che sussume i precedenti lavori di diversi ricercatori.

Di lì a poco venne introdotto anche il Klippel Distortion Analyzer, uno strumento di misura capace di identificare i parametri caratteristici degli altoparlanti attraverso processi di misura non invasivi, che divenne in breve tempo uno standard de-facto per industria degli altoparlanti [SK01, Kli00].

Da allora, molti tentativi sono stati effettuati includendo il nuovo modello non lineare in un algoritmo di controllo model-based per ottenere la compensazione della distorsione degli altoparlanti.

Lo stesso Klippel ha proposto un algoritmo di controllo, che consiste in un controllo adattativo ad anello aperto basato sulle misure di tensione e corrente dell'altoparlante, tutt'ora stato dell'arte [Kli03, Kli98].

Altri lavori hanno proposto implementazioni basate su diverse architetture (anello aperto, retroazione), considerando misure di diverse grandezze caratteristiche dell'altoparlante (corrente, spostamento, velocità, accelerazione, pressione) e implementando l'algoritmo adattativo in modi diversi [BBNFS04, BSH94, PSR+13, CCCP81].

L'obiettivo principale di questa tesi è quello di sviluppare un sistema di controllo in grado di compensare le distorsioni introdotte dal comportamento non lineare di un altoparlante dinamico, sfruttando le misure dei relativi parametri, ottenute con il Klippel Distortion Analyzer, ed avendo accesso ad una misura dell'altoparlante.

L'altoparlante controllato dovrà produrre una distorsione armonica totale (THD: Total Harmonic Distortion) nulla, esibendo un comportamento equivalente ad un altoparlante lineare ideale in tutta la banda di lavoro considerata.

Il controllore, inoltre, dovrà essere in grado di sfruttare la linearizzazione dell'altoparlante per applicare tecniche di controllo lineare, migliorandone così la dinamica.

L'altoparlante considerato in questa tesi è un LF18x401 subwoofer da 18" prodotto da RCF, con una bobina secondaria avvolta sopra la bobina principale, utilizzata come sensore.

L'introduzione di una bobina secondaria non è un processo inusuale nella progettazione degli altoparlanti dinamici, ma di solito entrambe le bobine sono connesse ad un ingresso di potenza. In questo caso, solo la bobina principale è connessa ad un ingresso di potenza, mentre la bobina secondaria è utilizzata come sensore.

Al fine di sviluppare l'algoritmo di controllo, l'altoparlante e il sensore saranno modellati prima attraverso il modello di Klippel e successivamente attraverso una rappresentazione a spazio di stati. I modelli ottenuti saranno implementati in MATLAB Simulink e validati comparando il loro comportamento con equivalenti misure dell'altoparlante reale.

Una volta sviluppato un modello soddisfacente, si procederà con il progetto e l'implementazione del controllore, sempre in MATLAB Simulink. Simulazioni verranno effettuate per valutare l'efficacia del controllo implementato.

Infine, sarà discussa la possibilità di implementazione dell'algoritmo di controllo progettato su una delle architetture di DSP attualmente impiegate da RCF.

La tesi è organizzata come segue:

Nel primo capitolo è presentato l'altoparlante dinamico. La tipica struttura del trasduttore è descritta in dettaglio, illustrando tutte le parti fondamentali, il loro scopo nel processo di trasduzione e le relative caratteristiche peculiari. Sono anche illustrati i principi fisici coinvolti nella trasduzione.

Nel secondo capitolo è introdotto il metodo a spazio di stati per la rappresentazione di sistemi ed il relativo controllo. Le principali tecniche di controllo non lineare e di controllo della dinamica note in letteratura sono illustrate, fornendo esempi di architetture in anello aperto ed in retroazione, ed introducendo il concetto di "osservatore". Infine, sono presentati gli approcci adottati per lo sviluppo del controllo non lineare ed il relativo osservatore.

Nel terzo capitolo sono derivati i modelli dell'altoparlante successivamente utilizzati per il progetto del controllore, ricavando anche la relativa rappresentazione a spazio di stati. Sono illustrate le analogie elettroacustiche ed elettromeccaniche, utilizzate per definire il modello dell'altoparlante lineare. Sono introdotti gli studi di Klippel sugli altoparlanti, estendendo il modello lineare con parametri non lineari ed ottenendo così un modello non lineare dell'altoparlante.

Nel quarto capitolo è modellata la bobina secondaria utilizzando lo stesso approccio descritto nel terzo capitolo.

Nel quinto capitolo è presentato il Klippel Distortion Analyzer, impiegato per estrare da un altoparlante reale i parametri usati per caratterizzare i modelli precedentemente definiti. I modelli sono validati confrontando i risultati delle loro simulazioni con le misure effettuate sull'altoparlante.

Nel sesto capitolo è sviluppato il controllore, progettando la compensazione delle non linearità ed il controllo della dinamica dell'altoparlante linearizzato. Le prestazioni del controllo sono valutate, considerando anche una possibile implementazione su un DSP utilizzato da RCF.

Introduction

This thesis has been developed during an internship in the company RCF and in collaboration with the Università degli studi di Modena e Reggio Emilia.

RCF is an Italian company based in Reggio Emilia, world leader in design and production of high-technology professional and consumer audio products. The company is especially renowned for the design of cutting edge loudspeakers and professional audio systems, worldwide employed in cinema, theaters, concert halls, etc.

The standard configuration of a professional audio system is composed by three fundamental elements: the Digital Signal Processor (DSP), the power amplifier and the loudspeaker.

The DSP is a digital electronic component capable of modifying the input signal coming from an audio source.

In order to be processed, the input audio signal must be converted into a digital signal using an Analog to Digital converter (ADC), and then converted back into an analog signal after the processing, using a Digital to Analog converter (DAC).

Nowadays, all active professional audio systems are equipped with a DSP, which is exploited for many tasks: managing the output volume, applying digital filtering, both to achieve fine tuning of the audio system and to properly condition the input signal, implementing the audio system protection logic, that avoids damages to the other components of the audio system due to user misuse or failures.

The computational power of these components has steadily increased during the years, making them capable of even more complex signal processing. Conversely, their cost is in constant decline.

The available computational power of a DSP is rarely fully exploited, leaving room for more specific and refined system optimization techniques.

The power amplifier is an analog power electronic component that converts the low power signal produced by an audio source or the DSP into a high power signal, suitable for driving the loudspeaker to produce significant sound levels.

Depending on the specific audio system purpose, the amplifier architecture can be very different: high power audio systems, used in concerts or theaters, are mainly designed in switching architecture (class D), in order to deliver audio power with the highest possible efficiency, possibly sacrificing the audio quality up to a tolerable limit. Conversely, small power systems, used in recording studio systems, are mainly designed in linear architectures (class A, class AB), in order to achieve the best sound quality with lower power efficiency.

Both the architectures exhibit, up to some extent, nonlinear behaviors that are common in amplifiers and introduce distortion to the input signal, such as voltage clipping and current supply limit. Switching amplifiers may add further distortion due to the intrinsic nonlinearity of the technology. Nevertheless, the most recent switching architectures are capable of competing with class AB distortion levels.

For the purpose of this work the amplifier will be considered an ideal component, i.e. a fixed voltage gain capable of delivering to the loudspeaker any current value, without any distorting behavior.

The loudspeaker is an electroacoustic transducer, i.e. a device that converts an electric signal into an acoustic wave with enough energy to be heard by the human ear.

Depending on the specific purpose of the audio system, many different technologies and loudspeaker shapes are available. Subwoofers are the largest devices, reaching up to $55cm$ in diameter, and capable of conveying motion to a large amount of air. They are used to reproduce low frequencies ($20Hz$ - $200Hz$). Woofers are smaller devices used to reproduce a medium range of frequency ($100Hz$ - $5000Hz$). Tweeters are the smallest devices, used to reproduce the high frequency range ($5000Hz$ - $20000Hz$). Many intermediate sizes are also employed (midbass, midrange, etc.) and the development of special purpose devices is not rare.

The most common technology employed in professional audio systems is the dynamic loudspeaker, thanks to its versatility and overall sound quality.

A common problem with all transduction technologies is the introduction of distortion, which causes a quality degradation of the conveyed sound. This can be attributed to the fact that the energy injected into the transducer by the power input signal to impress motion to the air also affects the loudspeaker itself. A large input signal translates into stress and significant changes in many parts of the transducer, causing it not to behave as an ideal, linear physical system and introducing distortion.

It is important to notice that in professional audio systems the loudspeaker is the main source of sound distortion.

Up to now, the typical approach used to alleviate the effect of distortion has been to oversize the critical parts of the device. In this way it is possible to extend the input signal range where the loudspeaker acts as an ideal, linear physical system, paying the price of a higher cost and weight of the device.

This is currently the most crucial trade-off in the professional audio loudspeaker design, deeply affecting the overall performance of the audio system.

The mentioned components are always mounted on a box, which also influences the efficiency and the quality of the audio system. In professional audio systems the box is tailored to match the mounted loudspeaker (and vice versa), in order to enhance the overall performance.

There are two main typologies of boxes: the sealed enclosure, a simple design that avoids any air passage between the inside volume and the outside, and the vented enclosure, a more complex design that instead provides a passage for the air (vent), which in turns allows to obtain higher efficiency and a better loudspeaker behavior. The volume of the box, its shape and (if present) the vent design are all crucial to achieve a good matching between the loudspeaker and the box itself.

Since the loudspeaker performance is the most critical element regarding the sound quality of a professional audio system, many control techniques have been developed that allow to overcome its physical limitations.

Early techniques include analog electrical feedback, the use of ad hoc tuned PID regulators and the employment of multi input loudspeakers. Those approaches were mostly empirical, obtaining unsatisfying results.

An interesting leap forward has been achieved by the introduction of the first physical models of the loudspeakers (Beranek [Ber86], Thiele [Thi71a, Thi71b] and Small [Sma72, Sma73a, Sma73b, Sma73c]). These were simple, linear models, that provided a first theoretical foundation that could be used to tackle the problem.

The next attempts to the design of loudspeaker control systems were model-based, exploiting the new linear models in order to apply linear control on the loudspeaker through signal processing [Cat85]. These techniques were mainly focused on the bandwidth extension of the transducer, trying to obtain a satisfying reproduction of low frequencies with smaller, lighter devices that are usually unsuitable for that task, but have lower costs.

These techniques gave promising results with low level signals, where the loudspeaker still behaves as an ideal, linear system, actually improving the device bandwidth. Unfortunately, the same is not true for relatively large signals, when the nonlinear behavior of the loudspeaker dominates the dynamics: in that case the model fails and the controller is not capable of providing the correct control signal, often causing instability.

The nonlinear behavior of the loudspeaker was also recognized as an important factor for the audio quality, causing degradation especially at low frequencies. This lead to the first attempts of compensation of the nonlinearities by current drive [MH89].

A more recent approach, that is still matter of research, is the active compensation of the loudspeaker distortion performed through digital signal processing, which would allow to improve the audio quality of the sound system without actually modifying the physical device.

This would have both the benefit of being applicable to already existent devices and of improving the sound quality of suboptimal devices without significant increase of weight and costs. The compensation of the nonlinear part of the loudspeaker dynamics, would also allow to use the previously developed linear control technique without any drawbacks.

The first attempts of distortion compensation by signal processing tried to exploit nonlinear system control theory combined with nonlinear system identification, mainly through Volterra Series [Kai87, BDNR05]. Unfortunately this approach, being very general, cannot capture the common features exhibited by different loudspeakers: the physical system is modeled as a complex combination of parameters without any physical meaning, causing also the control to be very complex and computationally expensive. Due to those characteristics, this family of approaches has been cast aside.

The model-based approach offered a better alternative to tackle the control problem. The research in this direction started with the introduction of a complete nonlinear model of the loudspeaker [Kli05] that subsumes many antecedent works from many researchers.

The Klippel Distortion Analyzer was also introduced, that is a measurement system capable of identifying the characteristic parameters of any loudspeaker through a non invasive measurement procedure, that quickly became a de-facto industry standard [SK01, Kli00].

Since then, many attempts have been carried out to include the new, non linear model in a model-based control algorithm to achieve compensation of the loudspeaker distortion.

Klippel proposed a control algorithm for loudspeakers consisting in a feedforward, adaptive control based on current and voltage sensing, which is still the state of the art [Kli03, Kli98].

Other works proposed implementations of the distortion compensation exploiting different control architectures (feedforward, feedback), the sensing of different characteristic variables of the loudspeaker (current, displacement, velocity, acceleration, pressure) and implementing the adaptive algorithm in different ways [BBNFS04, BSH94, PSR+13, CCCP81].

The main objective of this thesis is to develop a control system capable of compensating the distortions introduced by the nonlinear behavior of an dynamic loudspeakers, exploiting the measurement of the loudspeaker parameters, performed with a Klippel Distortion Analyzer, and having access to some measurement of the loudspeaker.

The controlled loudspeaker should ideally produce zero Total Harmonic Distortion (THD), thereby exhibiting a motional behavior equivalent to an ideal, linear loudspeaker over the whole application bandwidth.

The controller should also being capable of exploiting the enforced loudspeaker linearization to apply linear control to the device, improving its dynamics to satisfy any reasonable working bandwidth requirement.

The target loudspeaker considered in this thesis is a 18” subwoofer LF18x401 manufactured by RCF, with a secondary coil wound over the main voice coil, used as sensor.

The introduction of a secondary coil is not an unusual process in the design and building of dynamic loudspeakers, but usually both coils are connected to a powered input. In this case only the main voice coil is powered, while the secondary coil is used as a sensor at almost zero cost.

In order to implement the control algorithm, the loudspeaker and the sensor will be first modeled, according to the Klippel model, and expressed in a state space representation. The obtained models will be implemented in MATLAB Simulink and real measurements will be obtained for model validation.

Once a satisfying model for the device has been developed, the control design will be carried out and implemented in MATLAB Simulink. Simulations will be carried out to evaluate the effectiveness of the implemented control.

Finally, the possible implementation of the designed control system on one of the DSP architectures currently employed by RCF will be discussed.

The thesis is organized as follows:

In the first chapter the dynamic loudspeaker technology is presented. The typical structure of the transducer is described in detail, displaying all its fundamental parts, their purpose in the transduction process and their peculiar characteristics. The operating principles involved in the transduction are also displayed.

In the second chapter the state-space method for system representation and control is introduced. The main techniques of nonlinear control and dynamic control found in literature are displayed, providing examples in both feedback and feedforward architecture, also introducing the concept of "observer". Finally, the adopted approach for the design of the nonlinear control and the relative observer is displayed.

In the third chapter the models of the loudspeaker, later employed for the development of the controller, are derived and represented in state-space form. The electromechanical and the electroacoustic analogies are displayed and exploited to define a linear model of the loudspeaker. The Klippel studies on the loudspeakers are then introduced, extending the linear model with nonlinear parameters to obtain a nonlinear model of the loudspeaker.

In the fourth chapter the secondary coil, used as a sensor, is modeled following the same approach described for the third chapter.

In the fifth chapter the Klippel Distortion Analyzer is presented and employed to extract the parameters used to characterize the developed models from a real loudspeaker specimen. The models are then validated comparing their simulation results with the measures performed on the loudspeaker specimen.

In the sixth chapter the controller is developed, designing a suitable compensation of the nonlinearities and a control of the dynamics of the linearized loudspeaker. The performance the controller are evaluated, also considering a possible implementation on a DSP employed by RCF.

Chapter 1

Dynamic loudspeakers

The development of loudspeakers started in the late 19$^{\text{th}}$ century, when Erns Werner Siemens patented the first dynamic loudspeaker in 1874, and few years later, in 1876, Graham Bell patented the first practical application of the device: the telephone. The device created by Siemens exploited a linear electric motor to put a small mass into motion, and transmitted that motion to the surrounding air with the help of a horn.

Since then, a lot of effort has been spent to improve the quality of sound and the efficiency of the transduction, leading to the development and the optimization of different technologies.

One of the most noticeable results is owed to Chester W. Rice and Edward W. Kellogg, that in 1925 published a famous paper about their studies on the direct radiator loudspeaker [RK25]. Although they did not invented the device, they defined its basic principle and formalized the underlying theory, allowing a further development of the technology.

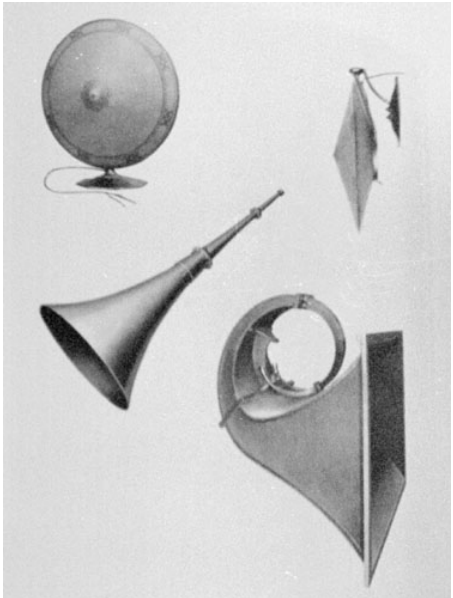

Figure 1.1: Collection of early loudspeakers designs. The bottom right device is the first horn coupled dynamic loudspeaker, patented E. W. Siemens in 1874.

Horn-coupled devices were unsuitable for a satisfactory reproduction of the whole audio bandwidth: in particular, the reproduction of medium and low frequencies was almost impossible. The direct radiator technology allowed to overcome this limitation, substituting the horn with a large surface attached to the vibrating element. This allowed to transmit motion to a larger amount of air and consequently reproduce with much more fidelity the lower part of the audio spectrum.

Nowadays, especially in professional audio applications, where high power output and transduction efficiency are critical, the most exploited loudspeaker technology is the Dynamic Loudspeaker, coupled with both a direct radiator or a horn according to the specific purpose of the device.

In consumer audio the trend is more various, with both medium power loudspeakers for personal audio reproduction, such as Hi-Fis, and small, low power loudspeakers for portable devices, such as the smartphones or notebooks.

Currently, this request is mainly satisfied by small, scaled versions of direct radiator Dynamic loudspeakers. For portable devices the miniaturization is pushed to the limit, with dimensions that can be less than 1 cm^2: those devices are usually referred as microspeakers. Other commonly employed technologies are the piezoelectric loudspeakers and the MEMS loudspeakers.

Nevertheless, there is still constant research for the development of new kinds of transduction principles and devices. The latest examples are the *ionic conduction speaker*, developed at the Harvard's University [KSF+13], and the *carbon nanotube termoacoustic speaker*, developed at the Tsinghua University [XCF+08].

Since the dynamic loudspeaker, in all its variants, is currently the mainly exploited loudspeaker technology, this work will focus on the development of a control system suitable for those specific devices.

In order to better understand the underlying physics, which is a key aspect for the definition of suitable models further used in the control development, and to familiarize with the specific technical terminology, the next chapter will be devoted to a high-level analysis of the direct radiator dynamic loudspeaker. All its functional parts will be illustrated separately in order to further describe the global principle of operation of this device.

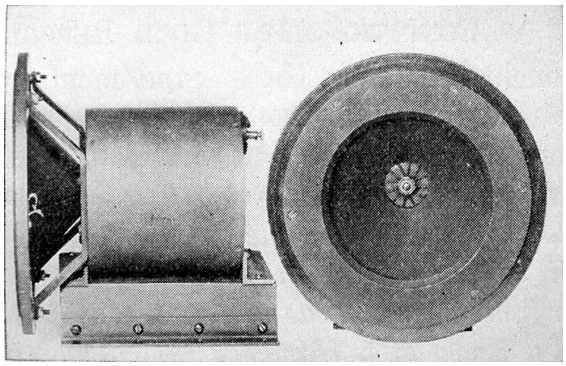

Figure 1.2: One of the direct radiator loudspeaker designs presented by W. Rice and E. W. Kellogg in 1925.

1.1 The structure

Figure fig. 1.3 represents the cross section of a typical direct radiator dynamic loudspeaker. For clarity, the same view is represented in fig. 1.4 highlighting all the main elements that characterize this typology of transducer.

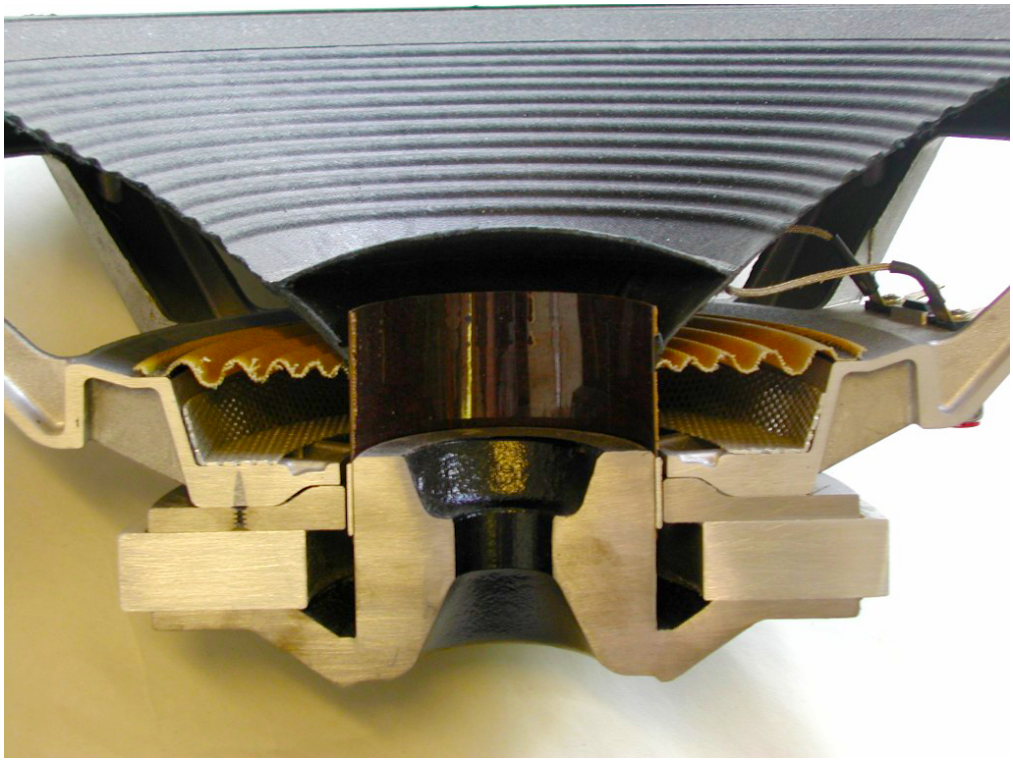

Figure 1.3: Cross section of a direct radiator dynamic loudspeaker.

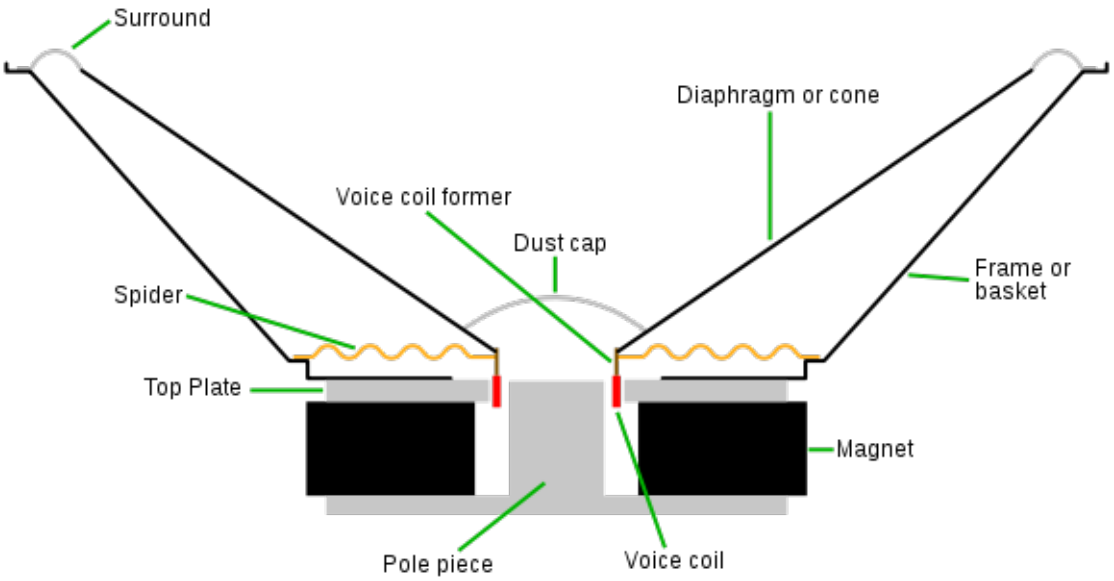

Figure 1.4: Simplified representation of a direct radiator cross section.

Even if this is the simplest configuration for this kind of devices, many parts are involved in the electroacoustic transduction. The fundamental elements of the dynamic loudspeaker will be now illustrated in detail.

The magnetic circuit is the first part of the loudspeaker's electric linear motor, composed by an annular permanent magnet placed between two metal parts, the top plate and the bottom plate (or pole piece, or T-yoke). The particular shaping of the two plates forms a small gap, called magnetic gap, where the voice coil is inserted without touching the sides.

The permanent magnet is built either in ferrite, an iron based ceramic compound, or in Neodymium based alloys. The first is the most used, due to the relatively low costs, having the drawback of a higher weight and worse performance, while the latter, despite its superior properties, is used only for high performance devices due to the high costs.

The plates, instead, are built in soft iron, a highly ferromagnetic material characterized by high level of saturation and low hysteresis. Those properties are fundamental in order to efficiently convey the permanent magnetic field. The only drawback of this material is represented by the generation of relatively high eddy currents, causing lower efficiency and undesirable heat generation.

The whole structure is a magnetic circuit, where the permanent magnet acts as a magnetic field generator, the two plates as magnetic short circuits and the magnetic gap as a relatively high reluctance.

The high reluctance scatters the magnetic flux in the surrounding air, decreasing the magnetic flux density in the magnetic gap, which is highly undesirable since the magnetic flux density in the magnetic gap is directly related to the force that the loudspeaker motor can exert.

In order to mitigate this effect the magnetic gap is kept as small as possible. Also, particular geometries for the top plate can be employed.

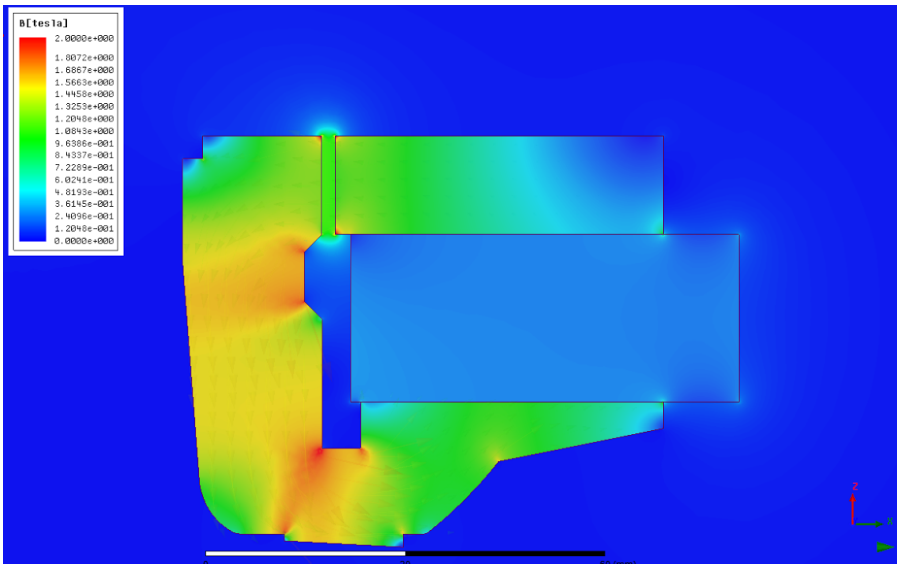

Figure 1.5: Magnetic circuit cross section with simulated magnetic flux density.

The voice coil is the second part of the loudspeaker electric linear motor, composed by a conductive wire coil wound around a rigid support, called former. The voice coil is rigidly attached to the diaphragm and inserted in the magnetic gap so as to be immersed into the stationary magnetic field.

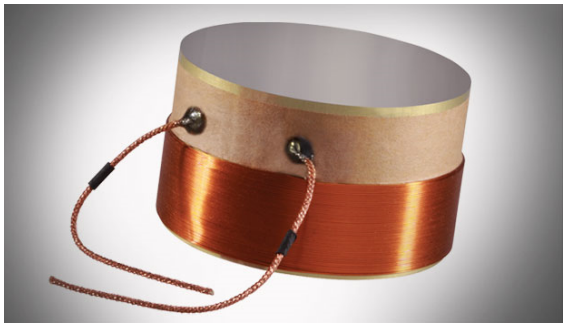

Figure 1.6: Copper wound voice coil.

The coil winding is made of insulated, metal wire (copper or aluminum), with variable gauge according to the design requirements. The length of the wire, the number of turns and the former size, are directly related to the force that the loudspeaker can exert and also to its electric impedance, two critical factors in the loudspeaker design. Moreover, there are three possible design configurations for the voice coil, depending on its height:

Under-hung: when the height of the voice coil winding is smaller than the magnetic gap height. This is the most compact design, with the serious drawback of having the coil exit the magnetic gap, thus experiencing a highly variable magnetic field.

Over-hung: when the height of the voice coil winding is larger than the magnetic gap height. This design ensures that a significant part of the coil is always inside the magnetic gap, which will experience a more stable magnetic field, while requiring larger geometries.

Equal-hung: when the height of the voice coil winding is equivalent to the magnetic gap height. This is an intermediate solution with respect two previously described designs.

Figure 1.7: Voice coil configurations, from left to right: over-hung, under-hung and equal-hung.

The diaphgram (or cone, or piston) is the surface of the direct radiator, rigidly connected to the voice coil former and attached to the basket through the suspensions (spider and surround).

Its purpose is to convert the mechanical motion of the voice coil into acoustical motion, moving the air and creating the actual sound wave.

Traditionally made of paper due to its low cost and good properties, nowadays it is produced with different materials depending on the specific application. Known alternatives are polymers (cellulose, Kevlar, polypropylene, etc) and even metals (titanium and magnesium), the most common choice being cellulose (which is also the main component of paper).

The required properties for the building material are low density, thus low mass, and high rigidity, thus not exhibiting flexure, acting as a perfect rigid body.

Unfortunately, no material exhibits perfect rigidity. At sufficiently high frequency undesired standing waves rise over the diaphragm surface due to its longitudinal and transversal resonance modes, both in radial and circumferential directions.

The net effect of the standing waves over the diaphragm is a variation of the effective radiation surface, and consequently of the overall transducer efficiency.

Since the vibration modes are strictly related to the diaphragm geometry, it turns out that the classical "cone" shape of the loudspeaker produces beneficial effects, increasing their damping.

Figure 1.8: Cellulose diaphragm attached to a voice coil, a spider and a surround.

The spider (or suspension) is an elastic annular disk, rigidly connected to the basket on the outer side and to the voice coil former on the inner side.

Its main purpose is to provide a restoring force to the voice coil and the diaphragm, in order to reposition the components at their rest position after an inward or outward excursion. It also used to center and guide the voice coil inside the magnetic gap, avoiding any contact between the two that would cause noise and distortion.

It is mainly built with Polycotton, a fabric made from a blend of 90% cotton and 10% plastic fibers (Polyester), impregnated with plastic resin and heated in order to properly modify the mechanical properties of the resin, in particular increasing its stiffness while keeping the cotton flexibility.

The spider structure is characterized by a corrugated radial pattern, whose ripples act as the coil of a spring during the voice coil motion: when the voice coil moves away from the rest position, the ripples are stretched apart assuming a flatter configuration, causing the rise of an inner structural force that tends to reestablish the original configuration. The corrugation can assume different shapes, typically being triangular for small displacements devices and sinusoidal for large displacements devices.

Unfortunately, being the most stressed component of the loudspeaker, it exhibits very large variations of its behavior, both during its operation and along all its lifetime. Three are the most influencing factors: the temperature variation (a high power loudspeaker can reach 100°C) and humidity, that may soften or harden the spider material, and the mechanical stress, that causes the degradation of the spider mechanical properties, leading to an hysteretic behavior (the spider restoring force is smaller than the moving force applied to it). Also, during large excursions the spider displays the loss of the elastic behavior, gradually acting as a rigid connection between voice coil and basket.

The spider is the most problematic component of the loudspeaker structure due to its erratic behavior. Yet it is still used in any dynamic loudspeaker design because there are no suitable alternatives.

Figure 1.9: Spiders of different sizes, used for different typologies of loudspeakers.

The surround (or edge suspension) is similar to a smaller version of the spider, consisting in an annular disk connected to the basket on the outer side and to the upper part of the diaphragm in the inner side.

Its main purpose is to keep the diaphragm centered, guiding its positioning during the excursions, while providing a minimal restoring force.

The material used to build the surround is mainly soft rubber, accurately shaped in order to achieve effective control of the off-axis movements of the diaphragm without damping the axial motion.

The dust cap is a cover placed over the hole left by the voice coil on the diaphragm surface in order to avoid the introduction of dust or other particles inside the loudspeaker structure.

Since the spacing left between the voice coil and the sides of the magnetic gap is usually in the order of a tenth of a millimeter, the presence of external particles would cause rubs and buzzes.

The basket is the rigid, fixed part of the loudspeaker structure, usually made in aluminum or steel, that provides a pivot for the moving parts.

All the rigid connections of the various components are made using special purpose glue, capable of withstanding the high stresses produced by the loudspeaker motion. The dried glue structure is also a critical element for the loudspeaker sound quality, as it may foster the rise of undesired vibration resonances: for this reason only amorphous glues are employed, that do not exhibit any preferential direction for vibrations in their dried structure.

From this short overview of the dynamic loudspeaker structure it is apparent that many of its constituent elements are characterized by non ideal properties and behaviors. The device will be fully characterized in chapter 3, with special attention on those non ideal features.

1.2 The operating principles

As said before, the dynamic loudspeaker exploits the linear motor principle to put into motion its mechanical system, which, in turn, thanks to the direct radiator implemented by the diaphragm, transmits that motion to the air producing audible sound waves.

This means that the dynamic loudspeaker actually exploits two transduction principles to convert an electric signal into an acoustic one: the electromechanical transduction of the linear electric motor and the mechanoacoustic transduction of the direct radiator.

Only the fundamental aspects of the two operating principles will be discussed. More information and fine details can be found in [Dav06, Ber86].

1.2.1 The Linear Electric Motor

A linear electric motor is a device that exploits the electromagnetic interaction between a fixed magnetic field and the current flowing in a conductor immersed in that field to produce a linear force on the conductor itself.

In a dynamic loudspeaker the electric motor is formed by the magnetic field present in the magnetic gap of the magnetic circuit, generated by the permanent magnet, and the voice coil wire that, being traversed by a current flow, experience a force.

According to the Lorenz Force Law, a conductive wire immersed in a magnetic field experiences a force $\mathbf{F}$ proportional to the current flow $\mathbf{i}$, the length of the wire $\mathbf{l}$ and the magnetic flux density $\mathbf{B}$, directed orthogonally to the current and the flux density direction:

$$\mathbf{F} = i\mathbf{l} \times \mathbf{B} \tag{1.1}$$

The electromechanical transduction is maximized when the magnetic flux density and the wire are perpendicular to each other, a condition in which the net force obtained becomes:

$$\mathbf{F} = Bli(\widehat{\mathbf{l}} \times \widehat{\mathbf{B}}) \tag{1.2}$$

In a dynamic loudspeaker this condition is met thanks to the specific radial geometry: the magnetic gap is in fact filled by a radial magnetic field that is always perpendicular to the wire of the voice coil, producing a force directed along its longitudinal axis.

Therefore, one of the fundamental quantities that characterize the dynamic loudspeakers is the product $\mathbf{Bl}$, called force factor, that is the conversion factor between the current flowing in the voice coil and the force produced on it due to the transduction.

Having a high force factor is important for a dynamic loudspeaker, as it is strictly related to the device efficiency.

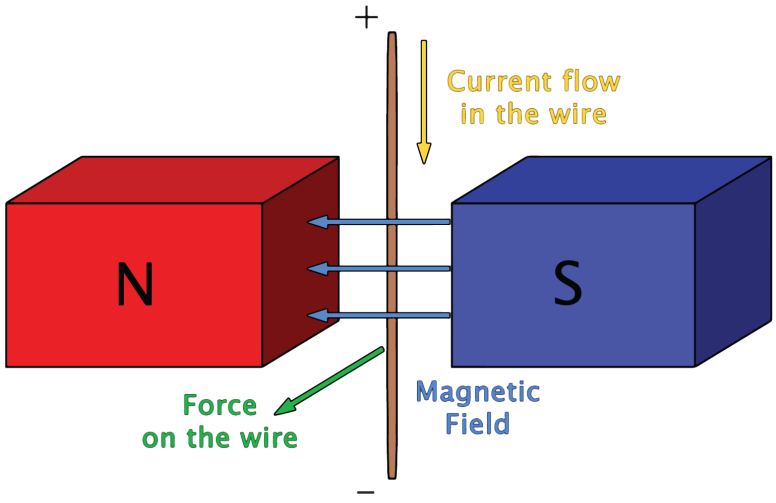

Figure 1.10: Electric linear motor principle.

For this reason, the transducers are designed by means of specific trade-offs:

- a longer wire increases the **l** contribution, but this will cause the voice coil to increase in height and/or in thickness, requiring a larger and/or thicker magnetic gap, thus reducing the **B** contribution;
- an alternative to increase **l** without requiring geometric changes of the magnetic circuit is the use of longer but thinner wires;
- longer or thinner wires will increase the voice coil electric resistance, limiting the current **i** and increasing heat generation;
- stronger magnets can be employed to increase **B** without any other change, but increasing the cost of the device

Electric motors are also characterized by a collateral, undesired behavior: the conductive wire displacement variation over time produces a motional electromotive force across the wire itself opposed to the voltage that generated the motion, which is the source voltage.

This phenomenon is caused by the electromagnetic interaction described by the Lorentz Force for moving charged particles in fixed magnetic fields:

$$V_{emf} = q\mathbf{v} \times \mathbf{B} \tag{1.3}$$

The electrons in the wire moving with velocity **v** experience a force that drives them to one end of the wire, producing an electromotive force.

In dynamic loudspeakers this effect is due to the motion of the voice coil inside the fixed magnetic field of the magnetic gap. Moreover, thanks to the radial geometry of the device, this undesired effect is maximized, producing a counter motional electromotive force $\mathbf{V_{emf}}$:

$$V_{emf} = Blv(\widehat{\mathbf{v}} \times \widehat{\mathbf{B}}) \tag{1.4}$$

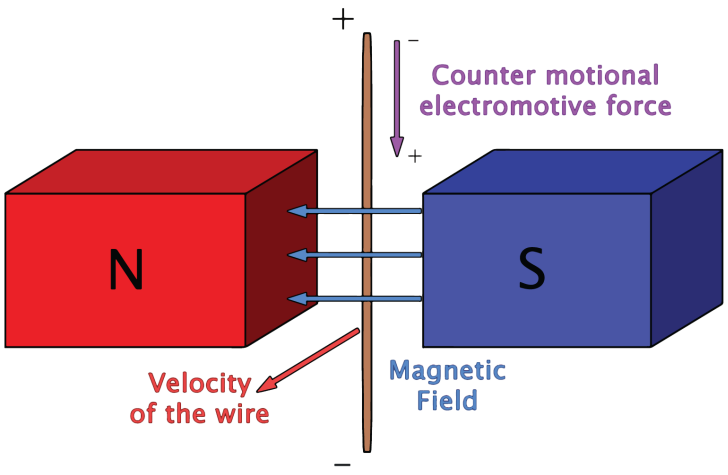

Figure 1.11: Generation of counter motional electromotive force.

However, this principle can be exploited for the development of a velocity sensor: a second conductive coil wounded over the voice coil, thus subjected to the same velocity, generates a voltage across its terminals proportional to their velocity.

Since in a linear electric motor the magnetic field **B**, the wire length **l** and the wire velocity **v** are perpendicular one another to maximize the electromechanical transduction, the direction of the force exerted on the voice coil (and consequently its velocity) is always axial and the motional electromotive force is always opposite to the source voltage. Thus, the respective directions can be disregarded, and the linear electric motor can be more simply characterized by means of two scalar equations:

$$\begin{cases} F = Bl\ i \\ V_{emf} = Bl\ v \end{cases} \tag{1.5}$$

1.2.2 The Direct Radiator

A direct radiator is simply an ideally rigid surface used to improve the amount of air that a mechanical system is capable of moving in order to produce sound waves, acting as a mechanoacoustic transducer characterized by two basic equations:

$$\begin{cases} p = \dfrac{F}{S_d} \\ U = S_d\ v \end{cases} \tag{1.6}$$

where the force **F** applied to the mechanical system is converted into the acoustic pressure **p** on the radiator surface, and the velocity of the mechanical system is converted into the volume velocity **U**. The conversion factor between the mechanic and the acoustic quantities is the radiator surface $\mathbf{S_d}$, assumed flat and perpendicular to the mechanical force.

Usually, the diaphragm is built with a conical or exponential geometry to achieve a better mechanoacoustic transduction, for which eq. (1.6) is not valid. However, it is common practice to define an equivalent flat surface of the specific diaphragm geometry for which eq. (1.6) applies.

In principle any mechanical system has an intrinsic direct radiator. For example, a dynamic loudspeaker is capable of producing sounds even without the diaphgram, exploiting the sole voice coil surface for the sound generation, obviously with inadequate results. The reasons for this lies in the air behavior and in the interaction between the mechanical and the acoustic domains.

The behavior of the air in contact with vibrating surfaces has been widely studied by Beranek [Ber86]: he observed that the air load, depending on the vibrating surface area and the stimulus frequency, exhibits different combinations of passive and reactive behaviors, that can be associated to an acoustic damping and mass respectively.

This equivalent acoustic system is fully described through the complex, frequency dependent acoustic impedance $\mathbf{Z_{AR}}(j\omega)$.

$$Z_{AR}(j\omega) = R_{AR}(j\omega) + j\omega M_{AR}(j\omega) \tag{1.7}$$

The real, passive part $\mathbf{R_{AR}}(j\omega)$ determines the fraction of power supplied by the mechanical system to the air being radiated as sound in the acoustic environment, while the imaginary, reactive part $\mathbf{M_{AR}}(j\omega)$ determines the fraction of power being stored in the moving air mass.

The two parts of the acoustic impedance are also dependent on the specific mounting of the loudspeaker.

In free air power is transmitted from both the front and the back surface of the diaphragm, which acts as an acoustic dipole, propagating sound in any direction. However, this setting is inefficient, especially at low frequencies (the air being "pushed" by one side is "pulled" by the other side instead of moving forward). If mounted on an infinite surface (infinite baffle mount) the two surfaces are completely separated, each one acting as a monopole source, propagating sound in a specific semi-space. The most practical configuration to achieve the sources separation is to use boxes as loudspeaker enclosures, achieving approximately omni directional sound propagation from the outer surface, while the inner one can be considered non propagating.

For the ease of exposition, the infinite baffle mount configuration is considered, but the same concepts are valid even for the other configurations.

It is often convenient to exploit eq. (1.6) to define an equivalent mechanical impedance of the air load $\mathbf{Z_{MR}}(j\omega)$.

$$Z_{MR}(j\omega) = R_{MR}(j\omega) + j\omega M_{MR}(j\omega) = \frac{F(j\omega)}{v(j\omega)} = \frac{S_d P(j\omega)}{\frac{U(j\omega)}{S_d}} = S_d^2 \frac{P(j\omega)}{U(j\omega)} = S_d^2 Z_{AR}(j\omega) \tag{1.8}$$

composed by an equivalent mechanical damping $\mathbf{R_{MR}}(j\omega)$ and mass $\mathbf{M_{MR}}(j\omega)$ of the air load experienced by the mechanical system.

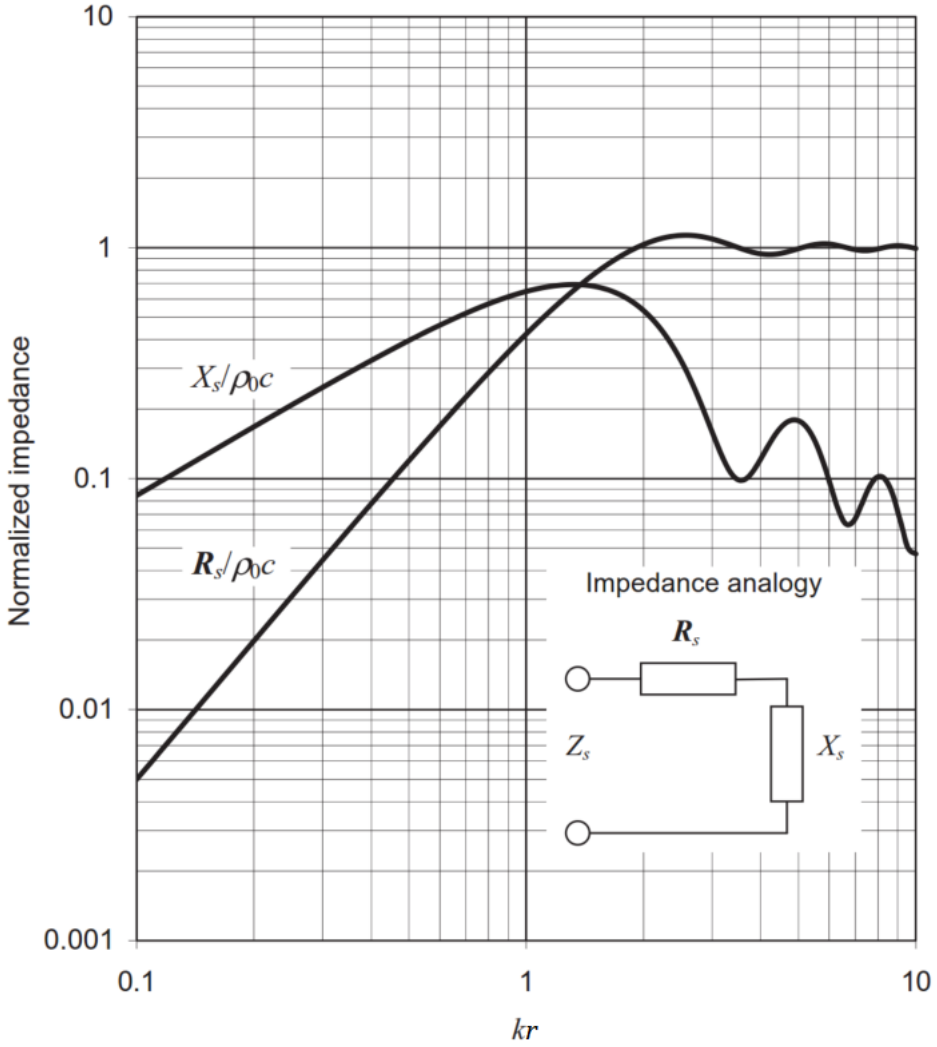

Figure 1.12: Real part ($\boldsymbol{R}_s$) and imaginary part (X_s) of the air load acoustic impedance on one side of a plain, circular direct radiator of radius r.

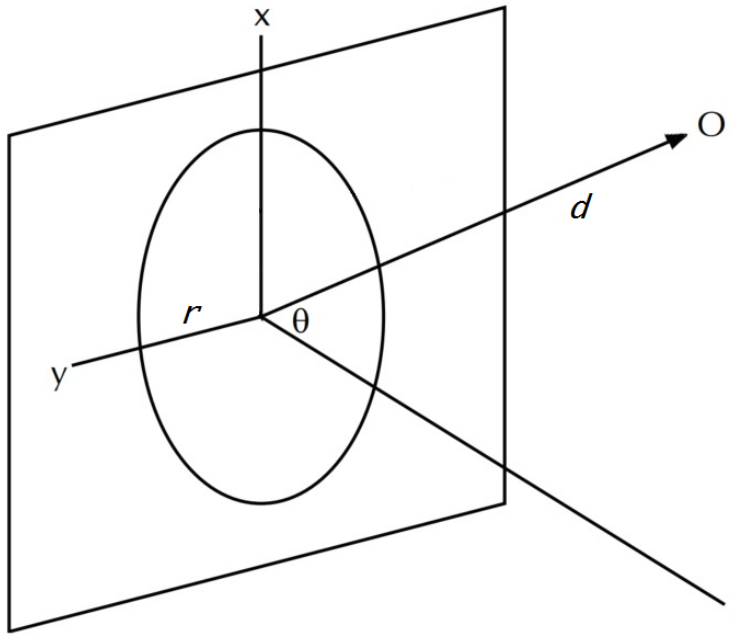

Figure 1.13: Frame of reference for a flat, circular direct radiator of radius radius r, in infinite baffle mounting.

From the observations of Beranek, two main behaviors of the air load can be broadly defined, depending on the size of the direct radiator radius **r** with respect to the wavelength of the reproduced signal λ:

- for relatively low frequencies ($\lambda > 2\pi r$) the air load is dominated by a reactive behavior, impeding the power transmission into the acoustic environment, while the resistive part appears to be a fraction of it. In this case the air is put into motion but in such a way that is not quite suitable to propagate power, thus sound, in the acoustic environment. The air on the radiator surface essentially acts as an excess mass attached to the mechanical system, storing and returning kinetic energy, thus propagating only a small fraction of power.

- for relatively high frequencies ($\lambda < 2\pi r$) the air load is dominated by a passive behavior, allowing power transmission to the acoustic environment, while the reactive part tends to disappear at higher frequencies. In this case the air is put into motion in a suitable way to propagate power, thus sound, into the acoustic environment. The air on the radiator surface essentially acts as an excess damping attached to the mechanical system, whose dissipated power corresponds to the generated acoustic power.

The second important aspect of the direct radiator is its role as impedance adapter between the mechanical system of the loudspeaker and the acoustic load of the air, improving the power transmission from the first to the latter.

As mentioned before in eq. (1.8), the air in contact with the vibrating surface acts as a mechanical impedance, related to the acoustic impedance by a proportional term that is the square of the equivalent radiator surface $\mathbf{S_d}^2$.

The radiator surface can be tailored in order to achieve, up to some extent, an impedance matching between the loudspeaker mechanical impedance and the air load equivalent mechanical impedance, consequently improving the power transfer between the two domains. The mechanical impedance mismatch can in fact lead to two opposite, undesirable conditions:

- if the air load equivalent mechanical impedance is too low, due to a small radiator surface, high volume velocity but low pressure are obtained. Conceptually, this is equivalent to moving a small amount of air very fast, but not creating enough pressure.
- if the air load equivalent mechanical impedance is too high, due to a large radiator surface, high pressure but low volume velocity are obtained. Conceptually, this is equivalent to pushing against a large mass of air without moving it properly.

These relationships can be exploited to determine with sufficient precision the size of the surface of a direct radiator in order to work in the resistive region throughout the required bandwidth and achieve mechanoacoustic impedance matching, thus maximizing the power transmission efficiency.

Nevertheless, in order to keep practical form factors, the direct radiator loudspeakers are equipped with under dimensioned radiators, that operate even in the reactive region and without achieving a perfect impedance matching. These configurations, while suboptimal, are capable of achieving better power propagation with respect to the use of a single small vibrating element.

Another important aspect of the direct radiator is its role in the loudspeaker's spatial response. In fact, a direct radiator loudspeakers do not propagate sound uniformly in space. Rather, they exhibit a directional behavior, especially at high frequencies.

Considering an infinite baffle mount direct radiator, in its far field (the region of the semi-space distant $d \gg r$ from the direct radiator) the produced pressure is:

$$p(d, \vartheta, t) = j\omega \frac{\rho_0 S_\mathrm{d}}{2\pi d} \left[\frac{2J_1(krsin\vartheta)}{krsin\vartheta} \right] v_m e^{j(\omega t - kd)} \tag{1.9}$$

where $\mathbf{d}$ is the distance from the direct radiator center and ϑ is the off-axis angle as in figure 1.13 , ρ_0 is the air density, $\mathbf{k}$ is the wavenumber associated to the pulsation ω and $\mathbf{v_m}$ is the RMS velocity of the diaphragm.

This equation can be considered as the combination of two contributions: one that accounts for the radiation at the points along the axis:

$$j\omega \; v_m e^{j(\omega t - kd)} \; \frac{\rho_0 S_\mathrm{d}}{2\pi d} \tag{1.10}$$

and a scaling factor due to the off axis position:

$$\frac{2J_1(krsin\vartheta)}{krsin\vartheta} \tag{1.11}$$

This last scaling factor, called directivity function, exploits the Bessel's function of the first kind and first order $\mathbf{J_1(x)}$.

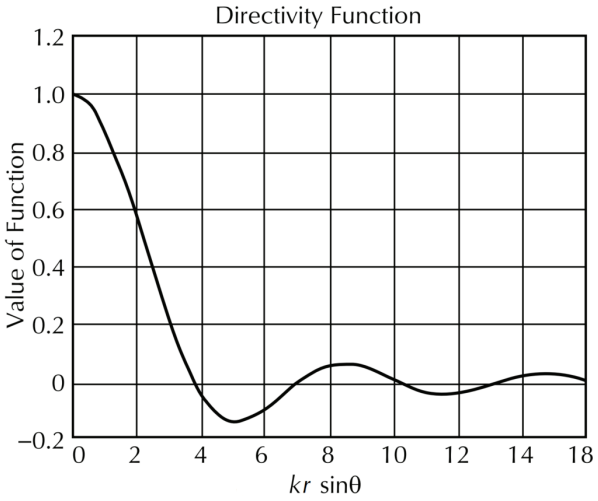

Figure 1.14: Directivity Function for a flat, circular direct radiator of radius r.

The directivity function shows that, regardless of the distance **d**, the pressure has its maximum value along the axis of the direct radiator and decreases for larger values of ϑ. Interestingly, the directivity function also exhibits local maxima and minima, corresponding to angles with higher pressure values, called lobes.

The position, number and shape of the lobes can be better appreciated through polar patterns, usually employed to evaluate the loudspeaker directivity and dispersion as function of the frequency.

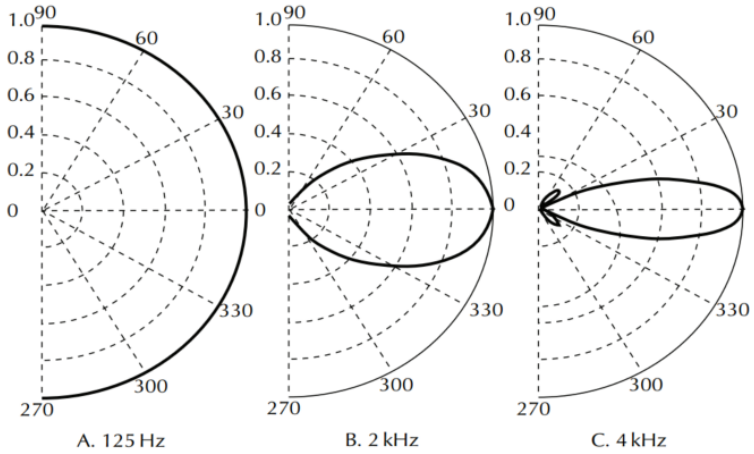

Figure 1.15: Polar patterns for the directivity function of a flat, circular direct radiator of radius $r = 0.1$m.

For relatively low frequencies ($\lambda > 2\pi$r) the directivity function can be considered constant in any direction, regardless of the aperture angle ϑ. In this condition the loudspeaker act as a spherical source, generating a pressure:

$$p(d,t) \approx j\omega \; v_m e^{j(\omega t - kd)} \; \frac{\rho_0 S_\mathrm{d}}{2\pi d} = a_m e^{j(\omega t - kd)} \; \frac{\rho_0 S_\mathrm{d}}{2\pi d} \tag{1.12}$$

where $\mathbf{a_m}$ is the RMS acceleration of the diaphragm.

Chapter 2

State-Space Control

Control theory has long been employed in order to modify and regularize the behavior of physical systems, with application in many different fields, such as mechanics, electronics, medicine, chemistry and even economics [Ast08].

Interestingly, it has already been employed in audio reproduction systems, as the electronic architecture of the amplifiers typically exploits an internal control to achieve high gains and low distortion figures.

The next step would be the application of control theory to the loudspeaker physical system, in order to achieve better performance both in sound quality, by reducing the nonlinearities that introduce distortions, and by controlling the device dynamics to overcome its physical limits and enhance low frequency reproduction.

In its most abstract form, any control system can be considered as the combination of two separate parts: a Plant and a Controller. The plant represents the controlled physical system, while the controller is the component designed to force the plant to exhibit a desired behavior, feeding it with an appropriate input signal.

Nowadays, two main families of methods are available for the plant description and the relative controller implementation:

The frequency response method , also called classical control, is based on the representation of physical LTI (linear time invariant) systems by means of their input-output transfer functions.

$$H(s) = \frac{Y(s)}{U(s)} \tag{2.1}$$

This approach, being the simplest and the most studied, is very popular for the characterization of LTI physical systems and the relative design of controllers.

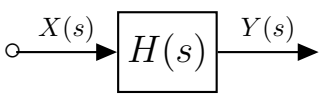

Figure 2.1: Transfer function representation of a linear time invariant system.

Its main limitation is that only LTI systems admit a transfer function. Thus it is unsuitable for the representation of non LTI systems and the design of non linear controllers.

The state-space method , sometimes referred as modern control, is based on the representation of physical systems by means of a set of first order differential equations in a vector-valued internal state $\mathbf{x}$ of the system.

$$\begin{aligned} \dot{\mathbf{x}}(t) &= \mathbf{f}(t, \mathbf{x}, u) \\ y(t) &= \mathbf{h}(t, \mathbf{x}, u) \end{aligned} \tag{2.2}$$

For any LTI system a state-space (SS) representation can be defined and conveniently expressed by a set of four matrices.

$$\begin{aligned} \dot{\mathbf{x}}(t) &= \mathbf{A}\mathbf{x}(t) + \mathbf{B}u(t) \\ y(t) &= \mathbf{C}\mathbf{x}(t) + \mathbf{D}u(t) \end{aligned} \tag{2.3}$$

The corresponding transfer function can easily be retrieved from the SS representation:

$$H(s) = \frac{Y(s)}{U(s)} = \mathbf{C}(s\mathbf{I} - \mathbf{A})^{-1}\mathbf{B} + \mathbf{D} \tag{2.4}$$

The SS representation can be used to characterize wider class of physical systems, including nonlinear time varying systems.

The definition of an internal state provides a richer representation of the system, describing not only the input output dynamics, but also the internal interactions that occur between the parts of the system, which is useful when dealing with complex systems.

It also provides new degrees of freedom for the control implementation: the controller may exploit, as well as the system output, even the system internal state, thus achieving a deeper control of the whole system compared to a plain output feedback.

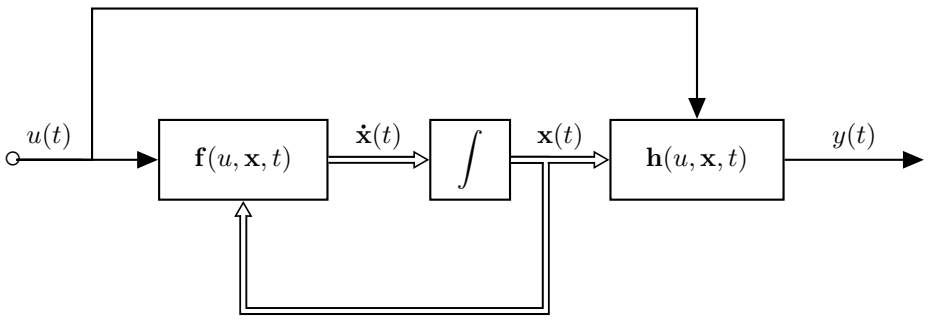

Figure 2.2: State-Space representation of a nonlinear time varying system.

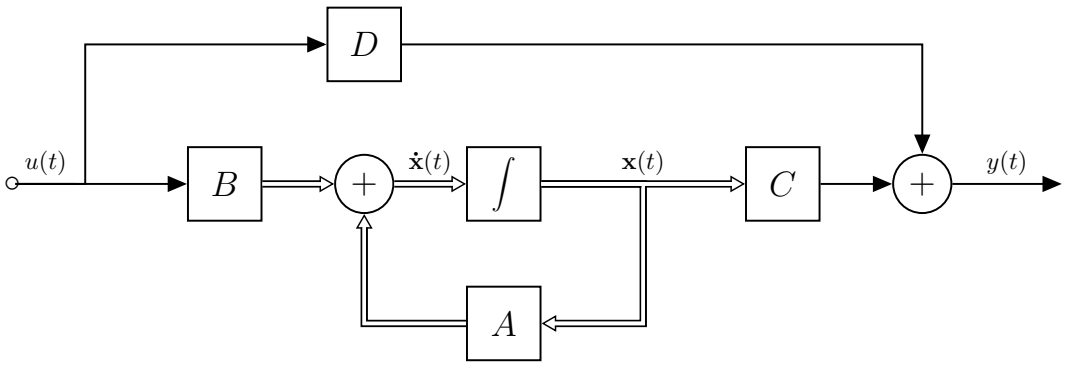

Figure 2.3: State-Space representation of a linear time invariant system.

The SS representation provides a powerful framework for the analysis of LTI systems. In [Kal59], Kalman defined the concepts of observability and controllability for LTI plants, which are key concepts for the design of SS controllers.

A plant is said to be observable if, for any possible sequence of states vectors and inputs, the current state can be determined using only the information retrieved from the outputs. The observability of a plant can be tested by checking the rank of the observability matrix:

$$\mathcal{O} = \begin{bmatrix} \mathbf{C} \\ \mathbf{CA} \\ \mathbf{CA}^2 \\ \vdots \\ \mathbf{CA}^{n-1} \end{bmatrix} \tag{2.5}$$

where $\mathbf{n}$ is the plant relative degree or, equivalently, the state vector length.

The plant is observable if the observability matrix is fullrank.

A plant is said to be controllable if there exists an inputs sequence capable of driving the state vector from a given initial value to a given final value in a finite time interval. The controllability of a plant can be tested by checking the rank of the controllability matrix:

$$\mathcal{C} = \begin{bmatrix} \mathbf{B} & \mathbf{AB} & \mathbf{A}^2\mathbf{B} & \cdots & \mathbf{A}^{n-1}\mathbf{B} \end{bmatrix} \tag{2.6}$$

The plant is controllable if the Controllability Matrix is fullrank.

The plant is stable if:

$$R_e[\lambda_i] < 0 \quad \forall \quad \lambda_i \in eig(\mathbf{A}) \tag{2.7}$$

Finally, if the plant is observable and controllable, then the poles of the transfer function correspond to the eigenvalues of the $\mathbf{A}$ matrix.

The rest of the chapter will illustrate the main SS approaches used to tackle the problems of the compensation of nonlinearities and the control of the dynamics.

2.1 Compensation of Nonlinearities

The aim of the compensation of the nonlinearities is to produce a control signal capable of driving the plant in such a way not to exhibit its non linearities, acting as much as possible like an ideal, linear system.

The fundamental idea behind all the compensation techniques is to implement a controller capable of processing the input signal with an appropriate nonlinear transformation, complementary to the plant nonlinearities, before being applied to the plant itself. In this way the nonlinear effects of the controller and the plant are mutually canceled out, so that the controlled plant exhibit only an ideal, linear behavior.

The processing implemented by the controller can also be interpreted as a predistortion of the input signal.

In order to produce the right predistortion, the controller needs updated informations about the plant behavior. This is achieved by defining a nonlinear SS model of the plant, that is exploited by the controller to track (or better, estimate) the plant internal state.

The development of models for the description of physical system is another huge branch of control theory, but it is not an important aspect at this point: for all the described techniques it is assumed that a suitable model is available. Obviously, the quality of the plant model is critical for the controller performances.

The compensation can be implemented by means of two different control architectures that will now be discussed: the feedback architecture and the feedforward architecture.

2.1.1 Feedback Techniques

Feedback techniques exploit a closed loop architecture, where some variable of the plant, often the actual plant output variable, is fed to the controller.

This architecture allows the controller to access information about the actual behavior of the controlled plant and evaluate the committed control error. In order to access even to variables that are not directly measured, the controller is combined with a state observer, that provides an estimate of the full plant state exploiting the plant model.

All those informations can be exploited by the controller to improve its performance, minimizing the control error and keeping the plant model aligned with the real plant.

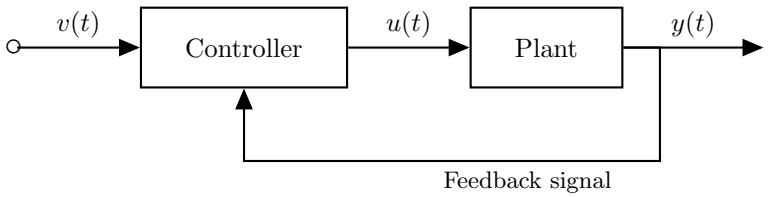

Figure 2.4: Structure of a feedback control system.

The feedback architecture has different drawbacks, mainly due to the requirements to measure the plant variable:

- the sensor used for the measurement may exhibit non ideal characteristics, like nonlinear behaviors or noise;
- the sensor affects the plant, for example by adding some mass, thus changing its theoretical behavior;
- the sensor may have a non negligible cost.

Moreover, if a digital controller is used, the required A/D and D/A operations will introduce delays in the acquisition of both the input signal and the control variable, and in the elaboration of the output control signal. This causes the loss of coherence between the plant and the controller's internal plant model, leading to performance degradation or even to control instability.

Due to its limitations, the pure feedback architecture has not been much exploited for the compensation of nonlinearities. The only noticeable application has been the Exact Feedback Linearization.

In this technique, shown in fig. 2.5 the plant is considered as a global nonlinear system to be compensated. The controller is designed in order to enforce a linear relationship between the controller input and the output of the controlled system such that:

$$y^{(n)}(t) = v(t) \tag{2.8}$$

where $\mathbf{n}$ is the relative degree of the plant and $\mathbf{y}^{(n)}(t)$ is the n^{th} derivative of the plant output.

The underlying idea is to transform the nonlinear description of the plant into a linear and controllable one, defining a new state vector by a coordinate transformation of the original state vector. Further details can be found in [Isi95].

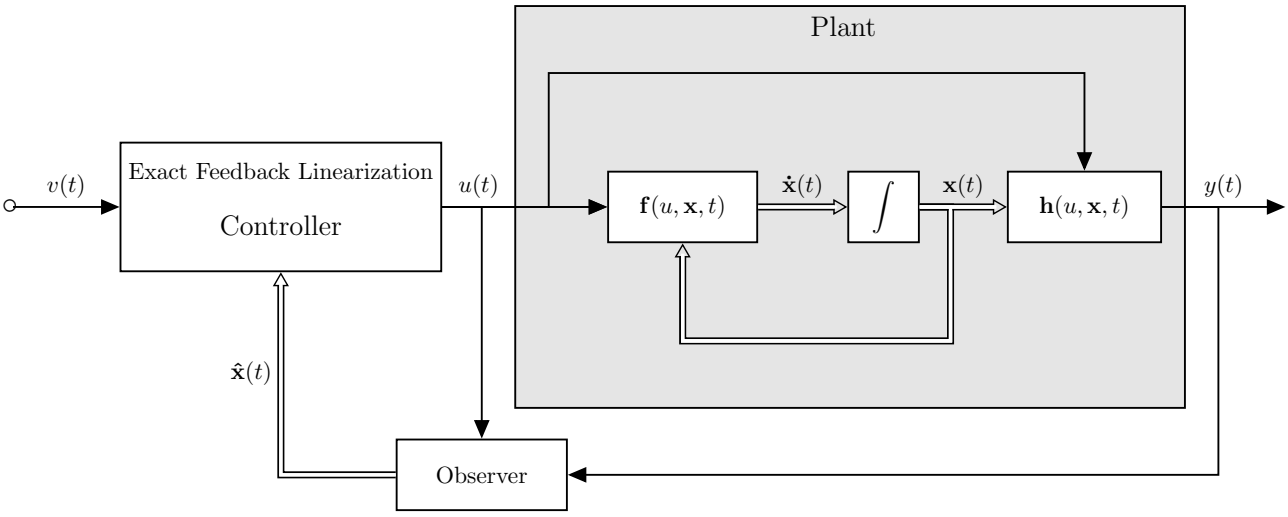

Figure 2.5: Exact Feedback Linearization control system.

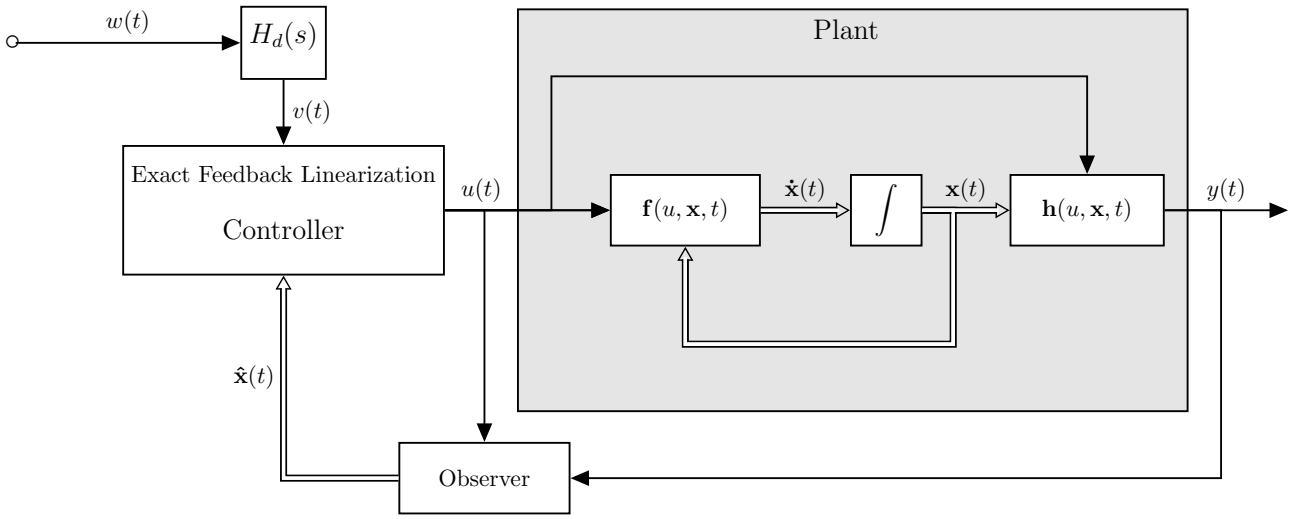

Figure 2.6: Exact Feedback Linearization control system, with reintroduction of the linear dynamics.

The original state vector information, required by the controller, is usually retrieved using of an observer.

From eq. (2.8) it is clear the controller compensates both the linear and the nonlinear behaviors of the plant. Any required linear dynamic, such as a low pass or high frequency roll-off, must be artificially introduced with an appropriate prefiltering of the input signal, as shown in fig. 2.6. The transfer function of the filter $H_d(s)$ should mimic the desired dynamic of the controlled plant.

2.1.2 Feedforward Techniques

Feedforward systems exploit an open loop architecture relying exclusively on the controller's internal plant model for the computation of the control signal.

This approach, that does not require any information about the real plant, solves all the problems relative to the plant measurements affecting the feedback architecture. Nevertheless, all the benefits that come from the observation of the plant are also lost: the controller is not aware of the real plant behavior and cannot exploit any information to adjust its control strategy.

This means that a purely feedforward controller is very sensitive to the misalignment between the plant model and the real plant, causing loss of robustness, performance degradation and even instability. The controller must be equipped with a perfect plant model and be perfectly initialized in order to work properly.

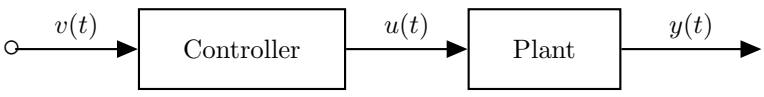

Figure 2.7: Structure of a feedforward control system.

Techniques that implement a pure feedforward nonlinear compensation can be derived from the Exact Feedback Linearization, retrieving the plant state without accessing to any plant measurement.

The main techniques are the Simulated State Observer, shown in fig. 2.8, and the Direct Integration, shown in fig. 2.9, that avoids the use of any observer.

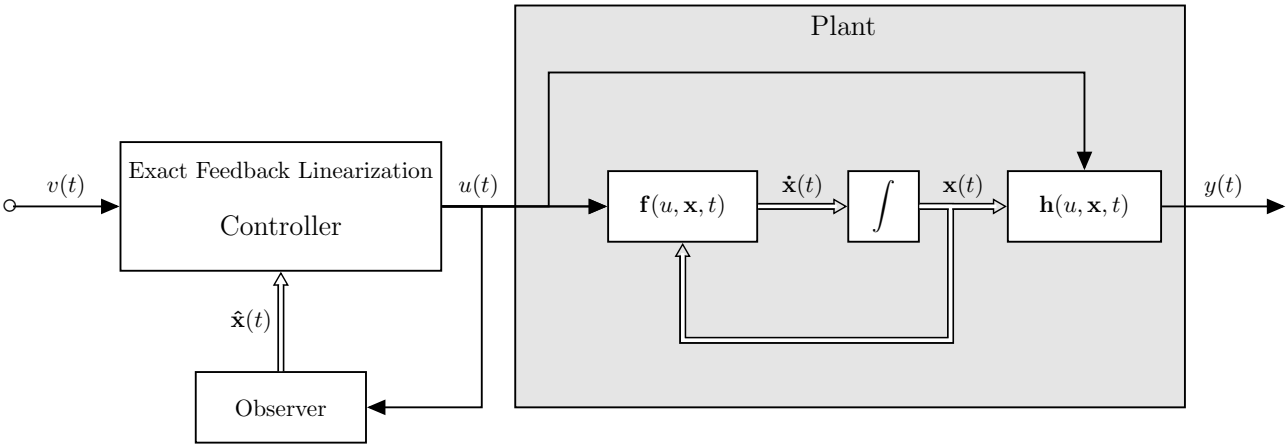

Figure 2.8: Feedforward implementation of the Exact Feedback Linearization control system, with Simulated State Observer.

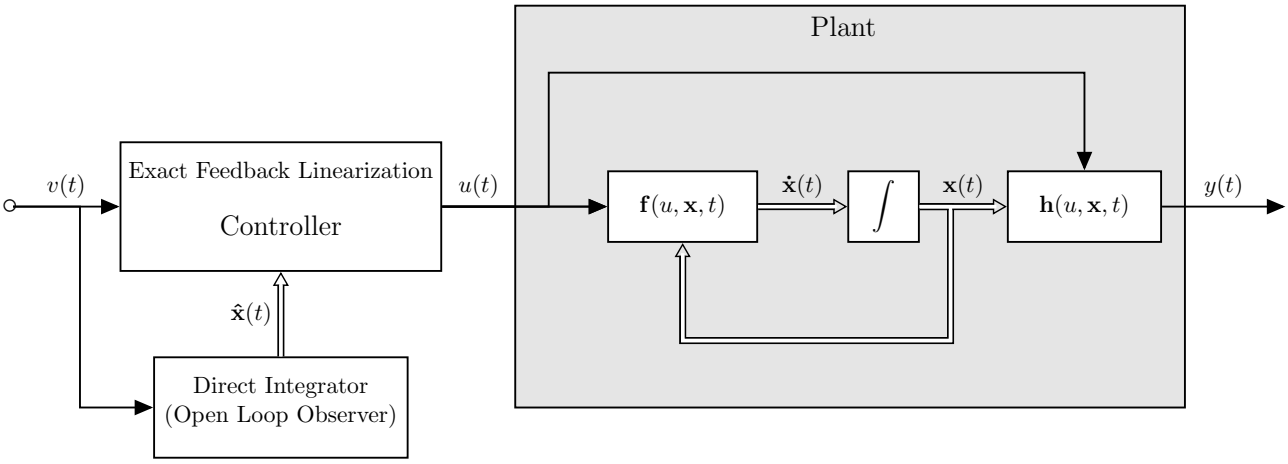

Figure 2.9: Feedforward implementation of the Exact Feedback Linearization control system, with Direct Integration of the state.

These techniques perform well when the plant is time invariant, and can be thus fully described by a fixed, nonlinear model, exploited by the controller. Conversely, they are not suitable for the control of time-varying nonlinear plants.

In order to deal with time varying plants, the controller must have some degree of adaptation, in order to follow the evolution of the characteristics of the plant. The only way to achieve this is, again, to access some measurement of the plant and modify the controller's plant model according to the sensed plant behavior. These techniques belong to the Adaptive Control category.

2.1.3 The adopted approach

All the presented approaches aim at the input-output linearization of the system.

Most physical systems exhibit an underlying linear behavior that, at large excitations, is modified by the intrinsic non idealities of the system itself. In that case, the system can be described as the combination of both a linear time invariant and a nonlinear time-varying contribution.

$$\begin{aligned} \dot{\mathbf{x}}(t) &= \mathbf{A}\mathbf{x}(t) + \mathbf{B}u(t) + \mathbf{a}(t,\mathbf{x})\mathbf{x}(t) + \mathbf{b}(t,\mathbf{x})u(t) \\ y(t) &= \mathbf{C}\mathbf{x}(t) + \mathbf{D}u(t) + \mathbf{c}(t,\mathbf{x})\mathbf{x}(t) + \mathbf{d}(t,\mathbf{x})u(t) \end{aligned} \tag{2.9}$$

The linearization of the physical system can then be achieved by compensating the nonlinear contributions without affecting the underlying linear dynamics.

The chosen approach follows this idea, and implements a controller capable of producing a control signal that compensates the nonlinear terms only. In order to do so, the controller requires information about the system internal state, that can be estimated by means of an observer, and also a complete and perfect characterization of the involved nonlinearities, possibly considering adaptation in case of time-varying systems.

This kind of controller could theoretically be implemented both with a feedback and a feedforward architecture, following the ideas of the already exposed approaches. However, since the adaptation will always require a measurement of the physical system, the same measurement can also be exploited for a more accurate state estimation, leading to a feedback implementation.

In this thesis it is assumed that the plant is nonlinear and time invariant, characterized by nonlinearities strictly dependent on its internal status, and that a perfect characterization of the nonlinearities dependencies is available.

$$\begin{aligned} \dot{\mathbf{x}}(t) &= \hat{\mathbf{A}}(\mathbf{x})\mathbf{x}(t) + \hat{\mathbf{B}}(\mathbf{x})u(t) = \mathbf{A}\mathbf{x}(t) + \mathbf{B}u(t) + \mathbf{a}(\mathbf{x})\mathbf{x}(t) + \mathbf{b}(\mathbf{x})u(t) \\ y(t) &= \hat{\mathbf{C}}(\mathbf{x})\mathbf{x}(t) + \hat{\mathbf{D}}(\mathbf{x})u(t) = \mathbf{C}\mathbf{x}(t) + \mathbf{D}u(t) + \mathbf{c}(\mathbf{x})\mathbf{x}(t) + \mathbf{d}(\mathbf{x})u(t) \end{aligned} \tag{2.10}$$

The designed controller generates a control signal $u(t)$ capable of driving the plant so as to exhibit its linear behavior only. The controlled system, driven by the desired input $v(t)$, act a linear time invariant system.

$$\begin{aligned} \dot{\mathbf{x}}_{\mathbf{lin}}(t) &= \mathbf{A}\mathbf{x}_{\mathbf{lin}}(t) + \mathbf{B}v(t) \\ y(t) &= \mathbf{C}\mathbf{x}_{\mathbf{lin}}(t) + \mathbf{D}v(t) \end{aligned} \tag{2.11}$$

It's important to remark that the state vector of the controlled plant $\mathbf{x}(t)$ and the state vector of the equivalent linear system $\mathbf{x}_{lin}(t)$ assume completely different behaviors.

The proposed control system is depicted in fig. 2.10

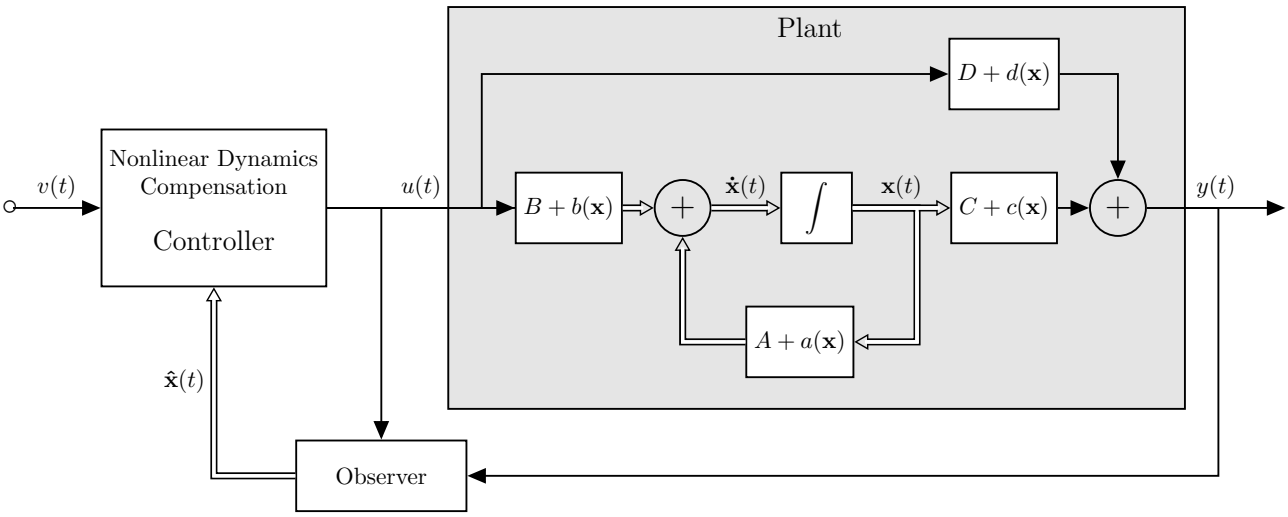

Figure 2.10: The implemented Nonlinear Dynamics Compensation, with nonlinear time invariant plant.

The proposed controller does not preclude the possible introduction of the plant time-variance, in which case an adaptive algorithm is required to ensure the constant alignment between the plant and its model used by the controller. For the purpose of this thesis, this enhancement is not considered and is left for future works.

2.2 Dynamic Control

The aim of the dynamic control is to produce a control signal capable of changing the behavior of a linear, time invariant plant. The controlled system is driven in such a way to exhibit a different behavior, acting as a physical system with different properties.

The dynamics of a linear, time invariant system is usually characterized by a transfer function, thus by its set of poles and zeros, and a gain. The fundamental idea behind dynamic control techniques is to tune the plant exhibited poles, and sometimes even the zeros, by means of an appropriate control signal.

If the plant is controllable and observable the poles of the transfer function correspond to the eigenvalues of the **A** matrix. The dynamic control problem is then recast as the tuning of the **A** matrix eigenvalues.

It is also possible to describe a relation between the four matrices of the SS representation and the zeros of the physical system. However, assuming that the plant is controllable and observable, it is usually much more convenient to design a dynamic control acting just on the poles, implementing the so called pole placement control.

The design of the controller just requires the SS representation of the plant model, which supplies all the needed information about the plant dynamics. The quality of the plant model is critical for the controller performance.

The very same techniques developed for the dynamic control of linear time invariant systems can easily be applied even to nonlinear systems that have been previously linearized. Thus, a single controller can be implemented to deal with both the plant linearization and the shaping of the dynamics.

As for the compensation of the nonlinearities, the dynamic control can be implemented either in a feedback or in a feedforward architecture.

2.2.1 Feedback Techniques

The feedback architecture exploited for dynamic control is conceptually identical to the one presented for the compensation of the nonlinearities in section 2.1.1.

The controller is designed to assign the closed-loop poles of the plant to arbitrary values (pole placement), in order to achieve satisfactory closed-loop system dynamics.

The typical approach, known as full-state feedback, implements the control action exploiting all the internal state variables of the plant. In particular, the control signal is produced by the controller as a linear combination of the plant state variables, and thus obtained multiplying the state vector with a proper feedback gain vector **K**.

$$u_{ctrl}(t) = -\mathbf{K}\mathbf{x}(t) \tag{2.12}$$

Since it is difficult to measure all the required internal variables, the controller is usually combined with a state observer, i.e. a system capable of computing an estimate of the full state vector from a meaningful measurement of the output of the plant. The observer design is also based on the SS model of the plant, causing

the state estimate to be affected by any misalignment between the plant and its model.

The design of the feedback gain vector is also crucial, as it actually defines the values of the closed-loop poles and consequently the closed-loop system dynamics.

$$\dot{\mathbf{x}}(t) = \mathbf{A}\mathbf{x}(t) + \mathbf{B}(u(t) + u_{ctrl}(t)) \tag{2.13}$$

$$\dot{\mathbf{x}}(t) = (\mathbf{A} - \mathbf{KB})\mathbf{x}(t) + \mathbf{B}u(t) \tag{2.14}$$

The closed-loop poles are determined by the eigenvalues of the matrix **(A-KB)**. The gain vector **K** is the only tuning factor involved in the control.

If the plant is controllable, then for each arbitrary combination of desired, stable poles there exists a value of the feedback gain vector that forces the plant closed-loop poles to those values, and such feedback gain vector can be easily found through the Ackermann's formula

$$\mathbf{K} = [\quad 0 \quad \cdots \quad 0 \quad 1 \quad]\mathcal{C}^{-1}\alpha_c(\mathbf{A}) \tag{2.15}$$

where $\mathcal{C}$ is the controllability matrix of the plant and $\alpha_c(\mathbf{A})$ is the characteristic polynomial of the desired closed loop matrix **(A-KB)** (which defines the desired closed loop dynamic of the system), solved for **A**.

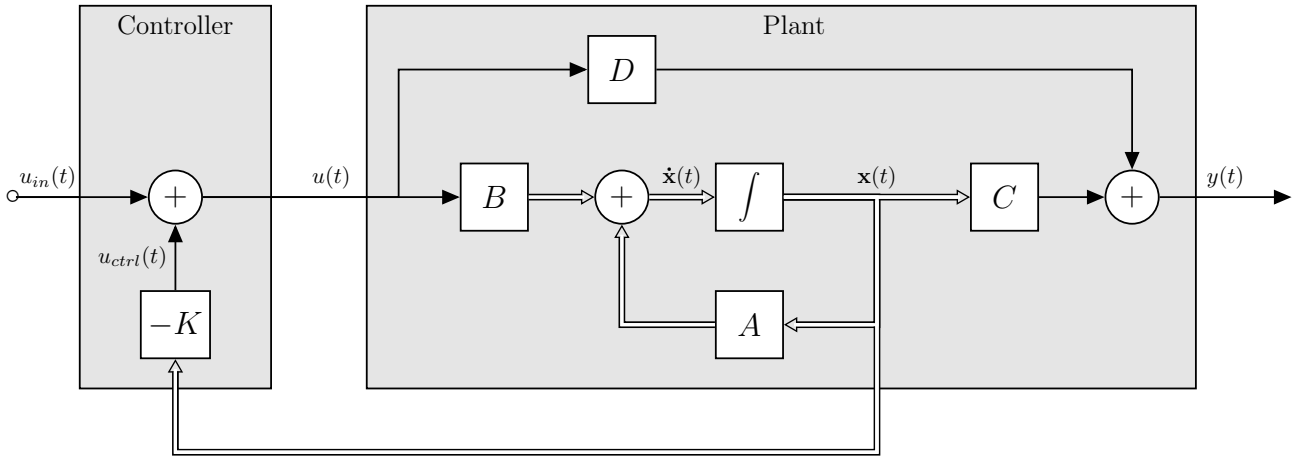

Figure 2.11: Full-State Feedback dynamic control system.

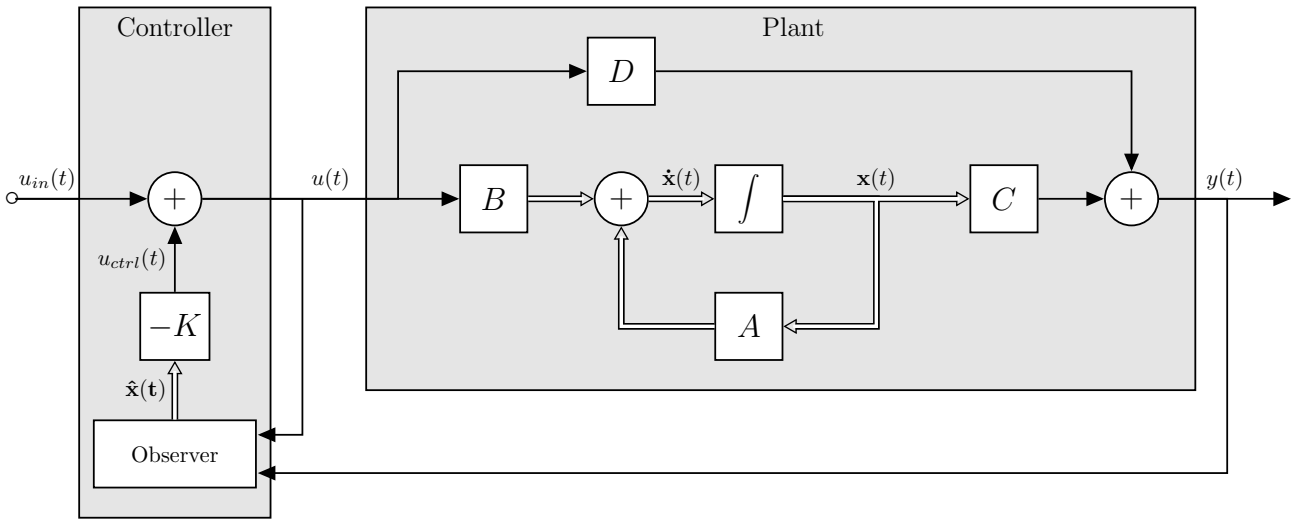

Figure 2.12: Full-State Feedback dynamic control system, with observer for the state estimation.

2.2.2 Feedforward Techniques

The feedforward architecture used for dynamic control is conceptually identical to the one discussed for the compensation of the nonlinearities in section 2.1.2. However, SS feedforward techniques are not typically employed for dynamic control.

The feedforward controller is obtained from the feedback controller, removing any measurement of the plant variables and exploiting other techniques to obtain an estimate of its internal state, as explained in section 2.1.2.

A common practice is the use of an open loop observer to estimate the controlled plant status, as shown in fig. 2.13.

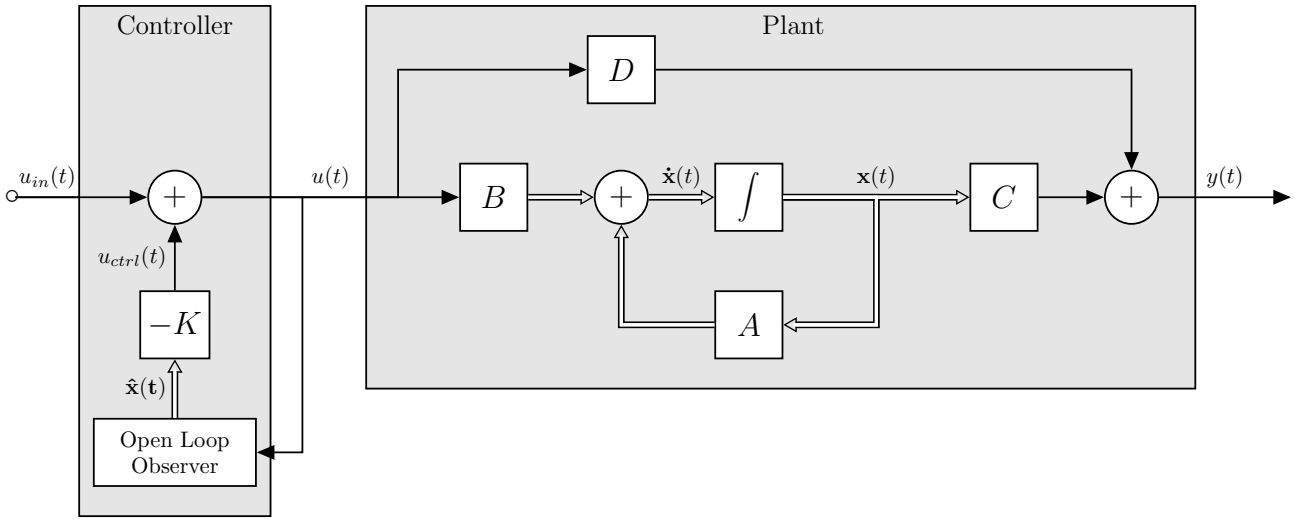

Figure 2.13: Full-State Feedback dynamic control system, with observer for the state estimation.

2.3 State Observers

All the described techniques require the access to the full state vector values to implement the control.

The direct measurement of all the states by means of sensors is usually impractical, if not impossible.

State observers are used to estimate the full state vector of the plant from output measurements of the plant itself, in some cases requiring just a single measurement. The obtained state estimate, denoted as $\hat{\mathbf{x}}$, is effectively used in place of the real plant state in the many control techniques.

Observers can be implemented in different ways (linear or nonlinear, time variant or time-varying) to match the nature of the controlled plant.

The simplest state observer architecture is the linear time invariant open loop observer, which is just a plain model of the dynamics of a linear time invariant plant:

$$\dot{\hat{\mathbf{x}}}(t) = \mathbf{A}\hat{\mathbf{x}}(t) + \mathbf{B}u(t) \tag{2.16}$$

This architecture can obtain satisfactory state estimation only if the plant model is perfectly characterized and the state is perfectly initialized. This last requirement is the most difficult to be satisfied and a poor initialization may greatly affect the state estimate quality.

The estimation error dynamics can be analyzed to determine the behavior of the open loop observer.

$$\mathbf{e}(t) = \mathbf{x}(t) - \hat{\mathbf{x}}(t) \tag{2.17}$$

$$\dot{\mathbf{e}}(t) = \dot{\mathbf{x}}(t) - \dot{\hat{\mathbf{x}}}(t) = \mathbf{A}\mathbf{e}(t) \tag{2.18}$$

The matrix $\mathbf{A}$ determines the rate at which the error tends to zero, that corresponds to the rate at which the state estimate tends to the real state. The convergence rate of the estimation error is limited by the speed of the $\mathbf{A}$ matrix eigenvalues, which correspond to the poles of the controlled plant.

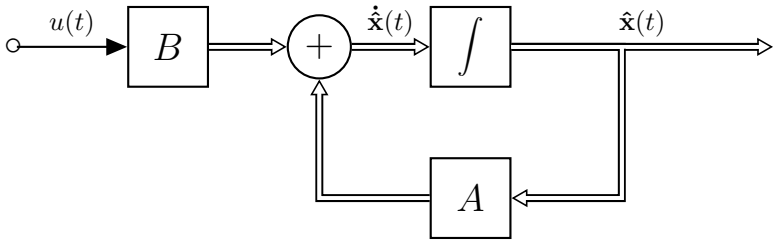

Figure 2.14: Open Loop observer.

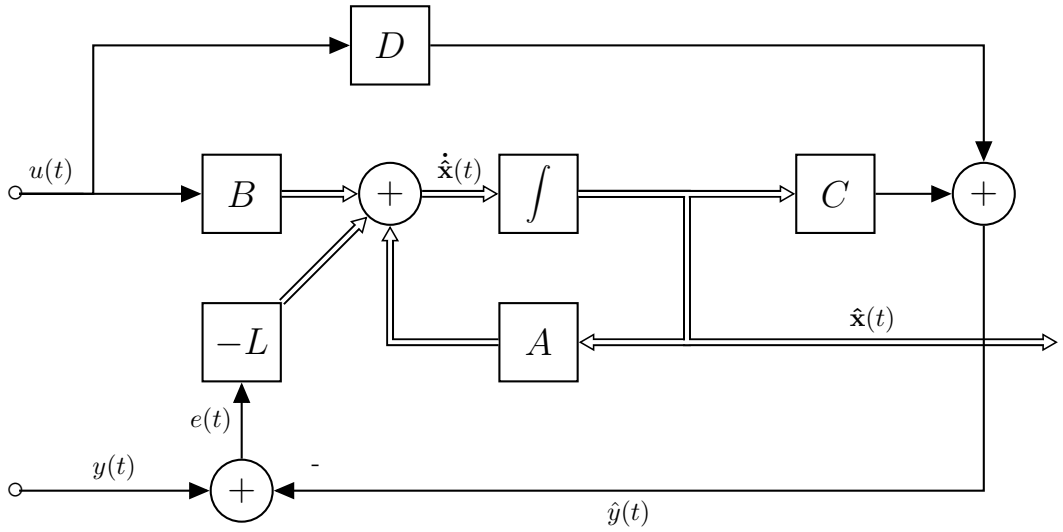

Figure 2.15: Luenberger observer (Closed Loop observer).

The linear time invariant closed loop observer, also called Luenberger observer, overcome this limitation allowing the tuning of the error dynamic eigenvalues to faster values. This is achieved by exploiting the measurement of the plant output and a feedback internal architecture.

The implementation is an extension of the open loop observer, where the internal model is continuously corrected with a feedback of the output estimation error (the difference between the measured and the estimated output) multiplied by a proper feedback gain vector $\mathbf{L}$.

The estimated state dynamic is described by:

$$\begin{aligned}\dot{\hat{\mathbf{x}}}(t) =& \mathbf{A}\hat{\mathbf{x}}(t) + \mathbf{B}u(t) + \mathbf{L}[y(t) - (\mathbf{C}\hat{\mathbf{x}}(t) + \mathbf{D}u(t))] \\ =& \mathbf{A}\hat{\mathbf{x}}(t) + \mathbf{B}u(t) + \mathbf{L}[\mathbf{C}\mathbf{x}(t) + \mathbf{D}u(t) - (\mathbf{C}\hat{\mathbf{x}}(t) + \mathbf{D}u(t))] \\ =& \mathbf{A}\hat{\mathbf{x}}(t) + \mathbf{B}u(t) + \mathbf{L}\mathbf{C}\mathbf{e}(t) \end{aligned} \tag{2.19}$$

Consequently, the state estimation error dynamic is described by the equation:

$$\begin{aligned}\dot{\mathbf{e}}(t) =& \mathbf{A}\mathbf{x}(t) + \mathbf{B}u(t) - [\mathbf{A}\hat{\mathbf{x}}(t) + \mathbf{B}u(t) + \mathbf{L}\mathbf{C}\mathbf{e}(t)] \\ =& (\mathbf{A} - \mathbf{L}\mathbf{C})\mathbf{e}(t) \end{aligned} \tag{2.20}$$

If the plant is observable and the internal model of the observer has been perfectly characterized, the feedback gain vector $\mathbf{L}$ can be chosen to tune the closed loop eigenvalues of the observer to arbitrary stable values.

The proper value of $\mathbf{L}$ can easily be found through the Ackermann's formula:

$$\mathbf{L} = \alpha_e(\mathbf{A})\mathcal{O}^{-1} \begin{bmatrix} 0 \\ \vdots \\ 0 \\ 1 \end{bmatrix} \tag{2.21}$$

where $\mathcal{O}$ is the observability matrix of the plant and $\alpha_e(\mathbf{A})$ is the characteristic polynomial of the desired closed loop matrix **(A-LC)** (which defines the desired closed loop dynamics of the state estimation error), solved for $\mathbf{A}$.

The eigenvalues of the matrix **(A-LC)** should be tuned faster than the eigenvalues of the closed loop matrix **(A-KB)**, as a rule of thumb by a factor of 2 to 6, to ensure faster decay of the state estimation error compared to the desired closed loop dynamics.

Tuning the observer eigenvalues to faster values increases the speed of response of the estimator but also increases its bandwidth, causing more sensor noise to be acquired. Conversely, tuning the eigenvalues to slower values decreases the observer bandwidth, achieving better noise smoothing but also interfering with the implemented control law dynamics. The right choice of the observer closed loop eigenvalues is a critical design step, affecting the overall performance of the implemented control system.

When the noise and the model uncertainties become critical, the Kalman Filter is often employed. It is an extension of the Luenberger observer capable of estimating the plant statue exploiting both the plant model and a noise model accounting for the uncertainties of the plant model itself. The peculiar feature of the Kalman Filter is that its feedback gain is time variant, adapted according to the internal noise model to achieve the best trade-off between the observation responsiveness and the noise smoothing. More details about the Kalman Filter can be found in [WB95].

Dealing with nonlinear time varying systems requires an observer which in turn is nonlinear time varying, capable of coping with the continuous evolution of the system and its nonlinear behavior.

Many approaches have been proposed for the design of nonlinear time varying observers [Pri96].

In this thesis, a nonlinear version of the Luenberger observer is employed.

The underlying idea is to use a linear version of the Luenberger observer, approximating the nonlinear plant behavior with a sequence of locally linear behaviors. This can be achieved periodically updating the linear observer plant model with a linear approximation of the nonlinear plant model at the current working point. If the update speed $\mathbf{T_{up}}$ is such to effectively track the plant nonlinear behavior, then the theory of the linear Luenberger observer can still be effectively applied locally.

Considering a generic SS representation of a nonlinear time-varying system of eq. (2.2), if $f(t, \mathbf{x}, u)$ and $h(t, \mathbf{x}, u)$ are differentiable, it can be linearized by means of Taylor's series:

$$\begin{aligned} \delta\dot{\mathbf{x}}(t) &\approx \left.\frac{\partial f(t,\mathbf{x},u)}{\partial \mathbf{x}}\right|_{\substack{\mathbf{x}=\mathbf{x_0}\\ u=u_0}} \delta\mathbf{x} + \left.\frac{\partial f(t,\mathbf{x},u)}{\partial u}\right|_{\substack{\mathbf{x}=\mathbf{x_0}\\ u=u_0}} \delta u \\ \delta y(t) &\approx \left.\frac{\partial h(t,\mathbf{x},u)}{\partial \mathbf{x}}\right|_{\substack{\mathbf{x}=\mathbf{x_0}\\ u=u_0}} \delta\mathbf{x} + \left.\frac{\partial h(t,\mathbf{x},u)}{\partial u}\right|_{\substack{\mathbf{x}=\mathbf{x_0}\\ u=u_0}} \delta u \end{aligned} \tag{2.22}$$

where $\mathbf{x_0} = \mathbf{x}(t_0)$ and $u_0 = u(t_0)$ are the state vector and the input value at the linearization time instant t_0, respectively.

Considering a perfectly characterized nonlinear time-invariant plant, as described in eq. (2.10), the linearized plant is expressed as follows:

$$\begin{aligned} \dot{\mathbf{x}}(t) &= f(t,\mathbf{x},u) = \hat{\mathbf{A}}(\mathbf{x})\mathbf{x}(t) + \hat{\mathbf{B}}(\mathbf{x})u(t) = \mathbf{A}\mathbf{x}(t) + \mathbf{B}u(t) + \mathbf{a}(\mathbf{x})\mathbf{x}(t) + \mathbf{b}(\mathbf{x})u(t) \\ y(t) &= h(t,\mathbf{x},u) = \hat{\mathbf{C}}(\mathbf{x})\mathbf{x}(t) + \hat{\mathbf{D}}(\mathbf{x})u(t) = \mathbf{C}\mathbf{x}(t) + \mathbf{D}u(t) + \mathbf{c}(\mathbf{x})\mathbf{x}(t) + \mathbf{d}(\mathbf{x})u(t) \end{aligned} \tag{2.23}$$

Therefore, the Taylor series of eq. (2.22) can be expressed as:

$$\begin{aligned} \delta\dot{\mathbf{x}}(t) &\approx \bar{\mathbf{A}}(\mathbf{x_0}, u_0)\delta\mathbf{x} + \bar{\mathbf{B}}(\mathbf{x_0}, u_0)\delta u \\ \delta y(t) &\approx \bar{\mathbf{C}}(\mathbf{x_0}, u_0)\delta\mathbf{x} + \bar{\mathbf{D}}(\mathbf{x_0}, u_0)\delta u \end{aligned} \tag{2.24}$$

where:

$$\bar{\mathbf{A}}(\mathbf{x},\mathbf{u}) = \left.\frac{\partial f(t,\mathbf{x},u)}{\partial \mathbf{x}}\right|_{\substack{\mathbf{x}=\mathbf{x_0}\\ u=u_0}} = \mathbf{A} + \mathbf{a}(\mathbf{x_0}) + \mathbf{x_0}\left.\frac{\partial \mathbf{a}(\mathbf{x})}{\partial \mathbf{x}}\right|_{\substack{\mathbf{x}=\mathbf{x_0}\\ u=u_0}} + u_0\left.\frac{\partial \mathbf{b}(\mathbf{x})}{\partial \mathbf{x}}\right|_{\substack{\mathbf{x}=\mathbf{x_0}\\ u=u_0}}$$

$$\bar{\mathbf{B}}(\mathbf{x},u) = \left.\frac{\partial f(t,\mathbf{x},u)}{\partial u}\right|_{\substack{\mathbf{x}=\mathbf{x_0}\\ u=u_0}} = \mathbf{B} + \mathbf{b}(\mathbf{x_0})$$

$$\bar{\mathbf{C}}(\mathbf{x},\mathbf{u}) = \left.\frac{\partial h(t,\mathbf{x},u)}{\partial \mathbf{x}}\right|_{\substack{\mathbf{x}=\mathbf{x_0}\\ u=u_0}} = \mathbf{C} + \mathbf{c}(\mathbf{x_0}) + \mathbf{x_0}\left.\frac{\partial \mathbf{c}(\mathbf{x})}{\partial \mathbf{x}}\right|_{\substack{\mathbf{x}=\mathbf{x_0}\\ u=u_0}} + u_0\left.\frac{\partial \mathbf{d}(\mathbf{x})}{\partial \mathbf{x}}\right|_{\substack{\mathbf{x}=\mathbf{x_0}\\ u=u_0}}$$

$$\bar{\mathbf{D}}(\mathbf{x},u) = \left.\frac{\partial f(t,\mathbf{x},u)}{\partial u}\right|_{\substack{\mathbf{x}=\mathbf{x_0}\\ u=u_0}} = \mathbf{D} + \mathbf{d}(\mathbf{x_0})$$

(2.25)

Neglecting the higher order terms, the considered nonlinear system can be described by the LTI SS representation, valid near the working point $\mathbf{x_0}$, u_0, t_0:

$$\begin{aligned}\dot{\mathbf{x}}(t) &= \hat{\mathbf{A}}(\mathbf{x_0})\mathbf{x}(t) + \hat{\mathbf{B}}(\mathbf{x_0})u(t) = \mathbf{A}\mathbf{x}(t) + \mathbf{B}u(t) + \mathbf{a}(\mathbf{x_0})\mathbf{x}(t) + \mathbf{b}(\mathbf{x_0})u(t) \\ y(t) &= \hat{\mathbf{C}}(\mathbf{x_0})\mathbf{x}(t) + \hat{\mathbf{D}}(\mathbf{x_0})u(t) = \mathbf{C}\mathbf{x}(t) + \mathbf{D}u(t) + \mathbf{c}(\mathbf{x_0})\mathbf{x}(t) + \mathbf{d}(\mathbf{x_0})u(t)\end{aligned} \tag{2.26}$$

The linearized Luenberger observer assumes the form:

$$\dot{\hat{\mathbf{x}}}(t) = \hat{\mathbf{A}}(\mathbf{x_0})\hat{\mathbf{x}}(t) + \hat{\mathbf{B}}(\mathbf{x_0})u(t) + \mathbf{L}[y(t) - (\hat{\mathbf{C}}(\mathbf{x_0})\hat{\mathbf{x}}(t) + \hat{\mathbf{D}}(\mathbf{x_0})u(t))] \tag{2.27}$$

Since the linearized matrices must be periodically updated, the plant model of the observer can be considered linear time varying, with matrices:

$$\begin{aligned}\hat{\mathbf{A}}(t) &= \mathbf{A} + \mathbf{a}(\mathbf{x_n}) \qquad \hat{\mathbf{B}}(t) = \mathbf{B} + \mathbf{b}(\mathbf{x_n}) \\ \hat{\mathbf{C}}(t) &= \mathbf{C} + \mathbf{c}(\mathbf{x_n}) \qquad \hat{\mathbf{D}}(t) = \mathbf{D} + \mathbf{d}(\mathbf{x_n})\end{aligned} \tag{2.28}$$

Where $\mathbf{x_n} = \mathbf{x}(t_n)$ is the nonlinear plant status vector associated to the n$^{\text{th}}$ linearization time instant $t_n = \lfloor \frac{t}{T_{up}} \rfloor$

Therefore, it is not possible to define a fixed feedback gain vector $\mathbf{L}$ that ensure the convergence of the estimation error at any instant, similarly to the linear time invariant Luenberger observer. A fixed gain, depending on the evolution in time of the linearized matrices, may suffice or lead to instability.

Assuming that the nonlinear plant locally preserves the observability property for any value of the state vector, it is possible to compute an observer time varying gain $\mathbf{L}$(t) through the Ackermann's Formula:

$$\mathbf{L}(t) = \alpha_e(\hat{\mathbf{A}}(t), t)\mathcal{O}^{-1}(t) \begin{bmatrix} 0 \\ \vdots \\ 0 \\ 1 \end{bmatrix} \tag{2.29}$$

where $\mathcal{O}(t)$ is the instantaneous observability matrix of the linearized plant:

$$\mathcal{O}(t) = \begin{bmatrix} \hat{\mathbf{C}}(t) \\ \hat{\mathbf{C}}(t)\hat{\mathbf{A}}(t) \\ \hat{\mathbf{C}}(t)\hat{\mathbf{A}}(t)^2 \\ \vdots \\ \hat{\mathbf{C}}(t)\hat{\mathbf{A}}(t)^{n-1} \end{bmatrix} \tag{2.30}$$

and $\alpha_e(\hat{\mathbf{A}}(t), t)$ is the instantaneous characteristic polynomial of the desired closed loop matrix $(\hat{\mathbf{A}}(t) - \mathbf{L}(t)\hat{\mathbf{C}}(t))$ (which defines the instantaneous desired closed loop dynamic of the state estimate error), solved for $\hat{\mathbf{A}}(t)$.

The proposed time varying linearized Luenberger observer, shown in fig. 2.16 assumes the form:

$$\dot{\hat{\mathbf{x}}}(t) = \hat{\mathbf{A}}(t)\hat{\mathbf{x}}(t) + \hat{\mathbf{B}}(t)u(t) + \mathbf{L}(t)[y(t) - (\hat{\mathbf{C}}(\mathbf{t})\hat{\mathbf{x}}(t) + \hat{\mathbf{D}}(t)u(t))] \tag{2.31}$$

The use of a time varying feedback gain allows to tune the closed loop poles of the observer to fixed values, preserving a fixed noise smoothing and allowing variations in the estimation responsiveness.

Conversely, it is also possible to update at runtime the closed loop poles in order to adapt the observer to the instantaneous poles of the plant, preserving a fixed estimation responsiveness and allowing noise smoothing variations.

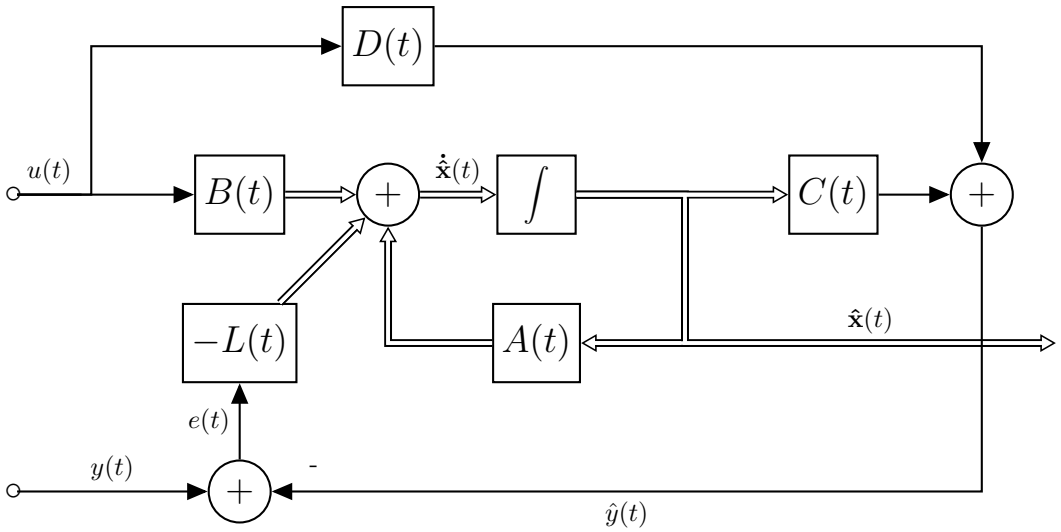

Figure 2.16: Proposed time varying linearized Luenberger observer for state estimation of nonlinear time variant system.

Chapter 3

Models for the Loudspeaker

In chapter 2 a recurrent requirement for the effectiveness of all the mentioned control techniques is to have a perfect characterization of the controlled physical system, in some cases requiring some kind of adaptive strategy in order to keep up with possible variations in time of the system properties.

For the ease of exposition, the working principles described in chapter 1 assumed an ideal, LTI dynamic loudspeaker. Unfortunately, as anticipated in section 1.1 each element of a real loudspeakers is affected by physical non idealities, causing the loudspeaker to exhibit a global nonlinear and time varying behavior.

The presence of the loudspeaker non idealities is fundamentally due to its working conditions.

In the small signals condition, the input signal is sufficiently low ($< 1V_{RMS}$) not to excite the physical system very much, producing a small current through the voice coil and consequently a relatively small diaphragm displacement ($< 1mm$ for woofers, even less for tweeters). In this case the assumption of linearity and time invariance are fulfilled, and the loudspeaker acts as an ideal device. Nevertheless, due to the small motion transmitted to the diaphragm, it cannot produce significant sound levels. For this reason no device is actually employed to work in the Small Signal condition.

In the large signals condition, the input signal ($> 1V_{RMS}$) produces a large current through the voice coil and consequently a relatively large diaphragm displacement (up to $20mm$ for woofers). In this way the physical system is sufficiently excited to exhibit a large number of non idealities, invalidating the assumption of linearity and time invariance. This is the typical working condition of a loudspeaker.

Since the first formal studies and researches on the dynamic loudspeaker different models have been proposed for its characterization, tailored on the specific purpose and conditions.

Contributions towards an effective modelization came from different researches, proposing linear, lumped element models capable of capturing the fundamental behavior of the dynamic loudspeaker (also considering the coupling with a box) in the small signals, low frequency condition [Sma72, Thi71a]. Many improvements to this first model have been proposed, extending the validity of the model even to higher frequencies [Ber86] and also introducing correction factors that account for the observed non idealities.

The fundamental breakthrough for the modeling of dynamic loudspeakers has been brought by Klippel that, summarizing the contributions of many different researches, proposed a simple and effective model for the characterization of the large signals behavior of loudspeakers [Kli05], and defined a convenient, non invasive procedure to measure all the model parameters [Kli00, SK01]. Nowadays, the model and the measurement procedure introduced by Klippel are the "de facto" standard employed by professional audio companies to characterize their products and analyze their quality.

In parallel, other techniques are employed for a more accurate study and design of loudspeakers, such as the FEM (finite element methods) and other kind of physical simulations. These approaches allow to perfectly simulate the whole physical behavior of the modeled device, requiring a very complex, ad hoc model of the device and large computational power.

For the target of this thesis, the Klippel model is the most attractive one, due to its rich but simple characterization of the dynamic loudspeaker nonlinearities. In order to achieve a better comprehension of the loudspeaker behavior, the simpler linear model will be presented first. Then, all the generalizations introduced by Klippel will be described, presenting the loudspeaker model that will be exploited for the design of the controller.

3.1 Small signals condition: the linear model

During the first half of the 20th century many publications suggested that the mechanical and the acoustic systems could be easily modeled and analyzed as if they were lumped elements electric circuits.

This is indeed possible when considering linear, time invariant systems: in that case the three physical domains (electric, mechanical and acoustic) share the same mathematical framework (linear differential equations) to model very different phenomena.

Particularly interesting is the work of Olson [Ols58], later extended by Beranek [Ber86], where all the analogies between the elements of the different physical domains are described in detail. Their results are summarized in fig. 3.1.

In his book, Beranek also proposes a methodology to model a linear dynamic loudspeaker exploiting the electromechanical and the electroacoustic analogies, considering each domain separately and defining the required inter-domain connections.

The dynamic loudspeaker is considered as the combination of an electric domain, composed by the voice coil; a mechanical domain, composed by the diaphragm and the spider; and an acoustic domain, defined by the surrounding acoustic environment, usually a box.

The electric domain interacts with the mechanical domain by means of the electroacoustic transduction of the electric linear motor, and in turn the mechanical domain interacts with the acoustic domain by means of the mechanoacoustic transduction of the direct radiator.

The model proposed by Beranek, being intrinsically linear and time invariant, is useful only to model the behavior of a dynamic loudspeakers in the small signal condition.

3.1.1 The electric domain

The electric domain includes all the dynamic loudspeaker parts whose behavior can be described in terms of voltage **V** and current **i**.

In a typical loudspeaker it is composed by the sole voice coil that, being a long solenoid of conducting wire, exhibits both a resistive and an inductive behavior.

The model proposed by Beranek is composed by the series of an electric resistance R_e and an electric inductance L_e, characterized by the equation:

$$V_{in}(t) = R_e i(t) + L_e \frac{\partial i}{\partial t} \tag{3.1}$$

Measurements of the electric impedance of the voice coil immersed in the loudspeaker magnetic field suggest that the electric inductance does not follow the expected $j\omega$ frequency dependence:

$$Z_e(j\omega) = R_e + j\omega L_e \tag{3.2}$$

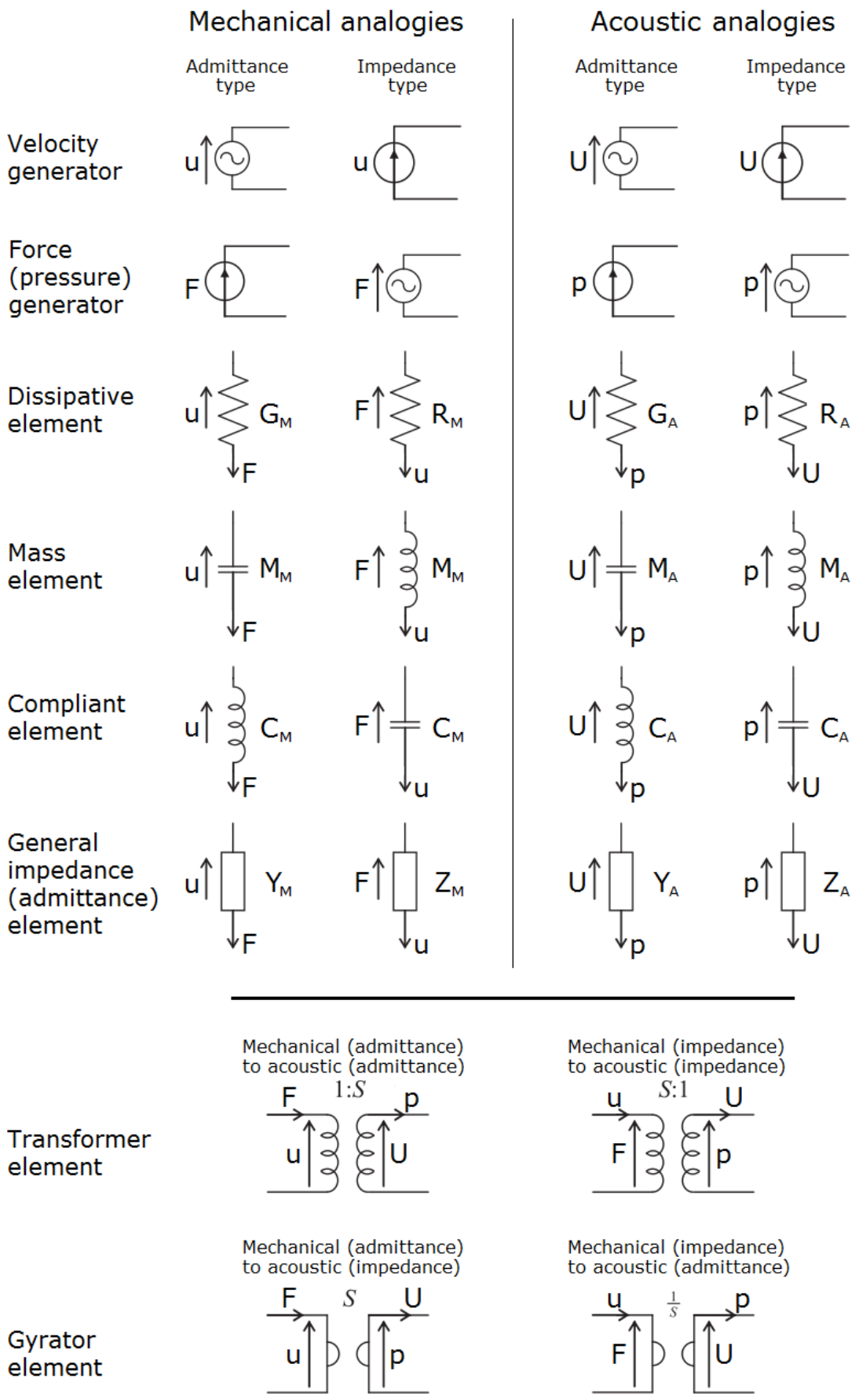

Figure 3.1: Electromechanical and electroacoustic analogies.

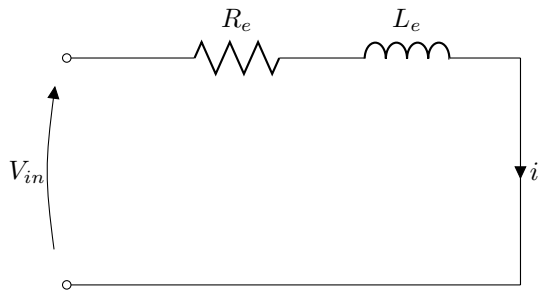

Figure 3.2: Simple equivalent circuit of the loudspeaker electric domain.

Vanderkooy in [Van89] verified that the electric inductance follows a "semi-inductive" behavior, characterized by a $\sqrt{j\omega}$ frequency dependence.

$$Z_e(j\omega) = R_e + \sqrt{j\omega}L_e \tag{3.3}$$

This is attributed to the electromagnetic interaction between the voice coil and the iron of the magnetic circuit, which can be considered equivalent to a large, single coil made of iron, wound around the voice coil.

Since the two coils are concentric, the voice coil and the equivalent coil of the magnetic circuit are almost perfectly coupled. This implies that the magnetic flux produced by the current flow in the voice coil strongly affects the magnetic flux of the magnetic circuit equivalent coil.

Therefore, due to Faraday's law of induction 3.4, the current flow variation in the voice coil causes the induction of an electromotive force in the iron and the generation of eddy currents in the iron with "semi-frequency" dependent ($\sqrt{j\omega}$) magnitude, due to the skin effect in the iron.

$$\mathcal{E}(t) = -\frac{\partial \Phi_B(t)}{\partial t} \tag{3.4}$$

In turn, the eddy currents flow in the iron produces a "semi-frequency" dependent magnetic field opposing the magnetic flux variation induced by the voice coil current. Thus, the magnetic flux generated by the eddy currents induces a "semi-frequency" dependent electromotive force on the voice coil $\mathcal{E}^{eddy}_{voice}$.

$$V_{in}(t) = R_e i(t) + L_e \frac{\partial i}{\partial t} + \mathcal{E}^{eddy}_{voice}(\sqrt{j\omega}, i, t) \tag{3.5}$$

The net effect of the complex electromagnetic interaction between the voice coil and the iron of the magnetic circuit is the exhibition of the "semi-frequency" dependency of the electric inductance, as described in eq. (3.3).

Since this relation cannot be expressed in linear terms, many models have been proposed to describe this feature or to approximate it [Lea02, Wri89, DKOB04].

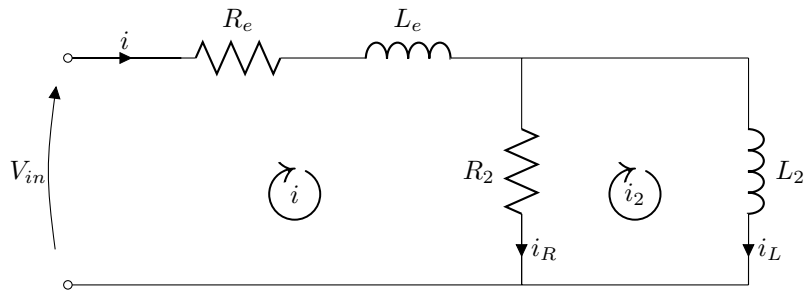

Figure 3.3: Equivalent circuit of the loudspeaker electric domain, with LR-2 model for eddy currents contribution.

The more interesting approach is the so called "LR-2 model", which adds to the model proposed by Beranek a second inductance L_2, shunted with a second resistance R_2.

Choosing the right values for L_2 and R_2 it is possible to obtain a satisfying linear model, capable of fitting the real behavior of the voice coil for a sufficiently large bandwidth.

The electric domain can then be characterized by the two equations:

$$\begin{cases} V_{in}(t) = R_e i(t) + L_e \dfrac{\partial i(t)}{\partial t} + R_2 i(t) - R_2 i_2(t) \\ \\ 0 = R_2 i_2(t) + L_2 \dfrac{\partial i_2(t)}{\partial t} - R_2 i(t) \end{cases} \tag{3.6}$$

where the "semi-frequency" dependent electromotive force generated by the eddy current is approximated by linear terms

$$\mathcal{E}^{eddy}_{voice}(\sqrt{j\omega}, i, t) = R_2 i(t) - R_2 i_2(t) \tag{3.7}$$

3.1.2 The mechanical domain

The mechanical domain includes all the parts of the dynamic loudspeaker whose behavior can be described in terms of force **F** and velocity **v**.

In a typical loudspeaker it is composed by the "voice coil + diaphragm" body and the spider, essentially acting as a rigid body of mass $\mathbf{M_{md}}$ and a spring of stiffness $\mathbf{K_{md}}$, respectively. Also a damping $\mathbf{R_{md}}$ effect is introduced due to the intrinsic mechanical losses.

The mechanical domain can be characterized by the equation:

$$F_{in}(t) = M_{md} \frac{\partial^2 x(t)}{\partial t^2} + R_{md} \frac{\partial x(t)}{\partial t} + K_{md} x(t) \tag{3.8}$$

The system globally act as a damped mechanical resonator, thus can be modeled by a spring-mass-damper system, characterized by a resonance frequency f_0 and a damping factor ζ_0.

$$f_0 = \frac{1}{2\pi} \sqrt{\frac{K_{md}}{M_{md}}} \qquad \zeta = \frac{R_{md}}{2} \frac{1}{\sqrt{K_{md} M_{md}}} \tag{3.9}$$

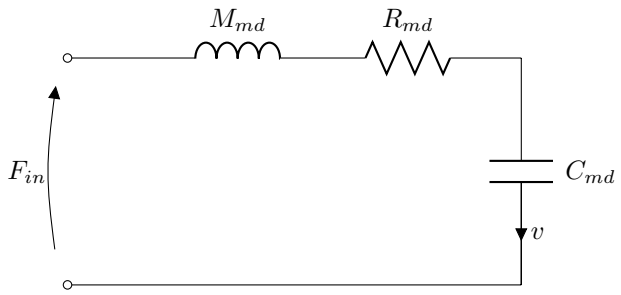

Figure 3.4: Equivalent circuit of the loudspeaker mechanical domain.

The described system clearly behaves like a series electric RLC resonator, justifying the conversion of the mechanical representation into an electric one.

Beranek defines both the impedance and the mobility conversions for the mechanical domain, but for the purpose of this thesis only the impedance form will be considered. In in the impedance form, the mechanical domain is converted into a electric circuit composed by the series of an inductance $\mathbf{M_{md}}$, representing the mechanical mass, a resistance $\mathbf{R_{md}}$, representing the mechanical damper, and a capacitor $\mathbf{C_{md}} = \dfrac{1}{\mathbf{K_{md}}}$, representing the mechanical compliance, i.e. the reciprocal of the mechanical stiffness.

3.1.3 The acoustic domain

The acoustic domain is not actually a proper part of the loudspeaker, being the acoustic environment surrounding the loudspeaker itself, described in terms of pressure $\mathbf{p}$ and volume velocity $\mathbf{U}$.

Three common acoustic configuration are considered for the loudspeaker mounting: the free air mount, the infinite baffle mount, the sealed enclosure and the vented enclosure.

In the free air mount the loudspeaker is simply immersed in air. In that case the acoustic domain is characterized by the sole air load, acting as as a combination of an acoustic mass and an acoustic damper.

The equivalent electric circuit in Impedance form is the series of an inductance $\mathbf{M_{AR}}(j\omega)$, representing the air load mass, and a resistance $\mathbf{R_{AR}}(j\omega)$, representing the acoustic radiation.

$$P_{in} = M_{AR}(j\omega)\frac{\partial U}{\partial t} + R_{AR}(j\omega)U \tag{3.10}$$

In the infinite baffle mount the loudspeaker is mounted on an infinite surface that acoustically insulates the two sides of the diaphragm. In that case, the acoustic domain is again characterized by the sole air load described in eq. (3.10), albeit with different behaviors of the air load parameters $M_{AR}(j\omega)$ and $R_{AR}(j\omega)$.

In the sealed enclosure mount, the loudspeaker is mounted on a closed box. The air cavity created by the box acts as an additional acoustic compliance $\mathbf{C_{ab}}$ that loads the loudspeaker. The equivalent counterpart of the box compliance in the acoustic circuit is a capacitor $\mathbf{C_{ab}}$.

In the vented enclosure mount, the loudspeaker is mounted on a box with a tuned port that connects the inner side of the box with the rest of the acoustic environment. This configuration introduces, in addition to the air cavity contribution as a compliance, also an acoustic mass $\mathbf{M_{ap}}$, due to the air inside the port, and an acoustic damping $\mathbf{R_{al}}$, due to the air losses, mainly friction and turbulence. The acoustic system formed by the vented box alone acts as a parallel resonator.

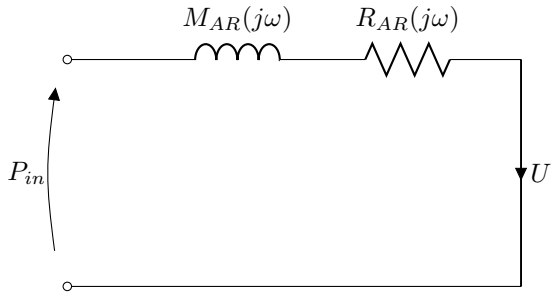

Figure 3.5: Equivalent circuit of the loudspeaker's acoustic domain, in either the free air or the infinite baffle mounting configuration.

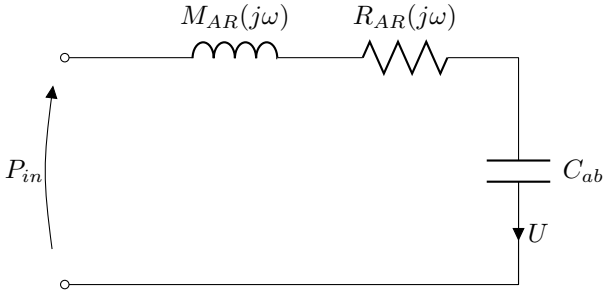

Figure 3.6: Equivalent circuit of the loudspeaker's acoustic domain, in the sealed enclosure mounting configuration.

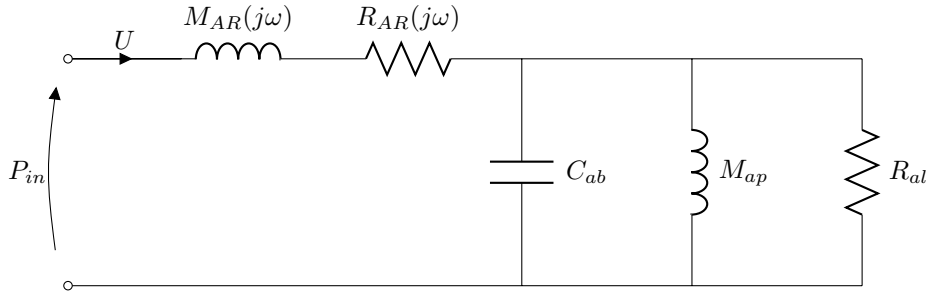

Figure 3.7: Equivalent circuit of the loudspeaker's acoustic domain, in the vented enclosure mounting configuration.

3.1.4 The electro-mechanic transduction

The electro-mechanic transduction allows the connection between the electric domain and the mechanical domain implementing an energy preserving conversion between the different physical variables of the two domains.

In a loudspeaker, the electro-mechanic transduction is performed by means of the linear electric motor, whose working principle has already been discussed in section 1.2.1.

The typical behavior of the linear electric motor in a loudspeaker can be described by the two equations:

$$\begin{cases} F(t) = Bl\ i(t) \\ V_{emf}(t) = Bl\ v(t) \end{cases} \tag{3.11}$$

The linear motor converts the electric current **i** flowing in the voice coil into a mechanical force **F** with a conversion factor equal to the motor force factor **Bl**. Conversely, the mechanical body's velocity **v** is converted into an electric voltage $\mathbf{v_{emf}}$, again with a conversion factor equal to **Bl**.

Beranek associates this behavior to a gyrator-like element with conductance equal to the motor force factor **Bl**.

3.1.5 The mechano-acoustic transduction

The mechano-acoustic transduction allows the connection between the mechanical domain and the acoustic domain implementing an energy preserving conversion between the different physical variables of the two domains.

In a loudspeaker, the mechano-acoustic transduction is performed by means of the direct radiator, whose working principle has already been discussed in section 1.2.2.

The typical behavior of the direct radiator in a loudspeaker can be described by the two equations:

$$\begin{cases} p(t) = \dfrac{F(t)}{S_d} \\ U(t) = S_d\ v(t) \end{cases} \tag{3.12}$$

The direct radiator converts the mechanical Force **F** exerted on the radiator into acoustic pressure **p** with a conversion factor equal to the reciprocal of the surface of the radiator $\dfrac{1}{\mathbf{S_d}}$. Similarly, the mechanical velocity **v** is converted into volume velocity **U** with a conversion factor equal to $\mathbf{S_d}$.

Beranek associates this behavior to a transformer-like element with turns ratio equal to the surface $\mathbf{S_d}$.

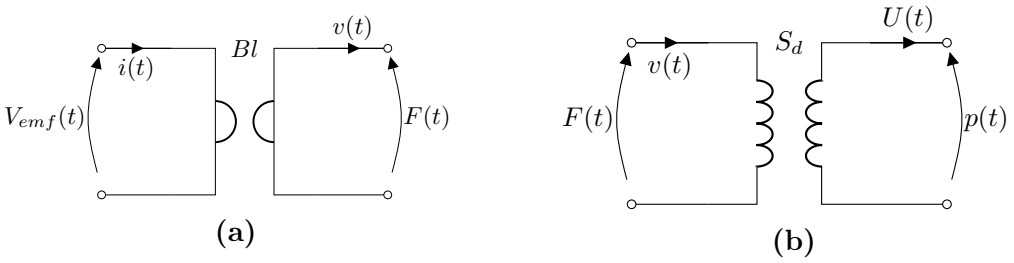

Figure 3.8: a) Equivalent circuit of the electro-mechanic transduction, performed by the electric linear motor; b) Equivalent circuit of the mechano-acoustic transduction, performed by the direct radiator

3.1.6 The complete linear model

Connecting the equivalent electrical, electromechanical and electroacoustic circuits derived in sections 3.1.1 to 3.1.3 with the transduction element described in sections 3.1.4 and 3.1.5, the complete linear model of the loudspeaker is obtained.

Considering a loudspeaker in the free air mounting configuration, the equivalent electro-mechano-acoustic model is shown in fig. 3.9.

A common simplification of the complete model consists in the translation of the air acoustic impedance $\mathbf{Z_{AR}}(j\omega)$ from the acoustic domain to the mechanical domain, exploiting the definition of the air equivalent mechanical impedance of eq. (1.8).

Thus, the acoustic mass $\mathbf{M_{AR}}(j\omega)$ and the acoustic damping $\mathbf{R_{AR}}(j\omega)$ of the acoustic domain are converted into an equivalent mechanical mass $\mathbf{M_{MR}}(j\omega)$ and mechanical damping $\mathbf{R_{MR}}(j\omega)$ respectively, directly connected to the mechanical domain.

Both the air mechanical mass and the air mechanical damping are usually much smaller than the loudspeaker mass and damping, allowing to consider them small constant values for the whole loudspeaker working bandwidth.

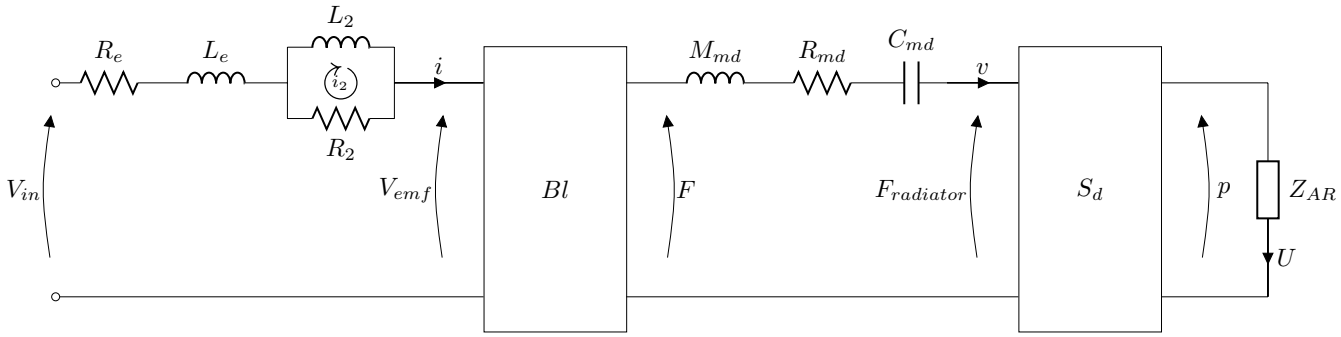

Figure 3.9: Equivalent circuit of the full loudspeaker system, in the free air mounting configuration.

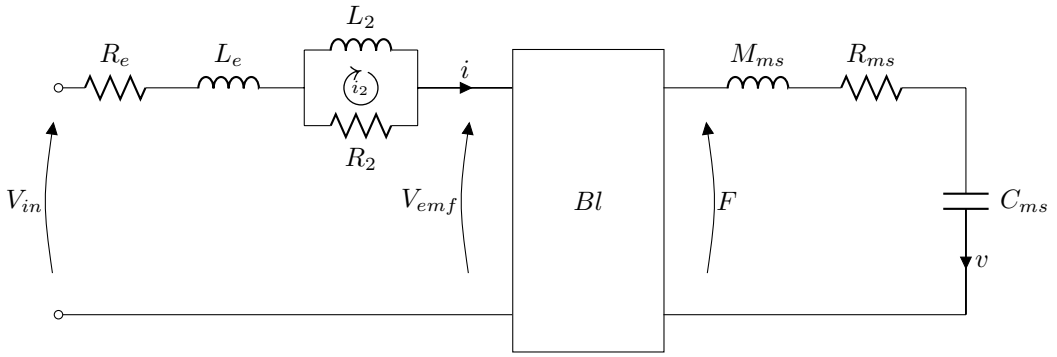

Figure 3.10: Equivalent circuit of the full loudspeaker system, in the free air mounting configuration and considering the mechanical equivalent contribution of the air acoustic impedance.

The mechanical contributions can then be reduced to a single, constant parameter for the mechanical mass, the mechanical damping and the mechanical compliance, respectively:

$$\begin{aligned} M_{ms} &= M_{md} + M_{MR} \\ R_{ms} &= R_{md} + R_{MR} \\ C_{ms} &= C_{md} \end{aligned} \tag{3.13}$$

The equivalent model is shown in figure fig. 3.10.

The equivalent mechanical system exhibit a slightly different resonance frequency f_s and a damping factor ζ_s with respect to those exhibited in the free air mounting configuration.

$$f_s = \frac{1}{2\pi}\sqrt{\frac{K_{ms}}{M_{ms}}} \qquad \zeta_s = \frac{R_{ms}}{2}\frac{1}{\sqrt{K_{ms}M_{ms}}} \tag{3.14}$$

More complex acoustic environments, such a sealed enclosure or a vented enclosure, can also be simplified converting the acoustic elements into mechanical equivalents.

For a sealed enclosure, the acoustic compliance of the box cavity $\mathbf{C_{ab}}$ is converted to an equivalent mechanical compliance $\mathbf{C_{mb}}$ that can be combined with the Spider compliance contribution into a single parameter.

$$C_{mb} = C_{ab}{S_d}^2 \tag{3.15}$$

$$C_{ms} = \frac{C_{md}C_{mb}}{C_{md} + C_{mb}} \tag{3.16}$$

The equivalent model is still the one shown in figure fig. 3.10, using the mechanical compliance in eq. (3.16). The equivalent mechanical system exhibit an even different resonant frequency and damping factor with respect to those exhibited in the free air mounting configuration, that can still be calculated using eq. (3.14).

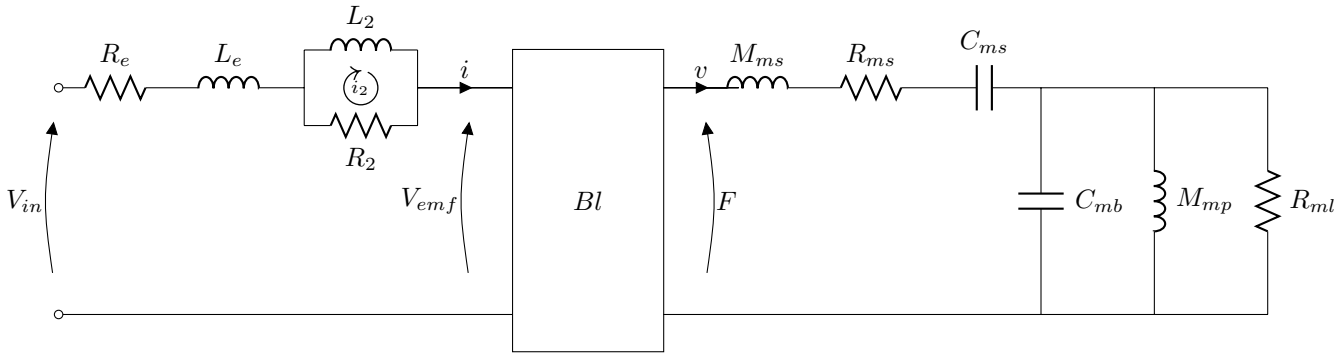

Figure 3.11: Equivalent circuit of the full loudspeaker system, in the vented enclosure mounting configuration and considering the mechanical equivalent contribution of the acoustic environment.

For a vented enclosure the conversion to the mechanical domain does not allow any further simplification of the model. The acoustic elements are converted into the respective mechanical counterparts:

$$\begin{aligned} M_{mp} &= M_{ap} {S_d}^2 \\ R_{ml} &= R_{al} {S_d}^2 \\ C_{mb} &= \frac{1}{K_{mb}} = C_{ab} {S_d}^2 \end{aligned} \tag{3.17}$$

The equivalent model is shown in figure fig. 3.11, using the parameters in eqs. (3.13) and (3.17). The equivalent mechanical system exhibit two resonant frequencies: one due to the mechanical resonance, still calculated using eqs. (3.13) and (3.14), and one due to the air port acoustic resonance, using eq. (3.17):

$$f_{s2} = \frac{1}{2\pi}\sqrt{\frac{K_{mb}}{M_{mp}}} \qquad \zeta_{s2} = \frac{R_{ml}}{2}\frac{1}{\sqrt{K_{mb} M_{mp}}} \tag{3.18}$$

3.1.7 SS representation of the linear model

This thesis focuses on the behavior of loudspeakers in the free air mount configuration. This choice is not arbitrary: the free air mount is indeed the simplest mounting configuration and allows a precise analysis of the transducer behavior without any influence from the acoustic environment.

Moreover, the analysis carried out for the free air mount can be later generalized for both the sealed enclosure mount, and the vented enclosure mount exploiting the models developed in section 3.1.6.

The model of the free air mounted loudspeaker previously developed fig. 3.9 is LTI and characterized by lumped elements that can be expressed in SS form.

First of all, it is necessary to define the input(s) and the output(s) of the system to be modeled. The loudspeaker is a SISO (single input - single output) system, whose usually considered input is the voltage applied to the voice coil by an audio source, say a power amplifier. The quantity to be considered as the loudspeaker output is not clearly defined instead.

Usually, the pressure produced by the direct radiator, or some related metric (Sound Pressure Level (SPL), the Sound Power (P) or the Sound Intensity (I)) is taken as the output. However, all the acoustic domain measurements are strongly affected by the sensor (microphone) noise, its positioning and disturbances (acoustic reflections), making it difficult to effectively evaluate the loudspeaker behavior. Moreover, the frequency dependent behavior of the direct radiator, described in section 1.2.2, makes it even harder.

The solution is to define a loudspeaker output a quantity that is not affected by the acoustic domain, but is related to the produced pressure. A good candidate comes from eq. (1.12), which relates the pressure generated by the loudspeaker to its acceleration.

Acceleration is indeed a more suitable quantity to be evaluated, since it belongs to the mechanical domain, and is directly related to the maximum pressure achievable by the loudspeaker.

The equations that characterize the free air mounted linear loudspeaker have been defined in sections 3.1.1, 3.1.2 and 3.1.4 and are here reported:

$$\begin{cases} V_{in}(t) - V_{emf}(t) = R_e i(t) + L_e \dfrac{\partial i(t)}{\partial t} + R_2 i(t) - R_2 i_2(t) \\ 0 = R_2 i_2(t) + L_2 \dfrac{\partial i_2(t)}{\partial t} - R_2 i(t) \\ F(t) = M_{ms} \dfrac{\partial^2 x(t)}{\partial t^2} + R_{ms} \dfrac{\partial x(t)}{\partial t} + K_{ms} x(t) \\ F(t) = Bl\ i(t) \\ V_{emf}(t) = Bl\ \dfrac{\partial x(t)}{\partial t} \end{cases} \tag{3.19}$$

Rearranging the equations as follows

$$\begin{cases} V_{in}(t) = (R_e + R_2) i(t) - R_2 i_2(t) + L_e \dfrac{\partial i(t)}{\partial t} + Bl\ \dfrac{\partial x(t)}{\partial t} \\ 0 = R_2 i_2(t) + L_2 \dfrac{\partial i_2(t)}{\partial t} - R_2 i(t) \\ Bl\ i(t) = M_{ms} \dfrac{\partial^2 x(t)}{\partial t^2} + R_{ms} \dfrac{\partial x(t)}{\partial t} + K_{ms} x(t) \end{cases} \tag{3.20}$$

the coupling between the electric and the mechanic domain becomes evident.

The equations can be further rearranged to form a system of first order differential equations, required for the definition of a SS model.

$$\begin{cases} \dfrac{\partial i(t)}{\partial t} = \dfrac{-(R_e + R_2)i(t) + R_2 i_2(t) - Bl\ v(t)}{L_e} + \dfrac{V_{in}(t)}{L_e} \\ \dfrac{\partial i_2(t)}{\partial t} = \dfrac{R_2 i(t) - R_2 i_2(t)}{L_2} \\ \dfrac{\partial x(t)}{\partial t} = v(t) \\ \dfrac{\partial v(t)}{\partial t} = \dfrac{Bl\ i(t) - K_{ms} x(t) - R_{ms} v(t)}{M_{ms}} \end{cases} \tag{3.21}$$

The state vector $\mathbf{x}$(t), the input u(t) and the output y(t) are defined as follows:

$$\mathbf{x} = \begin{bmatrix} i(t) & i_2(t) & x(t) & v(t) \end{bmatrix}^T \tag{3.22}$$

$$u(t) = V_{in}(t) \qquad y(t) = a(t) = \frac{\partial v(t)}{\partial t} = \frac{\partial^2 x(t)}{\partial t^2} \tag{3.23}$$

Then the SS representation of the loudspeaker in free air is given by the matrices:

$$\mathbf{A} = \begin{bmatrix} -\dfrac{R_e + R_2}{L_e} & \dfrac{R_2}{L_e} & 0 & -\dfrac{Bl}{L_e} \\ \dfrac{R_2}{L_2} & -\dfrac{R_2}{L_2} & 0 & 0 \\ 0 & 0 & 0 & 1 \\ \dfrac{Bl}{M_{ms}} & 0 & -\dfrac{K_{ms}}{M_{ms}} & -\dfrac{R_{ms}}{M_{ms}} \end{bmatrix} \qquad \mathbf{B} = \begin{bmatrix} \dfrac{1}{L_e} \\ 0 \\ 0 \\ 0 \end{bmatrix} \tag{3.24}$$

$$\mathbf{C} = \begin{bmatrix} \dfrac{Bl}{M_{ms}} & 0 & -\dfrac{K_{ms}}{M_{ms}} & -\dfrac{R_{ms}}{M_{ms}} \end{bmatrix} \qquad \mathbf{D} = \begin{bmatrix} 0 \end{bmatrix}$$

3.2 Large signals condition: the nonlinear model

The LTI model for the loudspeaker developed so far is not sufficient to characterize the device in typical working conditions.

For example, at its limit conditions, a subwoofer loudspeaker can be driven by voltage values up to 100V and currents up to 15A, producing a mechanical displacement of its moving parts up to 30mm (peak values).

Under such conditions, the large variations over time of the electrical and mechanical quantities undergone by the speaker will strongly affect its structure and its properties. The resulting behavior exhibited by the loudspeaker is nonlinear and time varying.

The analysis of loudspeakers in the large signals condition requires the definition of a different model, capable of capturing the nonlinear and time varying characteristics.

Among the various model proposals for the large signal loudspeaker characterization, the most suitable for the purpose of this thesis is the model proposed by Klippel.

3.2.1 Extension of the linear model: the Klippel model

The model proposed by Klippel is a lumped element, nonlinear time-invariant loudspeaker model, directly derived by the linear model described in section 3.1.

It has been developed for the analysis of the large signals behavior of loudspeakers and for the development of loudspeaker control systems. Lately, thanks to its proven effectiveness, it has substituted the Thiele-Small model and the Beranek model, becoming the new standard "de facto" for loudspeakers characterization.

The Klippel model extends the linear model described in section 3.1.6 characterizing some of the lumped elements with parameters which vary with the model's internal state, thus making the model itself nonlinear. These nonlinear parameters are described by means of nonlinear curves of the parameter value versus a state variable.

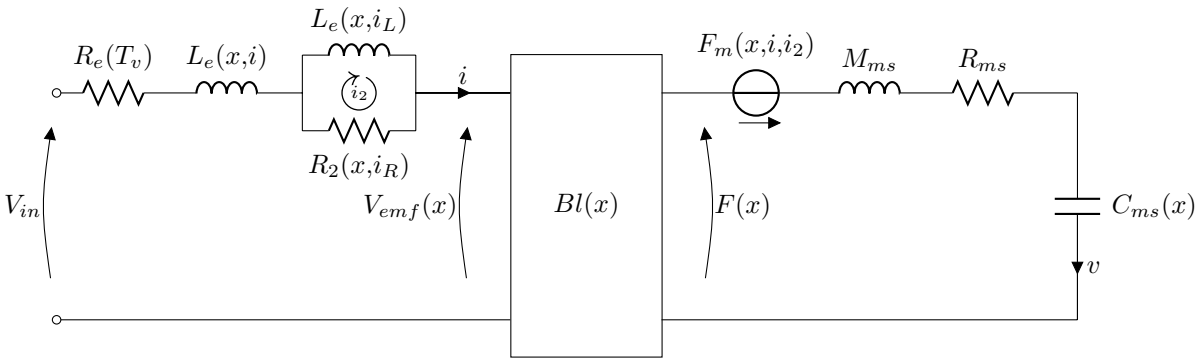

Figure 3.12: Klippel model for loudspeakers in the free air mounting configuration.

Even if not formally introduced in the model definition, time variance can be taken into account allowing the model parameters to change over time. Up to now it is not possible to fully characterize the evolution in time of the loudspeaker parameters, so the time variance is introduced only for control purposes, if it is possible to update the model parameters at runtime by means of an adaptive algorithm.

For the purpose of this thesis the loudspeaker is considered as a nonlinear time invariant system. Therefore the Klippel model provides a suitable framework for the its characterization. Also, it fosters the introduction of the loudspeaker time variance, which can be developed in future works.

3.2.2 The loudspeaker nonlinearities

In the Klippel model, as well as in the linear model to which is inspired, each parameter has a well defined physical meaning and is associated to a specific element of the loudspeaker structure. For this reason, the characterization of the nonlinearities can be carried out analyzing in detail the behavior of each element when working in the large signals condition.

It is important to point out that each kind of loudspeaker (woofer, tweeter, microspeaker, etc) exhibits different dominant nonlinearities. For the purpose of this thesis, only the main nonlinear effects affecting the woofers and subwoofers loudspeaker will be considered.

Electric inductance

The voice coil electric inductance exhibits both a displacement and a current dependency. This means that the correct characterization would require the definition of a nonlinear surface of the electric inductance value versus the displacement-current pair, instead of a simple curve.

$$L_e(x,i) = {L_e}^0 \, f(x,i) \tag{3.25}$$

where ${L_e}^0$ is the value of $L_e(0,0)$, the electric inductance value at rest.

This behavior is approximated assuming that the displacement and the current contributions are independent of each other, allowing the characterization of the nonlinear inductance parameter by means of two curves, each one with a single variable dependency.

$$L_e(x,i) \approx {L_e}^0 \, [1 + \xi(x) + \iota(i)] \tag{3.26}$$

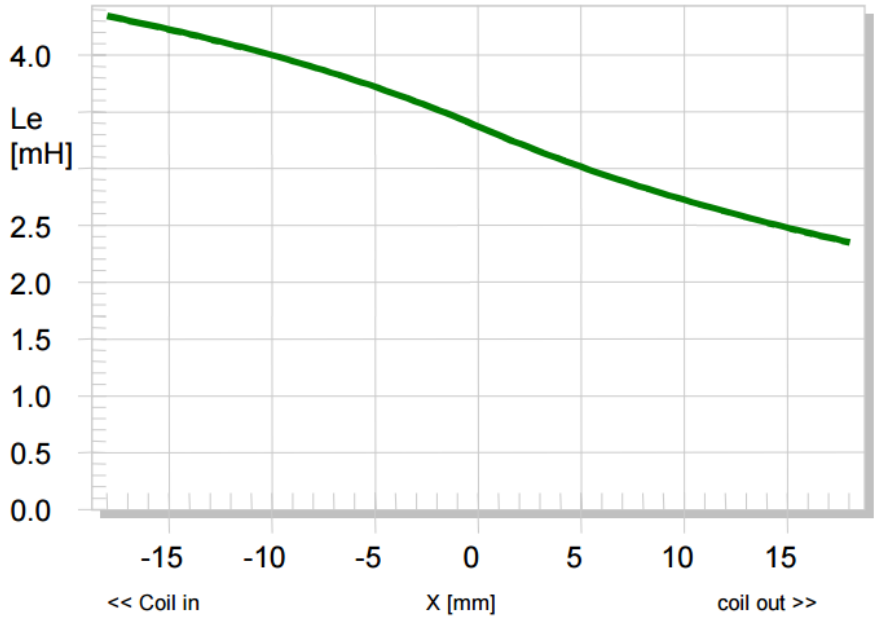

Figure 3.13: Voice coil inductance displacement dependency $L_e(x, i = 0)$.

The displacement dependency is due to the modulation of the magnetic permeability experienced by the voice coil during its motion back and forth in the magnetic gap.

At negative displacements, the voice coil is almost completely immersed in the magnetic circuit iron, characterized by a high magnetic permeability, while at positive displacements it is mostly immersed in air, characterized by a lower magnetic permeability.

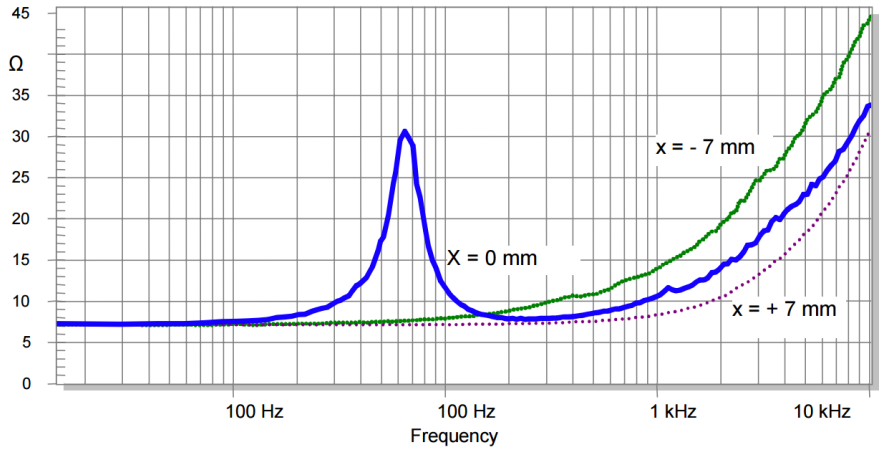

Figure 3.14: Variations of the electric impedance of a loudspeaker caused by the voice coil displacement.

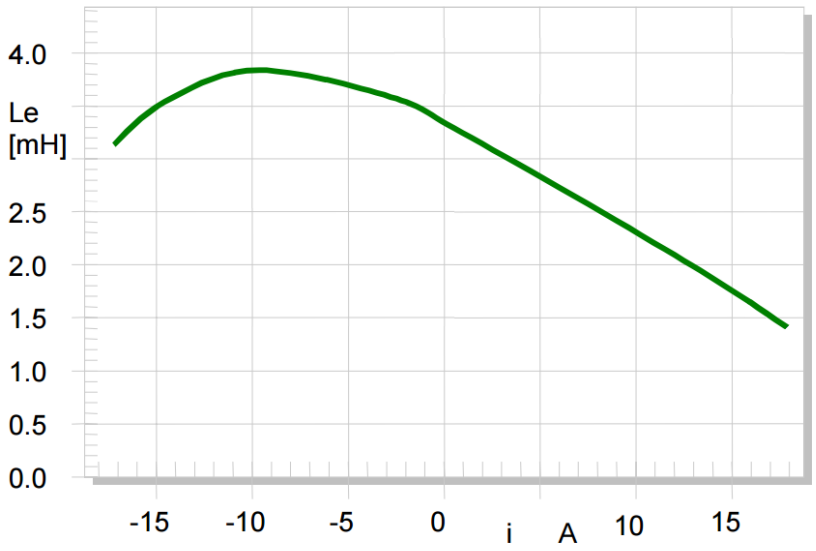

Figure 3.15: Voice coil inductance current dependency $L_e(x = 0, i)$.

The current dependency is due to the modulation of the magnetic permeability of the iron of the magnetic circuit, caused by the nonlinear relation between the magnetic field strength **H** of the permanent magnet and the magnetic flux density **B** in the iron.

Without any current flowing in the voice coil, the permanent magnet is the only magnetic field strength source. It enforces the working point on the **H**-**B** curve of fig. 3.16, i.e. with the iron magnetic permeability and magnetic flux density **B** at rest.

A large current flow in the voice coil acts as another magnetic field strength source, changing the total magnetic field strength. This causes a shift of the working point on the **H**-**B** curve, affecting the iron magnetic permeability.

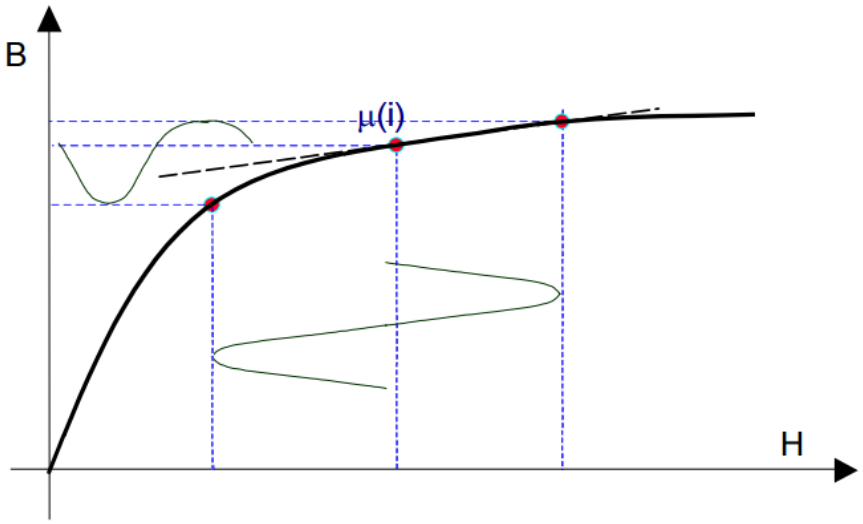

Figure 3.16: Magnetic flux density **B** versus magnetic field strength **H** in iron and the modulation effects due to the voice coil current.

The modulation of the magnetic permeability experienced by the voice coil due to current and displacement causes the modulation of its exhibited electrical inductance value, approximately following the long solenoid relation:

$$L_e(x,i) \propto \mu(x,i)\frac{N^2 A}{l} \tag{3.27}$$

Unfortunately, this relation is not strictly valid for a typical voice coil due to its geometry (short and wide), but it clearly highlights the dependency between the effective magnetic permeability $\mu(x,i)$ and the electric inductance $\mathbf{L_e}(x,i)$.

When using an LR-2 model to cope with the "semi-inductive" behavior of the electric inductance, parameters $\mathbf{L_2}$ and $\mathbf{R_2}$ are also affected by the magnetic permeability modulation. Rather than defining other two nonlinear curves for each parameter, Dodd in [DKOB04] and Klippel in [Kli05] suggested that, for most applications, the behaviors of $\mathbf{L_2}(x,i_L)$ and $\mathbf{R_2}(x,i_R)$ can be approximated to scaled version of the behavior of $\mathbf{L_e}(x,i)$.

In that case, the following relations hold:

$$L_2(x,i) = {L_2}^0\,[1+\xi(x)+\iota(i)] \qquad L_2(x,i) = {L_2}^0\,[1+\xi(x)+\iota(i)] \tag{3.28}$$

with

$$\xi(x) = \frac{L_e(x,0)}{{L_e}^0} \approx \frac{L_2(x,0)}{{L_2}^0} \approx \frac{R_2(x,0)}{{R_2}^0} \tag{3.29}$$

$$\iota(i) = \frac{L_e(0,i)}{{L_e}^0} \approx \frac{L_2(0,i)}{{L_2}^0} \approx \frac{R_2(0,i)}{{R_2}^0} \tag{3.30}$$

where $\mathbf{{L_2}^0}$ and $\mathbf{{R_2}^0}$ are the values of $\mathbf{L_2}(0,0)$ and $\mathbf{R_2}(0,0)$ respectively.

Finally, the variation of the electric inductance value over the displacement also generates an additional reluctance force $\mathbf{F_m}(i,i_L,x)$ that sums up to the linear motor driving force, causing a spurious drive of the mechanical system.

$$F_m(i,i_2,x) \approx -\frac{i(t)^2}{2}\frac{\partial L_e(x,i)}{\partial x} - \frac{i_L(t)^2}{2}\frac{\partial L_2(x,i)}{\partial x} \tag{3.31}$$

However, the reluctance force is generally negligible.

Force factor

The electric linear motor force factor mainly exhibits a dependency on the displacement.

$$Bl(x) = Bl^0 \, \beta(x) \tag{3.32}$$

where $\mathbf{Bl^0}$ is the value of $\mathbf{Bl}(0)$.

The force factor is given by the product of the voice coil wire length and the magnetic flux density experienced by each infinitesimal part of the wire.

Clearly, the wire length is fixed and the magnetic flux density produced by the permanent magnet in the magnetic gap and its surroundings can be considered with good approximation stationary. However, the magnetic flux density is not homogeneous in space, being almost constant inside the magnetic gap, where it assumes its maximum value, and exhibiting a rapid decay in its surroundings, often asymmetrically due to the magnetic circuit shape.

When the coil is at rest ($x = 0$), it is immersed in the strongest magnetic flux density, exhibiting a large force factor. Conversely, when the coil is at an arbitrary displacement, the magnetic flux density experienced by the coil is less the farther it is from its rest position.

The geometry of the voice coil can mitigate the force factor dependency on the displacement: an over-hung coil exhibits an approximately constant force factor for larger displacements, the so called "plateau", but also a more rapid decay once it passes a certain displacement threshold, as can be seen in section 3.2.2

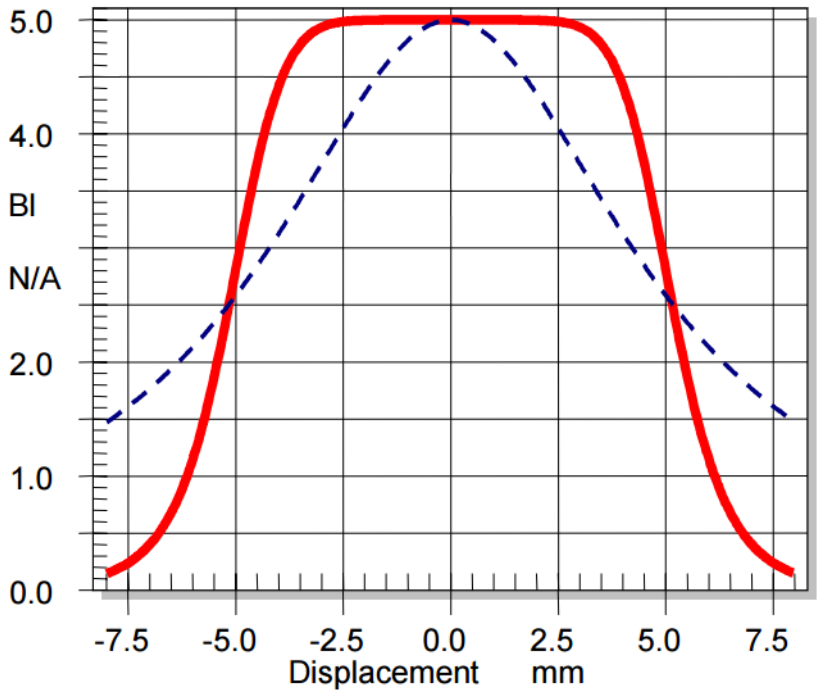

Figure 3.17: Force factor displacement dependency for over-hung (red) and equal-hung coils (blue).

The force factor decay due to the displacement strongly afflicts all the loudspeakers and is a major cause of sound distortion, as it directly influences the generation of the driving force.

The force factor also exhibit a weak current dependency. As explained in section 3.2.2, the presence of a large current in the voice coil causes the modulation of the iron magnetic permeability. This in turns affects also the magnetic flux density $\mathbf{B}$, as depicted in fig. 3.16. However, the effect of the current on the force factor is usually negligible, especially when using strong magnets capable to saturate the iron of the magnetic circuit.

Mechanical Stiffness

The mechanical stiffness exhibits a dependency on the displacement.

$$K_{ms}(x) = {K_{ms}}^{0}\, \kappa(x) \tag{3.33}$$

where $\mathbf{{K_{ms}}^{0}}$ is the value of $\mathbf{K_{ms}}(0)$.

The main source of the mechanical stiffness is the spider, while the surround is influential only at very large displacements.

The spider structure is characterized by a corrugation pattern that, acting as a spring, allows it to exhibit an almost linear behavior, at least for small displacements. Conversely, during large displacements, the waves of the corrugation tend to be overstretched, causing the spider to exhibit a stiffer behavior the farther the loudspeaker is from its rest condition ($x = 0$).

The geometry of the wave pattern can mitigate the stiffness dependency on the displacement: increasing the number of waves of the corrugation and/or increasing their size can help stabilizing the stiffness value for larger displacement values. The same applies for the surround but, since it is usually a very flexible rubber ring, its effects are negligible unless it is severely overstretched.

The stiffness nonlinearity is a major cause of sound distortion, as its value is subject to very large variations.

Another common non ideal behavior of the suspensions (spider and surround) is the occurrence of viscoelastic effects, referred as "creep", at frequencies much smaller that the loudspeaker resonant frequency. The net effect is a reduction of the stiffness at those frequencies.

Fortunately, the creep effect usually occurs at frequencies below the specific loudspeaker bandwidth, and can thus be neglected.

Other effects

The Klippel model introduces also other nonlinearities and non idealities that are not included in the older models, making it even more flexible and suitable for other typologies of loudspeakers or mounting configurations.

The most important of these contributions is the temperature dependency of the electric resistance $\mathbf{R_e}(T_v)$.

In normal working conditions the loudspeaker is subject to temperatures up to 100°, due to the Joule heating of the voice coil. The rise in temperature of the voice

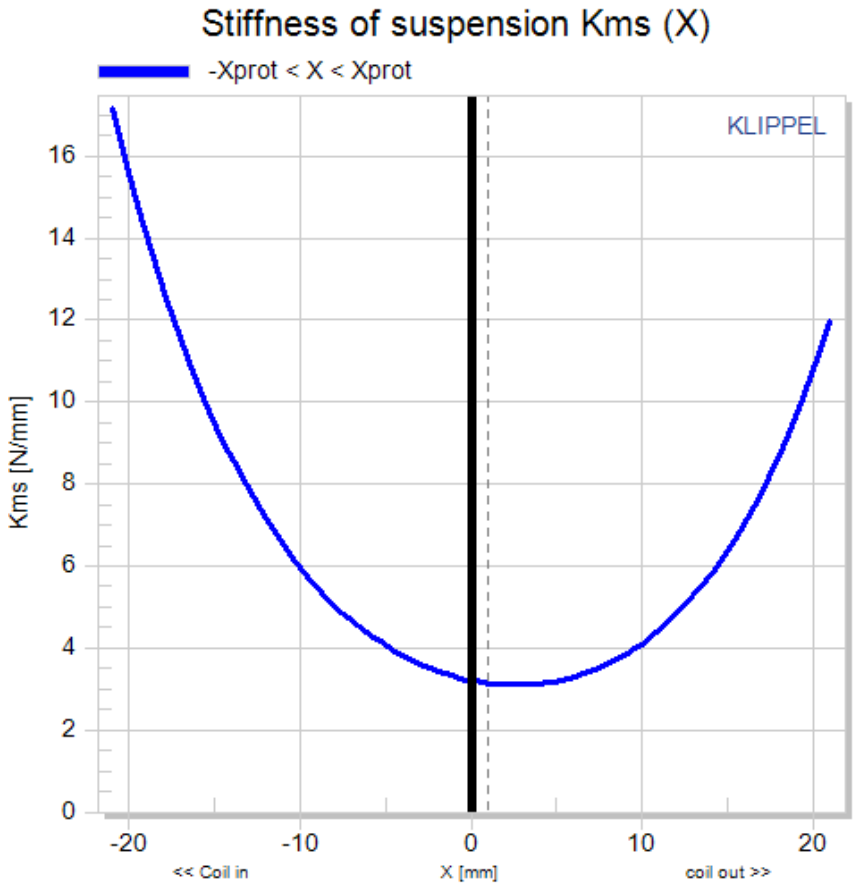

Figure 3.18: Mechanical stiffness displacement dependency.

coil causes the increase of the wire electrical resistance (which can even double its value) and consequently the reduction of the current flow.

The net effect of the higher temperature of the voice coil is a reduction of the loudspeaker output pressure, known as "thermal compression".

Unfortunately, the temperature is not included in the system state vector and it is difficult to accurately estimate it without a dedicated sensor. However, a thermal model of the loudspeaker has been proposed by Klippel [Kli04] that can be exploited for future extensions.

For the purpose of this thesis, the electric resistance $\mathbf{R_e}$ in the nonlinear characterization will be considered constant with value equal to the maximum recorded in the measurements (worst case scenario).

Other known effects that can be modeled are the dependence of the mechanical resistance $\mathbf{R_{ms}}(v)$ on the velocity, and that of the radiator surface $\mathbf{S_d}(f)$ on the frequency [Kli05].

For the purpose of this thesis, these effects are not considered.

3.2.3 SS representation of the nonlinear model

The development of a nonlinear SS model that includes the described nonlinearities is straightforward, since the Klippel model is based on the linear model that has already been discussed and represented in SS form.

The fundamental difference lies in the nonlinearity of some of the model parameters.

The proposed SS model includes the main nonlinear contributions previously presented: the electric inductance nonlinearity, the force factor nonlinearity and the mechanical stiffness nonlinearity.

The equations that describe the Klippel model are the following:

$$\begin{cases} V_{in}(t) - V_{emf}(x,t) = R_e i(t) + \dfrac{\partial L_e(x,i) i(t)}{\partial t} + R_2(x,i) i(t) - R_2(x,i) i_2(t) \\ 0 = R_2(x,i) i_2(t) + \dfrac{\partial L_2(x,i) i_2(t)}{\partial t} - R_2(x,i) i(t) \\ F(x,t) = M_{ms} \dfrac{\partial^2 x(t)}{\partial t^2} + R_{ms} \dfrac{\partial x(t)}{\partial t} + K_{ms}(x) x(t) \\ F(x,t) = Bl(x)\ i(t) \\ V_{emf}(x,t) = Bl(x)\ \dfrac{\partial x(t)}{\partial t} \end{cases} \tag{3.34}$$

The derivative over time of the inductances can be developed as follows:

$$\frac{\partial L_e(x,i) i(t)}{\partial t} = L_e(x,i) \frac{\partial i(t)}{\partial t} + i(t) \frac{\partial L_e(x,i)}{\partial t} \tag{3.35}$$

Following the steps shown for the development of the linear model in section 3.1.7, the following set of equations is obtained:

$$\begin{cases} \dfrac{\partial i(t)}{\partial t} = \dfrac{-\left[R_e + R_2(x,i) + \dfrac{\partial L_e(x,i)}{\partial t}\right] i(t) + R_2(x,i) i_2(t) - Bl(x)\ v(t)}{L_e(x,i)} + \dfrac{V_{in}(t)}{L_e(x,i)} \\ \dfrac{\partial i_2(t)}{\partial t} = \dfrac{R_2(x,i) i(t) - \left[R_2(x,i) + \dfrac{\partial L_2(x,i)}{\partial t}\right] i_2(t)}{L_2(x,i)} \\ \dfrac{\partial x(t)}{\partial t} = v(t) \\ \dfrac{\partial v(t)}{\partial t} = \dfrac{Bl(x)\ i(t) - K_{ms}(x) x(t) - R_{ms} v(t)}{M_{ms}} \end{cases} \tag{3.36}$$

Let the state vector $\mathbf{x}$(t), the input u(t) and the output y(t) be respectively defined as:

$$\mathbf{x} = \begin{bmatrix} i(t) & i_2(t) & x(t) & v(t) \end{bmatrix}^T \tag{3.37}$$

$$u(t) = V_{in}(t) \qquad y(t) = a(t) = \frac{\partial v(t)}{\partial t} = \frac{\partial^2 x(t)}{\partial t^2} \tag{3.38}$$

Then 3.36 can be represented in pseudo SS form:

$$\hat{\mathbf{A}}(\mathbf{x}) = \begin{bmatrix} -\dfrac{R_e + R_2(x,i) + \dfrac{\partial L_e(x,i)}{\partial t}}{L_e(x,i)} & \dfrac{R_2(x,i)}{L_e(x,i)} & 0 & -\dfrac{Bl(x)}{L_e(x,i)} \\ \dfrac{R_2(x,i)}{L_2(x,i)} & -\dfrac{R_2(x,i) + \dfrac{\partial L_2(x,i)}{\partial t}}{L_2(x,i)} & 0 & 0 \\ 0 & 0 & 0 & 1 \\ \dfrac{Bl(x)}{M_{ms}} & 0 & -\dfrac{K_{ms}(x)}{M_{ms}} & -\dfrac{R_{ms}}{M_{ms}} \end{bmatrix}$$

$$\hat{\mathbf{B}}(\mathbf{x}) = \begin{bmatrix} \dfrac{1}{L_e(x,i)} \\ 0 \\ 0 \\ 0 \end{bmatrix}$$

$$\hat{\mathbf{C}}(\mathbf{x}) = \begin{bmatrix} \dfrac{Bl(x)}{M_{ms}} & 0 & -\dfrac{K_{ms}(x)}{M_{ms}} & -\dfrac{R_{ms}}{M_{ms}} \end{bmatrix}$$

$$\hat{\mathbf{D}}(\mathbf{x}) = \begin{bmatrix} 0 \end{bmatrix} \tag{3.39}$$

The loudspeaker is indeed a physical system that exhibits an underlying linear behavior, as described in 3.1, that, in the large signals condition, is corrupted by the described nonlinearities. Thus, it can be expressed in the SS form described in 2.10 by the following matrices:

$$\mathbf{A} = \begin{bmatrix} -\frac{R_e + {R_2}^0}{{L_e}^0} & \frac{{R_2}^0}{{L_e}^0} & 0 & -\frac{Bl^0}{{L_e}^0} \\ \frac{{R_2}^0}{{L_2}^0} & -\frac{{R_2}^0}{{L_2}^0} & 0 & 0 \\ 0 & 0 & 0 & 1 \\ \frac{Bl^0}{M_{ms}} & 0 & -\frac{{K_{ms}}^0}{M_{ms}} & -\frac{R_{ms}}{M_{ms}} \end{bmatrix} \qquad \mathbf{B} = \begin{bmatrix} \frac{1}{{L_e}^0} \\ 0 \\ 0 \\ 0 \end{bmatrix}$$

$$\mathbf{C} = \begin{bmatrix} \frac{Bl^0}{M_{ms}} & 0 & -\frac{{K_{ms}}^0}{M_{ms}} & -\frac{R_{ms}}{M_{ms}} \end{bmatrix} \qquad \mathbf{D} = \begin{bmatrix} 0 \end{bmatrix}$$

$$\mathbf{a}(\mathbf{x}) = \begin{bmatrix} \frac{R_e[\xi(x) + \iota(i)] - \frac{\partial L_e(x,i)}{\partial t}}{{L_e}^0[1 + \xi(x) + \iota(i)]} & 0 & 0 & \frac{Bl^0[1 + \xi(x) + \iota(i) - \beta(x)]}{{L_e}^0[1 + \xi(x) + \iota(i)]} \\ 0 & -\frac{\frac{\partial L_2(x,i)}{\partial t}}{{L_2}^0[1 + \xi(x) + \iota(i)]} & 0 & 0 \\ 0 & 0 & 0 & 0 \\ \frac{Bl^0[\beta(x) - 1]}{M_{ms}} & 0 & -\frac{{K_{ms}}^0(\kappa(x) - 1)}{M_{ms}} & 0 \end{bmatrix}$$

$$\mathbf{b}(\mathbf{x}) = \begin{bmatrix} -\frac{\xi(t) + \iota(i)}{{L_e}^0[1 + \xi(x) + \iota(i)]} \\ 0 \\ 0 \\ 0 \end{bmatrix} \qquad \mathbf{c}(\mathbf{x}) = \begin{bmatrix} \frac{Bl^0[\beta(x) - 1]}{M_{ms}} & 0 & -\frac{{K_{ms}}^0(\kappa(x) - 1)}{M_{ms}} & 0 \end{bmatrix} \qquad \mathbf{d}(\mathbf{x}) = [0] \tag{3.40}$$

where:

$$\begin{aligned}\frac{\partial L_e(x,i)}{\partial t} &= \frac{\partial}{\partial t}\left[{L_e}^0(1+\xi(x)+\iota(i)\right] = {L_e}^0\left[\frac{\partial \xi(x)}{\partial t}+\frac{\partial \iota(i)}{\partial t}\right] = \\ &= {L_e}^0\left[\frac{\partial x(t)}{\partial t}\frac{\partial \xi(x)}{\partial x}+\frac{\partial i(t)}{\partial t}\frac{\partial \iota(i)}{\partial i}\right] = \\ &= {L_e}^0\left[v(x)\nabla\xi(x)+\frac{\partial i(t)}{\partial t}\nabla\iota(i)\right] \end{aligned} \tag{3.41}$$

and similarly:

$$\frac{\partial L_2(x,i)}{\partial t} = {L_2}^0\left[v(x)\nabla\xi(x)+\frac{\partial i(t)}{\partial t}\nabla\iota(i)\right] \tag{3.42}$$

Chapter 4

Velocity sensor model

The implementation of a feedback SS control system, as shown in chapter 2, requires the acquisition of at least one of the plant physical variables from which the entire system is observable to estimate the full state vector and generate the control output.

Therefore, a sensor must be introduced in the plant to convert one of the plant physical variables into an electrical signal, suitable to be processed by the controller.

Different kinds of sensors can be employed to measure the many physical variables that characterize the loudspeaker.

Common sensors used for loudspeaker measurement are microphones (to measure the generated pressure), the laser Doppler velocimeter and the laser displacement sensor (to measure the diaphragm velocity or displacement). The use of those sensors in a control system is definitely impractical in real working conditions due to space and cost constraints.

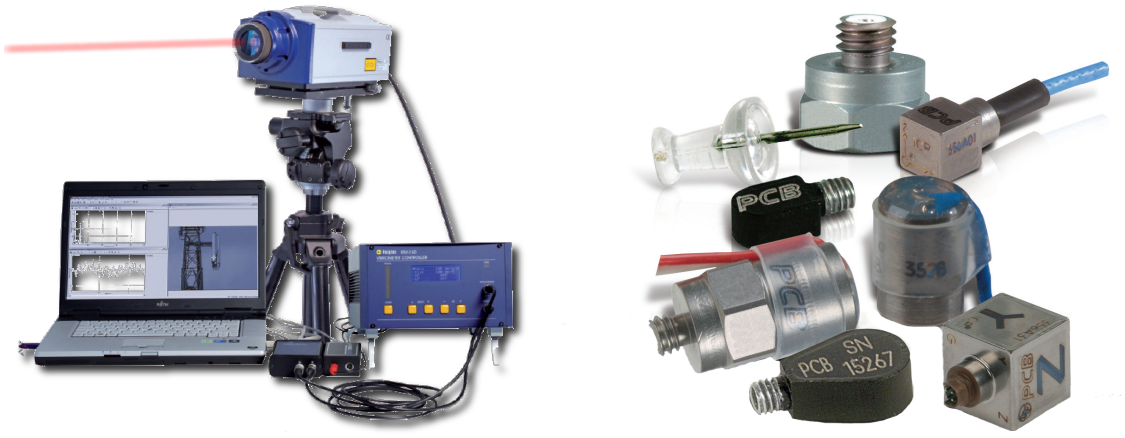

(a) **(b)**

Figure 4.1: a) Laser Doppler velocimeter; b) Collection of miniature accelerometers.

Cheaper, smaller sensors, suitable for control purposes, are accelerometers, magnetic velocimeters and current sensors. The main drawback of these sensors is that they change, up to some extent, the behavior of the loudspeaker, adding mass to the diaphragm (accelerometer,velocimeter) or increasing the input electric impedance of the loudspeaker (current sensor).

In this thesis a magnetic velocimeter is exploited to measure the loudspeaker velocity, mitigating the negative effects of the sensor embedding it in the loudspeaker structure.

The magnetic velocimeter is composed by two main parts, a conductive coil and a permanent magnet, and measures their relative velocity generating a counter motional electromotive force as explained in section 1.2.1. In order to measure the absolute velocity of a body, one of the two components, either the coil or the magnet, must be rigidly attached to the moving body, while the other must be kept at a fixed point in space.

A typical magnetic velocimeter is not particularly suitable to be used on a loudspeaker, since a non negligible mass is added to the moving body and the required magnet would interfere with the permanent magnet.

A solution is to embed the sensor components in the loudspeaker structure during its design: the sensor magnet can be completely replaced by the loudspeaker permanent magnet, while the sensor coil can be wound over the voice coil to maximize its sensitivity (equivalent to the linear motor force factor) and be designed arbitrarily small to minimize the added mass. This ideally provides a cheap and non intrusive access to the velocity information of the loudspeaker mechanical system.

This approach has already been proposed [CCCP81] and proved effective. However, the cited article does not define a correct electrical model for the sensor, characterizing it by means of a fitted transfer function instead of using the measured electrical parameters.

For the purpose of this thesis, a SS model of the described velocity sensor is required. In the rest of the chapter the SS sensor model is developed for both the small signals and the large signals condition.

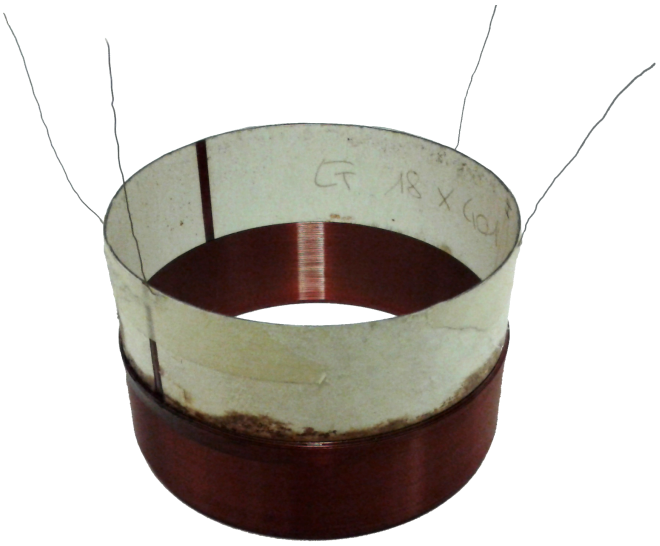

Figure 4.2: Voice coil with secondary coil used as sensor wound over.

4.1 Physical principles

The embedded magnetic velocimeter is as a secondary moving coil, wound over the voice coil and rigidly attached to it, immersed in the magnetic field generated by the permanent magnet and surrounded by the iron of the magnetic circuit.

Due to the peculiar configuration, there are three main contributions to the sensor output voltage: the counter motional electromotive force of the sensor coil, the inductive coupling between the sensor coil and the voice coil, and the inductive coupling between the sensor coil and the magnetic circuit equivalent coil.

Motional electromotive force

The underlying physical principle of this contribution has already been described in section 1.2.1. In short, the motion of the sensor coil in a stationary magnetic field generated by the permanent magnet induces a counter motional electromotive force across the coil itself.

$$\mathcal{E}_s^{motion}(t) = Bl_s v(t) \tag{4.1}$$

This is the working principle of the common magnetic velocimeter, where the induced output voltage is directly proportional to the moving body velocity. The sensor coil force factor $\mathbf{Bl_s}$ is equivalent to the velocimeter sensitivity.

Voice coil coupling

Since the sensor coil is wound directly over the voice coil, the two are perfectly coupled. This implies that the two coils share the same magnetic flux and flux variation.

$$\Phi_{voice}(t) = \Phi_{sensor}(t) \qquad \frac{\partial \Phi_{voice}(t)}{\partial t} = \frac{\partial \Phi_{sensor}(t)}{\partial t} \tag{4.2}$$

Therefore, due to Faraday's law of induction 3.4, the current flow variation in one coil causes the induction of an electromotive force in the other coil, opposing to the variation of the shared magnetic flux.

The current variation on one coil and the induced electromotive force on the other are related by means of the coils mutual inductance $\mathbf{M}$. For perfectly coupled coils, the mutual inductance is directly related to the self inductances of the single coils:

$$M = \sqrt{L_{voice} L_{sensor}} \tag{4.3}$$

The electromotive force generated by the voice coil on the sensor coil due to the coils mutual inductance is:

$$\mathcal{E}_{sensor}^{mutual}(t) = M\frac{\partial i_{voice}(t)}{\partial t} = M\frac{\partial i(t)}{\partial t} \tag{4.4}$$

Similarly, if traversed by a time varying current, the sensor coil produces an electromotive force across the voice coil.

This is an unwanted effect and must be avoided. Thus, to be effectively used as a velocity sensor, the sensor coil must be connected to a high impedance load, such as a preamplifier, to ensure no current flow.

Magnetic circuit equivalent coil coupling

As explained in section 3.1.1, the magnetic circuit can be considered equivalent to a large, single coil made of iron, wound around the voice coil. Since the voice coil and the magnetic circuit equivalent coil are almost perfectly coupled, the current variation on the voice coil induces eddy currents in the iron of the magnetic circuit, that, in turn, influence the voice coil inductance value. This has been approximated through the LR-2 model, introducing a corrective term for the voice coil inductance value (see eqs. (3.5) to (3.7)).

The corrective term, usually considered as a frequency dependent inductive contribution, can also be considered as an induced electromotive force on the voice coil due to the eddy currents.

$$\mathcal{E}_{voice}^{eddy}(t) = [R_2 i(t) - R_2 i_2(t)] \tag{4.5}$$

Since the sensor coil is wound directly over the voice coil, it is almost perfectly coupled with the magnetic circuit equivalent coil as well as the voice coil. This implies that the sensor coil is affected by (and may affect) the eddy currents.

More specifically, if traversed by a time varying current, the sensor coil produces an electromotive force in the iron, generating new eddy currents. This is an unwanted effect and must be avoided. Again, the sensor coil must be connected to a high impedance load, such as a preamplifier, to ensure no current flow.

The effects of the eddy currents on the sensor coil can be approximated, exploiting the perfect coupling between the sensor coil and the voice coil and approximating the effects of the eddy currents on the sensor coil with the same LR-2 model used for the voice coil correction.

Recalling that two perfectly coupled coils share the same magnetic flux:

$$\Phi_{voice}(t) = \Phi_{sensor}(t) \tag{4.6}$$

Faraday's law of induction for solenoids:

$$\mathcal{E}(t) = -N \frac{\partial \Phi_B(t)}{\partial t} \tag{4.7}$$

and considering the sole contribution of the eddy currents to the shared magnetic flux, the electromotive force generated by the eddy currents on the sensor coil can be related to the electromotive force generated by the same eddy currents on the voice coil

$$\frac{\partial \Phi^{eddy}(t)}{\partial t} = -\frac{\mathcal{E}^{eddy}_{voice}(t)}{N_{voice}} = -\frac{\mathcal{E}^{eddy}_{sensor}(t)}{N_{sensor}} \tag{4.8}$$

$$\begin{aligned} \mathcal{E}^{eddy}_{sensor}(t) &= \frac{N_{sensor}}{N_{voice}} \mathcal{E}^{eddy}_{voice}(t) \\ &= T_r \left[R_2 i(t) - R_2 i_2(t)\right] \end{aligned} \tag{4.9}$$

where $\mathbf{T_r}$ is the turns ratio of the two coils.

For perfectly coupled coils the turns ratio is directly related to the self inductances of the single coils and consequently to their mutual inductance

$$T_r = \frac{N_{sensor}}{N_{voice}} = \sqrt{\frac{L_{sensor}}{L_{voice}}} = \frac{M}{L_{voice}} = \frac{M}{L_e} \tag{4.10}$$

4.2 Small signals condition: the linear model

Considering the small signal condition described in chapter 3, all the parameters of both the loudspeaker and the sensor can be considered linear and time invariant.

The sensor coil, similarly to the voice coil, is a solenoid of conducting wire characterized by the series of an electrical resistance $\mathbf{R_s}$, an electrical inductance $\mathbf{L_s}$ and three electromotive force generators that account for the electromotive contributions previously presented.

If the sensor coil is connected to a high impedance load, as previously described, then the three electromotive contributions are exactly those described in eqs. (4.1), (4.4) and (4.9).

The high impedance load ensures zero current flow in the sensor coil and zero voltage drop across $\mathbf{R_s}$ and $\mathbf{L_s}$. Thus, the output voltage of the proposed sensor is determined by the sum of the three electromotive contributions:

$$\begin{aligned} V_{sensor}(t) &= \mathcal{E}^{motion}_{sensor}(t) + \mathcal{E}^{mutual}_{sensor}(t) + \mathcal{E}^{eddy}_{sensor}(t) \\ &= Bl_s v(t) + M\frac{\partial i(t)}{\partial t} + T_r\left[R_2 i(t) - R_2 i_2(t)\right] \end{aligned} \tag{4.11}$$

The voice coil current derivative can be expanded exploiting eq. (3.21):

$$\begin{aligned} V_{sensor}(t) = Bl_s v(t) + \frac{M}{L_e}\left[-R_e i(t) - R_2 i(t) + R_2 i_2(t) - Blv(t) + V_{in}(t)\right] \\ + T_r\left[R_2 i(t) - R_2 i_2(t)\right] \end{aligned} \tag{4.12}$$

The mutual inductance $\mathbf{M}$ is related to the turns ratio $\mathbf{T_r}$ as expressed in eq. (4.10), so the voltage across the sensor coil is simplified as follows:

$$V_{sensor}(t) = -T_r R_e i(t) + [Bl_s - T_r Bl]v(t) + T_r V_{in}(t) \tag{4.13}$$

It is interesting to notice that even if the sensor has initially been designed to be a velocity sensor, the generated output voltage exhibits stronger dependencies on the voice coil current and input voltage. In particular, in a perfectly built, ideal sensor the velocity contribution becomes zero. In fact:

$$Bl_s = B\, l_{sensor} = B\, N^{turns}_{sensor}\, 2\pi r = T_r B\, N^{turns}_{voice}\, 2\pi r = B\, l_{voice} = T_r Bl \tag{4.14}$$

However, thanks to the slight differences between the two coils due to the intrinsic approximations of the manufacturing process, the sensor output voltage detect also a small velocity contribution.

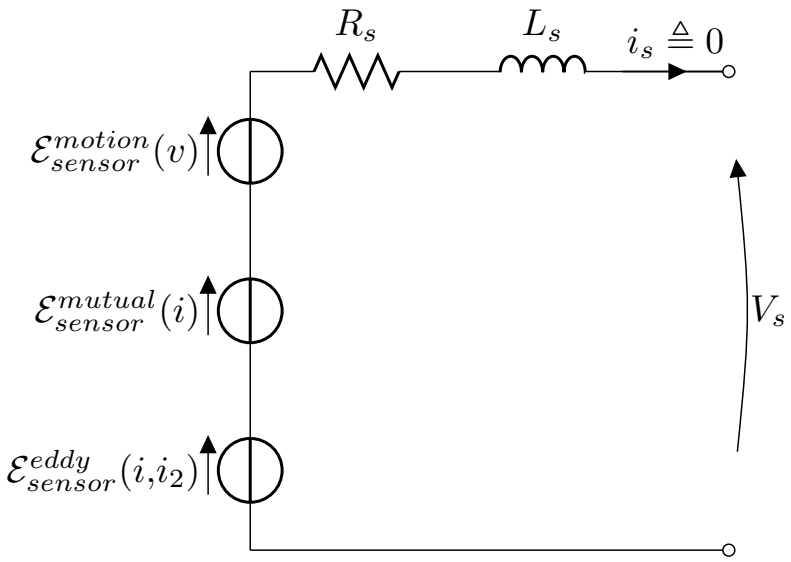

Figure 4.3: Electric circuit of the proposed sensor in the small signals condition, assuming high impedance load.

4.2.1 SS representation of the linear sensor

The output voltage of the sensor coil expressed in eq. (4.13) can be considered a second output of the linear SS model described in eq. (3.24), characterized by the following matrices:

$$\mathbf{C}_{sensor} = \begin{bmatrix} -T_r R_e & 0 & 0 & (Bl_s - T_r Bl) \end{bmatrix} \qquad \mathbf{D}_{sensor} = \begin{bmatrix} T_r \end{bmatrix} \tag{4.15}$$

4.3 Large signals condition: the nonlinear model

Considering the large signals condition described in chapter 3, all the parameters of both the loudspeaker and the sensor can be considered nonlinear and time invariant.

The nonlinear behavior of the sensor coil in the large signals condition is modeled extending the linear model proposed in section 4.2, introducing nonlinear contributions similar to those introduced by the Klippel model. The sensor coil is indeed a conductive coil moving inside the loudspeaker magnetic gap and is in principle identical to the voice coil. Thus, the sensor coil is subjected to all the nonlinearities that afflict the voice coil, described in section 3.2.2.

The displacement dependency of the sensor coil force factor is modeled by means of a nonlinear curve, similarly to the voice coil force factor:

$$Bl_s(x) = {Bl_s}^0 \, \beta_s(x) \tag{4.16}$$

where $\mathbf{Bl_s}^0$ is the value of $\mathbf{Bl_s}(0)$.

The turns ratio and the mutual inductance of the two coils exhibit dependencies on both the displacement and the current, related to the nonlinear dependencies of their electrical inductances:

$$T_r(x,i) = \sqrt{\frac{L_s(x,i)}{L_e(x)}} = \sqrt{\frac{{L_s}^0[1+\xi(x)+\iota(i)]}{{L_e}^0[1+\xi_s(x)+\iota_s(i_s)]}} = {T_r}^0 \sqrt{\frac{1+\xi_s(x)+\iota_s(i_s)}{1+\xi(x)+\iota(i)}} \tag{4.17}$$

$$M(x,i) = \sqrt{L_e(x,i)L_s(x)} = M^0 \sqrt{[1+\xi(x)+\iota(i)][1+\xi_s(x)+\iota_s(i_s)]} \tag{4.18}$$

where $\mathbf{L_s}^0$ is the value of $\mathbf{L_s}(0)$, $\mathbf{T_r}^0$ is the value of $\mathbf{T_r}(0,0)$ and $\mathbf{M}^0$ is the value of $\mathbf{M}(0,0)$.

The three electromotive contributions are also affected by the nonlinear behavior of the system, and are derived from eqs. (4.1), (4.4) and (4.9) introducing the appropriate nonlinear behavior in the parameters.

It is important to remark that eqs. (4.1), (4.4) and (4.9) are valid only if the sensor coil is connected to a high impedance load, and the same applies to their nonlinear extension. In this condition the sensor coil current flow and the current dependency of the nonlinearities are negligible.

The nonlinear equations that describe the three electromotive forces generated by the sensor coil in the large signals condition are the following:

$$\begin{cases} \mathcal{E}_{sensor}^{motion}(x,t) = Bl_s(x)v(t) \\ \mathcal{E}_{sensor}^{mutual}(x,i,t) = \dfrac{\partial M(x,i)i(t)}{\partial t} = M(x,i)\dfrac{\partial i(t)}{\partial t} + i(t)\dfrac{\partial M(x,i)}{\partial t} \\ \mathcal{E}_{sensor}^{eddy}(x,i,t) = T_r(i,x)\,[R_2(i,x)i(t) - R_2(i,x)i_2(t)] \\ M(x,i) = \sqrt{L_e(x,i)L_s(x)} = M^0\sqrt{[1+\xi(x)+\iota(i)][1+\xi_s(x)]} = M^0\mu(x,i) \\ T_r(x,i) = \sqrt{\dfrac{L_s(x,i)}{L_e(x)}} = {T_r}^0\sqrt{\dfrac{1+\xi_s(x)}{1+\xi(x)+\iota(i)}} = {T_r}^0\tau(x,i) \end{cases} \tag{4.19}$$

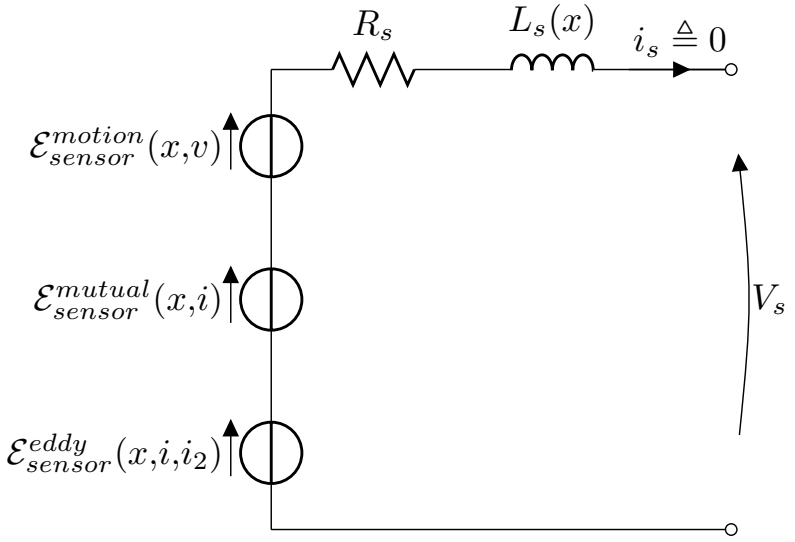

Figure 4.4: Electric circuit of the proposed sensor in the large signals condition, assuming high impedance load.

The high impedance load ensures zero current flow in the sensor coil and zero voltage drop across $\mathbf{R_s}$ and $\mathbf{L_s}(x)$. Thus, the output voltage of the nonlinear proposed sensor is determined by the sum of the three electromotive contributions of eq. (4.19):

$$\begin{aligned} V_{sensor}(t) &= \mathcal{E}^{motion}_{sensor}(x,t) + \mathcal{E}^{mutual}_{sensor}(x,i,t) + \mathcal{E}^{eddy}_{sensor}(x,i,t) \\ &= Bl_s(x)v(t) + M(x,i)\frac{\partial i(t)}{\partial t} + i(t)\frac{\partial M(x,i)}{\partial t} + T_r(x,i)\,[R_2(x,i)i(t) - R_2(x,i)i_2(t)] \end{aligned} \tag{4.20}$$

The voice coil current derivative can be expanded exploiting eq. (3.36)

$$\begin{aligned} V_{sensor}(t) = Bl_s(x)v(t) + i(t)\frac{\partial M(x,i)}{\partial t} + T_r(x,i)\,[R_2(x,i)i(t) - R_2(x,i)i_2(t)] + \\ + \frac{M(x,i)}{L_e(x,i)}\left[-R_e i(t) - R_2(x,i)i(t) - i(t)\frac{\partial L_e(x,i)}{\partial t} + R_2(x,i)i_2(t) - Bl(x)v(t) + V_{in}(t)\right] \end{aligned} \tag{4.21}$$

The mutual inductance $\mathbf{M}(x,i)$ is related to the turns ratio $\mathbf{T_r}(x,i)$ as expressed in eq. (4.19), so that the voltage across the sensor coil is simplified as follows:

$$\begin{aligned} V_{sensor}(t) = &\left[-T_r(x,i)R_e + \frac{\partial M(x,i)}{\partial t} - T_r(x,i)\frac{\partial L_e(x,i)}{\partial t}\right]\, i(t) + \\ &+ \left[Bl_s(x) - T_r(x,i)Bl(x)\right]\, v(t) + \\ &+ T_r(x,i)\, V_{in}(t) \end{aligned} \tag{4.22}$$

4.3.1 SS representation of the nonlinear sensor

The output voltage of the sensor coil expressed in eq. (4.22) can be considered a second output of the nonlinear SS model described in eq. (3.39), characterized by the following matrices:

$$\hat{\mathbf{C}}_{\mathbf{sensor}}(\mathbf{x}) = \left[\left[-T_r(x,i)R_e + \frac{\partial M(x,i)}{\partial t} - T_r(x,i)\frac{\partial L_e(x,i)}{\partial t}\right] \quad 0 \quad 0 \quad [Bl_s(x) - T_r(x,i)Bl(x)]\right]$$

$$\hat{\mathbf{D}}_{\mathbf{sensor}}(\mathbf{x}) = \left[T_r(x,i)\right] \tag{4.23}$$

or, equivalently, as a second output of the nonlinear SS model described in 3.40 by the following matrices:

$$\mathbf{C}_{\mathbf{sensor}} = \left[-{T_r}^0 R_e \quad 0 \quad 0 \quad ({Bl_s}^0 - {T_r}^0 Bl^0)\right]$$

$$\mathbf{D}_{\mathbf{sensor}} = \left[{T_r}^0\right]$$

$$\mathbf{c}_{\mathbf{sensor}}(\mathbf{x}) = \begin{bmatrix} -{T_r}^0 R_e[\tau(x,i) - 1] + \dfrac{\partial M(x,i)}{\partial t} - {T_r}^0 \tau(x,i)\dfrac{\partial L_e(x,i)}{\partial t} \\ 0 \\ 0 \\ {Bl_s}^0[\beta_s(x) - 1] - {T_r}^0 Bl^0[\tau(x,i)\beta(x) - 1] \end{bmatrix}^T \tag{4.24}$$

$$\mathbf{d}_{\mathbf{sensor}}(\mathbf{x}) = \left[{T_r}^0(\tau(x,i) - 1)\right]$$

The time derivative of $\mathbf{L_e}(x,i)$ can be expressed as 3.41. Conversely, the time derivative of $\mathbf{M}(x,i)$ cannot be easily related to other known quantities.

A blunt approximation is to neglect the current dependency from the voice coil ($\iota(i) = 0$) and consider the displacement dependencies of the two coils identical ($\xi(x) = \xi_s(x)$). With those assumptions one has that:

$$M(x,i) \approx M^0[1 + \xi(x)] \qquad \frac{\partial M(x,i)}{\partial t} \approx M^0 v(t) \nabla \xi(x) \tag{4.25}$$

Chapter 5

Measurement of the loudspeaker parameters

The measurement of the loudspeaker physical parameters for analysis purposes is an historical problem. For the first half of the 20^{th} century it was considered impossible to characterize a loudspeaker without dismantling it and measuring the characteristics of all its parts separately.

In the '70s Thiele and Small proposed a simple model for the analysis of the loudspeaker behavior in different acoustic configurations, providing also a noninvasive methodology for the extraction of the model parameters, the so called "Thiele-Small parameters", mainly through the measurement of the loudspeaker impedance frequency response.

This was possible because the proposed model was an extreme simplification of the loudspeaker system, being valid only at low frequency, in the small signals condition. However, the Thiele-Small model and the Thiele-Small parameters remained for years the standard tool for the loudspeakers and audio systems characterization, enabling huge advancements in the audio field.

Lately, the introduction of the Klippel nonlinear model allowed to characterize also the behavior of the loudspeakers in the large signals condition and at relatively high frequencies. Klippel also proposed a noninvasive methodology for the extraction of the parameters required for its model, based on model identification and parameter fitting.

The measurement (or better, the estimation) of the Klippel parameters is indeed much more complex with respect to the procedure proposed by Thiele and Small. Nowadays, the Klippel parameters can be easily measured using the Klippel Distortion Analyzer, a complex measurement instrument that implements and automates the Klippel methodology.

For the purpose of this thesis, the loudspeaker parameters have been measured using a Klippel Distortion Analyzer, property of RCF.

5.1 The Klippel Distortion Analyzer

The Distortion Analyzed is an hardware platform that performs the generation, acquisition and digital signal processing required for the analysis of the loudspeaker behavior and the estimation of its characteristic parameters in both small signals (linear) and large signals (nonlinear) conditions.

In the typical configuration, the loudspeaker is fixed on a rigid structure in free air and connected with special cables to the amplified output of the Distortion Analyzer. Other configurations are used to analyze loudspeakers in closed or vented enclosures.

The Distortion Analyzer is capable of measuring three physical variables of the loudspeaker: the voice coil current, the diaphragm displacement and the generated pressure.

The voice coil current is measured without any further connection: the special cables used to connect the Distortion Analyzer to the loudspeaker enable the simultaneous voltage driving of the voice coil and its current sensing. The displacement is measured using a laser triangulation sensor, tailored to measure displacements of $\pm 50mm$ with resolution of $0.2mm$ at $1000Hz$. The pressure is measured using a special purpose measurement microphone with flat frequency response in the audio band.

The Distortion Analyzer is connected to a PC running the software dB-Lab, which serves as a user interface to the instrument.

Through dB-Lab the user can extract information and perform different characterizations of the analyzed loudspeaker, access the extracted data and manage the data extracted from different loudspeaker samples for comparison.

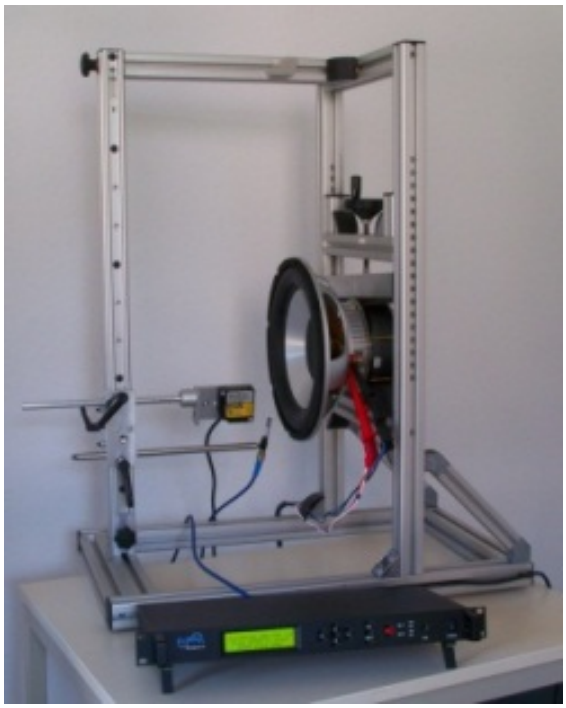

Figure 5.1: Full setup of the Distortion Analyzer in the free air mount configuration.

The user is only required to provide a small set of parameters about the analyzed loudspeaker, that are crucial for a correct and safe measurement but inaccessible to the Distortion Analyzer, such as the analyzed loudspeaker typology, its surface area, its nominal impedance, is design maximum electrical power and the voice coil material.

On the basis of this information, the dB-Lab exploits the measurements retrieved from the Distortion Analyzer to extract the required data.

The loudspeaker analysis performed by the dB-Lab is based on a grey-box system identification procedure: instead of directly measuring the required information, dB-Lab employs a suitable loudspeaker model, linear or nonlinear depending on the specific analysis, and fits its parameters upon the sensed behavior of the analyzed loudspeaker.

To do so, the Distortion Analyzer applies an input voltage signal to the loudspeaker, optimized for the specific analysis, and measures the produced displacement, pressure and current. The parameters of the dB-Lab model are periodically updated to minimize the RMS error between the model behavior and the analyzed loudspeaker sensed behavior, fitting the acquired measurements.

For the purpose of this thesis the Distortion Analyzer has been used to perform two specific loudspeaker analysis: the Linear Parameter Measurement (LPM) and the Large Signal Identification (LSI).

5.1.1 Linear Parameter Measurement (LPM)

The Linear Parameter Measurement is the specific measurement procedure through which is possible to determine the electrical and the mechanical parameters of a loudspeaker in the small signal condition.

The fundamental parameters that are extracted are the ones that characterize the linear model described in section 3.1.

R_e	Electrical resistance of the voice coil at DC
L_e	Frequency independent part of the electrical inductance of the voice coil
R_2	Electrical resistance of the LR-2 model
L_2	Electrical inductance of the LR-2 model
Bl	Loudspeaker force factor
M_{ms}	Mechanical mass of the equivalent mechanical system including the air load
R_{ms}	Mechanical damping of the equivalent mechanical system including the air load
K_{ms}	Mechanical stiffness of the equivalent mechanical system including the air load
f_s	Resonance frequency of the equivalent mechanical system including the air load

These data are used to derive other important factors for the loudspeaker evaluation and design, such as the efficiency, the sensitivity and the electrical, mechanical and total Q-factors.

In the typical (and suggested) measurement configuration, the parameters are estimated fitting the loudspeaker electrical impedance frequency response, obtained measuring the voice coil current, and the loudspeaker displacement frequency response, obtained measuring the diaphragm displacement with the laser sensor.

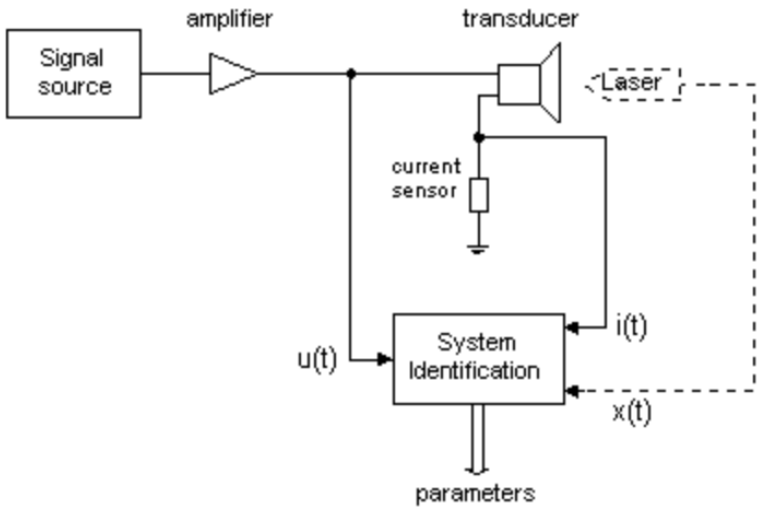

Figure 5.2: LPM typical configuration: current and displacement sensing.

Other measurement configurations can be employed, choosing to use the sole current measurement and/or to add the microphone measurement.

The dB-Lab software also allows the customization of the measurement procedure, acting on the stimulus amplitude, the fitting resolution, the considered bandwidth and other factors.

5.1.2 Large Signal Identification (LSI)

The Large Signal Identification is the specific measurement procedure through which is possible to characterize the loudspeaker behavior in the large signal condition, estimating the parameter of the Klippel model that match the analyzed device.

The extracted information include the displacement and current dependency curves of the nonlinear parameters, the values of the nonlinear parameters at rest ($x = 0$, $i = 0$), the evolution in time of the physical quantities (voltage, current, displacement,etc) and the behaviors of the device time-varying parameters (electric resistance, stiffness rest value, resonant frequency, etc). All the data is available in real time during the measurement process for monitoring purposes and stored as time series for later analysis.

This information is used to evaluate the global behavior of the analyzed device and possibly determine its weakest part to enable further design improvements.

In the typical measurement configuration, the loudspeaker model parameters and the nonlinear dependency curves are estimated in real time accessing to the measurements of the voice coil current and voltage, exploiting the counter motional electromotive force to extract information about the mechanical domain.

In practice, the voice coil act both as an electric and a mechanical transducer. However, the laser displacement measurement can be added to the setup to enhance the accuracy of the results. This last configuration has been used in the performed measurements.

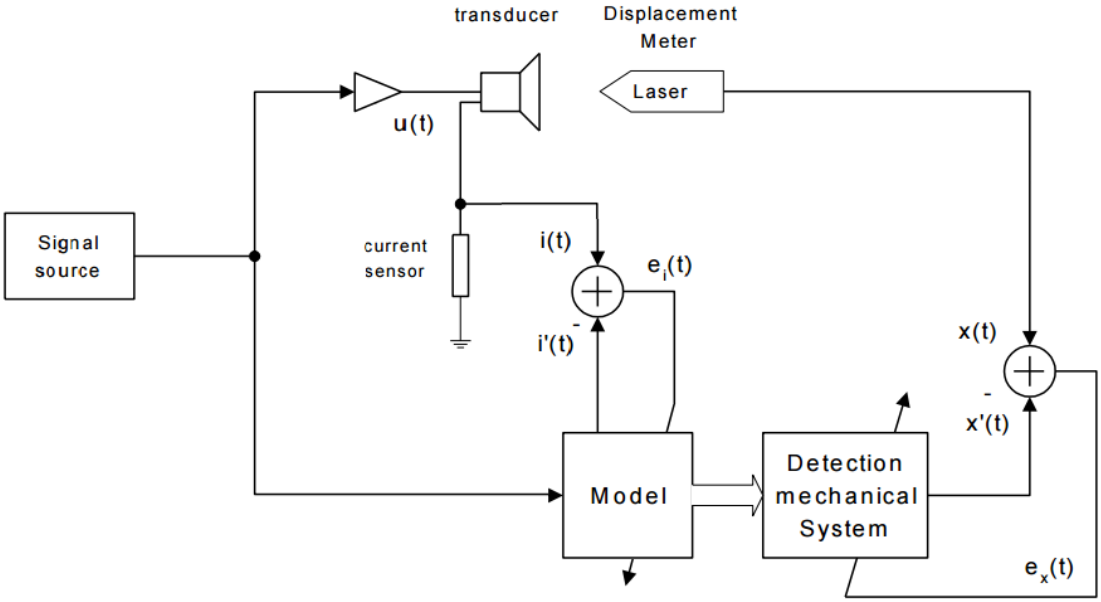

Figure 5.3: LSI full configuration: current and displacement sensing.

The measurement procedure includes a nonlinear system identification process based on adaptive inverse control. The analyzed loudspeaker is excited with a large amplitude, noise-like signal, especially designed to enable a complete and effective identification of the device dynamics. The characterization of the loudspeaker behavior is obtained through the fitting of the Klippel model nonlinear parameters, driven by the minimization of the RMS model error.

For the purpose of this thesis, the LSI is employed to extract the Klippel model parameters of the examined loudspeaker, along with the related dependency curves. Those informations are used to characterize the proposed nonlinear models of the loudspeaker and the sensor.

The extracted dependency curves of interest are:

Force Factor Bl(x)

The curve shows the decay of the force factor of the analyzed loudspeaker versus the displacement of the diaphragm with respect to the rest position ($x = 0$).

From this curve it is possible to characterize the values $\mathbf{Bl^0}$ and $\beta(x)$ of the proposed nonlinear model.

$$Bl^0 = Bl(x = 0) \qquad \beta(x) = \frac{Bl(x)}{Bl^0} \tag{5.1}$$

Mechanical Stiffness $\mathbf{K_{ms}}$(x)

The curve shows the increase of the suspension stiffness of the analyzed loudspeaker versus the displacement of the diaphragm with respect to the rest position ($x = 0$).

From this curve it is possible to characterize the values $\mathbf{K_{ms}^0}$ and $\kappa(x)$ of the proposed nonlinear model.

$$K_{ms}{}^0 = Kms(x = 0) \qquad \kappa(x) = \frac{K_{ms}(x)}{K_{ms}{}^0} \tag{5.2}$$

Electric Inductance $\mathbf{L_e}$(x)

The curve shows the variation of the electrical inductance of the analyzed loudspeaker versus the displacement of the diaphragm with respect to the rest position ($x = 0$).

From this curve it is possible to characterize the values $\mathbf{L_e^0}$ and $\xi(x)$ of the proposed nonlinear model.

$$L_e^0 = L_e(x = 0) \qquad \xi(x) = \frac{L_e(x)}{L_e^0} \tag{5.3}$$

Electric Inductance $\mathbf{L_e}$(i)

The curve shows the variation of the electrical inductance of the analyzed loudspeaker versus the current in the voice coil with respect to the rest current value ($i = 0$).

From this curve it is possible to characterize the values $\mathbf{L_e^0}$ and $\iota(x)$ of the proposed nonlinear model.

$$L_e^0 = L_e(i = 0) \qquad \iota(x) = \frac{L_e(x)}{L_e^0} \tag{5.4}$$

Clearly, the value of $L_e(i = 0)$ coincides with the value of $L_e(x = 0)$.

Other extracted parameters of interest are:

$R_e(T_v)$	Electrical resistance of the voice coil at DC at the working temperature T_v
$R_2(0)$	Electrical resistance of the LR-2 model at rest ($x = 0, i = 0$)
$L_2(0)$	Electrical inductance of the LR-2 model at rest ($x = 0, i = 0$)

5.1.3 Parameter drift

The main limitation of the LPM and LSI measurements is that the extracted parameters and dependency curves are assumed time invariant.

This is evident in LPM, where a single set of parameters is extracted, but is also true for LSI, where the parameters of the analyzed loudspeaker are monitored throughout the measurement process but the proposed parameters and dependency curves are relative to the final instant of the measurement process.

This limitation is due to the time invariance of the loudspeaker models exploited by both the measurement processes, that are the small signals linear model for the LPM and the large signals Klippel model for the LSI.

A real loudspeaker is indeed a time-varying system, constantly subject to temperature, pressure and humidity variations, as well as aging. All these factors affect the structure and behavior of the loudspeaker and, since they are not modeled, they determine a constant and unpredictable parameter drift.

This can be appreciated from the curves of fig. 5.4, result of a LSI measurement performed on a loudspeaker while simulating environmental climatic changes, switching from cold winter to hot summer temperatures.

The result of the sole temperature variation is a shift of the loudspeaker parameters that lead to a severe variation of its behavior, for example shifting the resonance frequency an octave up.

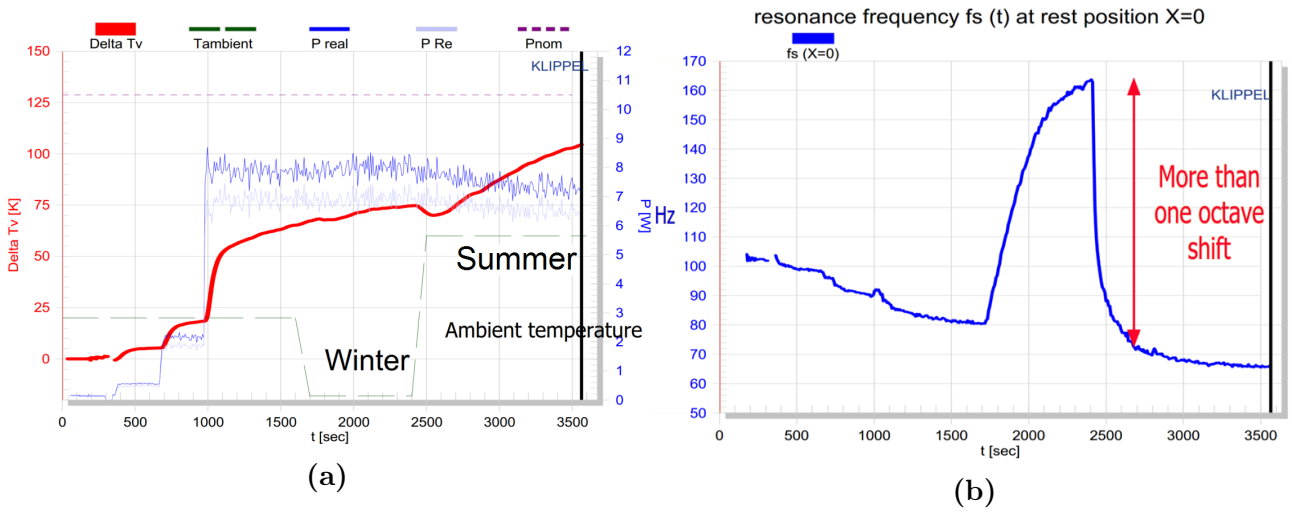

Figure 5.4: a) Temperature evolution versus time during the climate change simulation; b) Resonance frequency versus time during the climate change simulation.

The most significant example of parameter drifting in a loudspeaker is given by the time variance of the mechanical stiffness.

Considering the small signals condition, the value of parameter K_{ms} is affected by environmental factors (temperature, humidity) and aging. Two LPM measurements performed in different environmental conditions clearly show a variation of the mechanical stiffness, which becomes softer (K_{ms} reduction) at high temperatures and vice versa. This is the main reason of the resonance frequency shift in the test of fig. 5.4. Similarly, two measurements performed at two different and distant times show the aging effects.

Considering the large signals condition instead, the values of the curve $K_{ms}(x)$ are also influenced by the structural fatigue of the suspensions. Monitoring the evolution of the curve estimate during the LSI process, one observes the constant reduction of the mechanical stiffness around the rest position (near $x = 0$). This is shown in fig. 5.5.

Up to some extent, all the loudspeaker parameters are subject to drifts, introducing a potential degradation of the model's quality.

For the purpose of this thesis, it is assumed that the loudspeaker parameters are time invariant and that the parameters extracted by the LPM and LSI measurements perfectly characterize the loudspeaker.

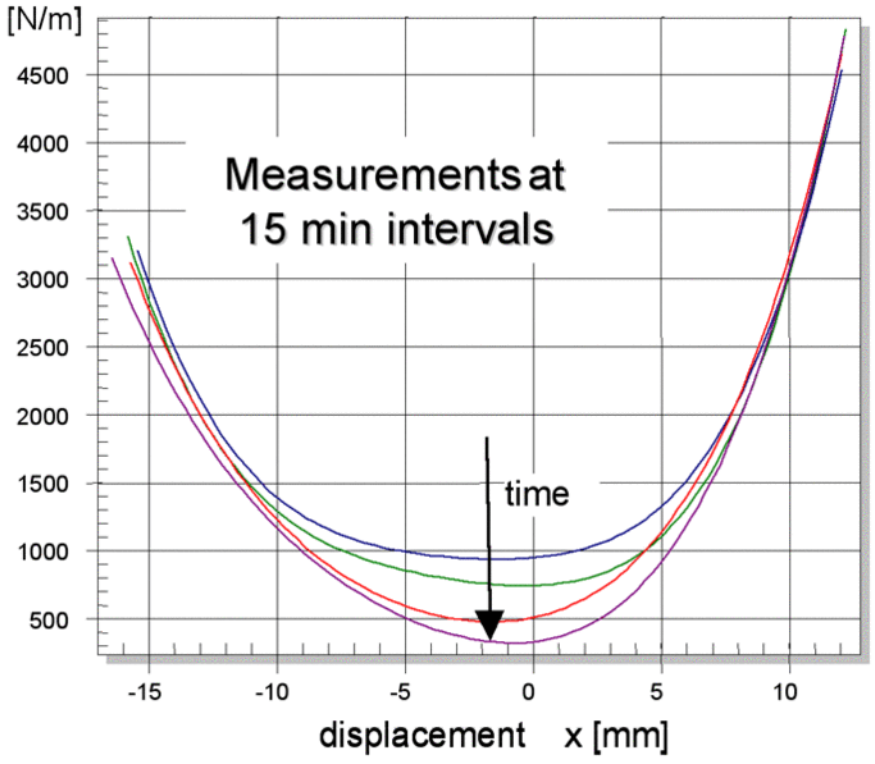

Figure 5.5: Evolution of the estimate curve of the mechanical stiffness versus displacement.

5.2 The studied loudspeaker: LF18x401 with double voice coil

The studied loudspeaker is the LF18X401 subwoofer, manufactured by RCF. It is a 18" $(45,72cm)$ subwoofer with cellulose-based conical diaphragm and ferrite permanent magnet and copper, dual layer voice coil.

The nominal frequency range of the transducer is $25-1000Hz$. However, devices of this kind are usually employed in audio systems, combined with other loudspeakers, for the reproduction of the $25-200Hz$ range only.

For this reason, the considered working bandwidth is $25-200Hz$.

The nominal maximum displacement range of the transducer is $50mm$ peak-to-peak, or equivalently $\pm 25mm$. This means that if the diaphragm displacement exceeds the specified threshold, the transducer will suffer of structural damages and, if the overstimulation is prolonged in time, may be destroyed.

For this reason, the considered working displacement range is $\pm 20mm$.

The considered LF18X401 has been customized to be equipped with a secondary voice coil, used as sensor as described in chapter 4. The introduction of the sensor coil requires the enlargement of the magnetic gap, to fit the additional thickness.

The major effects of this structural change are a slight reduction of the maximum force factor **Bl**, caused by the reduction of the magnetic flux density **B** in the magnetic gap and a small increase in the mechanical moving mass, due to the sensor coil copper. To minimize the effects of the sensor voice coil on the loudspeaker behavior, it should be made as short as possible, to minimize the excess mass, and as thin as possible, to minimize also the enlargement of the magnetic gap.

For the ease of construction and analysis, the sensor coil has been designed to be identical in material, thickness and height to the voice coil, but with half the number of turns.

The voice coil is designed to be made of 130 turns of $0.45mm$ thick insulated copper wire, wound on a $100mm$ diameter former and distributed on two overlapped layers $292.5mm$ high, for a total length of $40.84m$. The sensor coil has the same form factor of the voice coil with but with a single layer, for a total length of $20.42m$.

Figure 5.6: The studied loudspeaker: the LF18X401.

5.2.1 Extracted parameters

The Distortion Analyzer and the dB-Lab software have been exploited for the estimation of the fundamental parameters of the loudspeaker, both in small and large signals conditions.

To fully characterize the device the measurement processes have been performed on both the loudspeaker coils.

The results of interest of the LPM measurement processes are shown in tables 5.1a to 5.1c.

From the extracted parameter values one can notice that quantities that should be identical among the two measurements, like the mechanical mass, appear to be different.

This is one of the limits of the identification-based algorithm exploited by the Distortion Analyzer. The parameters are not actually measured but estimated, introducing small variations of the extracted parameter values between different measurements of the same devices. However, the estimation error is always less than 5%.

It is also important to notice that, as explained in section 4.2, the small differences from the theoretical design introduced by the manufacturing process lead to a slightly smaller effective turns ratio. The theoretically null velocity contribution to the sensor output voltage, in the real device actually appears.

$$Bl_s - T_r Bl = -0.2017 \tag{5.5}$$

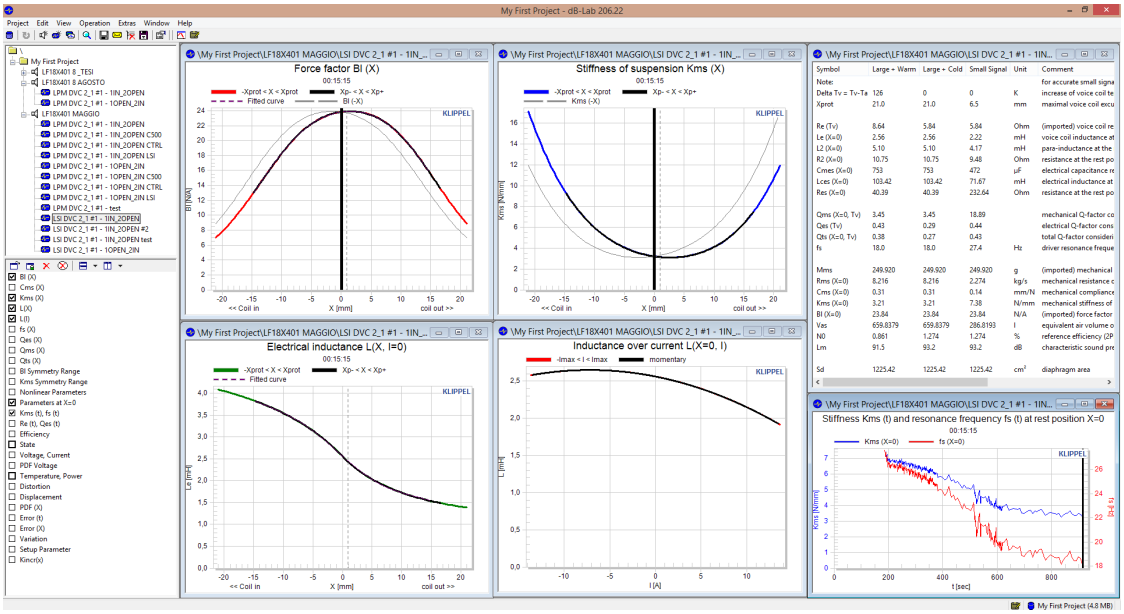

Figure 5.7: Window of the dB-Lab software with the LSI measurement results shown.

R_e	5.86	Ω
L_e	2.923	mH
R_2	6.12	Ω
L_2	3.665	mH
Bl	23.408	N/A
M_{ms}	251.669	g
R_{ms}	5.121	kg/s
K_{ms}	7936	N/m
f_s	28.3	Hz

(a) Voice coil linear parameters.

R_s	3.19	Ω
L_s	0.705	mH
R_{2s}	1.45	Ω
L_{2s}	0.841	mH
Bl_s	11.294	N/A
$\hat{M}_{ms}$	247.715	g
$\hat{R}_{ms}$	5.297	kg/s
$\hat{K}_{ms}$	7633	N/m
$\hat{f}_s$	27.9	Hz

(b) Sensor coil linear parameters.

M	1.436	mH
T_r	0.4911	

(c) Derived linear parameters.

Table 5.1: Extracted linear parameters from the LPM procedure.

	at t(start)	at t(end)	
T_v	0	126	°C
$R_e(T_v)$	5.84	8.64	Ω
${L_e}^0$	2.22	2.56	mH
${R_2}^0$	9.48	10.75	Ω
${L_2}^0$	4.17	5.10	mH
Bl^0	23.84	23.84	N/A
M_{ms}	249.920	249.920	g
R_{ms}	2.274	8.216	kg/s
${K_{ms}}^0$	7380	3210	N/m
f_s	27.4	18	Hz

(a) Voice coil parameters at rest.

	at t(start)	at t(end)	
T_v	0	128	°C
$R_s(T_v)$	3.03	4.50	Ω
${L_s}^0$	0.58	0.59	mH
${R_{2s}}^0$	2.47	2.41	Ω
${L_{2s}}^0$	1.09	1.28	mH
${Bl_s}^0$	11.46	11.46	N/A
$\hat{M}_{ms}$	241.100	241.100	g
$\hat{R_{ms}}$	7.395	8.936	kg/s
$\hat{K}^0_{ms}$	5170	2940	N/m
$\hat{f}_s$	23.3	17.6	Hz

(b) Sensor coil parameters at rest.

	at t(start)	at t(end)	
M^0	1.229	1.135	mH
${T_r}^0$	0.480	0.511	

(c) Derived parameters at rest.

Table 5.2: Estimated parameters at rest from the LSI procedure.

The LSI measurement process extracts the same fundamental parameters also extracted with the LPM procedure, with the addition of the tracking of the parameters evolution in time during the large signals stimulation and the set of the nonlinear parameters curves.

The comparison between the extracted parameters corresponding to the rest position ($x = 0$) at the start and at the end of the measurement process is shown in tables 5.2a to 5.2c.

Again, variations of the theoretically fixed parameters between the two LSI measurements, and also between the LSI starting measurements and the LPM results, can be noticed. However, the final result of the two measurements is consistent, since both the mechanical stiffness $\mathbf{K_{ms}}$ and the resonant frequency $\mathbf{f_s}$ at $t(end)$ converge to similar values as can be seen in fig. 5.8.

Those curves appear very different in the first part of the measurement process, suggesting a different response of the loudspeaker to the LSI stimuli. Indeed, the voice coil measure has been done first, after a very long period of rest of the device, while the sensor coil measure has been carried out after just few hours.

This means that spider the loudspeaker has had the time to recover its elastic behavior, but not its entire strength, exhibiting a more compliant behavior with respect to the first measure.

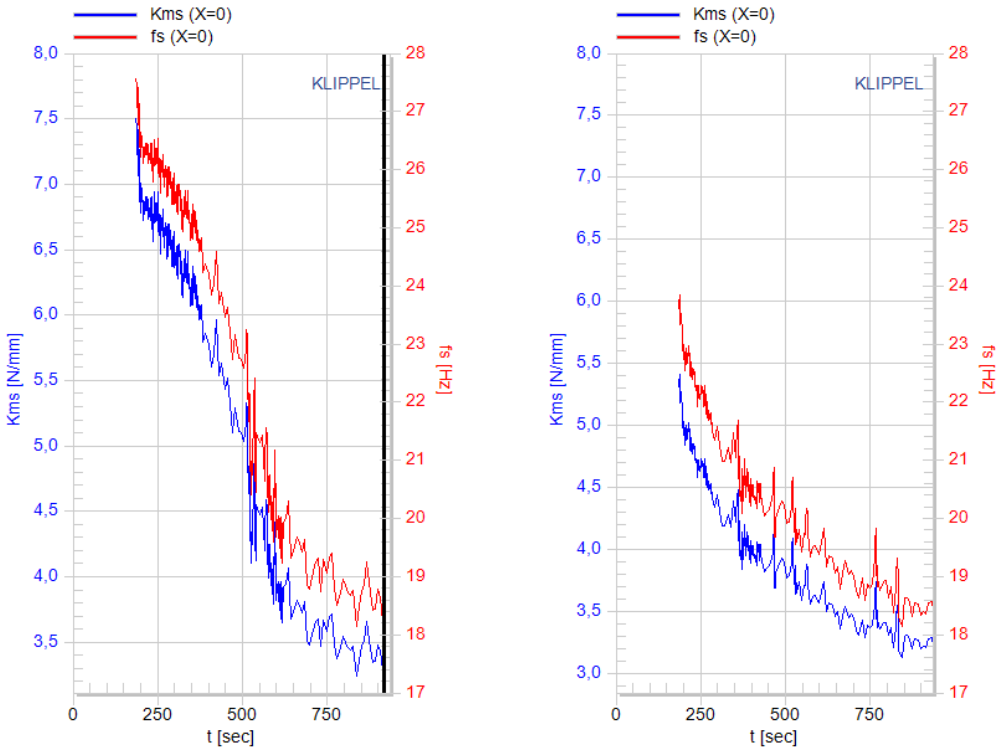

(a) Variations detected from the voice coil.

(b) Variations detected from the sensor coil.

Figure 5.8: Variations of K_{ms} and f_s during the LSI measurement process.

The extracted nonlinear parameter curves are shown in fig. 5.9.

From the those curves it is possible to derive the four basic nonlinear dependency curves $\xi(x), \iota(i), \beta(x)$, $\kappa(x)$ and $\beta_s(x)$ described in sections 3.2.2 and 4.3 along with their relative gradients, used in sections 3.2.3 and 4.3.1 to simplify the defined nonlinear state space models, avoiding the use of the derivative operation in the matrices coefficients. Those curves are shown in figs. 5.10 to 5.15

The displacement dependency curves are characterized by 100 data points over a displacement excursion of $\pm 21mm$, for a resolution $\Delta x = 0.42mm$. The current dependency curve is characterized by 1000 data points over a current excursion of $\pm 13.6A$, for a resolution $\Delta i = 27.2mA$.

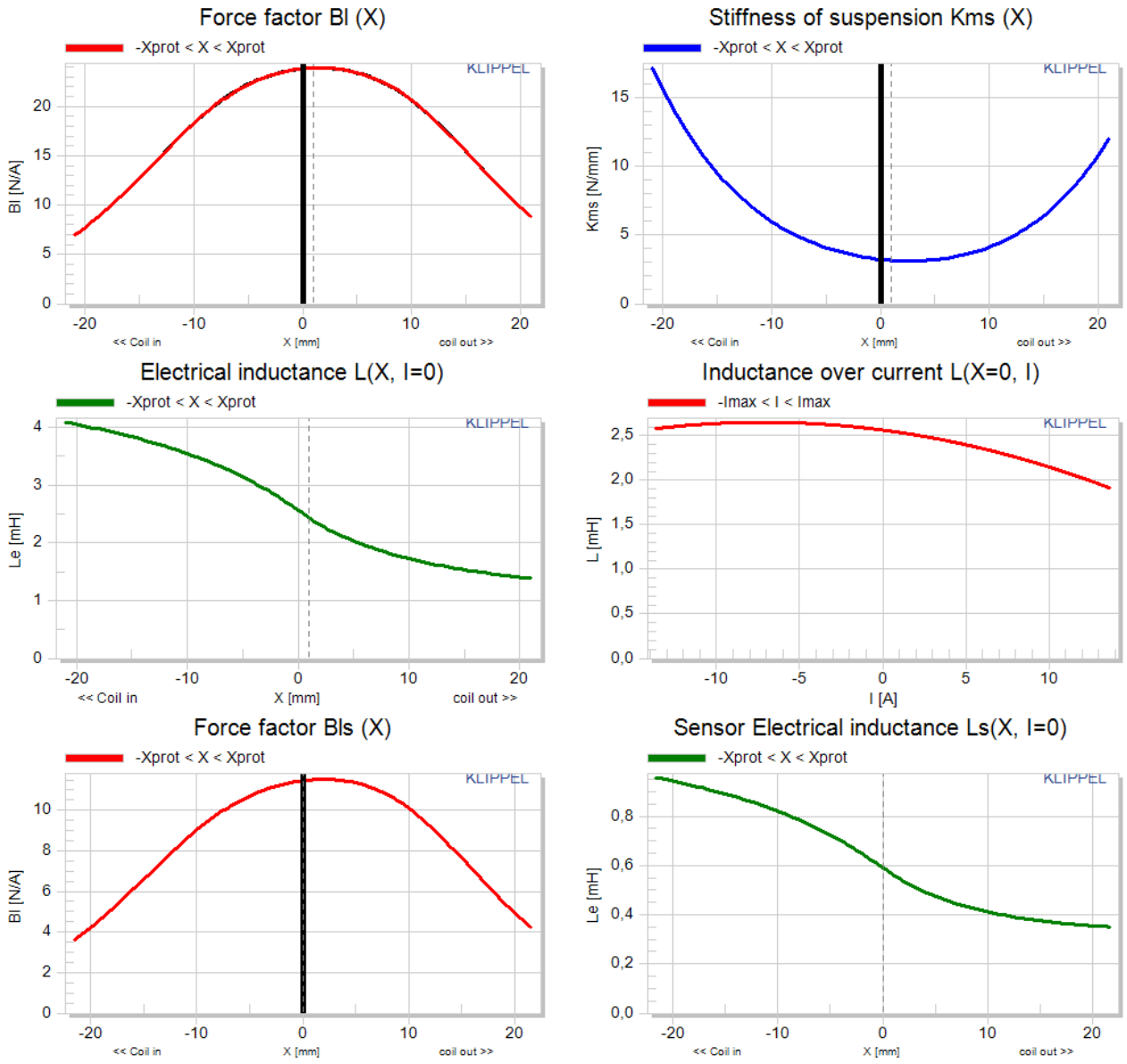

Figure 5.9: Nonlinear parameters curves.

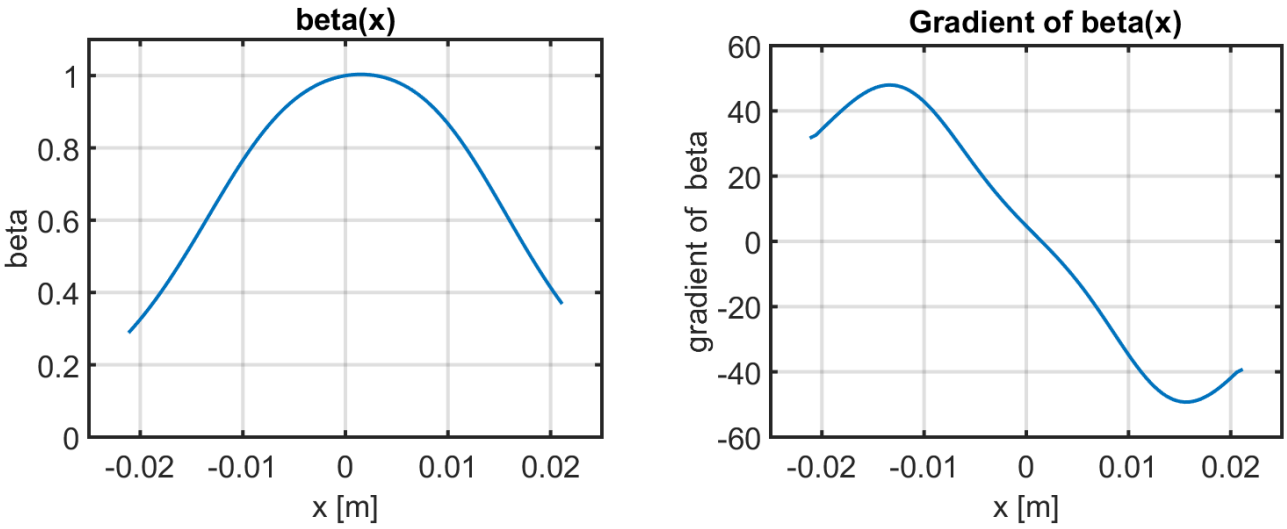

Figure 5.10: Voice coil force factor nonlinear dependency curve $\beta(x)$ and gradient $\nabla\beta(x)$.

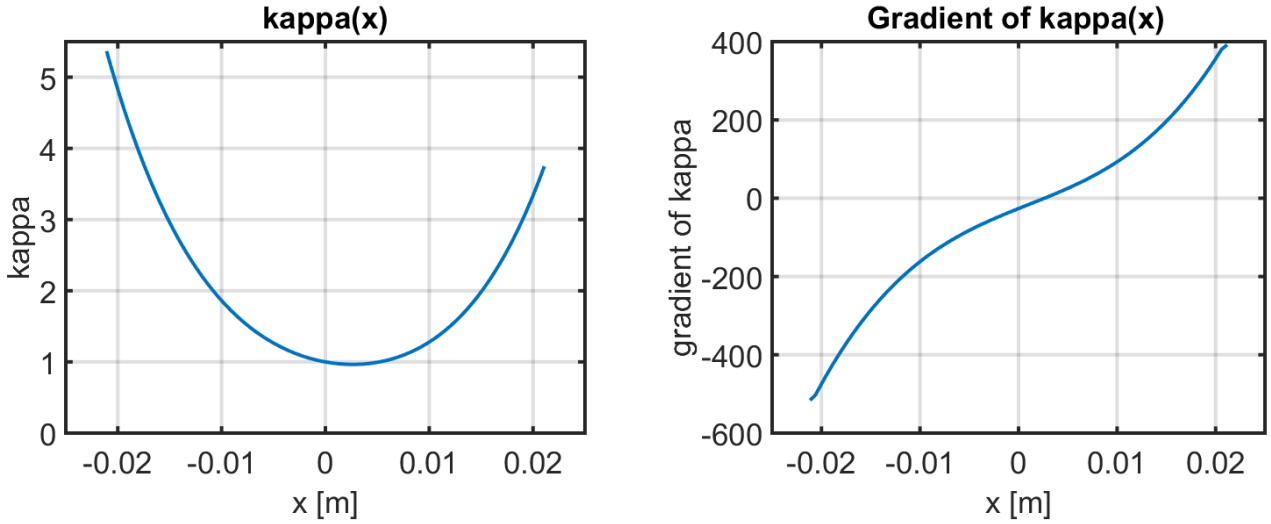

Figure 5.11: Mechanical stiffness nonlinear dependency curve $\kappa(x)$ and gradient $\nabla\kappa(x)$.

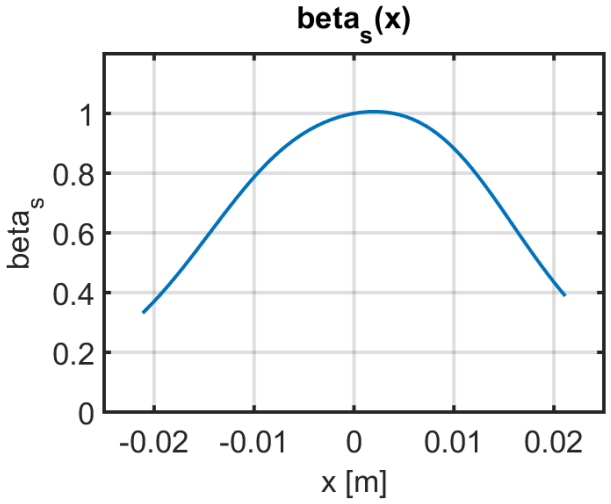

Figure 5.12: Sensor coil force factor nonlinear dependency curve $\beta_s(x)$.

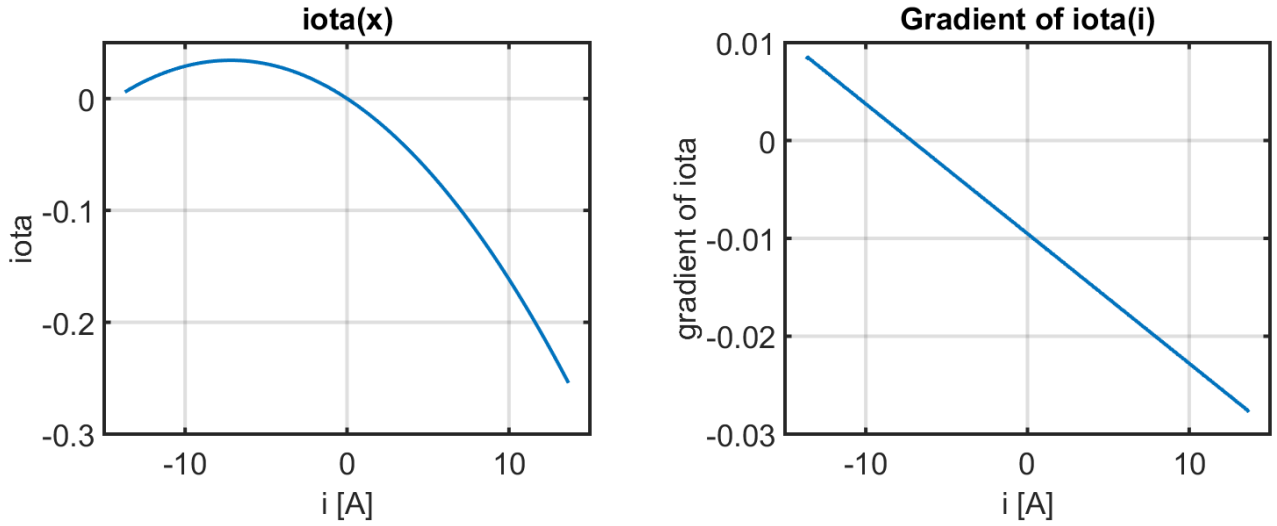

Figure 5.13: Voice coil inductance nonlinear dependency curve $\iota(i)$ and gradient $\nabla\iota(i)$.

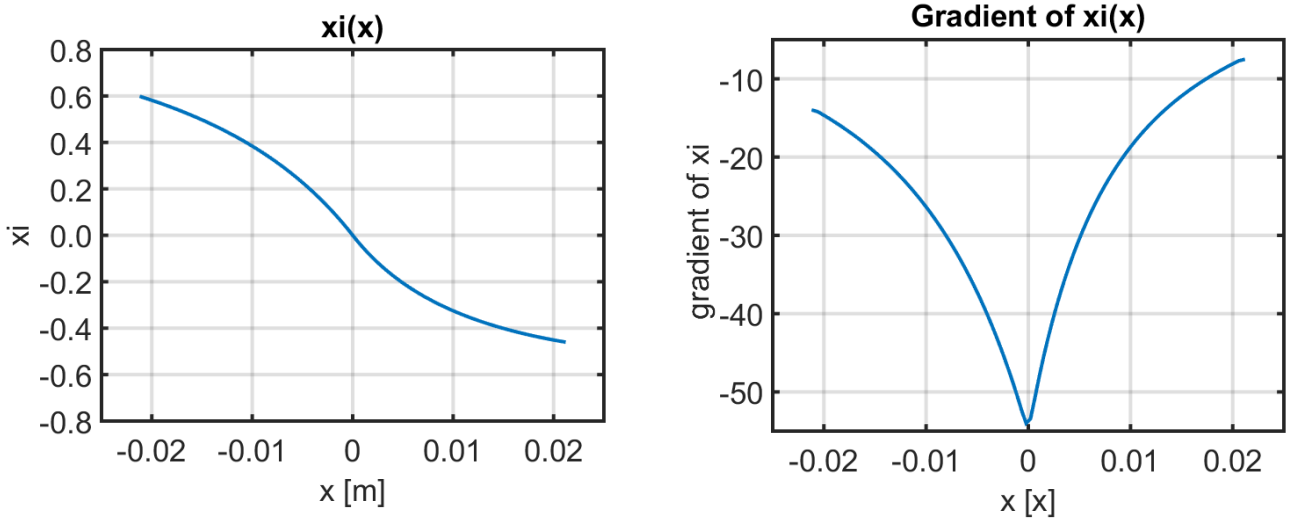

Figure 5.14: Voice coil inductance nonlinear dependency curve $\xi(x)$ and gradient $\nabla\xi(x)$.

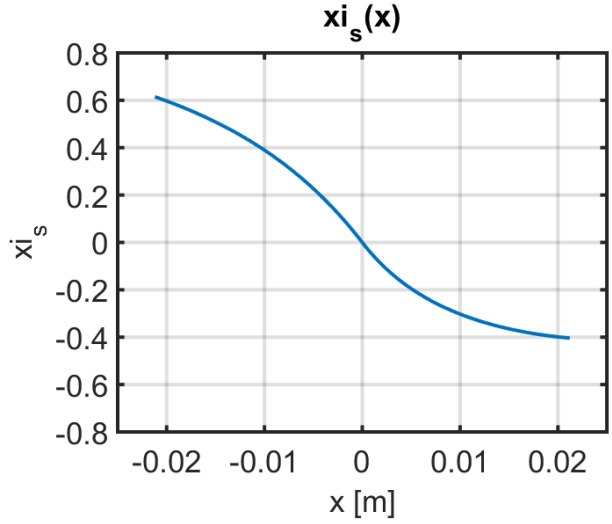

Figure 5.15: Sensor coil inductance nonlinear dependency curve $\xi_s(x)$.

5.2.2 The Loudspeaker Models in Simulink

The loudspeaker and sensor models presented so far have been implemented in Mathworks Simulink for validation purposes.

The loudspeaker models developed in chapter 3 and the sensor models developed in chapter 4 have been condensed in just two models, one for each of the described loudspeaker working conditions. The models, in fact, use the same internal state vector, allowing to consider the sensor coil output voltage as a second output of a loudspeaker system.

$$\mathbf{x}(t) = \begin{bmatrix} i(t) & i_2(t) & x(t) & v(t) \end{bmatrix}^T \tag{5.6}$$

$$u(t) = V_{in}(t) \qquad \mathbf{y}(t) = \begin{bmatrix} a(t) & V_{sensor}(t) \end{bmatrix}^T \tag{5.7}$$

For the small signal conditions, the complete model for the loudspeaker with sensor coil can be expressed as the SIMO (Single Input - Multiple Output) SS model of eq. (5.8)

$$\mathbf{A} = \begin{bmatrix} -\dfrac{R_e + R_2}{L_e} & \dfrac{R_2}{L_e} & 0 & -\dfrac{Bl}{L_e} \\ \dfrac{R_2}{L_2} & -\dfrac{R_2}{L_2} & 0 & 0 \\ 0 & 0 & 0 & 1 \\ \dfrac{Bl}{M_{ms}} & 0 & -\dfrac{K_{ms}}{M_{ms}} & -\dfrac{R_{ms}}{M_{ms}} \end{bmatrix} \qquad \mathbf{B} = \begin{bmatrix} \dfrac{1}{L_e} \\ 0 \\ 0 \\ 0 \end{bmatrix}$$

$$\mathbf{C} = \begin{bmatrix} \dfrac{Bl}{M_{ms}} & 0 & -\dfrac{K_{ms}}{M_{ms}} & -\dfrac{R_{ms}}{M_{ms}} \\ -T_r R_e & 0 & 0 & (Bl_s - T_r Bl) \end{bmatrix} \qquad \mathbf{D} = \begin{bmatrix} 0 \\ T_r \end{bmatrix} \tag{5.8}$$

The Simulink implementation of the small signal linear model is obtained using a State Space block, properly initialized with the four matrices of eq. (5.8). The matrices are created in the MATLAB environment with the parameters extracted through the LPM procedure and stored in the workspace to be freely used by the Simulink simulation engine.

For the large signal conditions, the complete model for the loudspeaker with sensor coil can be expressed as the SIMO nonlinear time invariant SS model of eq. (5.9).

$$\mathbf{A}(\mathbf{x}) = \begin{bmatrix} -\dfrac{R_e + R_2(x,i) + \dfrac{\partial L_e(x,i)}{\partial t}}{L_e(x,i)} & \dfrac{R_2(x,i)}{L_e(x,i)} & 0 & -\dfrac{Bl(x)}{L_e(x,i)} \\ \dfrac{R_2(x,i)}{L_2(x,i)} & -\dfrac{R_2(x,i) + \dfrac{\partial L_2(x,i)}{\partial t}}{L_2(x,i)} & 0 & 0 \\ 0 & 0 & 0 & 1 \\ \dfrac{Bl(x)}{M_{ms}} & 0 & -\dfrac{K_{ms}(x)}{M_{ms}} & -\dfrac{R_{ms}}{M_{ms}} \end{bmatrix}$$

$$\mathbf{B}(\mathbf{x}) = \begin{bmatrix} \dfrac{1}{L_e(x,i)} \\ 0 \\ 0 \\ 0 \end{bmatrix}$$

$$\mathbf{C}(\mathbf{x}) = \begin{bmatrix} \dfrac{Bl(x)}{M_{ms}} & 0 & -\dfrac{K_{ms}(x)}{M_{ms}} & -\dfrac{R_{ms}}{M_{ms}} \\ \left[-T_r(x,i)R_e + \dfrac{\partial M(x,i)}{\partial t} - T_r(x,i)\dfrac{\partial L_e(x,i)}{\partial t}\right] & 0 & 0 & [Bl_s(x) - T_r(x,i)Bl(x)] \end{bmatrix}$$

$$\mathbf{D}(\mathbf{x}) = \begin{bmatrix} 0 \\ T_r(x,i) \end{bmatrix} \tag{5.9}$$

A new block has been defined to implement the nonlinear model, exploiting the characteristic differential equations of the nonlinear loudspeaker and sensor, shown in eqs. (3.34) and (4.19).

For ease of construction, the model has been split in six subparts, later connected and encapsulated in a single functional block to form the full nonlinear model: two for the electric domain in figs. 5.18 and 5.19, one for the mechanical domain in fig. 5.20, one for the electromechanic transduction in fig. 5.21, one for the sensor output fig. 5.22 and one for the constant update of the nonlinear parameter values in fig. 5.23.

The model is characterized using the parameters and nonlinear dependency curves extracted through the LSI measurement process. The measured parameters, due to the intrinsic time variance of the loudspeaker physical system, also exhibit time variance during the whole measurement process.

For the purpose of this thesis, the loudspeaker is considered a nonlinear time invariant system, characterized by the last extracted parameter at time $t(end)$, thus under mechanical stress.

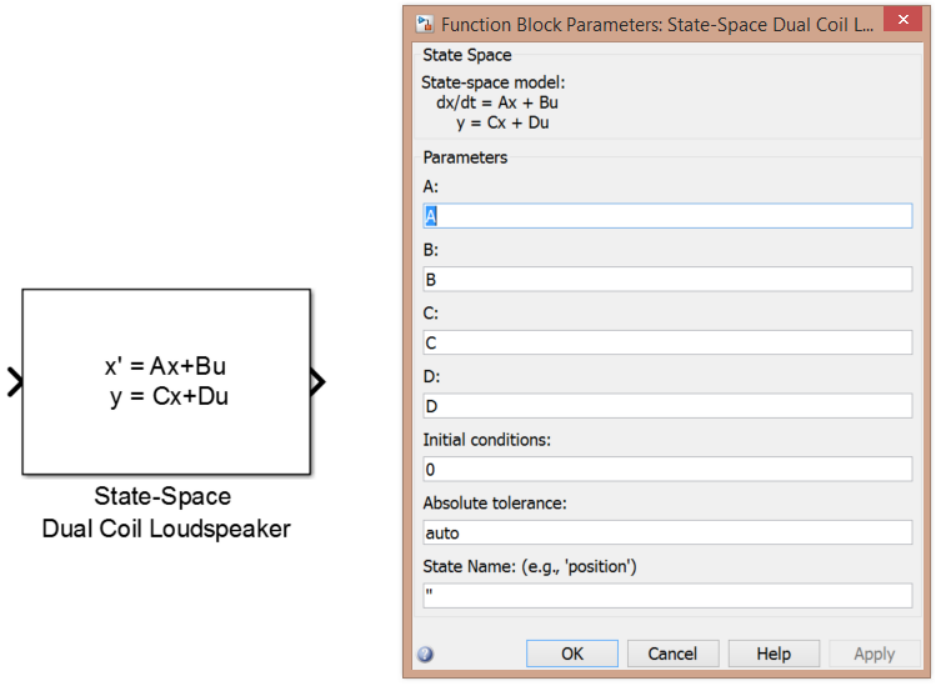

Figure 5.16: State Space Simulink block, initialized with the matrix to implement the loudspeaker small signal model.

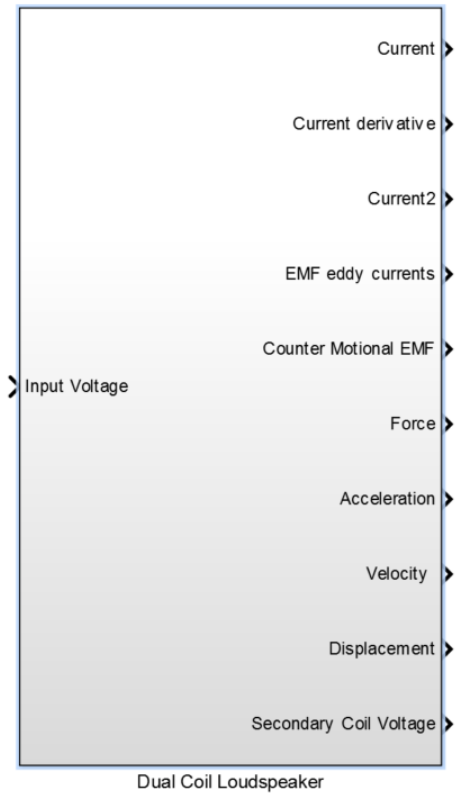

Figure 5.17: The custom Simulink block, implementing the nonlinear loudspeaker large signal model.

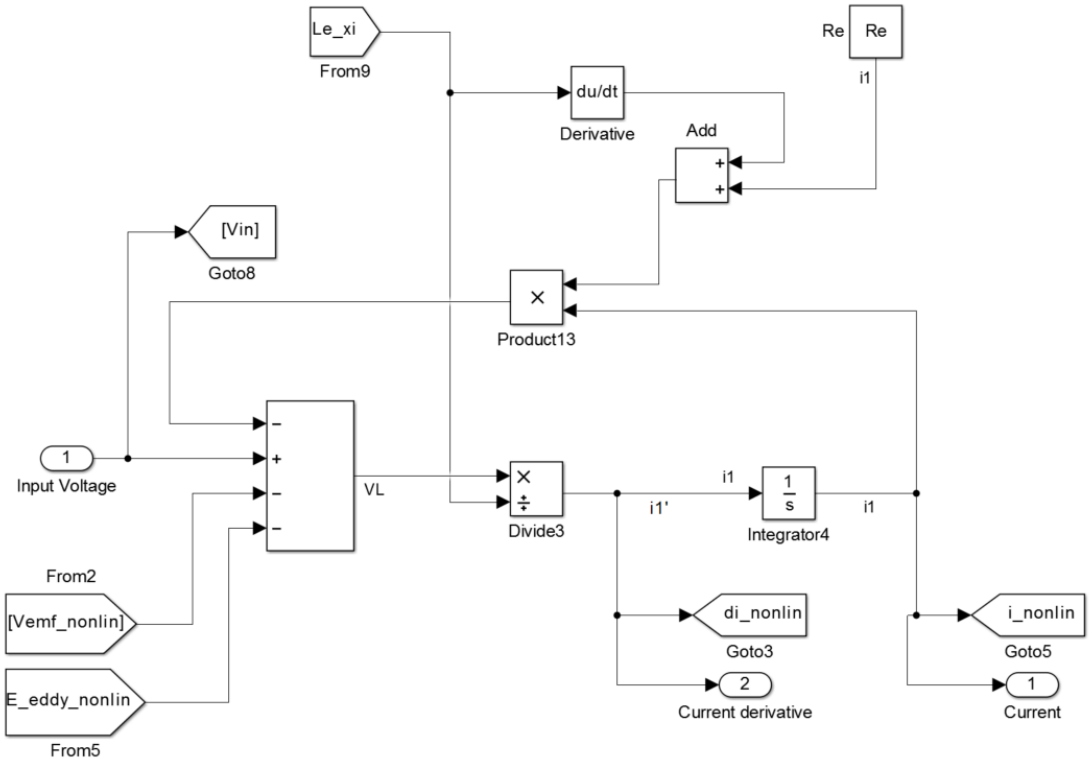

Figure 5.18: Modeling of the voice coil current.

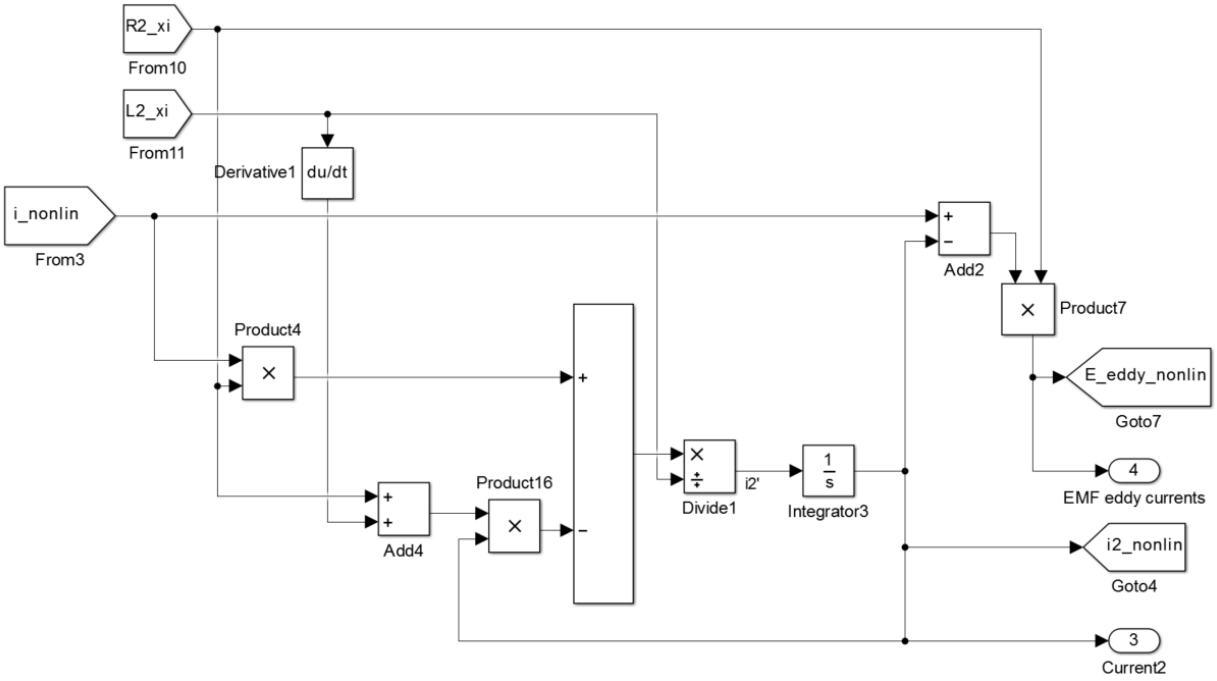

Figure 5.19: Modeling of the eddy currents contribution with LR-2 model.

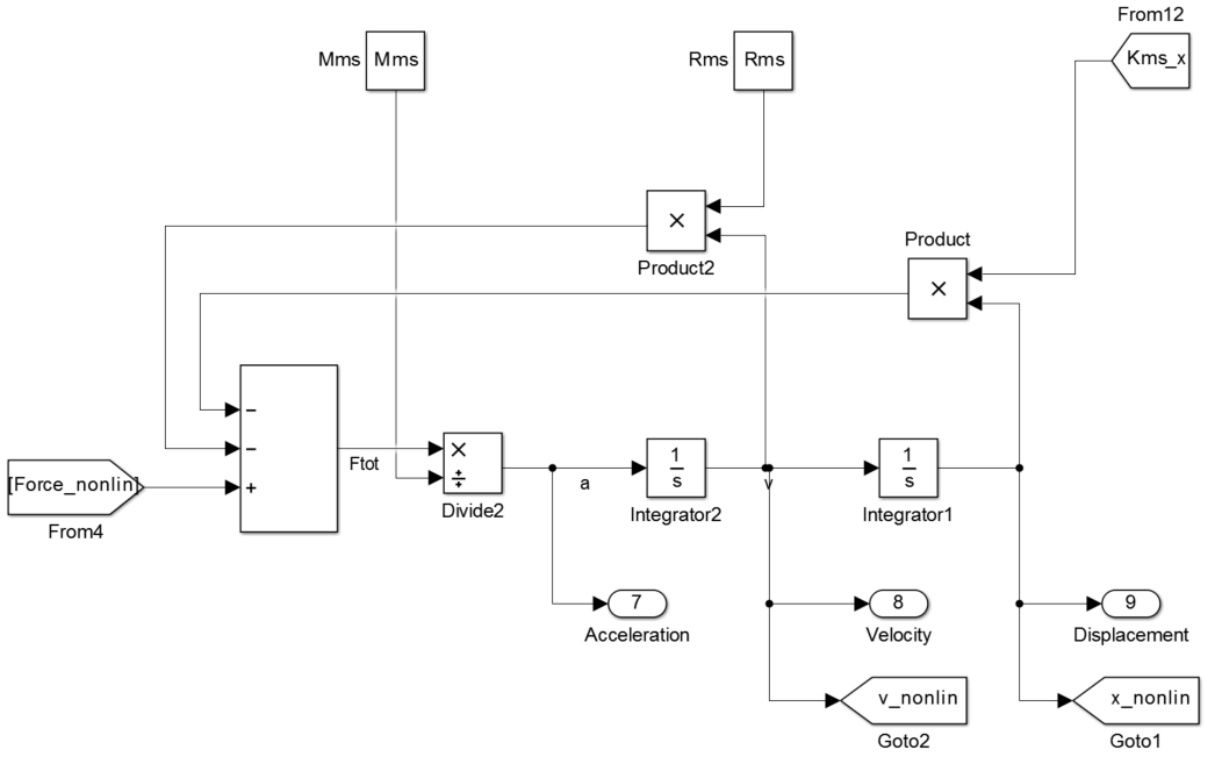

Figure 5.20: Modeling of the mechanical domain.

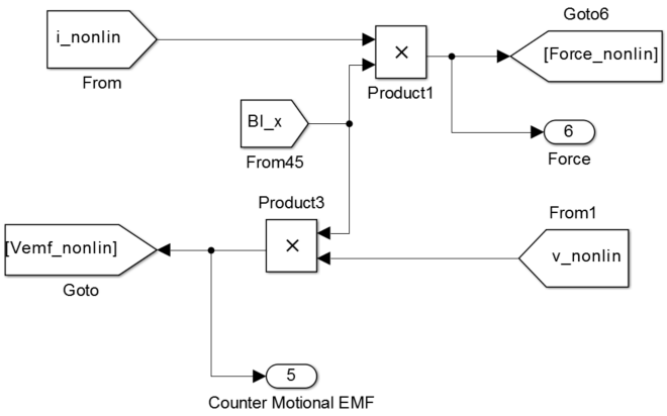

Figure 5.21: Modeling of the electromechanical transduction.

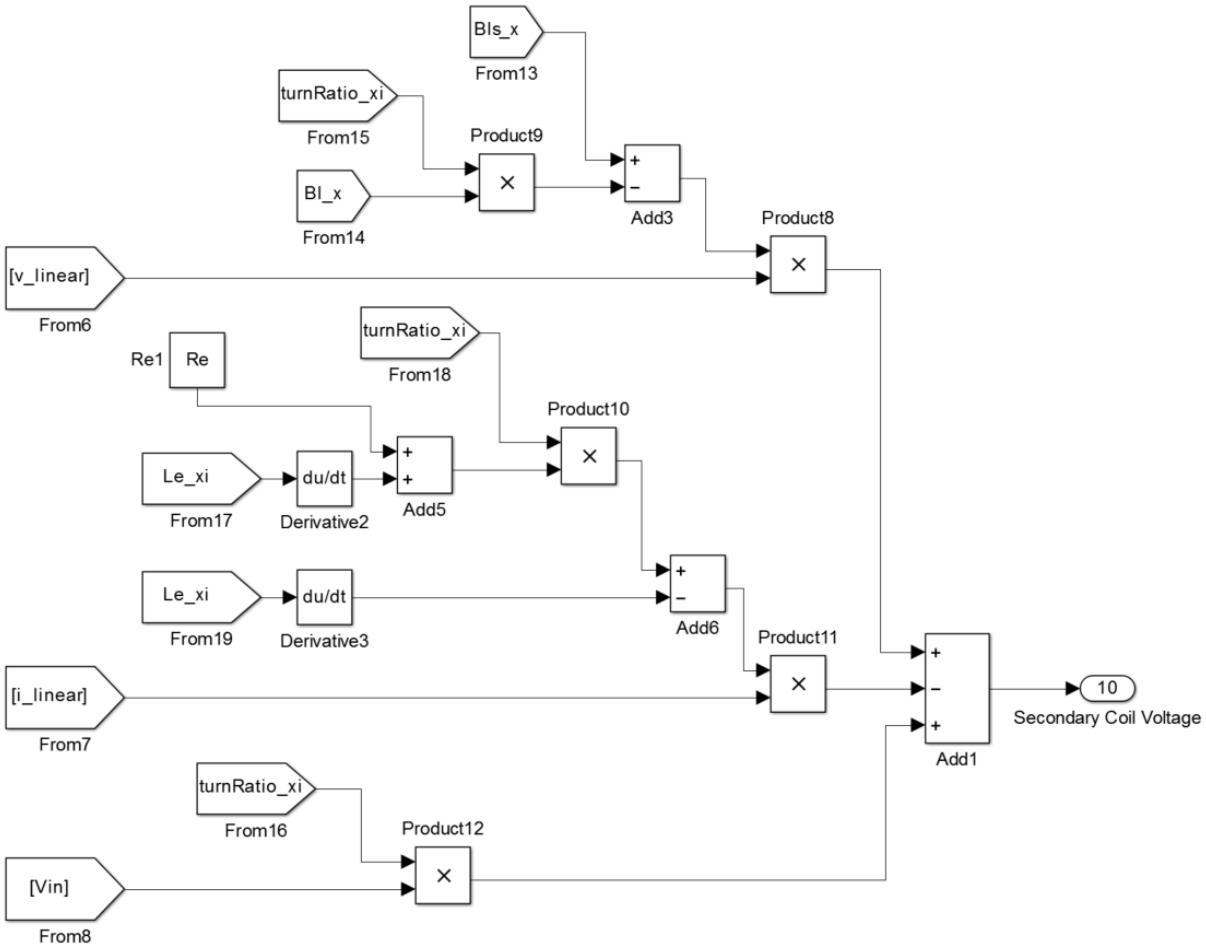

Figure 5.22: Modeling of the output voltage of the sensor coil.

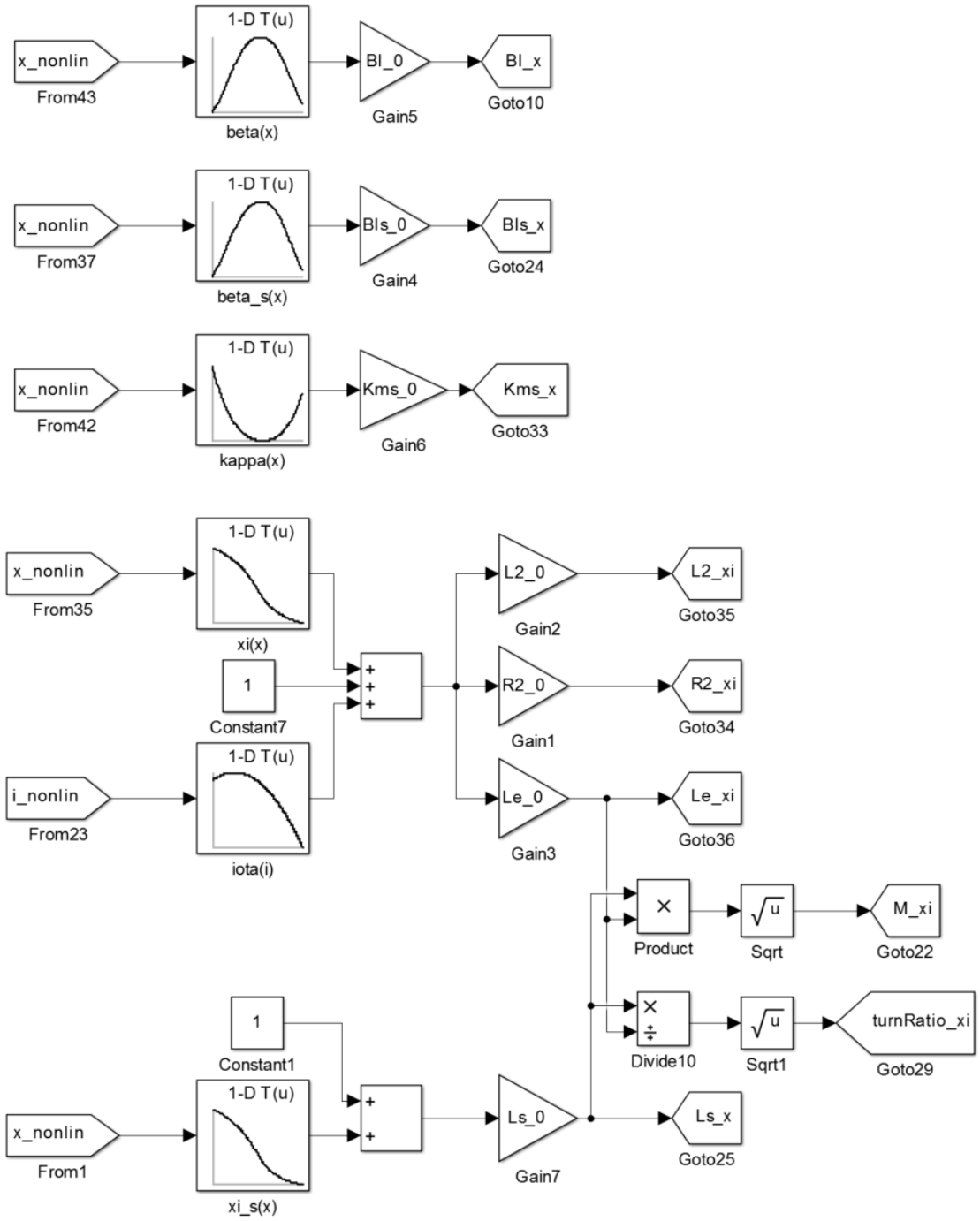

Figure 5.23: State-based update of the nonlinear parameters, using of LUT of the extracted dependency curves.

5.2.3 Small signals model validation

The developed linear model of the loudspeaker has been evaluated considering different frequency domain features, comparing the model and the real device behaviors.

The main tools for the characterization of LTI systems, as the loudspeaker in the small signals condition, are its transfer functions.

With the measuring instrument available in the RCF laboratories, it was possible to measure three loudspeaker transfer functions: the electric impedance

$$Z_e(s) = \frac{I(s)}{V_{in}(s)} \tag{5.10}$$

the voltage input to sensor output transfer function

$$H_{coils}(s) = \frac{V_s(s)}{V_{in}(s)} \tag{5.11}$$

and the voltage input to displacement transfer function

$$H_x(s) = \frac{X(s)}{V_{in}(s)} \tag{5.12}$$

These three transfer functions have been measured using CLIO, a professional instrument typically used for acoustic measurements of audio systems. The measurement process consists in driving of the analyzed loudspeaker with an exponential sine sweep while recording one of its output physical variables with a suitable sensor. To ensure the small signals condition, the sine sweep has been set to $-6dBV = 0.5V_{RMS}$

At the end of the sine sweep, CLIO automatically calculates the magnitude and phase of the considered transfer function using the recorded signal. The measured data are then imported and processed in MATLAB to extract the full transfer functions.

The model transfer function has been computed directly in MATLAB using eq. (2.4).

The comparisons between the measured and simulated transfer functions are shown in figs. 5.24 to 5.26. The transfer functions of the proposed models, which includes the effects of the eddy currents with the LR-2 model, show a very good fit on the measured transfer functions.

The semi-inductive behavior of the electric inductance in fig. 5.24 is evident. The measured phase tends to 50°instead of 90°and the magnitude rises of +3dB/decade instead of +6dB/decade.

Employing the LR-2 model, the semi-inductive behavior is effectively emulated up to $1000Hz$, while the plain model appears to be already ineffective at $200Hz$.

The same can be said regarding the sensor coil transfer function, where the beneficial effect of the introduction of the eddy current contribution is even more evident.

Figure 5.25 shows in yellow the model proposed in [CCCP81], and in red the model proposed in this thesis, which exploits the LR-2 model. The improvement is considerable, but the sensor coil model is still not perfect, showing a $3dB$ error at the dip around $95Hz$.

Parameter L_2, and especially R_2, can be slightly modified to achieve a better modeling of the sensor coil, losing accuracy at high frequency but matching the real behavior in the working bandwidth. However, for the rest of this thesis the extracted parameters L_2 and R_2 are considered good enough.

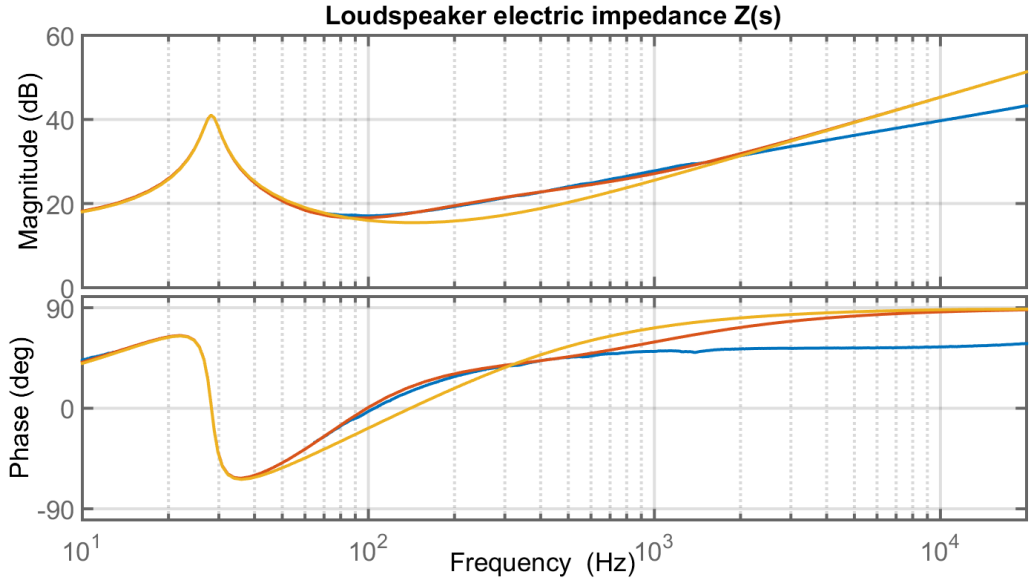

Figure 5.24: Loudspeaker electric impedance: blue) measured; red) model with LR-2; yellow) model without LR-2.

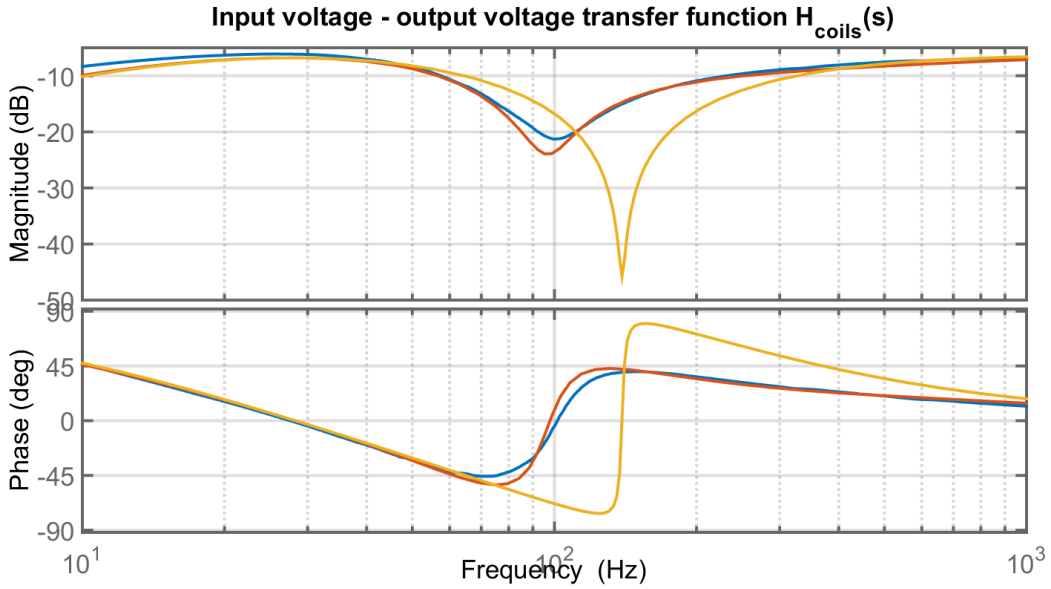

Figure 5.25: Loudspeaker voice coil input to sensor coil output transfer function: blue) measured; red) model with LR-2; yellow) model without LR-2.

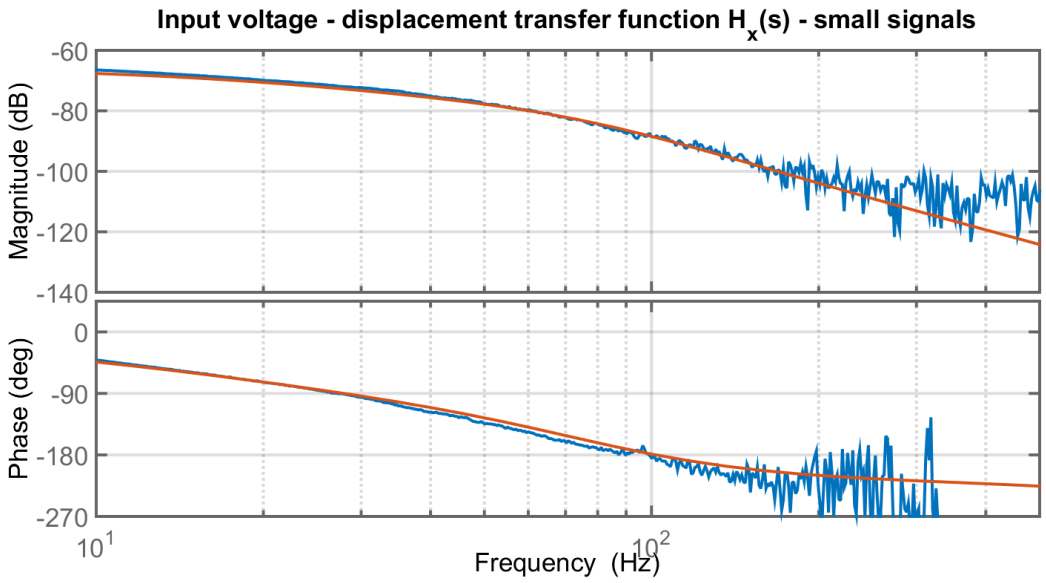

Figure 5.26: Loudspeaker voice coil input to displacement transfer function: blue) measured; red) model

Finally, in fig. 5.26 a very high noise can be noticed above $100Hz$. This is due to the limits of the displacement laser sensor, that is not sensitive enough to effectively measure the very small displacement of the diaphragm at high frequencies. However, given the good fit at low frequency, the model can be trusted.

Another significant series of measurements carried out to evaluate the quality of the model are the power spectra of its outputs.

The analyzed loudspeaker and the model have been driven with the same input, recording their relative output responses in the time domain. The recorded time series have been used to estimate the output power spectra.

Two loudspeaker output quantities have been considered: the displacement and the sensor coil output voltage. Moreover, two inputs have been considered: a sinusoid at $25Hz$ and a sinusoid at $50Hz$, both with amplitude of $-6dBV$ to ensure the small signals condition.

The two frequencies have been chosen because are one above and one below the resonant frequency of the loudspeaker, allowing to characterize both the conditions and detect possible differences. Also, considering the measured displacement transfer function of fig. 5.26, the input frequencies must be sufficiently low not to be corrupted by the sensor noise.

The input and output signals have been measured with CLIO, producing a driving signal while recording the measured quantity. The data have been imported into MATLAB to compute the power spectra that characterize the loudspeaker and to simulate the power spectra that characterize the model.

In this case, the recorded input signal drives the Simulink model, producing a simulated output used to estimate the model power spectra.

Figures 5.27 and 5.28 display the spectra of the input signals. A significant difference Can be noticed between the declared $-6dB$ and the measured $-10dB$. This is caused by the windowing process used during the spectra calculation, that caused the loss of $4dB$ in all the presented spectra.

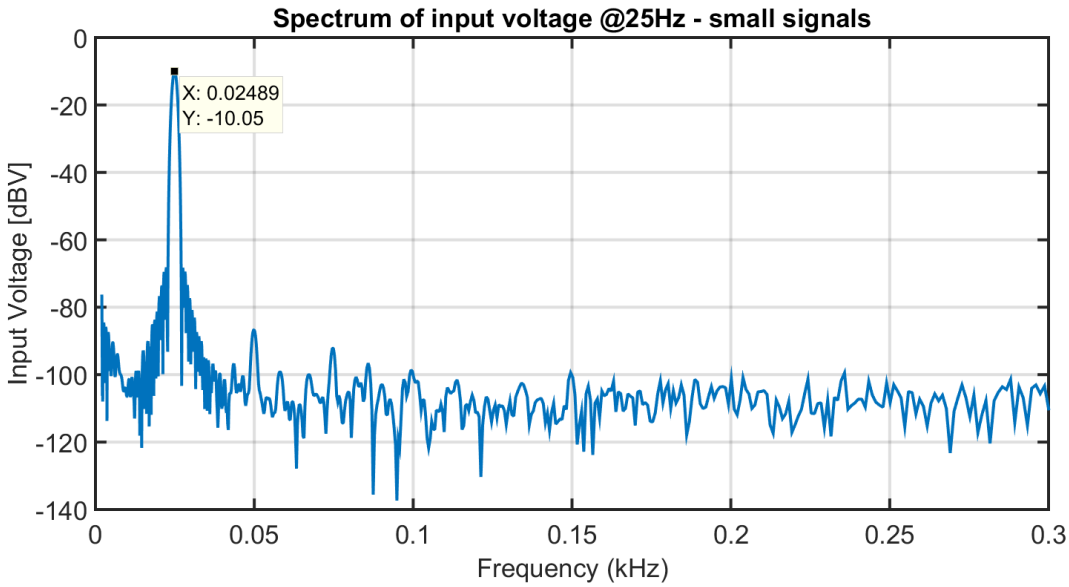

Figure 5.27: First input signal for the measurement of the output spectrum, -6dB @25Hz.

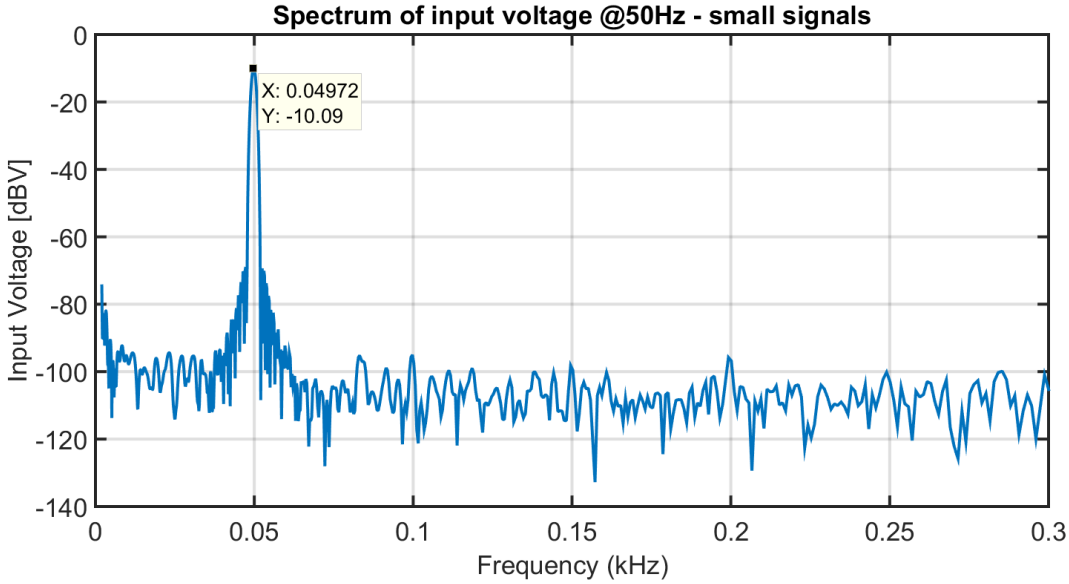

Figure 5.28: Second input signal for the measurement of the output spectrum, -6dB @50Hz

Figures 5.29 and 5.30 and figs. 5.31 and 5.32 show the spectra of the sensor coil output voltages and displacements, respectively.

In the measured spectra of the sensor coil output, it is interesting to notice the presence of very weak harmonic components, not predicted by the model. However, these contributions are absolutely neglectable, being $50dB$ smaller than the fundamental.

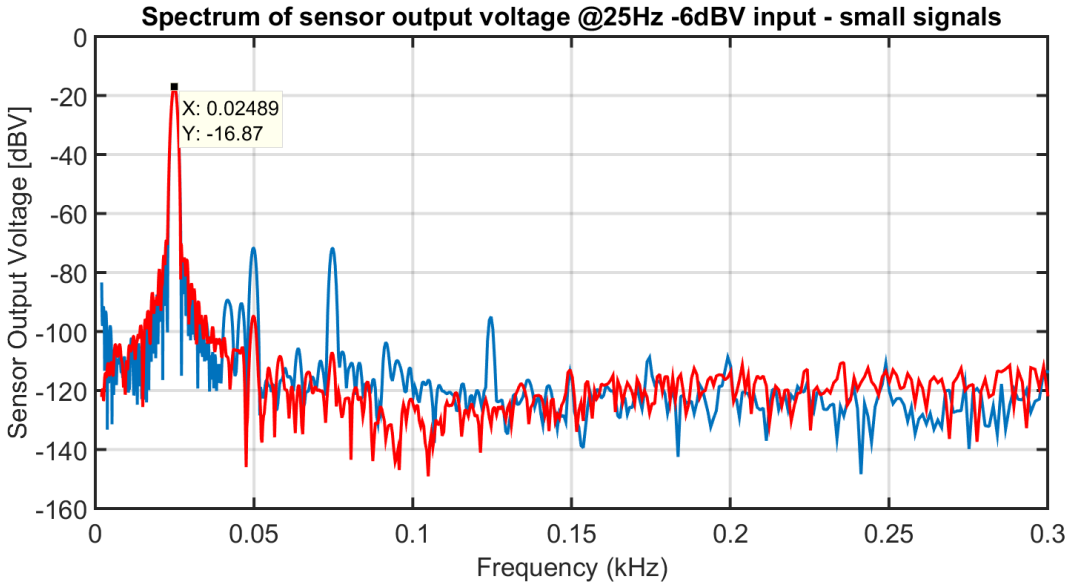

Figure 5.29: Output spectra of the sensor coil voltage @25Hz: blue) measured; red) model.

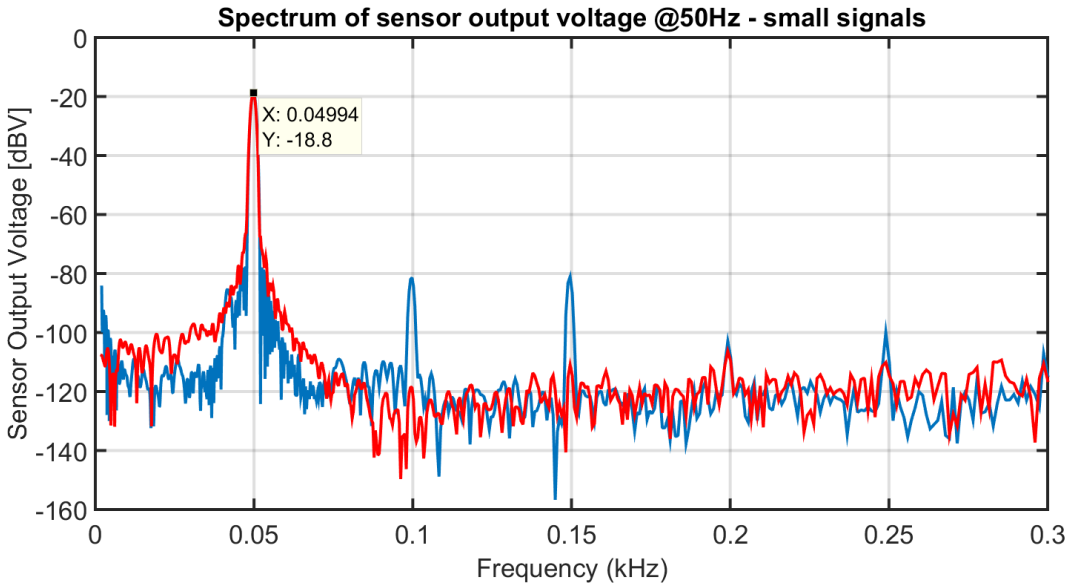

Figure 5.30: Output spectra of the sensor coil voltage @50Hz: blue) measured; red) model.

In conclusion, the developed linear model of the loudspeaker in the small signals condition appears to be coherent with the measurements performed on the real device, within the defined working bandwidth $25 - 200Hz$.

Significant errors are found with the model of the sensor coil output where, however, it is possible to tune the parameters L_2 and R_2 to achieve better performance and match the measured behavior.

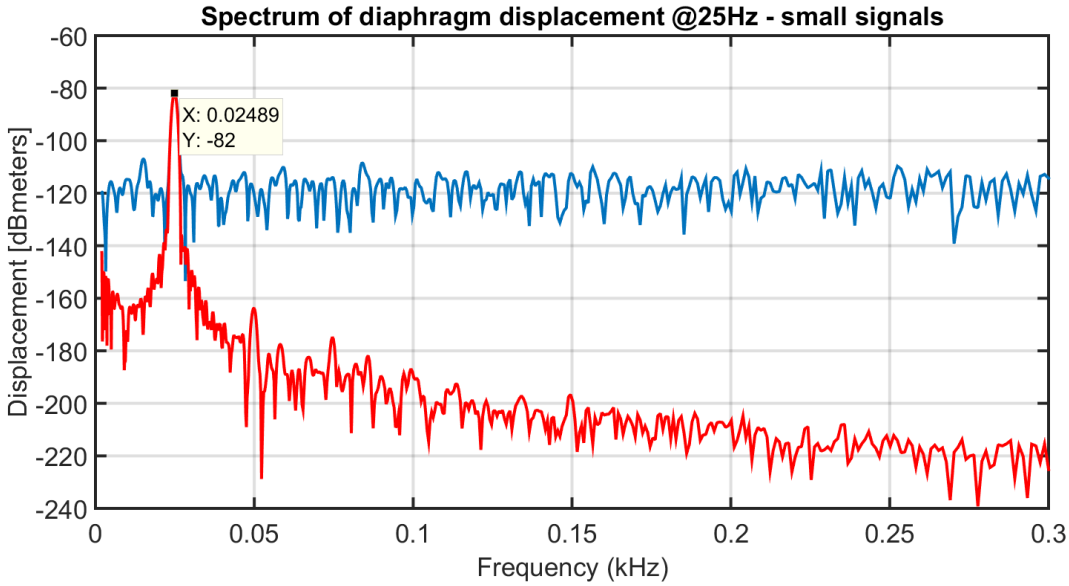

Figure 5.31: Output spectra of the displacement @25Hz: blue) measured; red) model.

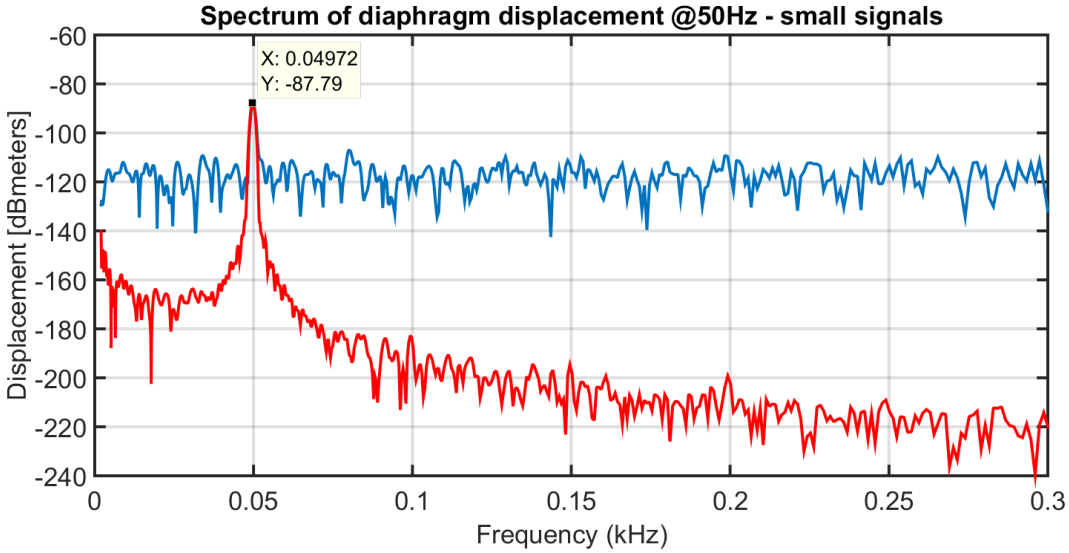

Figure 5.32: Output spectra of the displacement @50Hz: blue) measured; red) model.

5.2.4 Large signal model validation

Since in the large signals condition the loudspeaker cannot be considered a linear system, it is not possible to evaluate te quality of the model by means of transfer functions.

The developed nonlinear model of the loudspeaker has been evaluated considering the power spectra of its output.

Similarly to the process described for the small signal validation, the analyzed loudspeaker and the model have been driven with the same known input, recording their relative output responses in the time domain. The recorded time series have been used to estimate the outputs power spectra.

Again, the loudspeaker measured quantities are the sensor coil output voltage and the displacement. The chosen inputs are two sinusoids at $25Hz$ and $50Hz$, both with an amplitude of $+30dBV$ to ensure the large signals condition.

The two frequencies have been chosen to be equal to those used in the small signals validation process, that can be used as a reference for the model quality. Also, at low frequencies the nonlinearities are more pronounced, allowing to better appreciate their effects.

Figures 5.33 and 5.34 show the spectra of the input signals. In addition to the $4dB$ loss due to the windowing process, previously described, the presence of many harmonic components can be noticed.

These components are due to the harmonic distortion of the amplifier employed for the input sound generation. However, their effectcan be safely neglected, being $50dB$ smaller than the fundamental.

Figures 5.35 and 5.36 and figs. 5.37 and 5.38 show the spectra of the sensor coil output voltages and displacements respectively.

In this case, one can notice a huge discrepancy between the measurements and the Simulink model simulation both in the sensor coil output voltage and the displacement. In particular, the model is always underestimating the harmonic components, with errors that reach $20dB$ in the sensor coil output simulation and $10dB$ in the displacement simulation, while the fundamental is much better modeled.

This is mainly attributed to the fact that, due to the extreme time variability of the loudspeaker, the used model parameters are not aligned with the exhibited loudspeaker behavior.

For any practical use of the proposed model, the exhibited differences are not neglectable, underlining the need of an adaptive algorithm to keep the model always aligned with the real device.

In the rest of this thesis, the described discrepancies are neglected assuming that the extracted parameters perfectly characterize the analyzed loudspeaker, keeping in mind that an adaptation algorithm will be required.

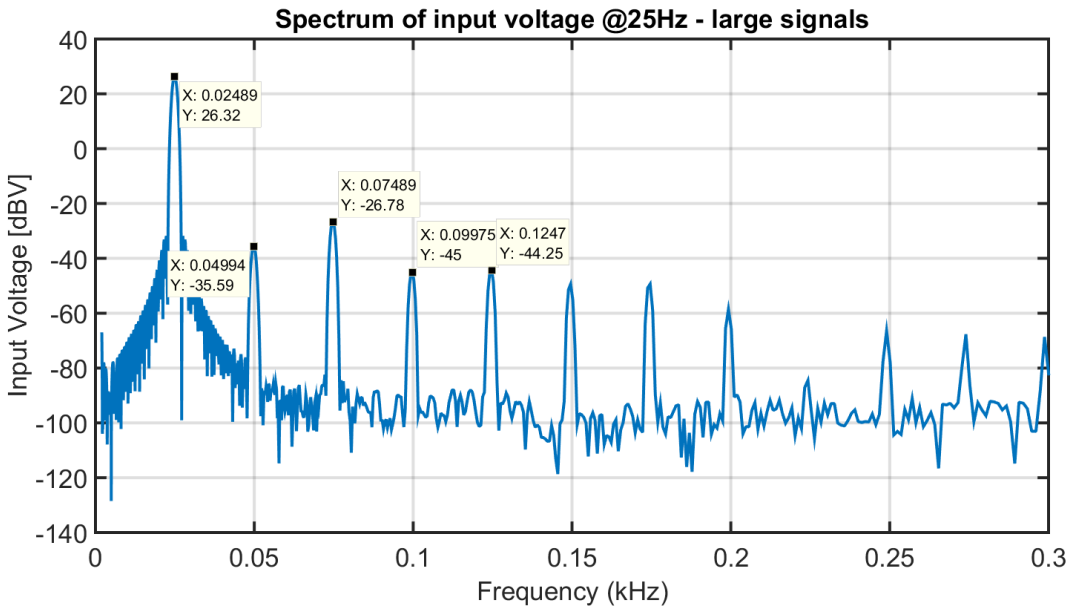

Figure 5.33: First input signal for the measurement of the output spectrum, 30dB @25Hz.

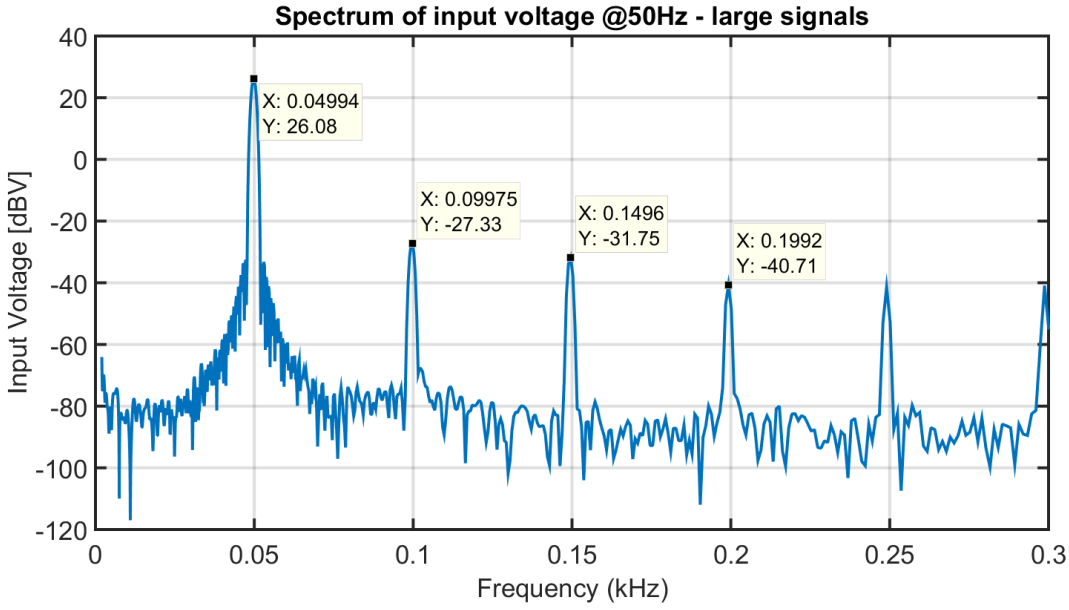

Figure 5.34: Second input signal for the measurement of the output spectrum, 30dB @50Hz

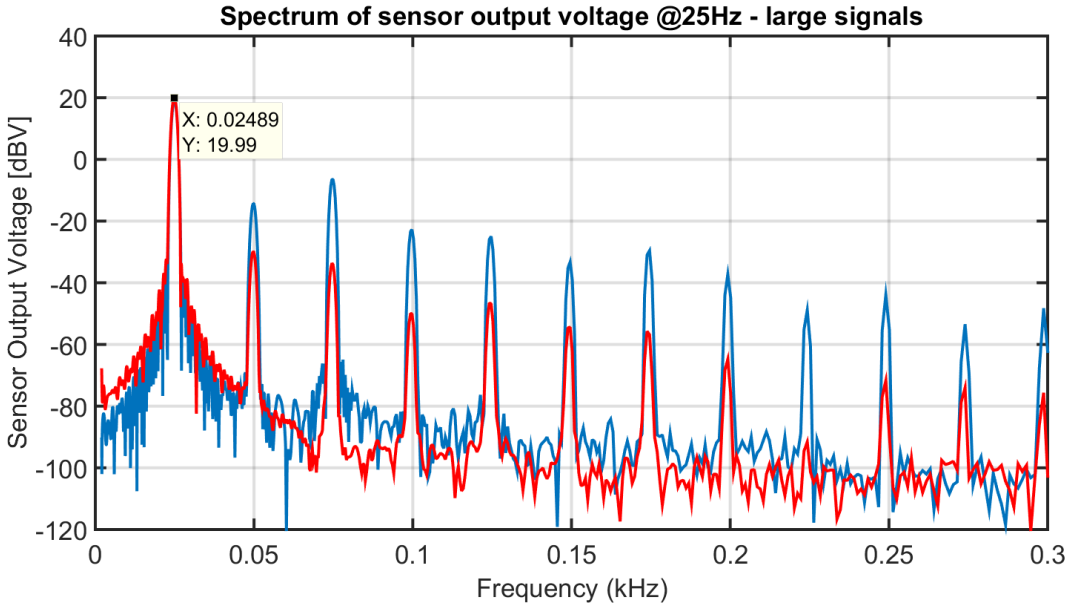

Figure 5.35: Output spectra of the sensor coil voltage @25Hz: blue) measured; red) model.

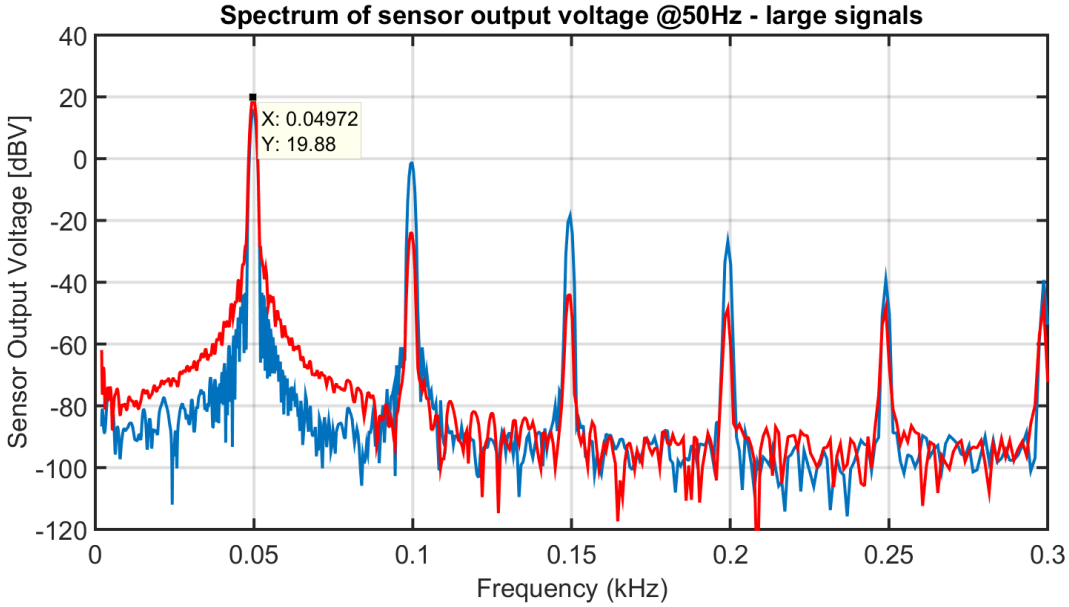

Figure 5.36: Output spectra of the sensor coil voltage @50Hz: blue) measured; red) model.

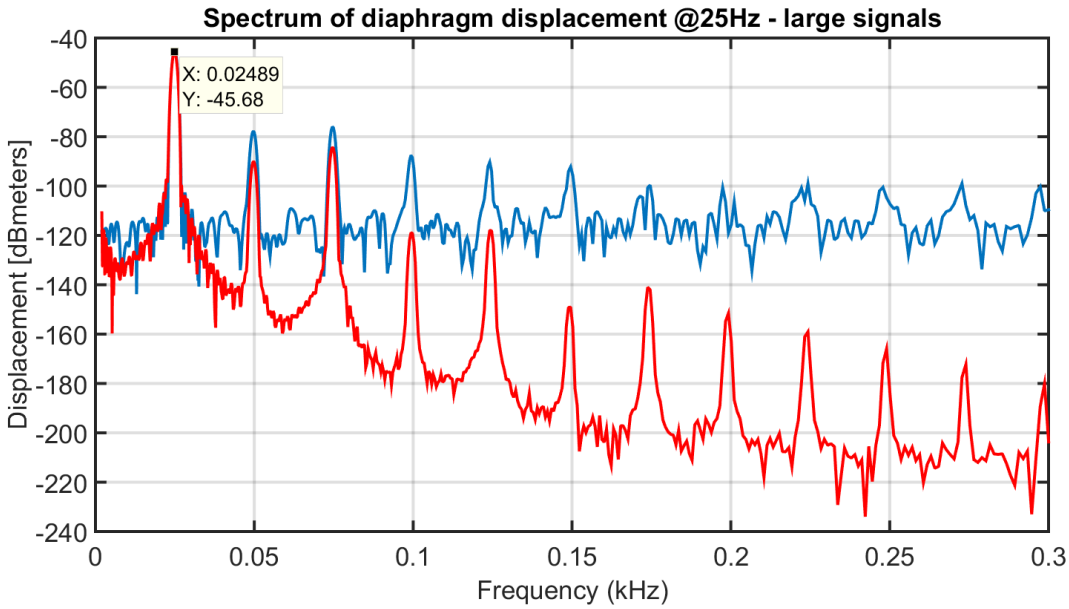

Figure 5.37: Output spectra of the displacement @25Hz: blue) measured; red) model.

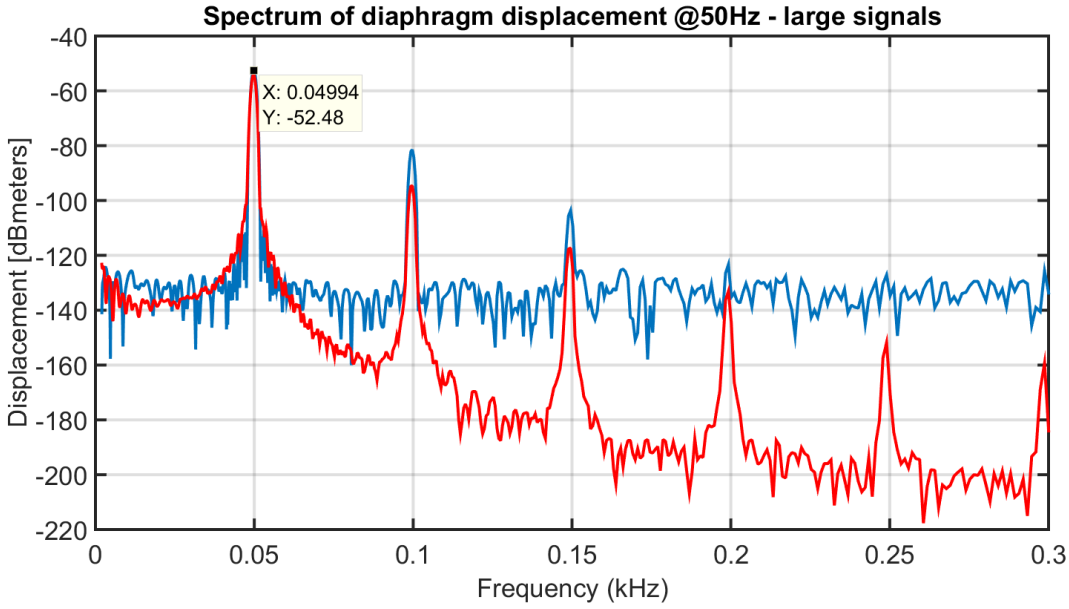

Figure 5.38: Output spectra of the displacement @50Hz: blue) measured; red) model.

Chapter 6

Control of the loudspeaker

The main purpose of this thesis is the design of a control system to compensate the nonlinearities exhibited by a loudspeaker in the large signals condition, which are the main cause of sound distortions in audio systems, and to control the dynamic of the linearized transducer, extending the desired working frequency range and shaping the frequency response function.

The controller here presented is specifically designed for the control of the device characterized in chapter 5, an RCF LF18X401 subwoofer loudspeaker, equipped with a secondary sensor coil. However, the same approach can also be employed for the control of similar, low frequency devices, such as woofers and mid-bass, provided they are equipped with a sensor coil.

The proposed controller is divided into two functional parts, the first dedicated to the compensation of the nonlinearities, implemented following the approach presented in section 2.1.3, while the second implements the dynamics control using a pole placement technique as described in section 2.2.

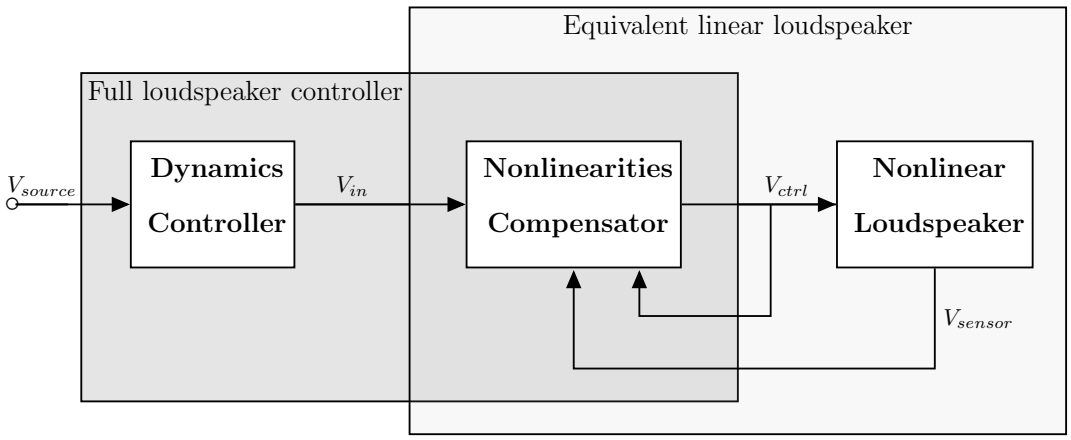

Figure 6.1: Block diagram of the proposed controller.

The two functionalities are interdependent, as the nonlinearities compensation is fundamental for the implementation of the dynamic control. In fact, the pole placement technique can only be applied to controllable LTI systems, while the loudspeaker, here considered in the large signals condition, is strongly nonlinear. The nonlinearities compensation, forcing the loudspeaker to act as linear system, enables the use of linear control techniques on the linearized transducer.

For the design of the controller, the target loudspeaker is considered as a nonlinear time-invariant system, described by the SIMO SS model of eq. (5.9), characterized by the parameters extracted in chapter 5 with the Distortion Analyzer.

In chapter 5 it has been shown that, due to the time varying behavior commonly exhibited by the loudspeakers, the adopted model is not accurate enough in the medium-long term, displaying significant differences between the simulations and the real device measurements. A possible solution is the introduction of an adaptation technique, allowing the model to cope with the real device time varying behavior by updating its parameters. This is not the purpose of this thesis and it is left for future works.

For the rest of the chapter it is assumed that the considered loudspeaker model and the extracted parameters perfectly characterize the real device. This condition corresponds to the use of a set of recently updated parameters.

Considering a possible implementation on a DSP, the controller has been designed and implemented in discrete-time form in MATLAB Simulink, considering a base sampling frequency $\mathbf{f_s} = 48000Hz$, a typical value employed for high quality audio signal processing, corresponding to a sampling time $\mathbf{T_s} = 20.8\overline{3}\mu sec$. The same environment has been used to evaluate the controller performances in the working bandwidth $25 - 200Hz$.

6.1 Compensation of the nonlinearities

The first part of the controller is the Nonlinearities Compensator, whose purpose is to produce a control signal $V_{ctrl}(k)$ capable of driving the controlled loudspeaker so as not to exhibit its nonlinear behaviors, forcing it to act as an equivalent linear loudspeaker driven by the input signal $V_{in}(k)$. This is achieved introducing a compensation signal $V_{comp}(k)$, such that:

$$V_{ctrl}(k) = V_{in}(k) + V_{comp}(k) \tag{6.1}$$

The nonlinearities compensator can be divided into three functional parts, as depicted in fig. 6.2: the compensation generator, the extended observer and the internal model.

The compensation generator implements the proposed compensation algorithm and produces the required compensation signal $V_{comp}(k)$. To fulfill this task, it exploits the estimate of the controlled loudspeaker state and other required variables, provided by the extended observer as an extended state $\mathbf{x_{ext}}(k)$, and the updated values of the nonlinear parameters of the controlled loudspeaker, provided by the internal model.

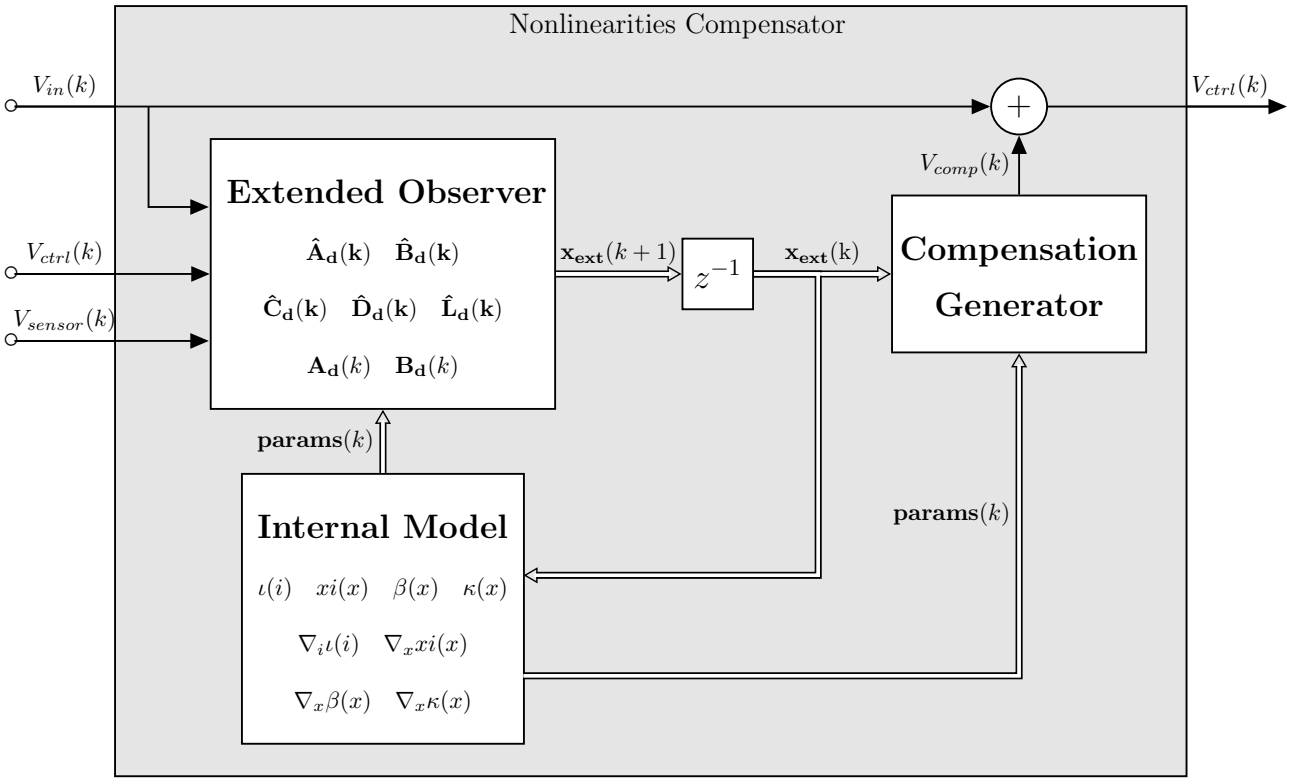

Figure 6.2: Block diagram of the proposed nonlinearities compensator.

The extended observer is used to estimate all the variables required by the compensation generator to implement the control algorithm. The estimated variables include the state of the controlled loudspeaker, the time derivative of the voice coil current of the controlled loudspeaker and the simulated state of the equivalent linear loudspeaker. The collection of those variables can be considered an extended state vector $\mathbf{x_{ext}}(k)$. It is estimated exploiting the information of the input signal $V_{in}(k)$, the control signal applied to loudspeaker $V_{ctrl}(k)$, the measurement of the sensor coil output signal $V_{sensor}(k)$, and the updated values of the nonlinear parameters of the controlled loudspeaker, provided by the internal model.

The internal model provides updated values of the nonlinear parameters of the controlled loudspeaker to the compensation generator and the extended observer. This is achieved by exploiting the controlled loudspeaker state estimate, provided by the extended observer, and the nonlinear dependency curves extracted with the Distortion Analyzer.

The compensation of the nonlinearities is designed considering the model of the loudspeaker sensor output, expressed through the nonlinear time invariant model:

$$\begin{aligned} \dot{\mathbf{x}}(t) &= \hat{\mathbf{A}}(\mathbf{x})\mathbf{x}(t) + \hat{\mathbf{B}}(\mathbf{x})u(t) = \mathbf{A}\mathbf{x}(t) + \mathbf{B}u(t) + \mathbf{a}(\mathbf{x})\mathbf{x}(t) + \mathbf{b}(\mathbf{x})u(t) \\ y(t) &= \hat{\mathbf{C}}(\mathbf{x})\mathbf{x}(t) + \hat{\mathbf{D}}(\mathbf{x})u(t) = \mathbf{C}\mathbf{x}(t) + \mathbf{D}u(t) + \mathbf{c}(\mathbf{x})\mathbf{x}(t) + \mathbf{d}(\mathbf{x})u(t) \end{aligned} \tag{6.2}$$

with:

$$\mathbf{x}(t) = \begin{bmatrix} i(t) & i_2(t) & x(t) & v(t) \end{bmatrix}^T \tag{6.3}$$

$$u(t) = V_{in}(t) \qquad y(t) = V_{sensor}(t) \tag{6.4}$$

and characterized by the following matrices:

$$\hat{\mathbf{A}}(\mathbf{x}) = \mathbf{A} + \mathbf{a}(\mathbf{x}) \qquad \hat{\mathbf{B}}(\mathbf{x}) = \mathbf{B} + \mathbf{b}(\mathbf{x}) \qquad \hat{\mathbf{C}}(\mathbf{x}) = \mathbf{C} + \mathbf{c}(\mathbf{x}) \qquad \hat{\mathbf{D}}(\mathbf{x}) = \mathbf{D} + \mathbf{d}(\mathbf{x}) \tag{6.5}$$

$$\mathbf{A} = \begin{bmatrix} -\dfrac{R_e + {R_2}^0}{{L_e}^0} & \dfrac{{R_2}^0}{{L_e}^0} & 0 & -\dfrac{{Bl}^0}{{L_e}^0} \\ \dfrac{{R_2}^0}{{L_2}^0} & -\dfrac{{R_2}^0}{{L_2}^0} & 0 & 0 \\ 0 & 0 & 0 & 1 \\ \dfrac{{Bl}^0}{M_{ms}} & 0 & -\dfrac{{K_{ms}}^0}{M_{ms}} & -\dfrac{R_{ms}}{M_{ms}} \end{bmatrix} \qquad \mathbf{B} = \begin{bmatrix} \dfrac{1}{{L_e}^0} \\ 0 \\ 0 \\ 0 \end{bmatrix} \tag{6.6}$$

$$\mathbf{C} = \begin{bmatrix} -{T_r}^0 R_e & 0 & 0 & ({Bl_s}^0 - {T_r}^0 {Bl}^0) \end{bmatrix} \qquad \mathbf{D} = \begin{bmatrix} {T_r}^0 \end{bmatrix}$$

$$\mathbf{a}(\mathbf{x}) = \begin{bmatrix} \dfrac{R_e[\xi(x)+\iota(i)] - \dfrac{\partial L_e(x,i)}{\partial t}}{{L_e}^0[1+\xi(x)+\iota(i)]} & 0 & 0 & \dfrac{Bl^0[1+\xi(x)+\iota(i)-\beta(x)]}{{L_e}^0[1+\xi(x)+\iota(i)]} \\ 0 & -\dfrac{\dfrac{\partial L_2(x,i)}{\partial t}}{{L_2}^0[1+\xi(x)+\iota(i)]} & 0 & 0 \\ 0 & 0 & 0 & 0 \\ \dfrac{Bl^0[\beta(x)-1]}{M_{ms}} & 0 & -\dfrac{{K_{ms}}^0(\kappa(x)-1)}{M_{ms}} & 0 \end{bmatrix}$$

$$\mathbf{b}(\mathbf{x}) = \begin{bmatrix} -\dfrac{\xi(t)+\iota(i)}{{L_e}^0[1+\xi(x)+\iota(i)]} \\ 0 \\ 0 \\ 0 \end{bmatrix}$$

$$\mathbf{c}(\mathbf{x}) = \begin{bmatrix} -{T_r}^0 R_e[\tau(x,i)-1] + \dfrac{\partial M(x,i)}{\partial t} - {T_r}^0\tau(x,i)\dfrac{\partial L_e(x,i)}{\partial t} \\ 0 \\ 0 \\ {Bl_s}^0[\beta_s(x)-1] - {T_r}^0 Bl^0[\tau(x,i)\beta(x)-1] \end{bmatrix}^T \tag{6.7}$$

$$\mathbf{d}(\mathbf{x}) = \left[{T_r}^0(\tau(x,i)-1)\right]$$

where:

$$\frac{\partial L_e(x,i)}{\partial t} = {L_e}^0\left[v(x)\nabla\xi(x) + \frac{\partial i(t)}{\partial t}\nabla\iota(i)\right] \tag{6.8}$$

$$\frac{\partial L_2(x,i)}{\partial t} = {L_2}^0\left[v(x)\nabla\xi(x) + \frac{\partial i(t)}{\partial t}\nabla\iota(i)\right] \tag{6.9}$$

$$\frac{\partial M(x,i)}{\partial t} = M^0 v(x)\nabla\xi(x) = \sqrt{{L_e}^0{L_s}^0}\,v(x)\nabla\xi(x) \tag{6.10}$$

In the considered model, the time derivative of the mutual inductance $M(x,i)$ has been approximated as described in section 4.3.1, neglecting the current contribution.

The parameters of the model have been extracted with the Distortion Analyzer and are summarized in section 5.2.1.

6.1.1 The compensation generator

The nonlinearities compensation has been developed analytically, exploiting the continuous-time characteristic equations of the nonlinear time invariant loudspeaker of eq. (3.34). The discrete-time control signal has been derived through the discretization of the defined continuous-time control signal.

The compensation algorithm has been designed to cancel the effects of the three main nonlinear behaviors exhibited by the loudspeakers, described in chapter 3: the mechanical stiffness dependency on the displacement, the force factor dependency on the displacement and the electric inductance dependency on the displacement and on current.

The algorithm has been developed defining the linearization constraints for each part of the loudspeaker, one at a time. First, the sole mechanical domain is considered. Then the electromechanical transduction is added and finally also the electric domain.

At each step, the specific driving quantity (force, current and voltage) of the considered loudspeaker parts has been designed to force the ideal, linear behavior of the device.

Compensation of the mechanical domain: Kms(x)

The first step aims at the compensation of the nonlinearities of the sole mechanical system, thus at the linearization of the nonlinear behavior of the mechanical stiffness $K_{ms}(x)$.

The mechanical domain characteristic equations of the real, nonlinear loudspeaker and the ideal, linear loudspeaker are shown in eq. (6.11).

$$\begin{cases} F_{NL}(x_{NL},t) = M_{ms}\dfrac{\partial^2 x_{NL}(t)}{\partial t^2} + R_{ms}\dfrac{\partial x_{NL}(t)}{\partial t} + K_{ms}(x_{NL})x_{NL}(t) \\ \\ F_{LIN}(t) = M_{ms}\dfrac{\partial^2 x_{LIN}(t)}{\partial t^2} + R_{ms}\dfrac{\partial x_{LIN}(t)}{\partial t} + {K_{ms}}^0 x_{LIN}(t) \end{cases} \tag{6.11}$$

The driving quantity of the mechanical domain is the force $F_{NL}(x_{NL},t)$, exerted on the real, nonlinear loudspeaker mechanical system.

The target of the compensation is to force the real, nonlinear loudspeaker to exhibit the same motion of the ideal, linear loudspeaker. This leads to the following constraints:

$$\begin{gathered} \frac{\partial^2 x_{NL}(t)}{\partial t^2} = \frac{\partial^2 x_{LIN}(t)}{\partial t^2} = \frac{\partial^2 x(t)}{\partial t^2} \\ \frac{\partial x_{NL}(t)}{\partial t} = \frac{\partial x_{LIN}(t)}{\partial t} = \frac{\partial x(t)}{\partial t} \\ x_{NL}(t) = x_{LIN}(t) = x(t) \end{gathered} \tag{6.12}$$

The required driving force $F_{NL}(x_{NL}, t)$ that satisfies the constraints of eq. (6.12) is found subtracting the two equations in eq. (6.11).

$$\begin{aligned} F_{NL}(x,t) &= F_{LIN}(t) + K_{ms}(x)x(t) - {K_{ms}}^0 x(t) \\ &= F_{LIN}(t) + {K_{ms}}^0(\kappa(x) - 1)x(t) \\ &= F_{LIN}(t) + F_{comp}(x,t) \end{aligned} \tag{6.13}$$

The compensation of the mechanical system nonlinearities requires the exertion of an additional compensation force $F_{comp}(x, t)$:

$$F_{comp}(x,t) = {K_{ms}}^0[\kappa(x) - 1]x(t) \tag{6.14}$$

The compensation force $F_{comp}(x, t)$ exhibit a displacement dependent behavior that follows the nonlinear stiffness dependency curve $\kappa(x)$, compensating for the variation of the mechanical stiffness.

At large displacements, the loudspeaker suspensions become stiffer and hamper the diaphragm motion introducing distortion. The additional compensation force overdrives the diaphragm, allowing it to move as if the mechanical stiffness of the loudspeaker were linear.

Compensation of the electromechanical transduction: Bl(x) and Kms(x)

The second step aims at the compensation of the nonlinearities of the system composed by the electric motor and the mechanical domain, thus at the simultaneous linearization of the nonlinear behaviors of the force factor $Bl(x)$ and the mechanical stiffness $K_{ms}(x)$.

The electromechanical transduction characteristic equations of the real, nonlinear loudspeaker and the ideal, linear loudspeaker are shown in eq. (6.15).

$$\begin{cases} F_{NL}(x,t) = Bl(x)\ i_{NL}(x,t) \\ \\ F_{LIN}(t) = Bl^0\ i_{LIN}(t) \end{cases} \tag{6.15}$$

The electromechanical transduction driving quantity is the current $i_{NL}(x, t)$, applied to the real, nonlinear loudspeaker electric motor.

The compensation of the mechanical stiffness nonlinearity is fulfilled considering eq. (6.13) as a constraint. The required driving current $i_{NL}(x,t)$ that achieves the linearization of both the mechanical stiffness and the force factor is then found subtracting the two equations in eq. (6.15).

$$\begin{aligned} i_{NL}(x,t) &= \frac{Bl^0\, i_{LIN}(t) + F_{NL}(x,t) - F_{LIN}(t)}{Bl(x)} \\ &= \frac{Bl^0\, i_{LIN}(t) + {K_{ms}}^0[\kappa(x)-1]x(t)}{Bl(x)} \\ &= \frac{1}{\beta(x)}\, i_{LIN}(t) + \frac{{K_{ms}}^0}{Bl^0}\frac{[\kappa(x)-1]}{\beta(x)}\, x(t) \end{aligned} \tag{6.16}$$

The driving current $i_{NL}(x,t)$ is composed by two contributions, one proportional to the ideal, desired current $i_{LIN}(t)$ and one proportional to the displacement $x(t)$.

The first contribution exhibit a displacement dependent behavior that follows the nonlinear force factor dependency curve $\beta(x)$, compensating for the variation of the force factor.

At large displacements, the magnetic field in which the voice coil is immersed quickly decays, reducing the generated driving force and introducing distortion. The factor $\frac{1}{\beta(x)}$ increases the driving current to compensate for the force factor decay.

The second contribution corresponds to the additional control force F_{comp} introduced in section 6.1.1 for the compensation of the mechanical stiffness nonlinearity, compensated in turn to account for the force factor decay.

The electromechanical transduction is also characterized by a second equation that affects the electric domain, here reported for the real, nonlinear loudspeaker and for the ideal, linear loudspeaker:

$$\begin{cases} V_{emf_{NL}}(x,t) = Bl(x)\,\dfrac{\partial x(t)}{\partial t} \\ \\ V_{emf_{LIN}}(t) = Bl^0\,\dfrac{\partial x(t)}{\partial t} \end{cases} \tag{6.17}$$

Those equations will be exploited in the next subsection.

The full compensation algorithm: Le(x,i), Bl(x) and Kms(x)

The third step aims at the full compensation of the nonlinearities of the loudspeaker system, composed by the electric domain, the electric motor and the mechanical domain, thus at the simultaneous linearization of the nonlinear behaviors of the electric inductance $L_e(x,i)$, the force factor $Bl(x)$ and the mechanical stiffness $K_{ms}(x)$.

The electric domain characteristic equations of the real, nonlinear loudspeaker and the ideal, linear loudspeaker are shown in eq. (6.18).

$$\begin{cases} V_{in_{NL}}(t) - V_{emf_{NL}}(x,t) = R_e i_{NL}(t) + \dfrac{\partial L_e(x, i_{NL}) i_{NL}(t)}{\partial t} \\ \qquad\qquad + R_2(x, i_{NL}) i_{NL}(t) - R_2(x, i_{NL}) i_{2_{NL}}(t) \\ V_{in_{LIN}}(t) - V_{emf_{LIN}}(t) = R_e i_{LIN}(t) + L_e^0 \dfrac{\partial i_{LIN}(t)}{\partial t} \\ \qquad\qquad + R_2^0 i_{LIN}(t) - R_2^0 i_{2_{LIN}}(t) \end{cases} \tag{6.18}$$

The electric domain driving quantity is the voltage $V_{in_{NL}}(t)$ applied to the real loudspeaker voice coil, while the voltage $V_{in_{LIN}}(t)$ is the driving voltage of the equivalent ideal, linear loudspeaker. This means that:

$$\begin{cases} V_{in_{NL}}(t) = V_{ctrl}(t) \\ V_{in_{LIN}}(t) = V_{in}(t) \end{cases} \tag{6.19}$$

The compensation of the mechanical stiffness nonlinearity and the force factor nonlinearity is fulfilled considering eqs. (6.16) and (6.17) as a constraint. The required driving voltage $V_{in_{NL}}(t)$ that achieves the linearization of the loudspeaker is then found subtracting the two equations in eq. (6.18).

$$\begin{aligned} V_{in_{NL}}(t) =& V_{in_{LIN}}(t) + V_{emf_{NL}}(x,t) - V_{emf_{LIN}}(t) + R_e i_{NL}(t) - R_e i_{LIN}(t) \\ &+ L_e(x, i_{NL}) \frac{\partial i_{NL}(t)}{\partial t} + \frac{\partial L_e(x, i_{NL})}{\partial t} i_{NL}(t) - L_e^0 \frac{\partial i_{LIN}(t)}{\partial t} \\ &+ R_2(x, i_{NL}) i_{NL}(t) - R_2^0 i_{LIN}(t) - R_2(x, i_{NL}) i_{2_{NL}}(t) + R_2^0 i_{2_{LIN}}(t) \end{aligned} \tag{6.20}$$

$$\begin{aligned} V_{in_{NL}}(t) = & V_{in_{LIN}}(t) \\ & + \left[R_e + R_2(x, i_{NL}) + \frac{\partial L_e(x, i_{NL})}{\partial t} \right] i_{NL}(t) \\ & - R_2(x, i_{NL}) i_{2_{NL}}(t) \\ & + L_e(x, i_{NL}) \frac{\partial i_{NL}(t)}{\partial t} \\ & - [R_e + R_2^0] i_{LIN}(t) \\ & + R_2^0 i_{2_{LIN}}(t) \\ & - L_e^0 \frac{\partial i_{LIN}(t)}{\partial t} \\ & + [Bl(x) - Bl^0] \frac{\partial x(t)}{\partial t} \end{aligned} \tag{6.21}$$

Recalling the constraint of eq. (6.16), all the instances of $i_{LIN}(t)$ and can be expressed in terms of $i_{NL}(x,t)$ and $x(t)$.

$$i_{LIN}(t) = \beta(x) i_{NL}(x,t) - \frac{{K_{ms}}^0}{Bl^0}[\kappa(x) - 1]\, x(t) \tag{6.22}$$

$$\frac{\partial i_{LIN}(t)}{\partial t} = \beta(x)\frac{\partial i_{NL}(x,t)}{\partial t} + \frac{\partial \beta(x)}{\partial t} i_{NL}(x,t) - \frac{{K_{ms}}^0}{Bl^0}\left[\frac{\partial \kappa(x)}{\partial t} x(t) + [\kappa(x) - 1]\frac{\partial x(t)}{\partial t}\right] \tag{6.23}$$

Therefore, the equation for the voltage compensation is the following:

$$\begin{aligned}
V_{in_{NL}}(t) =& V_{in_{LIN}}(t) + V_{comp}(t) \\
=& V_{in_{LIN}}(t) \\
&+ \left[R_e - Re\beta(x) + R_2(x, i_{NL}) - R_2^0\beta(x) + \frac{\partial L_e(x, i_{NL})}{\partial t} - {L_e}^0\frac{\partial \beta(x)}{\partial t}\right] i_{NL}(t) \\
&- R_2(x, i_{NL}) i_{2_{NL}}(t) \\
&+ [L_e(x, i_{NL}) - {L_e}^0\beta(x)]\frac{\partial i_{NL}(t)}{\partial t} \\
&+ R_2^0 i_{2_{LIN}}(t) \\
&+ \left[Bl(x) - Bl^0 + {L_e}^0\frac{{K_{ms}}^0}{Bl^0}[\kappa(x) - 1]\right]\frac{\partial x(t)}{\partial t} \\
&+ \left[{L_e}^0\frac{{K_{ms}}^0}{Bl^0}\frac{\partial \kappa(x)}{\partial t} + \frac{{K_{ms}}^0}{Bl^0}[\kappa(x) - 1]({R_e} + {R_2}^0)\right] x(t)
\end{aligned} \tag{6.24}$$

Recalling eq. (6.19) and expressing all the nonlinear parameters as a function of the extracted nonlinear dependency curves, the expression of the voltage compensation is the following:

$$\begin{aligned}
V_{ctrl}(t) =& V_{in}(t) + V_{comp}(t) \\
=& V_{in}(t) \\
&+ \left[R_e[1 - \beta(x)] + R_2[1 + \iota(i) + \xi(x) - \beta(x)] + {L_e}^0\left[\frac{\partial \iota(i)}{\partial t} + \frac{\partial \xi(x)}{\partial t} - \frac{\partial \beta(x)}{\partial t}\right]\right] i_{NL}(t) \\
&- {R_2}^0[1 + \iota(i) + \xi(x)] i_{2_{NL}}(t) \\
&+ {L_e}^0[\iota(i) + \xi(x) - \beta(x)]\frac{\partial i_{NL}(t)}{\partial t} \\
&+ R_2^0 i_{2_{LIN}}(t) \\
&+ \left[Bl^0[\beta(x) - 1] + {L_e}^0\frac{{K_{ms}}^0}{Bl^0}[\kappa(x) - 1]\right]\frac{\partial x(t)}{\partial t} \\
&+ \left[{L_e}^0\frac{{K_{ms}}^0}{Bl^0}\frac{\partial \kappa(x)}{\partial t} + \frac{{K_{ms}}^0}{Bl^0}[\kappa(x) - 1]({R_e} + {R_2}^0)\right] x(t)
\end{aligned} \tag{6.25}$$

Finally, applying the time discretization:

$$
\begin{aligned}
V_{ctrl}(k) &= V_{in}(k) + V_{comp}(k) \\
&= V_{in}(k) \\
&+ \left[R_e[1-\beta(x)] + R_2[1+\iota(i)+\xi(x)-\beta(x)] + {L_e}^0 \left[\frac{\partial \iota(i)}{\partial k} + \frac{\partial \xi(x)}{\partial k} - \frac{\partial \beta(x)}{\partial k} \right] \right] i_{NL}(k) \\
&- {R_2}^0[1+\iota(i)+\xi(x)] i_{2_{NL}}(k) \\
&+ {L_e}^0[\iota(i)+\xi(x)-\beta(x)] \frac{\partial i_{NL}(k)}{\partial k} \\
&+ R_2^0 i_{2_{LIN}}(k) \\
&+ \left[Bl^0[\beta(x)-1] + {L_e}^0 \frac{{K_{ms}}^0}{Bl^0}[\kappa(x)-1] \right] v(k) \\
&+ \left[{L_e}^0 \frac{{K_{ms}}^0}{Bl^0} \frac{\partial \kappa(x)}{\partial t} + \frac{{K_{ms}}^0}{Bl^0}[\kappa(x)-1](R_e + {R_2}^0) \right] x(k)
\end{aligned}
\tag{6.26}
$$

The compensation generator has been implemented to produce the compensation signal $V_{comp}(k)$ according to eq. (6.26), exploiting the extended state $\mathbf{x_{ext}}(k)$ provided by the extended observer.

In fact, $V_{comp}(k)$ depends not only on the controlled loudspeaker state, but also on the current related to the LR-2 model of the equivalent linear loudspeaker $i_{2_{LIN}}(k)$ and the time derivative of the voice coil current of the real, nonlinear loudspeaker $\frac{\partial i_{NL}(k)}{\partial k}$. All the other parameters and the relative derivatives are provided by the internal model component.

The designed controller output $V_{ctrl}(k)$ drives the real, nonlinear loudspeaker compensating all the considered nonlinearities and forcing it to exhibit a motional behavior identical to that of an ideal, linear transducer driven by the voltage $V_{in}(k)$.

6.1.2 The extended observer

The extended observer provides the compensation generator and the internal model with updated estimates of the extended state $\mathbf{x_{ext}}(k)$.

$$\mathbf{x_{ext}}(k) = \begin{bmatrix} i_{NL}(k) \\ i_{2_{NL}}(k) \\ x_{NL}(k) \\ v_{NL}(k) \\ \dfrac{i_{NL}(k)}{\partial k} \\ i_{LIN}(k) \\ i_{2_{LIN}}(k) \\ x_{LIN}(k) \\ v_{LIN}(k) \end{bmatrix} = \begin{bmatrix} \mathbf{x}(k) \\ \dfrac{i_{NL}(k)}{\partial k} \\ \mathbf{x_{LIN}}(k) \end{bmatrix} \tag{6.27}$$

The defined extended state includes the controlled loudspeaker state $\mathbf{x}(k)$, the derivative of the current of the controlled loudspeaker voice coil $\frac{i_{NL}(k)}{\partial k}$ and the state of the equivalent linear loudspeaker $\mathbf{x_{LIN}}(k)$.

As already explained in section 6.1.1, the compensation algorithm requires more information than the controlled loudspeaker state alone, and the extended observer is used to estimate all the required variables.

The extended observer is mainly composed by two parallel observers: a nonlinear observer for the estimation of the nonlinear loudspeaker state $\mathbf{x}(k)$, and a linear open-loop observer for the estimation of the state $\mathbf{x_{LIN}}(k)$ of the target linear loudspeaker.

It is important to remark that the open-loop linear observer is not a proper observer, since it does not exploit any measurement of the plant to estimate the state vector. However, it will be denoted as "linear observer" since this is its role in the controller.

The derivative of the nonlinear loudspeaker voice coil current is estimated from the controlled loudspeaker state $\mathbf{x}(k)$.

The nonlinear observer

The employed nonlinear observer is based on a nonlinear version of the Luenberger observer, presented in its continuous-time form in section 2.3.

The proposed nonlinear observer estimates the state of a nonlinear time invariant plant locally applying the linear Luenberger observer theory. This can be achieved by periodically updating the observer internal model with an updated linear approximation of the plant behavior.

If the update speed of the observer internal model is sufficient to effectively track the nonlinear plant behavior and if the locally linear models approximating the plant behavior preserve the observability property, then the linear Luenberger observer theory can still be applied locally.

The described nonlinear observer can be considered as a linear time varying Luenberger observer characterized by the state equation:

$$\dot{\hat{\mathbf{x}}}(t) = \hat{\mathbf{A}}(\mathbf{t})\hat{\mathbf{x}}(t) + \hat{\mathbf{B}}(t)u(t) + \mathbf{L}(t)[y(t) - (\hat{\mathbf{C}}(\mathbf{t})\hat{\mathbf{x}}(t) + \hat{\mathbf{D}}(t)u(t))] \tag{6.28}$$

where the matrices $\hat{\mathbf{A}}(t)$, $\hat{\mathbf{B}}(t)$, $\hat{\mathbf{C}}(t)$ and $\hat{\mathbf{D}}(t)$ are the SS representation matrices of the locally linearized model of the plant at time t, defined in eq. (2.28), and the vector $\hat{\mathbf{L}}(t)$ is the time varying observer feedback gain vector defined in eq. (2.29).

The nonlinear observer of the considered nonlinear loudspeaker is:

$$\dot{\hat{\mathbf{x}}}(t) = \hat{\mathbf{A}}(\mathbf{t})\hat{\mathbf{x}}(t) + \hat{\mathbf{B}}(t)V_{in}(t) + \mathbf{L}(t)[V_{sensor}(t) - (\hat{\mathbf{C}}(\mathbf{t})\hat{\mathbf{x}}(t) + \hat{\mathbf{D}}(t)V_{in}(t))] \tag{6.29}$$

characterized by the matrices of eqs. (6.5) to (6.7).

The observer requires the time interval $\mathbf{T_{up}}$ between the internal model updates to be sufficiently small to guarantee the validity of the locally linearized models used for the state estimation. This is largely ensured using an updating period equal to the considered signal sampling time $\mathbf{T_{up}} = \mathbf{T_s}$.

It is also required that all the linear models used to locally approximate the loudspeaker nonlinear behavior preserve the observability property. This can be considered true during normal working conditions of the loudspeaker.

In fact, the nonlinear loudspeaker model at rest ($\mathbf{x} = 0$) is observable from the sensor output:

$$rank(\mathcal{O}) = rank\left(\begin{bmatrix} \hat{\mathbf{C}}(\mathbf{0}) \\ \hat{\mathbf{C}}(\mathbf{0})\hat{\mathbf{A}}(\mathbf{0}) \\ \hat{\mathbf{C}}(\mathbf{0})\hat{\mathbf{A}}(\mathbf{0})^2 \\ \hat{\mathbf{C}}(\mathbf{0})\hat{\mathbf{A}}(\mathbf{0})^3 \end{bmatrix}\right) = rank\left(\begin{bmatrix} \mathbf{C} \\ \mathbf{CA} \\ \mathbf{CA}^2 \\ \mathbf{CA}^3 \end{bmatrix}\right) = 4 \tag{6.30}$$

During normal working conditions the parameters of the matrices $\hat{\mathbf{C}}(\mathbf{x})$ and $\hat{\mathbf{A}}(\mathbf{x})$ are subjected to variations due to the nonlinearities, possibly leading to the loss of the observability. However, preliminary simulations of the nonlinear model demonstrated that the instantaneous observability and controllability properties are preserved in the large signals condition. This allows the local application of the linear Luenberger observer theory.

The observer is implemented in discrete-time form, by way of the discretization of eq. (6.29):

$$\hat{\mathbf{x}}(k+1) = \hat{\mathbf{A}}_\mathbf{d}(\mathbf{k})\hat{\mathbf{x}}(k)+\hat{\mathbf{B}}_\mathbf{d}(k)V_{ctrl}(k)+\mathbf{L_d}(k)[V_{sensor}(k)-(\hat{\mathbf{C}}_\mathbf{d}(k)\hat{\mathbf{x}}(k)+\hat{\mathbf{D}}_\mathbf{d}(k)V_{ctrl}(k))] \tag{6.31}$$

where:

$$\hat{\mathbf{A}}_\mathbf{d}(k) = e^{\hat{\mathbf{A}}(\mathbf{t})\mathbf{T_s}} \qquad \hat{\mathbf{B}}_\mathbf{d}(k) = \int_0^{T_s} \hat{\mathbf{B}}(t)e^{\hat{\mathbf{A}}(t)t}dt = \hat{\mathbf{A}}(t)^{-1}(\hat{\mathbf{A}}_\mathbf{d}(\mathbf{k}) - \mathbf{I})\hat{\mathbf{B}}(t)$$

$$\hat{\mathbf{C}}_\mathbf{d}(k) = \hat{\mathbf{C}}(\mathbf{t}) \qquad \hat{\mathbf{D}}_\mathbf{d}(k) = \hat{\mathbf{D}}(\mathbf{t}) \tag{6.32}$$

The discrete time observer feedback gain $\mathbf{L_d}(\mathbf{k})$ is again defined through Ackermann's formula:

$$\mathbf{L_d}(k) = \alpha_e(\hat{\mathbf{A}}_\mathbf{d}(k), k)\mathcal{O}^{-1}(k)\begin{bmatrix}0\\0\\0\\1\end{bmatrix} \tag{6.33}$$

where $\mathcal{O}(k)$ is the instantaneous observability matrix of the linearized model of the loudspeaker:

$$\mathcal{O}(k) = \begin{bmatrix}\hat{\mathbf{C}}_\mathbf{d}(k)\\ \hat{\mathbf{C}}_\mathbf{d}(k)\hat{\mathbf{A}}_\mathbf{d}(k)\\ \hat{\mathbf{C}}_\mathbf{d}(k)\hat{\mathbf{A}}_\mathbf{d}(k)^2\\ \hat{\mathbf{C}}_\mathbf{d}(k)\hat{\mathbf{A}}_\mathbf{d}(k)^3\end{bmatrix} \tag{6.34}$$

and $\alpha_e(\hat{\mathbf{A}_\mathbf{d}}(k), k)$ is the instantaneous characteristic polynomial of the desired closed loop matrix $(\hat{\mathbf{A}_\mathbf{d}}(k) - \mathbf{L_d}(k)\hat{\mathbf{C_d}}(t))$, solved for $\hat{\mathbf{A}_\mathbf{d}}(k)$.

The matrices $\hat{\mathbf{A}}_\mathbf{d}(k)$,$\hat{\mathbf{B}}_\mathbf{d}(k)$,$\hat{\mathbf{C}}_\mathbf{d}(k)$ and $\hat{\mathbf{D}}_\mathbf{d}(k)$, and the feedback gain vector $\mathbf{L_d}(k)$ are periodically computed by the extended observer using the updated information provided by the internal model.

The feedback gain vector can be designed to assign the local closed loop poles of the observer to fixed values, despite the time variance of the loudspeaker, or to adapt their placement to follow the evolution of the nonlinear loudspeaker poles and zeros.

Preliminary simulations of the nonlinear loudspeaker in the large signals condition have been performed to evaluate the evolution in time of its instantaneous poles and zeros. Figures 6.3 and 6.4 show the result for a $25Hz$ sinusoid at $+30dBV$, which is the simulated scenario that caused the most significant variations. While the zeros can be considered pretty much fixed, the poles are subject to large variations, some being shifted to more than twice the respective value at rest.

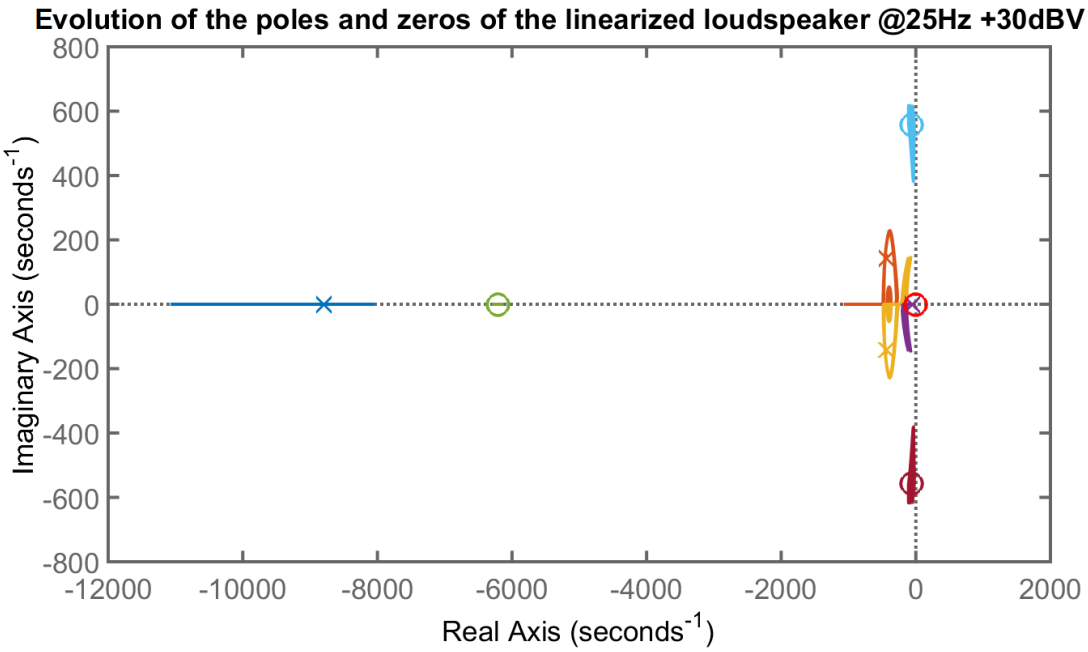

Figure 6.3: Evolution of the instantaneous poles and zeroes of the nonlinear loudspeaker.

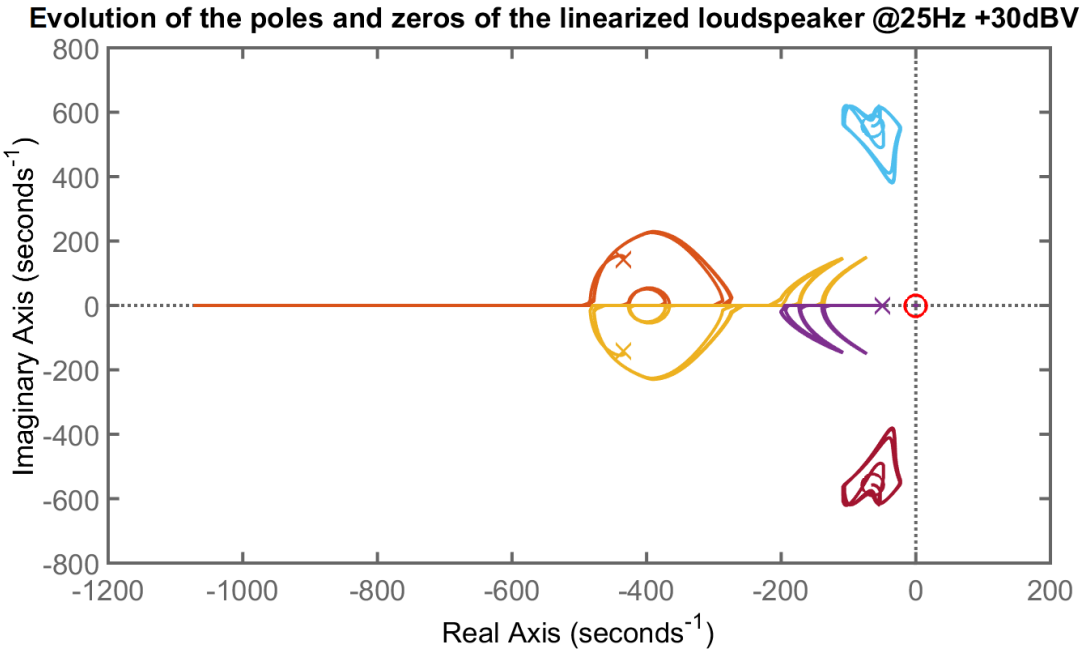

Figure 6.4: Detail of the evolution of the instantaneous poles and zeroes of the nonlinear loudspeaker.

When the plant model is subject to uncertainty, as in this case due to the plant time variance, it is common practice to place the observer closed loop poles near the plant zeros. This practice limits the contribution of the estimation error to the observer state estimate and consequently the responsiveness of the observer.

A faster observer response can be obtained designing its closed loop poles faster than the instantaneous poles of the loudspeaker. However, this may lead to instability if the poles are too fast, due to the overaggressive correction of the estimation error.

The extended observer must be provided with the desired closed loop poles values p_n or, equivalently, with the relative coefficients of the closed loop matrix characteristic polynomial c_n.

$$\begin{gathered}\alpha_e(\lambda) = \lambda^4 + \lambda^3 c_1 + \lambda^2 c_2 + \lambda c_3 + \mathbf{I} c_4 = (\lambda - p_1)(\lambda - p_2)(\lambda - p_3)(\lambda - p_4) \\ c_1 = -p_1 - p_2 - p_3 - p_4 \\ c_2 = p_1 p_2 + p_1 p_3 + p_1 p_4 + p_2 p_3 + p_2 p_4 + p_3 p_4 \\ c_3 = -p_1 p_2 p_3 - p_1 p_2 p_4 - p_1 p_3 p_4 - p_2 p_3 p_4 \\ c_4 = p_1 p_2 p_3 p_4\end{gathered} \tag{6.35}$$

The extended observer periodically computes the feedback gain vector $\mathbf{L_d}(k)$ through Ackermann's formula of eq. (6.33), using the updated information provided by the internal model, adapting its dynamics to the nonlinear loudspeaker instantaneous poles.

Alternatively, the extended observer can be designed to automatically calculate the optimal closed loop poles from the information provided by the internal model, adapting them to the nonlinear loudspeaker behavior. A simple strategy is to adapt the discrete-time closed loop poles of the observer enforcing a constant proportion between the equivalent continuous-time closed loop poles of the observer and the instantaneous poles of the loudspeaker.

Since the nonlinear loudspeaker has been proved to be controllable and observable in the considered large signals conditions, its instantaneous poles coincide with the eigenvalues of the matrix $\hat{\mathbf{A}}(t)$, that can be estimated with the information provided by the internal model.

The relative discrete-time closed loop poles of the observer are computed as follows:

$$p_{1:4}^{discrete} = e^{p_{1:4}^{continuous} T_s} = e^{m\ eig[\hat{\mathbf{A}}(t)] T_s} \tag{6.36}$$

where m is the chosen proportion factor between the poles.

Once the updated values of the closed loop poles have been computed, the computation of the feedback gain vector is identical to the fixed poles case.

The time derivative of the current of the controlled loudspeaker voice coil is estimated exploiting the continuous time definition of the current derivative of eq. (3.36), applying it to the discrete time state estimate of the controlled loudspeaker $\mathbf{x}(k)$ and the control signal $V_{control}(k)$.

$$\frac{\partial i_{NL}(k)}{\partial k} = \frac{V_{ctrl}(k) - \left[R_e + R_2(x, i_{NL}) + \dfrac{\partial L_e(x, i_{NL})}{\partial k}\right] i_{NL}(k) + R_2(x, i_{NL}) i_{2_{NL}}(k) - Bl(x)\, v(k)}{L_e(x, i_{NL})} \tag{6.37}$$

The internal model provides the extended observer with all the required information to compute vector $\mathbf{J}(\mathbf{k})$:

$$\mathbf{J}(k) = \begin{bmatrix} -\dfrac{R_e + R_2(x, i_{NL}) + \dfrac{\partial L_e(x, i_{NL})}{\partial k}}{L_e(x, i_{NL})} \\ \\ \dfrac{R_2(x, i_{NL})}{L_e(x, i_{NL})} \\ \\ 0 \\ \\ -\dfrac{Bl(x)}{L_e(x, i_{NL})} \\ \\ \dfrac{1}{L_e(x, i_{NL})} \end{bmatrix}^T \tag{6.38}$$

such that:

$$\frac{\partial i_{NL}(k)}{\partial k} = \mathbf{J}(k) \begin{bmatrix} \mathbf{x}(k) \\ \\ V_{ctrl}(k) \end{bmatrix} \tag{6.39}$$

It is important to notice that there exists an algebraic loop between the controller output voltage $V_{ctrl}(k)$ and the estimated current derivative $\frac{\partial i_{NL}(k)}{\partial k}$.

However, the chosen sampling time is sufficiently small to consider the current derivative almost constant between two subsequent samples, so that the algebraic loop can be solved introducing a one-sample delay, thus approximating the estimate of the current derivative at time k with the estimate at time $k-1$.

The linear observer

The linear observer is used to estimate the state of the equivalent linear loudspeaker driven by the input signal $V_{in}(k)$. Such loudspeaker is modeled in SS form by the matrices **A**, **B**, **C**, **D** of eq. (6.6).

The state of the ideal, linear loudspeaker is estimated with a discrete-time open loop observer:

$$\mathbf{x_{LIN}}(k+1) = \mathbf{A_d}\mathbf{x_{LIN}}(k) + \mathbf{B_d}V_{in}(k) \tag{6.40}$$

where:

$$\mathbf{A_d} = e^{\mathbf{A}\mathbf{T_s}} \qquad \mathbf{B_d} = \int_0^{T_s} e^{\mathbf{A}t}\,\mathbf{B}\,dt = \mathbf{A}^{-1}(\mathbf{A_d} - \mathbf{I})\mathbf{B} \tag{6.41}$$

6.1.3 The internal model

The internal model provides the updated values of the controlled loudspeaker nonlinear parameters and their relative time derivatives to the compensation generator and the extended observer, exploiting the estimated extended state vector.

The loudspeaker parameters are estimated by means of look-up tables of the nonlinearities dependency curves, extracted with the Distortion Analyzer.

The relative derivatives are indirectly calculated, using the identity:

$$\frac{\partial\beta(x)}{\partial t} = \frac{\partial\beta(x)}{\partial x}\frac{\partial x}{\partial t} = \nabla_x\beta(x)v(t) \tag{6.42}$$

that in discrete-time becomes:

$$\frac{\partial\beta(x)}{\partial k} = \nabla_x\beta(x)v(k) \tag{6.43}$$

and similarly for the other required time derivatives of the nonlinear parameters:

$$\frac{\partial\kappa(x)}{\partial k} = \nabla_x\kappa(x)v(k) \qquad \frac{\partial\xi(x)}{\partial k} = \nabla_x\xi(x)v(k) \qquad \frac{\partial\iota(i)}{\partial k} = \nabla_i\iota(i)\frac{\partial i}{\partial k} \tag{6.44}$$

6.2 Simulation of the nonlinear observer

The proposed nonlinear observers has been implemented in MATLAB Simulink and connected to the nonlinear loudspeaker model, already presented in section 5.2.2.

Two versions of the nonlinear observer have been proposed. The first follows a fixed closed loop poles design, computing at runtime the feedback gain vector $\mathbf{L_d}(t)$ that enforces the position of the observer closed loop poles to predefined values. The second follows a floating closed loop pole design, computing at runtime both the feedback gain vector and the optimal closed loop poles to follow the controlled loudspeaker evolution.

Both the fixed pole and the floating pole versions have been implemented to evaluate and compare their performance. In particular, the implemented floating pole version computes the optimal instantaneous values of the observer closed loop poles exploiting the information about the instantaneous loudspeaker poles, as explained in section 6.1.2.

To overcome the implementation complexity, the two nonlinear observers are implemented as MATLAB functions, called at runtime by the Simulink environment.

Here the simulation results of a fixed pole nonlinear observer are presented, with poles designed 5 times faster than the nonlinear loudspeaker poles at rest, together with those of a floating pole nonlinear observer, with poles designed to be 5 times faster than the nonlinear loudspeaker instantaneous poles.

Each implemented version has been simulated with two different sinusoidal inputs at $+30dBV$, oscillating at $25Hz$ and $200Hz$ respectively, considering a badly estimated initial state:

$$\mathbf{x_0} = \begin{bmatrix} i_0 \\ i_{20} \\ x_0 \\ v_0 \end{bmatrix} = \begin{bmatrix} 1.5 \\ -1.5 \\ -0.01 \\ 1 \end{bmatrix} \tag{6.45}$$

corresponding to large values relatively to the exhibited loudspeaker dynamics.

Figures 6.5 and 6.6 show the comparisons of the global estimation errors for the $25Hz$ and $200Hz$ input signal respectively.

First of all, one can be notice a relatively large initial estimation error, due to the setting of the initial state $\mathbf{x_0}$.

The two observers exhibit a similar behavior, converging to zero estimation error in approximately the same amount of time. However, the fixed pole design exhibits a stronger overshoot of the global estimation error.

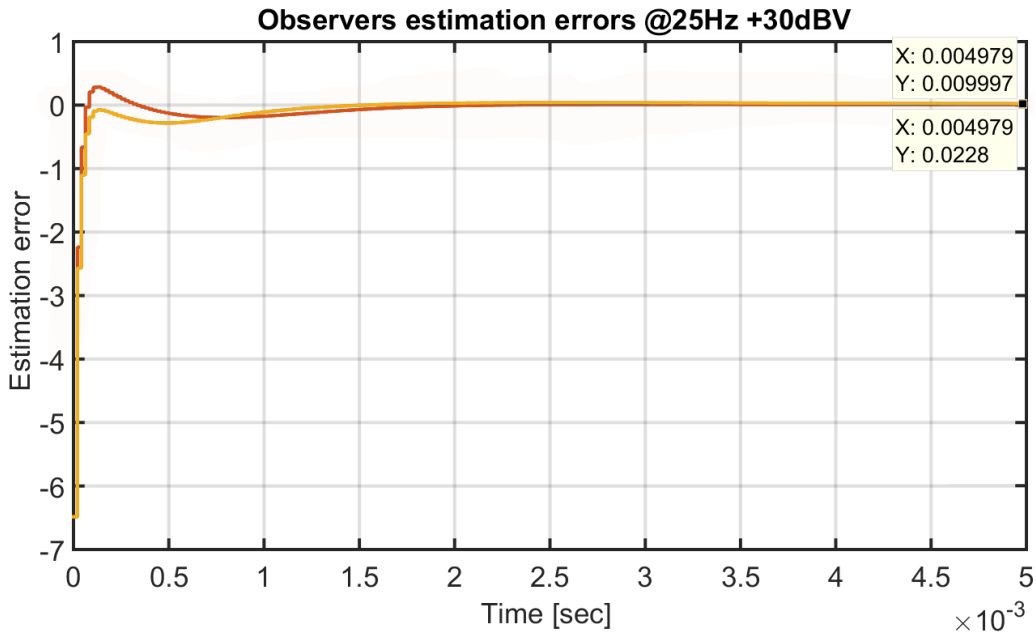

Figure 6.5: Global estimation errors of the two observers at 25Hz: red) fixed poles design; yellow) floating poles design.

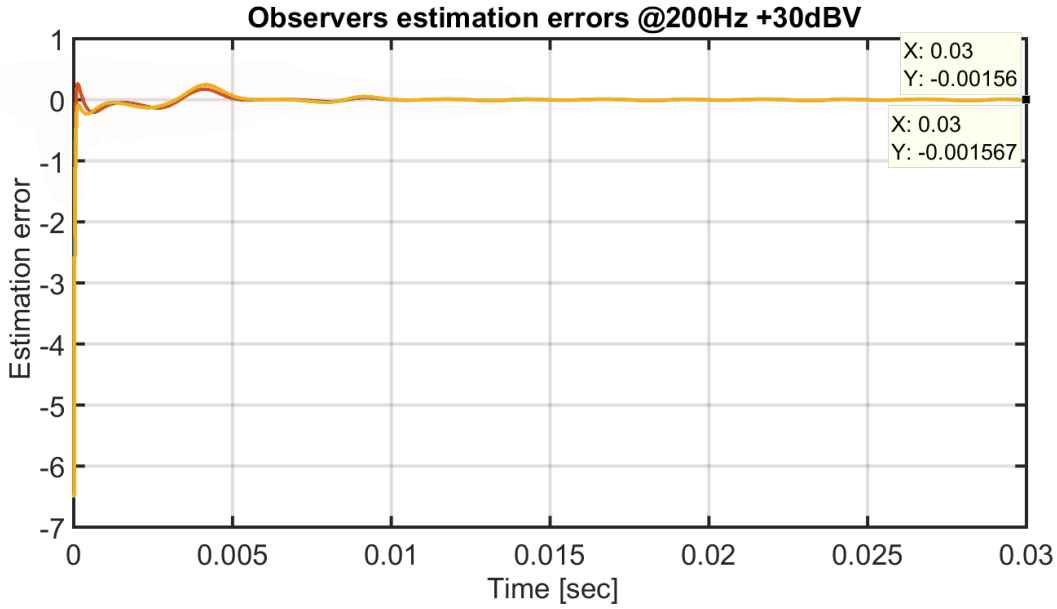

Figure 6.6: Global estimation errors of the two observers at 200 Hz: red) fixed poles design; yellow) floating poles design.

Moreover, the two observers show a better performance at $25Hz$, reaching a small estimation error under $5msec$. Conversely, at $200Hz$ the estimation error exhibit a more erratic behavior, showing a peak around $4msec$ and then converging to a small value in about $10msec$.

The cause of this difference can be better understood from the behaviors of the estimated state variables of the two implementations at $25Hz$ and $200Hz$, respectively shown in sections 6.2 and 6.2.

At $25Hz$, in both the implementation versions all the estimated state variables quickly converge to their respective real values. The slowest convergence is shown by the estimated displacements, which also exhibit an overshoot.

At $200Hz$, the convergence of the estimated velocities is clearly slower and with overshoots. More interestingly, the displacement estimates exhibit larger overshoots and do not converge to the relative real value.

This can be attributed to the approximations introduced in the loudspeaker model. The considered model approximates the nonlinear dependency on the displacement of the sensor coil electric inductance with the relative dependency of the voice coil electric inductance, assuming $\xi_s(x) = \xi(x)$. Moreover, the mutual inductance and its time derivative are calculated neglecting the nonlinear dependency on the current of the voice coil.

However, the displacement estimation error after the first two peaks is approximately of $\pm 0.2mm$, being sufficiently smaller with respect to the spatial resolution of the employed look-up tables $\Delta x = 0.42mm$ not to affect the performance of the compensation algorithm.

In conclusion, both the versions of the proposed nonlinear observer have demonstrated a good estimation capability, limited only by the quality of the employed plant model, and a remarkable robustness to errors in the initial state estimation.

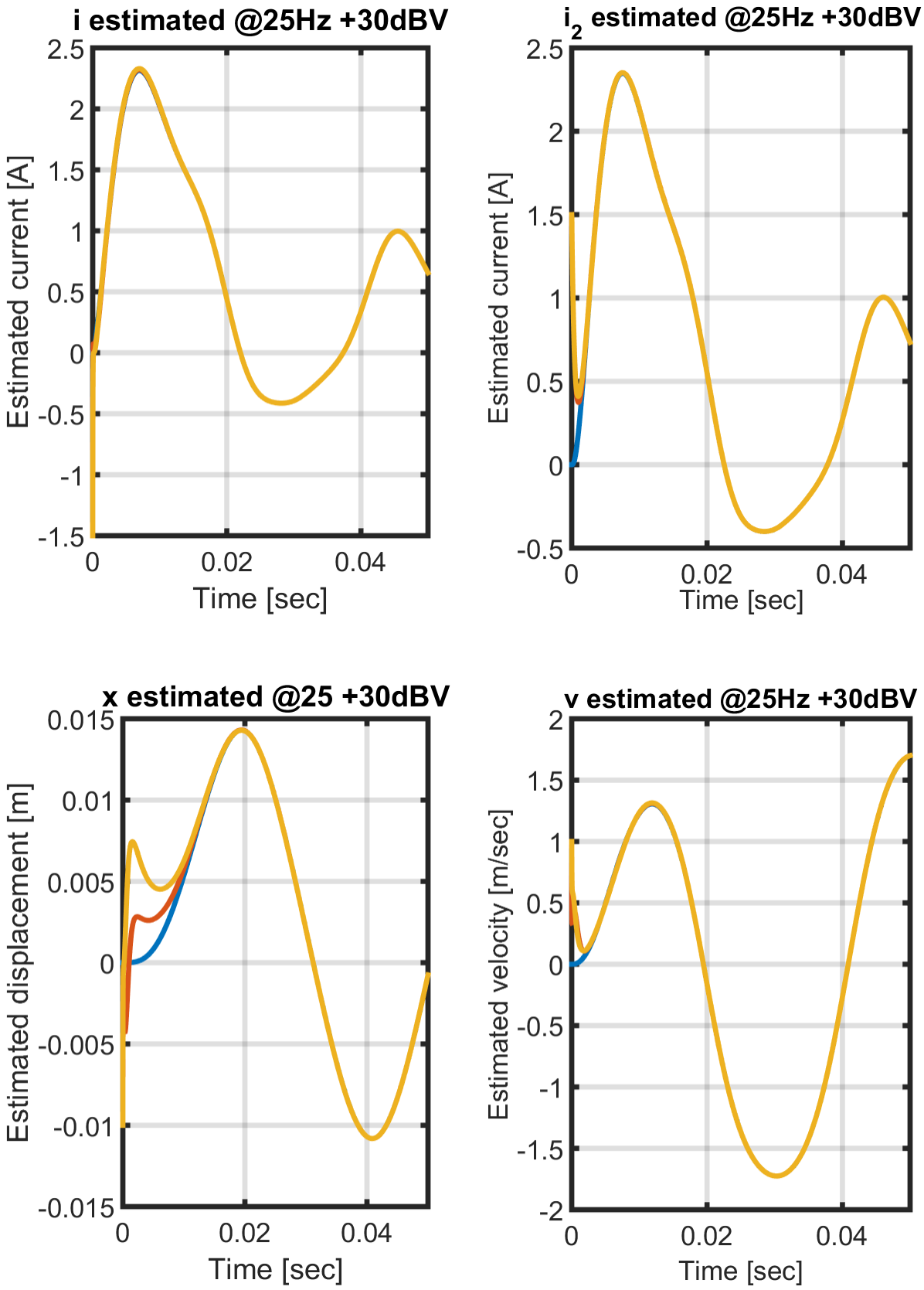

Figure 6.8: Estimated state variables at 25 Hz: red) fixed poles design; yellow) floating poles design; blue) real state

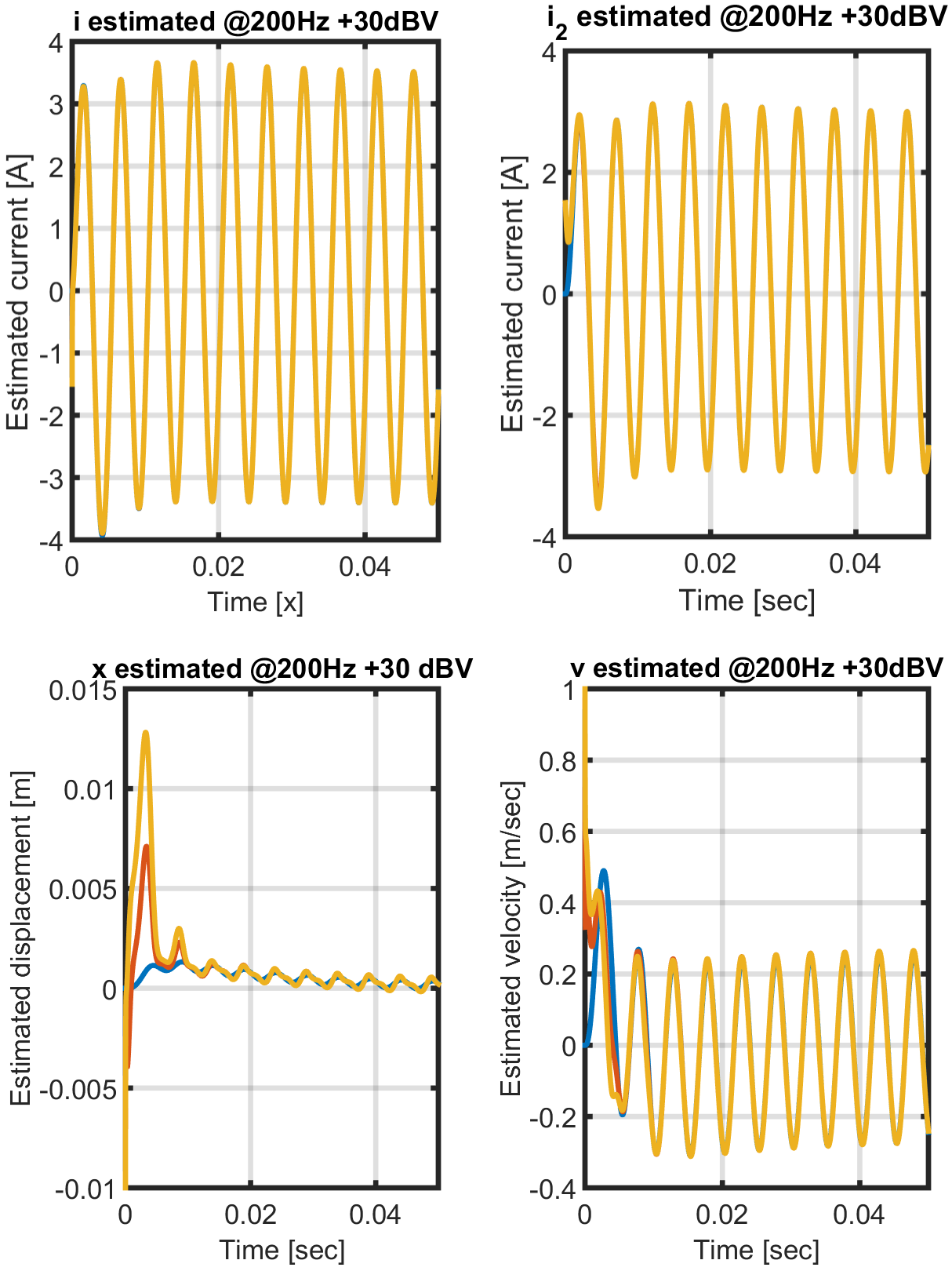

Figure 6.10: Estimated state variables at 200 Hz: red) fixed poles design; yellow) floating poles design; blue) real state

6.3 Simulation of the full compensation scheme

The proposed full nonlinearities compensator has been implemented in MATLAB Simulink and connected to the nonlinear loudspeaker model, already presented in section 5.2.2.

To overcome the complexity of the compensation generator and the extended observer, the two components are implemented as MATLAB functions, called at runtime by the Simulink environment.

In the presented simulations, the extended observer is implemented with fixed closed loop poles, designed 5 times faster than the nonlinear loudspeaker poles at rest.

Five simulations have been performed to evaluate the performance of the compensation algorithm throughout the working bandwidth $25 - 200Hz$, each one with a different input signal $V_{in}(k)$. The first four simulations employed a sinusoidal input at $+30dBV$, oscillating at $25Hz$, $50Hz$,$100Hz$ and $200Hz$ respectively. The last simulation employed a step input signal with $+15V$ amplitude.

The performance of the compensation algorithm is evaluated comparing the simulated acceleration of the controlled nonlinear loudspeaker with the simulated accelerations of other two devices: an uncontrolled loudspeaker, identical to the controlled one, and a linear loudspeaker with the same dynamics of the controlled loudspeaker. This last device is the reference for the target behavior of the controlled loudspeaker.

The acceleration of the loudspeaker diaphragm is considered a significant quantity for the evaluation of the reproduced sound quality as it is directly related to the generated sound pressure, as described in eq. (1.12). An undistorted diaphragm acceleration is theoretically related to the generation of an undistorted sound pressure.

For the step response simulation, the displacement is evaluated instead. The displacement step response emphasize the effects of the nonlinearities, that usually cause a bounce of the diaphragm.

The result of each simulation is a set of waveforms: the input signal $V_{in}(k)$, the compensation signal $V_{comp}(k)$, the control signal $V_{ctrl}(k)$, the acceleration (or displacement) of the controlled loudspeaker $a_{CTRL}(k)$ ($x_{CTRL}(k)$), the acceleration (or displacement) of the uncontrolled loudspeaker $a_{NL}(k)$ ($x_{NL}(k)$) and the acceleration (or displacement) of the target linear loudspeaker $a_{LIN}(k)$ ($x_{LIN}(k)$).

6.3.1 Time domain measurements

Figures 6.12 to 6.15 show the output acceleration waveforms of the the simulated devices driven with sinusoidal signals at different frequencies.

In the time domain it is difficult to properly evaluate the beneficial effects of the controller but, at least at $25Hz$ and $200Hz$ it is clear that the controlled loudspeaker assumes a behavior similar to the linear loudspeaker. At $50Hz$ and $100Hz$ the effects of the control are much less evident.

This happens because in a loudspeaker the most significant nonlinearities, such as the force factor and the mechanical stiffness variation, are related to the large displacement undergone by the diaphragm during the reproduction of frequencies lower or comparable to the mechanical system resonance frequency, while the inductance modulation becomes noticeable at high frequencies. At $50Hz$ and $100Hz$ the effects of the nonlinearities are much more subtle.

Figure 6.11 show the step response of the displacement. The control effectively force the controlled nonlinear loudspeaker to follow the step response exhibited by the linear loudspeaker. The uncontrolled nonlinear loudspeaker, instead, exhibits the typical bounce effect due to the simultaneous increase of the mechanical stiffness and the reduction of the force factor.

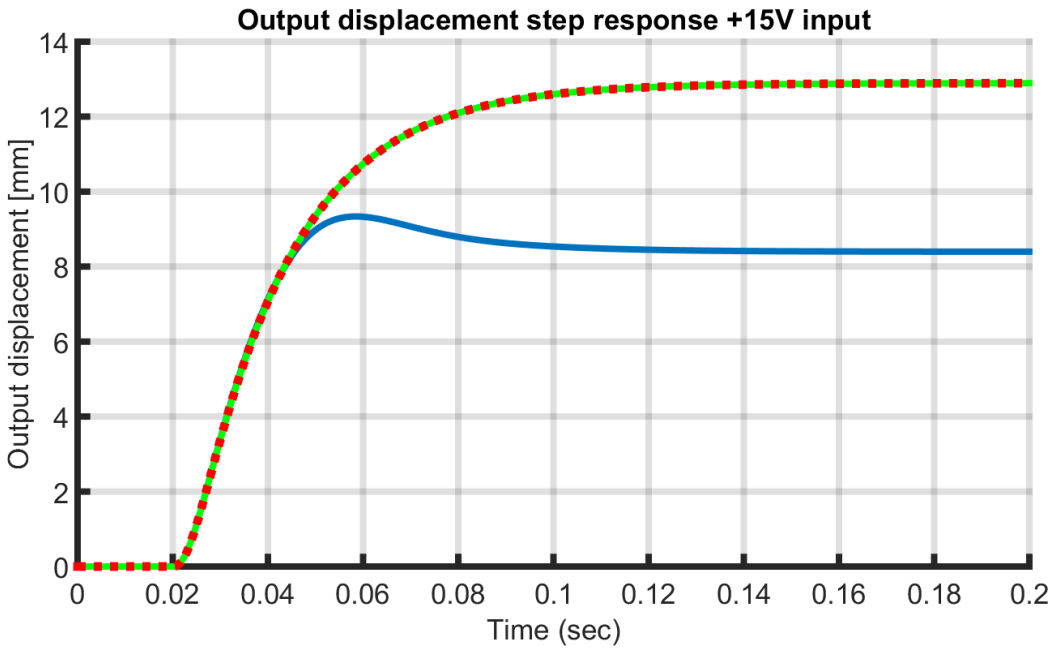

Figure 6.11: Displacement step response of the simulated loudspeakers: blue) nonlinear; green) linear; red) nonlinear compensated.

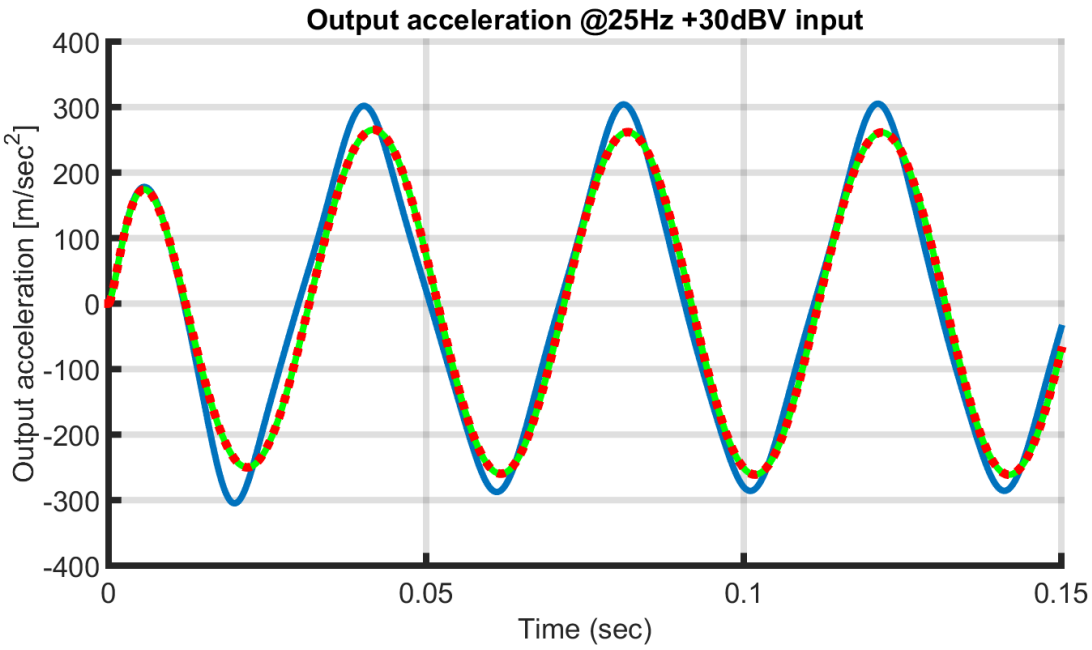

Figure 6.12: Acceleration of the simulated loudspeakers at 25Hz: blue) nonlinear; green) linear; dotted red) nonlinear compensated.

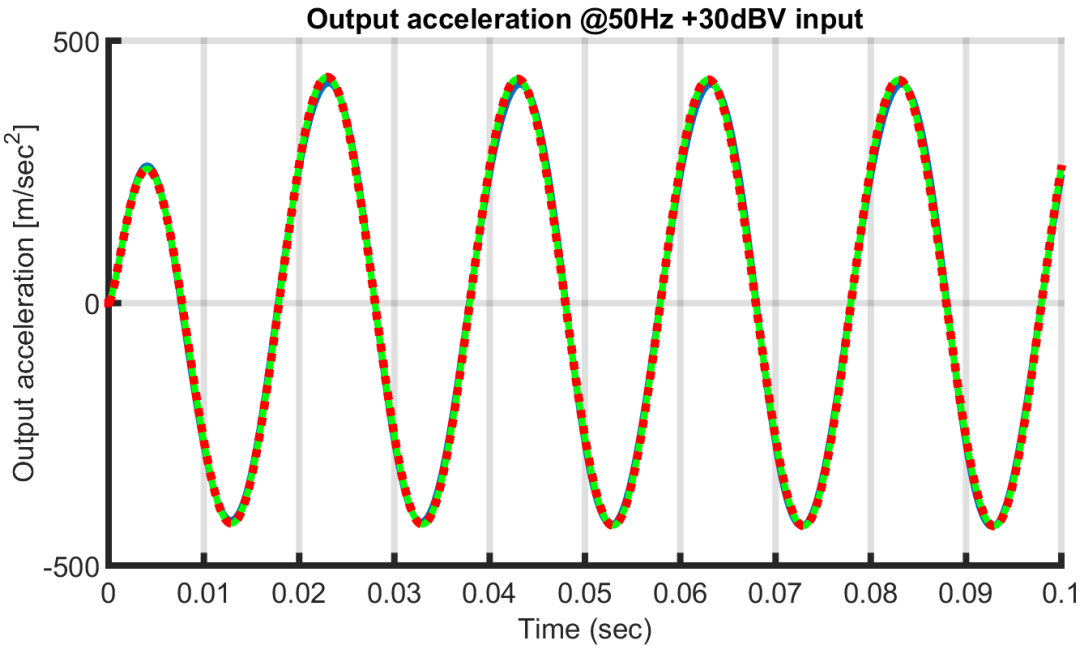

Figure 6.13: Acceleration of the simulated loudspeakers at 50Hz: blue) nonlinear; green) linear; dotted red) nonlinear compensated.

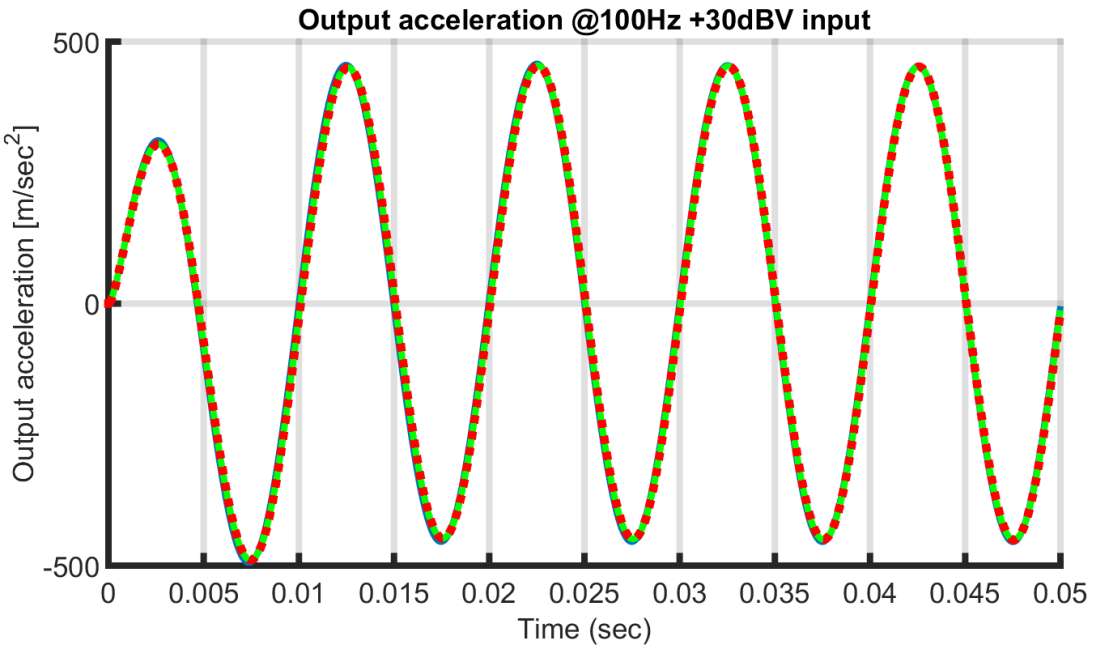

Figure 6.14: Acceleration of the simulated loudspeakers at 100Hz: blue) nonlinear; green) linear; dotted red) nonlinear compensated.

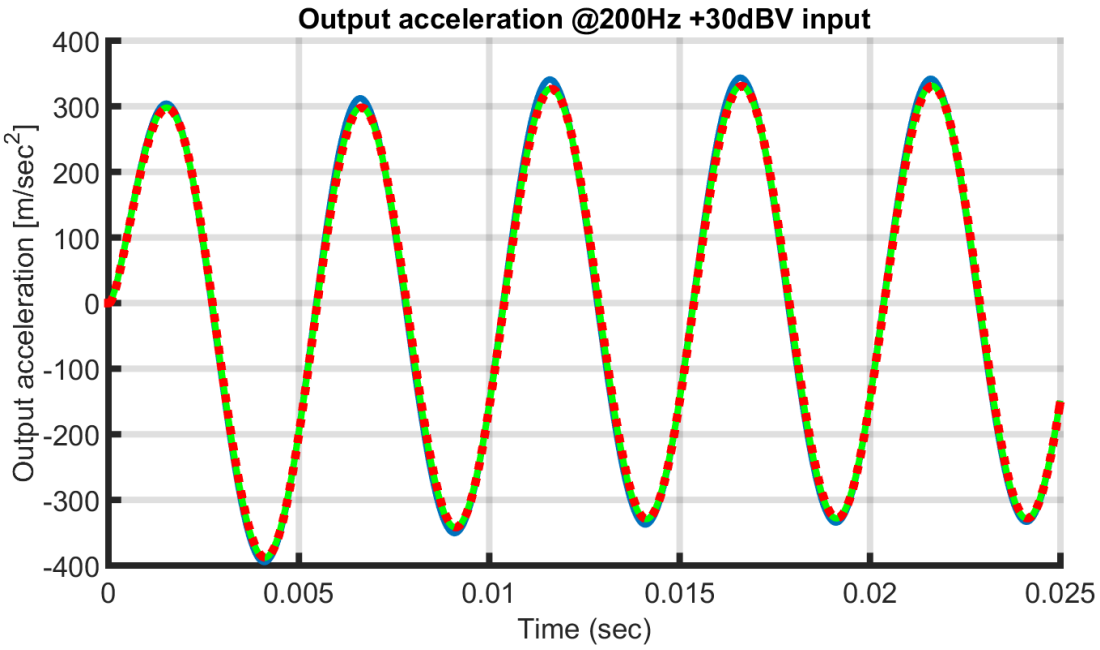

Figure 6.15: Acceleration of the simulated loudspeakers at 200Hz: blue) nonlinear; green) linear; dotted red) nonlinear compensated.

The measured input signal V_{in}, the compensation signal V_{comp} and the generated control signal V_{ctrl} are shown in figs. 6.11 to 6.15.

In the sinusoidal driven simulations, the compensation signal is generally much lower than the input signal, requiring just a small additional compensation to enhance the loudspeaker performances. The only exception is at $25Hz$, where the compensation signal shows a peak during the first period of control. This is due to the large effort required to drive the diaphragm against the increasing mechanical stiffness leveraging on a decaying force factor.

After the first period this large compensation effort is no more required, since the overdriven mechanical stiffness acts as a slingshot, providing the required kinetic energy. The compensation is just used to slightly correct the diaphragm motion.

In the step driven simulation, instead, the compensation signal is even larger than the input signal. Again, this is due to the large effort required to drive the diaphragm and keep it at the ideal displacement, counteracting the force applied by the mechanical stiffness.

In the considered situations, the control effort is not an issue, since the control voltage is not excessive to be handled for both the loudspeaker or a typical power amplifier. However, there are conditions in which the control effort becomes unsustainable for the amplifier, but are extreme situations in which the loudspeaker is subject to excessive displacement not belonging to the normal working condition.

A large control voltage also generate an large current on the voice coil. This can be a problem during the simulations, as the current dependency look-up table is limited at $\pm 13.6A$, preventing the controller from following the real loudspeaker state and consequently leading to instability.

Also, considering a real world application, the amplifier used to drive the controlled loudspeaker must be capable of providing the required control current.

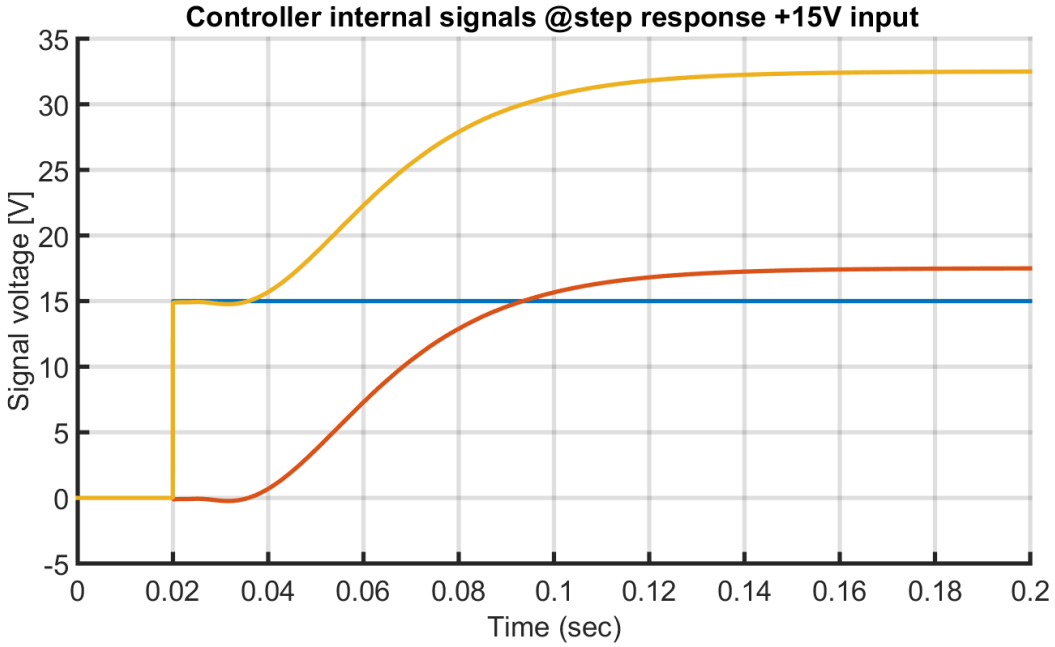

Figure 6.16: Signals of the simulated displacement step response: blue) input signal V_{in}; red) compensation signal V_{comp}; yellow) control signal V_{ctrl}.

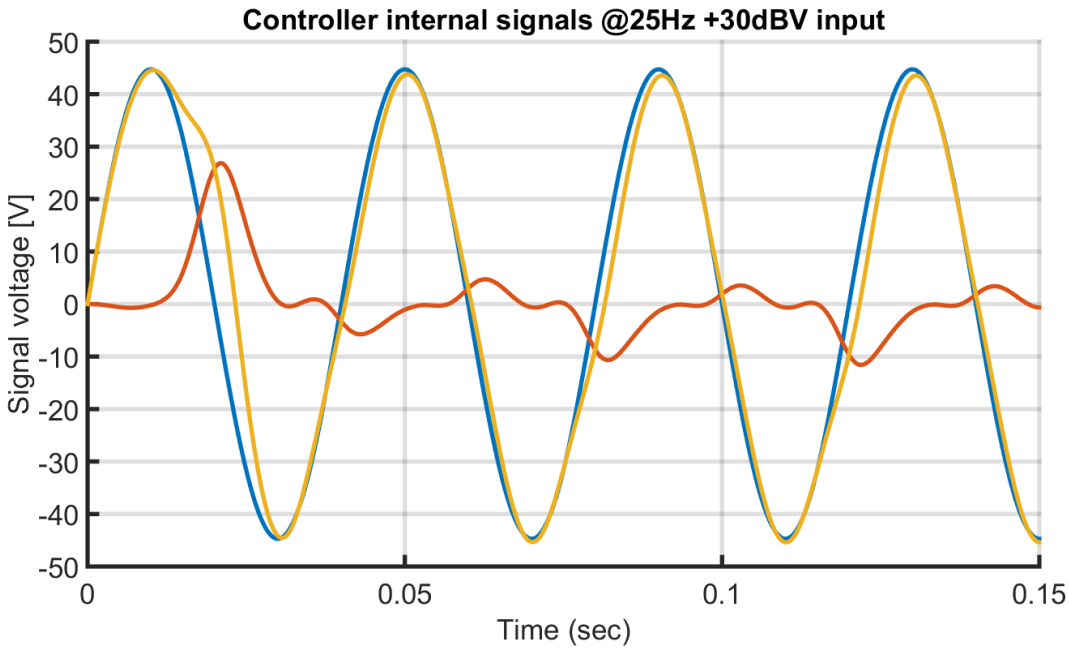

Figure 6.17: Signals of the simulated loudspeakers at 25Hz: blue) input signal V_{in}; red) compensation signal V_{comp}; yellow) control signal V_{ctrl}.

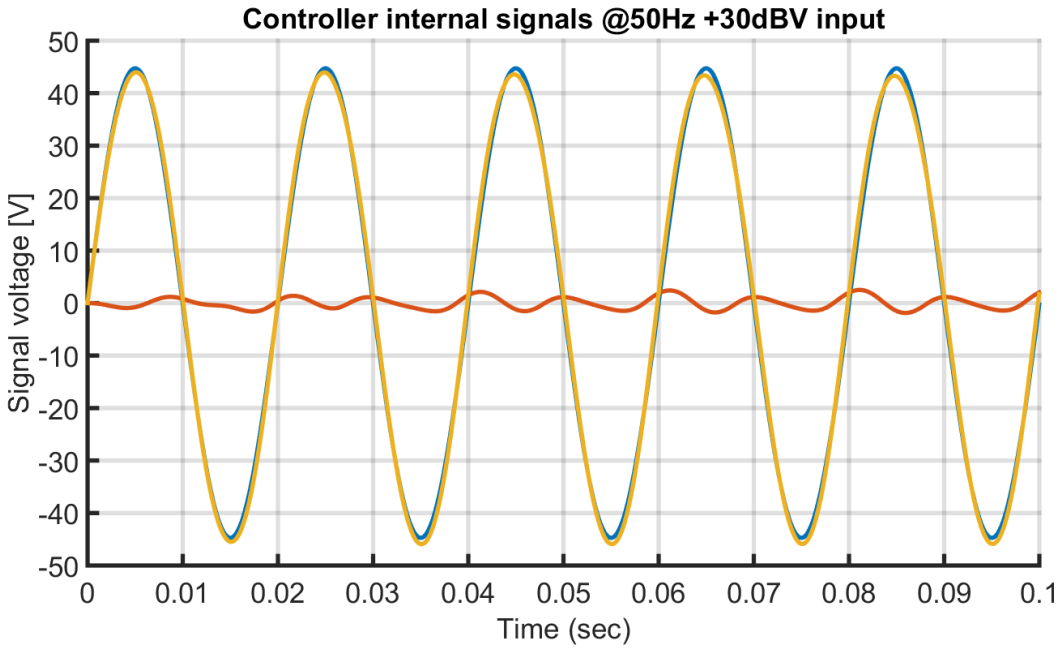

Figure 6.18: Signals of the simulated loudspeakers at 50Hz: blue) input signal V_{in}; red) compensation signal V_{comp}; yellow) control signal V_{ctrl}.

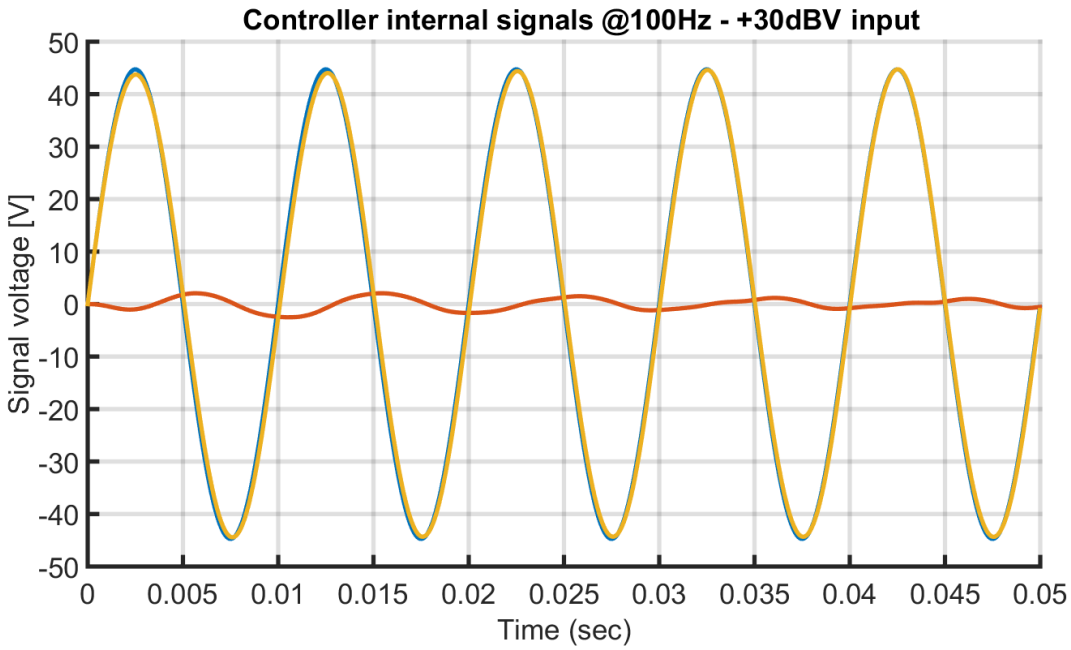

Figure 6.19: Signals of the simulated loudspeakers at 100Hz: blue) input signal V_{in}; red) compensation signal V_{comp}; yellow) control signal V_{ctrl}.

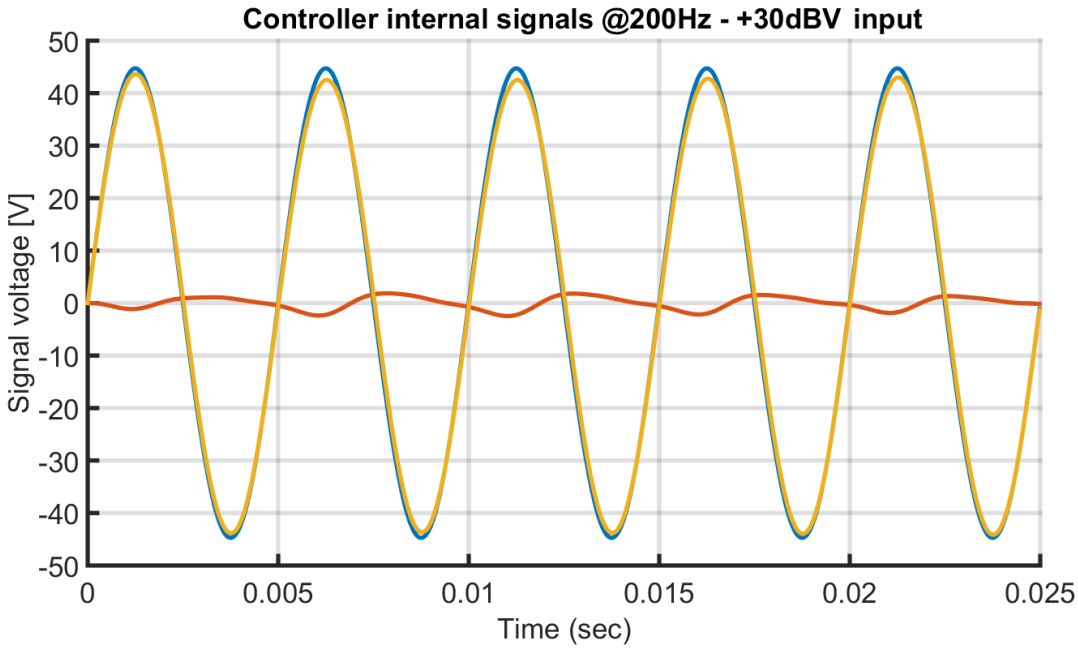

Figure 6.20: Signals of the simulated loudspeakers at 200Hz: blue) input signal V_{in}; red) compensation signal V_{comp}; yellow) control signal V_{ctrl}.

6.3.2 Frequency domain measurements

To properly evaluate the effect of the control the acceleration power spectra are computed from the simulation outputs. The resulting spectra are shown in figs. 6.21 to 6.24.

From the spectral analysis the beneficial effects of the proposed control are clear.

Especially at low frequencies, all the harmonics generated by the loudspeaker nonlinearities are largely attenuated, reaching a mean attenuation of about $40dB$ for a fundamental of $25Hz$ and $30dB$ for a fundamental of $50Hz$, and making the highest harmonic at least $70dB$ smaller that the fundamental in both cases.

At higher frequencies the linearization capabilities of the control are reduced, and at $200Hz$ the controller can only partially compensate the second harmonic.

Clearly, at high frequency the harmonics caused by the nonlinear effects are much less significant with respect to the fundamental: at $25Hz$ the first, second and third harmonics are respectively $39.95dB\frac{meter}{sec^2}$, $11.62dB\frac{meter}{sec^2}$ and $17.39dB\frac{meter}{sec^2}$, while at $200Hz$ they are respectively $41.96dB\frac{meter}{sec^2}$, $-0.81dB\frac{meter}{sec^2}$ and $-13.81dB\frac{meter}{sec^2}$. This means that the loudspeaker already exhibits an almost linear behavior, making the control less necessary.

However, the approximations used to model the displacement dependency of the sensor coil inductance and the time derivative of the mutual inductance may have affected the performances of the control. Simulations performed without considering the effects of the electric domain nonlinearities, both in the model and in the compensator, show a perfect compensation even at high frequencies, confirming this hypothesis.

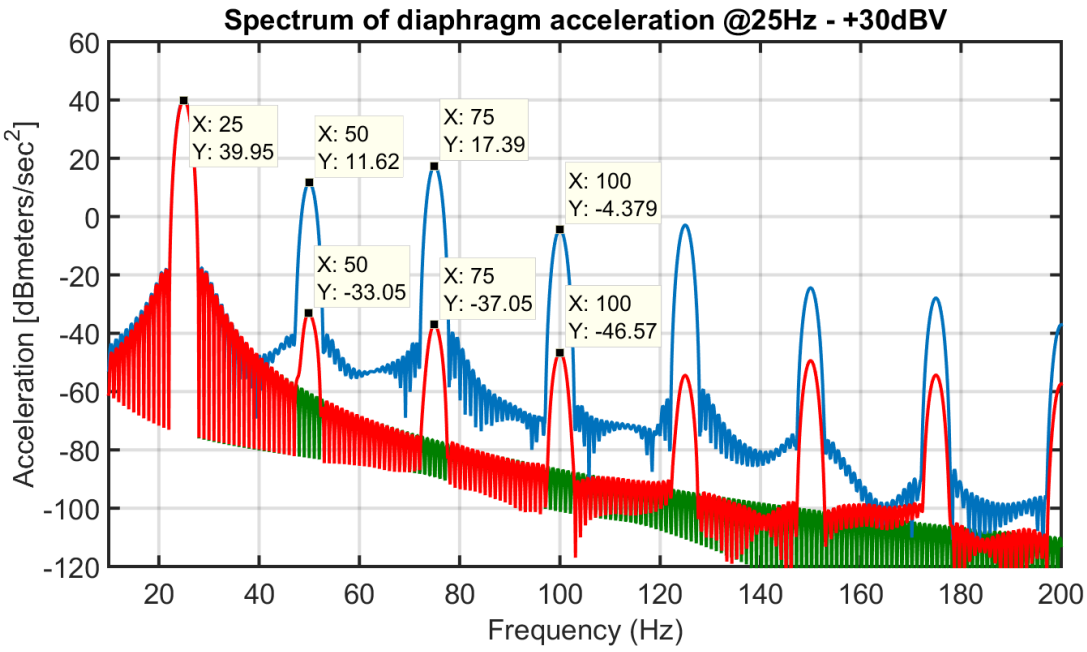

Figure 6.21: Spectra acceleration of the simulated loudspeakers at 25Hz: blue) nonlinear; green) linear; red) nonlinear compensated.

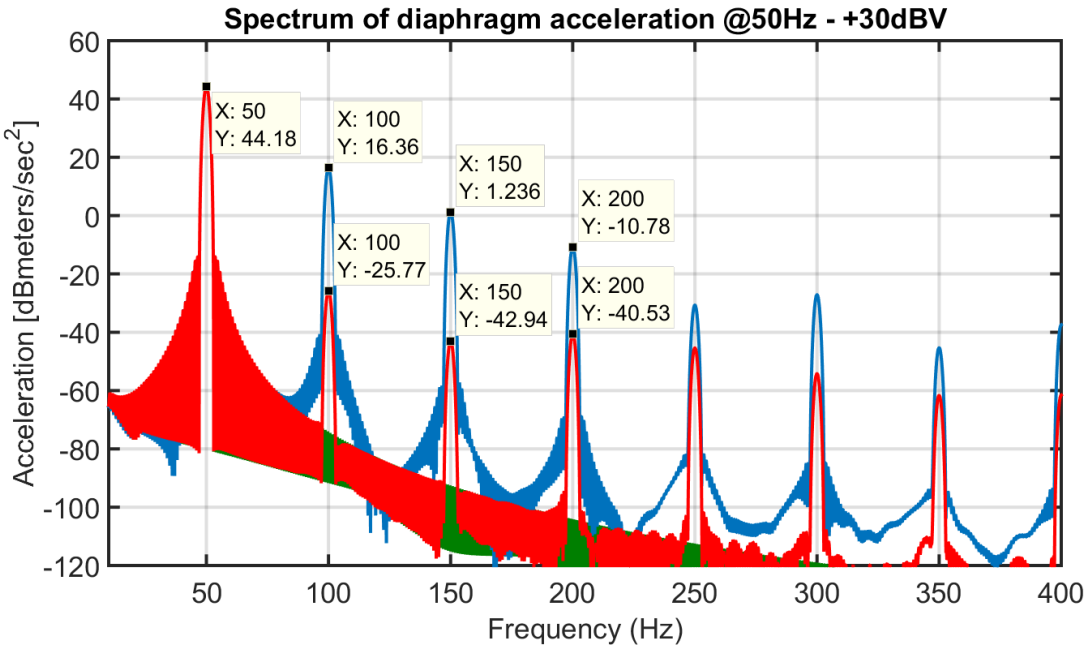

Figure 6.22: Spectra acceleration of the simulated loudspeakers at 50Hz: blue) nonlinear; green) linear; red) nonlinear compensated.

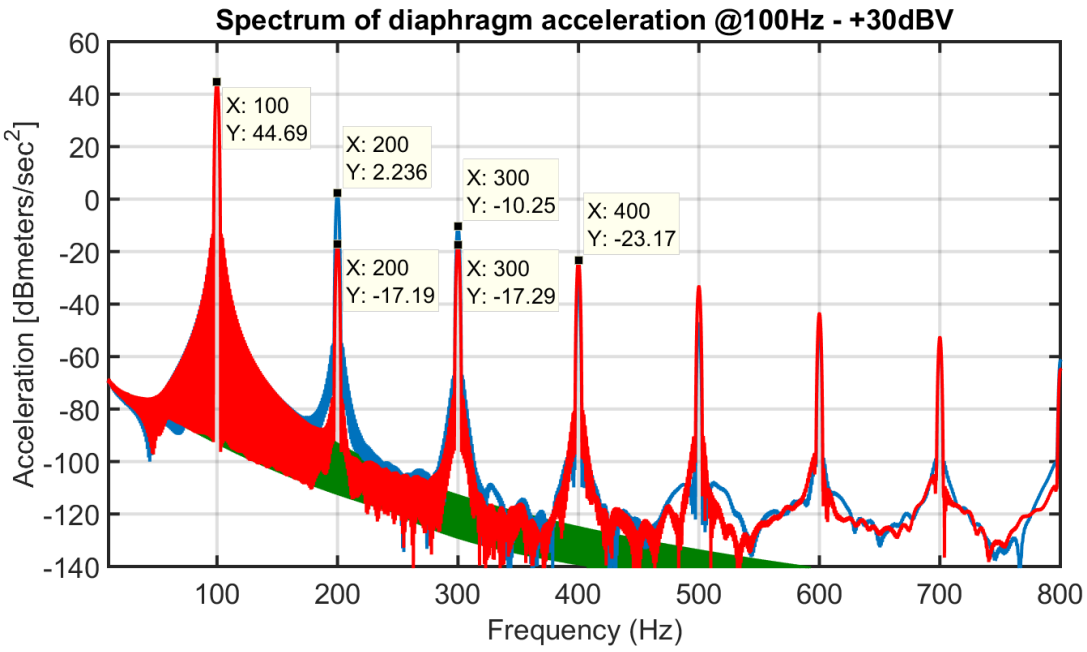

Figure 6.23: Spectra acceleration of the simulated loudspeakers at 100Hz: blue) nonlinear; green) linear; red) nonlinear compensated.

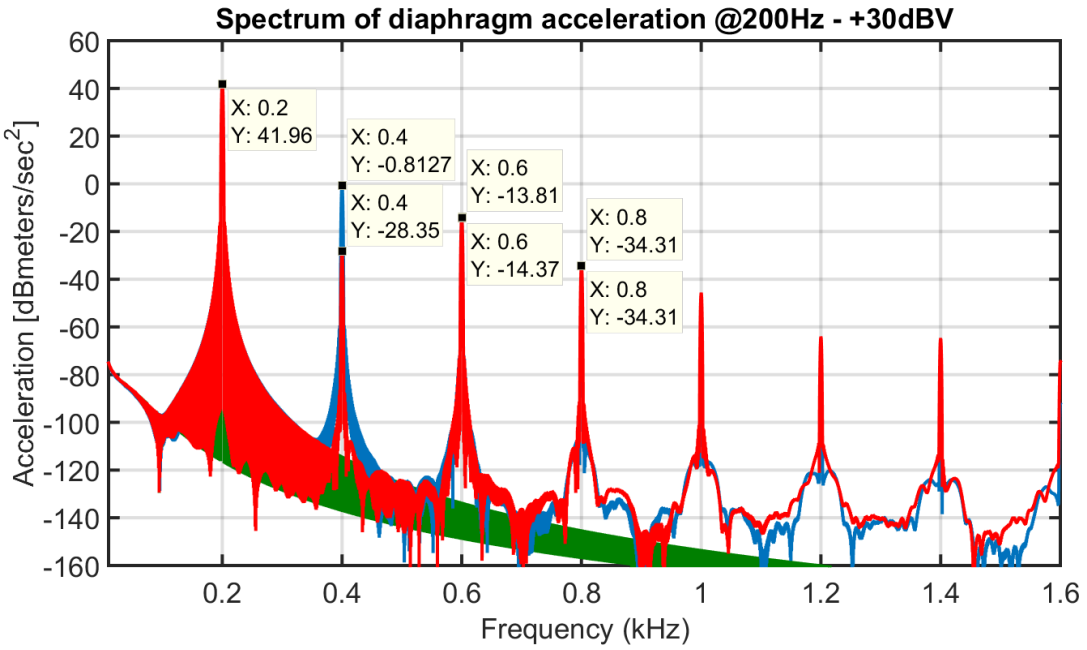

Figure 6.24: Spectra acceleration of the simulated loudspeakers at 200Hz: blue) nonlinear; green) linear; red) nonlinear compensated.

6.3.3 Total Harmonic Distortion

The Total Harmonic Distortion (THD) is a characteristic of a periodic signal, defined as the ratio of the RMS amplitude of the signal's higher harmonics to the RMS amplitude of the signal's first harmonic, often expressed in dB scale or in percentage:

$$THD = \frac{\sqrt{\sum_{i=2}^{\infty} A_i^2}}{A_1} \tag{6.46}$$

$$THD_{dB} = 20log(THD) \qquad THD_{\%} = 100\,THD$$

with the series of considered harmonics usually limited to 50.

The THD gives a measure of the harmonic purity of the analyzed signal: the less the harmonic content of the signal, the less the THD.

It is also a common figure of merit for the evaluation of audio systems, amplifiers and transducers quality: an audio device is typically characterized by the THD value exhibited by the device's output when driven by a pure sinusoidal tone input.

A $THD_{\%} \leq 1\%$ is considered sufficient for audio purposes. However, modern power amplifiers and Hi-Fi systems typically exhibit a $THD_{\%} \leq 0.1 - 0.3\%$.

The THD values relative to the simulated acceleration outputs of the compensated nonlinear loudspeaker and the uncompensated nonlinear loudspeaker are summarized in table 6.1.

From those data, the benefits of the compensation are evident. At low frequencies, the nonlinear loudspeaker reaches $THD_{\%} \geq 8\%$ at $25Hz$ and $\geq 4\%$ at $50Hz$, being clearly above the minimum recommendations for audio devices. A better behavior is experienced at the higher frequencies.

The implemented control effectively compensates the loudspeaker nonlinearities extremely well, reducing the exhibited $THD_{\%}$ of 400 times at $25Hz$. As already stated, at higher frequencies the compensation has a much lesser impact on the loudspeaker performances. However, it brings the exhibited $THD_{\%}$ well below the 0.3% threshold of high quality audio.

	THD nonlinear	THD compensated
$f_0 = 25$ Hz	8.032%	0.027%
$f_0 = 50$ Hz	4.150%	0.032%
$f_0 = 100$ Hz	0.7748%	0.121%
$f_0 = 200$ Hz	0.7418%	0.157%

Table 6.1: Total Harmonic Distortion of the simulated loudspeakers

6.4 Control of the linearized dynamics

The second part of the controller is the Dynamics Controller, whose purpose is to produce the signal $V_{in}(k)$ capable of driving the linearized loudspeaker so as to exhibit a satisfactory frequency response from the source input signal $V_{source}(k)$ to the output diaphragm acceleration $a(k)$, and thus to the generated sound pressure as eq. (1.12) implies.

This is achieved introducing a full-state feedback control signal $V_{FSF}(k)$, such that:

$$V_{in}(k) = V_{source}(k) + V_{FSF}(k) \tag{6.47}$$

allowing to assign the poles of the controlled linearized loudspeaker to arbitrary values.

The control signal $V_{FSF}(k)$ is computed by a discrete-time full-state feedback controller, described in section 2.2 in its continuous-time form.

In short, considering a continuous-time, controllable and observable LTI plant:

$$\begin{aligned} \dot{\mathbf{x}}(t) &= \mathbf{A}\mathbf{x}(t) + \mathbf{B}u(t) \\ y(t) &= \mathbf{C}\mathbf{x}(t) + \mathbf{D}u(t) \end{aligned} \tag{6.48}$$

it is possible to tune the poles exhibited by the plant adding a state feedback contribution $u_{FSF}(t)$ to the plant input, obtained as a linear combination of the plant state $\mathbf{x}(t)$.

$$u_{FSF}(t) = -\mathbf{K}\mathbf{x}(t) \tag{6.49}$$

$$\begin{aligned} \dot{\mathbf{x}}(t) =& \mathbf{A}\mathbf{x}(t) + \mathbf{B}[u(t) + u_{FSF}(t)] \\ =& (\mathbf{A} - \mathbf{B}\mathbf{K})\mathbf{x}(t) + \mathbf{B}u(t) \end{aligned}$$

The poles exhibited by the controlled plant are determined by the eigenvalues of the matrix $(\mathbf{A} - \mathbf{K}\mathbf{B})$, tuned by the feedback gain vector $\mathbf{K}$ defined in eq. (2.15)

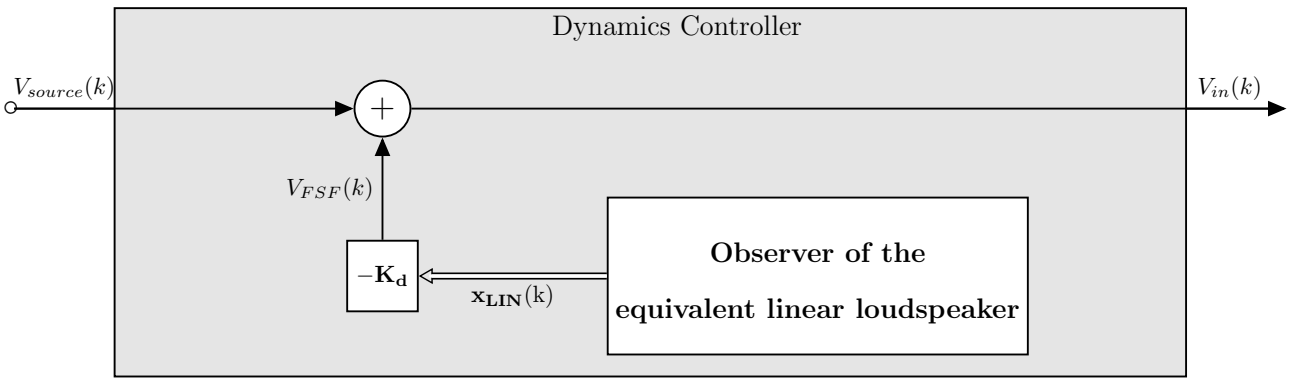

Figure 6.25: Block diagram of the proposed dynamics controller.

The same state feedback control can be implemented in discrete-time form considering a discretized version of the plant:

$$\mathbf{A_d} = e^{\mathbf{AT_s}} \qquad \mathbf{B_d} = \int_0^{T_s} e^{\mathbf{A}t}\,\mathbf{B}\,dt = \mathbf{A}^{-1}(\mathbf{A_d} - \mathbf{I})\mathbf{B}$$
$$\mathbf{C_d} = \mathbf{C} \qquad \mathbf{D_d} = \mathbf{D} \tag{6.50}$$

$$\begin{aligned}\mathbf{x}(k+1) =& \mathbf{A_d}\mathbf{x}(k) + \mathbf{B_d}[u(k) + u_{FSF}(k)] \\ =& (\mathbf{A_d} - \mathbf{B_d}\mathbf{K_d})\mathbf{x}(k) + \mathbf{B_d}u(k)\end{aligned}$$

The poles exhibited by the discretized, controlled plant are determined by the eigenvalues of the matrix $(\mathbf{A_d} - \mathbf{K_d}\mathbf{B_d})$, tuned by the gain vector $\mathbf{K_d}$ defined through Ackermann's formula:

$$\mathbf{K_d} = [\quad 0 \quad \cdots \quad 0 \quad 1 \quad]\mathcal{C}^{-1}\alpha_c(\mathbf{A_d}) \tag{6.51}$$

where $\mathcal{C}$ is the controllability matrix of the discretized plant and $\alpha_c(\mathbf{A_d})$ is the characteristic polynomial of the desired closed loop matrix $(\mathbf{A_d} - \mathbf{K_d}\mathbf{B_d})$, solved for $\mathbf{A_d}$.

The considered plant is the linearized loudspeaker system, composed by the nonlinearities compensator and the compensated nonlinear loudspeaker, characterized by the input $V_{in}(k)$ and the output $a(k)$.

The control action enforced by the nonlinearities compensator ensures that the considered system acts like an equivalent linear loudspeaker characterized by the sole linear behavior of the nonlinear controlled loudspeaker.

The dynamic control is designed considering the discrete-time model of the equivalent linear loudspeaker expressed through the LTI model:

$$\begin{aligned}\mathbf{x_{LIN}}(k+1) &= \mathbf{A_d}\mathbf{x_{LIN}}(k) + \mathbf{B_d}u(k) \\ y(k) &= \mathbf{C_d}\mathbf{x_{LIN}}(k) + \mathbf{D_d}u(k)\end{aligned} \tag{6.52}$$

with:

$$\begin{aligned}\mathbf{x_{LIN}}(k) &= \begin{bmatrix} i_{LIN}(k) & i_{2LIN}(k) & x_{LIN}(k) & v_{LIN}(k)\end{bmatrix}^T \\ &= \begin{bmatrix} i_{LIN}(k) & i_{2LIN}(k) & x(k) & v(k)\end{bmatrix}^T\end{aligned} \tag{6.53}$$

$$u(k) = V_{in}(k) \qquad y(k) = a_{LIN}(k) = a(k) \tag{6.54}$$

and characterized by the discrete matrices $\mathbf{A_d}$, $\mathbf{B_d}$, $\mathbf{C_d}$ and $\mathbf{D_d}$, obtained through the discretization method described in eq. (6.50) from the continuous-time matrices:

$$\mathbf{A} = \begin{bmatrix} -\frac{R_e + {R_2}^0}{{L_e}^0} & \frac{{R_2}^0}{{L_e}^0} & 0 & -\frac{Bl^0}{{L_e}^0} \\ \frac{{R_2}^0}{{L_2}^0} & -\frac{{R_2}^0}{{L_2}^0} & 0 & 0 \\ 0 & 0 & 0 & 1 \\ \frac{Bl^0}{M_{ms}} & 0 & -\frac{{K_{ms}}^0}{M_{ms}} & -\frac{R_{ms}}{M_{ms}} \end{bmatrix} \qquad \mathbf{B} = \begin{bmatrix} \frac{1}{{L_e}^0} \\ 0 \\ 0 \\ 0 \end{bmatrix} \tag{6.55}$$

$$\mathbf{C} = \begin{bmatrix} \frac{Bl^0}{M_{ms}} & 0 & -\frac{{K_{ms}}^0}{M_{ms}} & -\frac{R_{ms}}{M_{ms}} \end{bmatrix} \qquad \mathbf{D} = \begin{bmatrix} 0 \end{bmatrix}$$

The parameters of the model have been extracted with the Distortion Analyzer and are summarized in table 5.2.

The controller design has been carried out in the continuous-time framework and has afterwards been implemented in discrete-time.

Typically, loudspeakers are designed to exhibit a flat frequency response in their working frequency range, with a tolerance of $\pm 3dB$.

The target for the design of the controller pole placement is to enhance the frequency response behavior, restricting the admitted tolerance to less than $\pm 1dB$, preserving the maximum value.

The considered linear loudspeaker is characterized by following the transfer function, shown in fig. 6.26:

$$H_a(s) = \frac{A(s)}{V_{in}(s)} = \mathbf{C}(s\mathbf{I} - \mathbf{A})^{-1}\mathbf{B} + \mathbf{D} = \mathbf{C}(s\mathbf{I} - \mathbf{A})^{-1}\mathbf{B} \tag{6.56}$$

defined by the following poles and zeros, shown in fig. 6.27:

$$\begin{array}{rc} p_1 = & -8789,17 \\ p_2 = & -434,44 + j143,09 \\ p_3 = & -434,44 - j143,09 \\ p_4 = & -49,64 \end{array} \qquad \begin{array}{rc} z_1 = & -2107,84 \\ z_2 = & 0 \\ z_3 = & 0 \end{array} \tag{6.57}$$

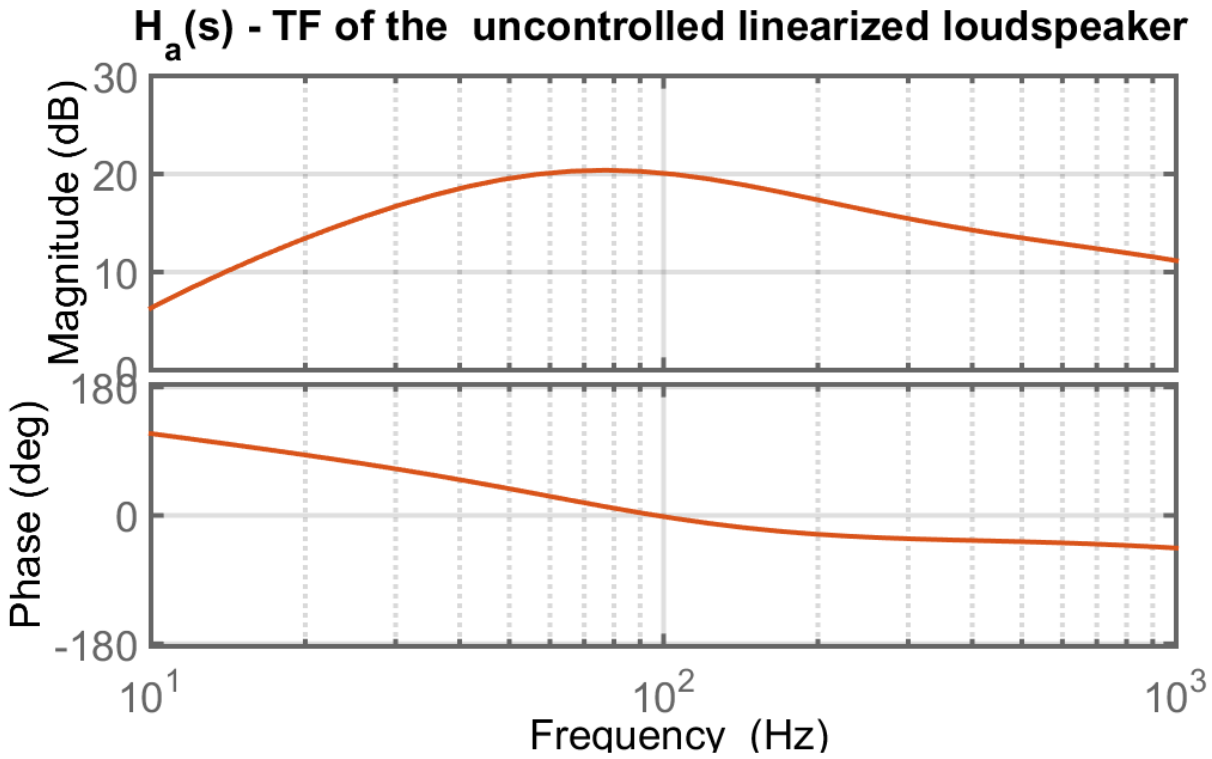

Figure 6.26: Transfer function of the uncontrolled linearized loudspeaker.

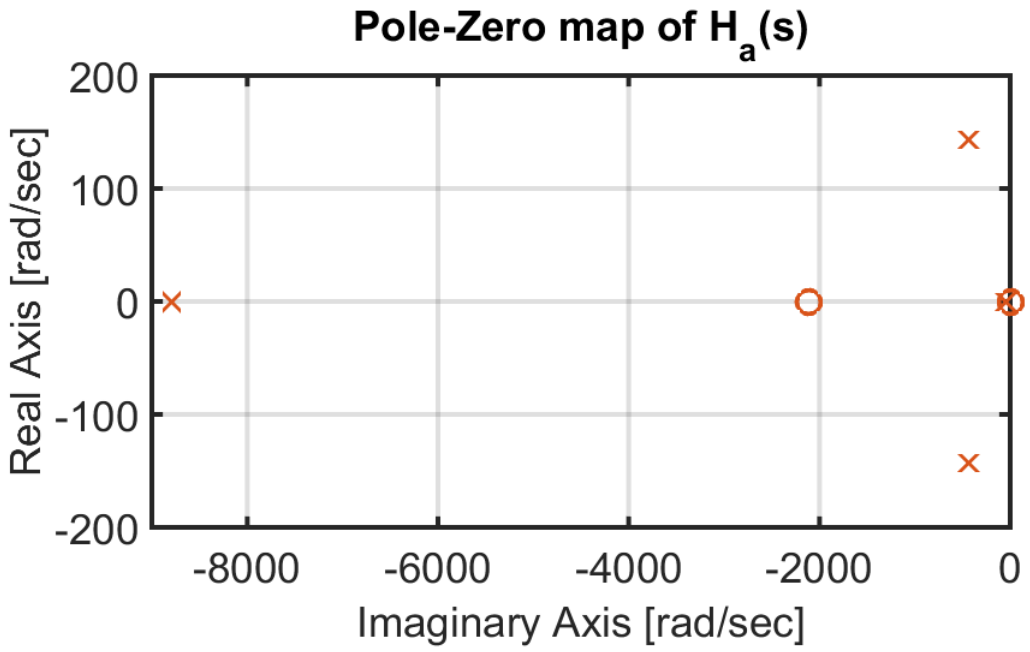

Figure 6.27: Pole-zero map of the uncontrolled linearized loudspeaker.

The transfer function of the linearized loudspeaker $H_a(s)$ actually fits the typical magnitude tolerance, exhibiting in the working bandwidth of $25 - 200Hz$ a maximum value of $20.4dB$ at $77Hz$ and a minimum value of $17.4dB$ at $25Hz$. This corresponds to a variation of $\pm 2.5dB$ around the halfway value of $18.9dB$.

However, a variation of $5dB$ between the maximum and the minimum values of the transfer function is not a particularly good feature for a loudspeaker.

A much better behavior can be obtained by properly designing the linearized loudspeaker poles, enforcing the designed values by means of the presented pole placement technique.

The two complex poles are redesigned to form a second order high-pass filter with cut-off frequency $f_c = 12.5Hz$ and damping $\zeta = 0.707$, i.e. a second order Butterworth filter.

The other two poles are designed to compensate for the effect of the zero $z1$. The best result in terms of flatness of the frequency response and preservation of the maximum value of the original transfer function is obtained placing those poles to form a second order low-pass filter with cut-off frequency $f_c = 435Hz$ and damping $\zeta = 1$.

The values of the designed the poles are the following:

$$\begin{array}{ll} p_1 = & -2733,19 \\ p_2 = & -2733,19 \\ p_3 = & -55,54 + j55,54 \\ p_4 = & -55,54 - j55,54 \end{array} \tag{6.58}$$

The relative continuous-time and discrete-time feedback gain vectors of the full-state feedback controller are defined through Ackermann's formula:

$$\mathbf{K} = \mathbf{K_d} = [\quad -10.58 \quad 11.21 \quad -659.90 \quad -16.62 \quad] \tag{6.59}$$

The designed transfer function of the controlled, linearized loudspeaker $H_a^{ctrl}(s)$, shown in fig. 6.28, is defined as follows:

$$H_a^{ctrl}(s) = \frac{A(s)}{V_{source}(s)} = \mathbf{C}(s\mathbf{I} - (\mathbf{A} - \mathbf{BK}))^{-1}\mathbf{B} \tag{6.60}$$

and is characterized by the pole-zero map shown in fig. 6.29.

The designed transfer function $H_a^{ctrl}(s)$ exhibits an extremely flat response in the working bandwidth of $25 - 200Hz$, with a maximum value of $20.4dB$ at $77Hz$ and minimum values of $20.2dB$ at $25Hz$ and $200Hz$.

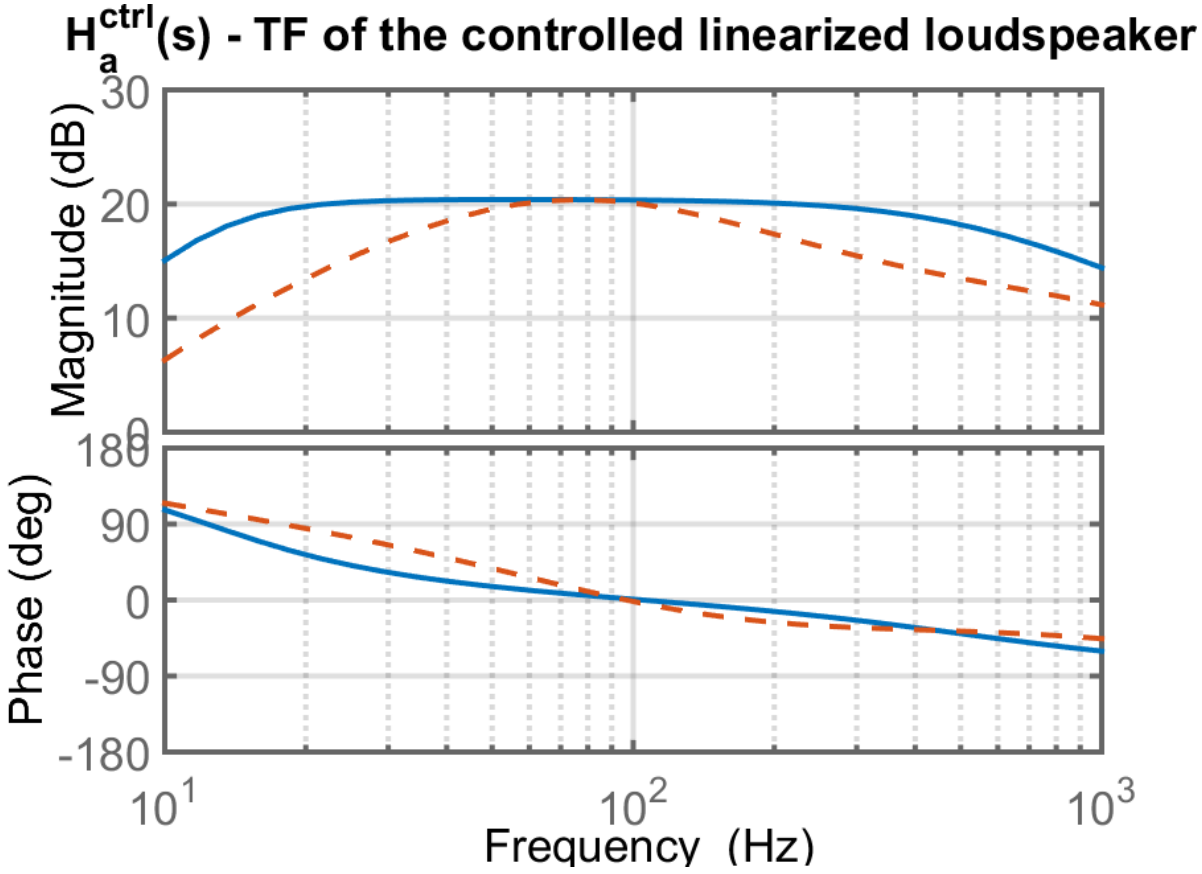

Figure 6.28: Designed transfer function of the controlled linearized loudspeaker (blue). The uncontrolled transfer function $H_a(s)$ (dashed red) is shown for comparison.

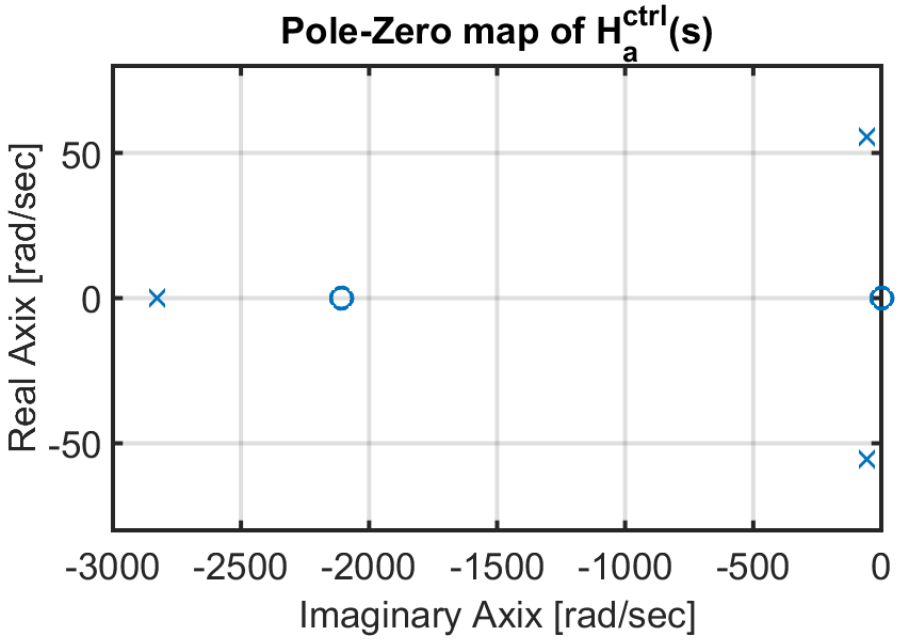

Figure 6.29: Designed pole-zero map of the controlled linearized loudspeaker.

The implementation of the designed full-state feedback controller requires the knowledge of the internal state of the equivalent linearized loudspeaker $\mathbf{x_{LIN}}(k)$.

Unfortunately, it is not possible to estimate the state of that linear system by means of a linear Luenberger observer exploiting the sensor coil signal $V_{sensor}(k)$. In fact, the nonlinearities compensation enforces the linearization of the loudspeaker motional behavior, while the sensor output is still nonlinear.

If a feedback observer is required, then a second nonlinear observer must be introduced.

However, since the compensator has proven its effectiveness, it can be assumed that, at any instant k, the linearized loudspeaker exhibits *exactly* the same behavior as the linear loudspeaker described by eq. (6.52), thus not requiring a closed-loop observer to correct the estimation error.

The state of the equivalent linearized loudspeaker $\mathbf{x_{LIN}}(k)$ can be effectively estimated by means of a discrete-time open loop observer:

$$\mathbf{x_{LIN}}(k+1) = \mathbf{A_d}\mathbf{x_{LIN}}(k) + \mathbf{B_d}V_{in}(k) \tag{6.61}$$

where:

$$\mathbf{A_d} = e^{\mathbf{A}\mathbf{T_s}} \qquad \mathbf{B_d} = \int_0^{T_s} e^{\mathbf{A}t}\,\mathbf{B}\,dt = \mathbf{A}^{-1}(\mathbf{A_d} - \mathbf{I})\mathbf{B} \tag{6.62}$$

The same open-loop observer is already implemented as a part of the extended observer used by the nonlinearities compensator, and there is no need to implement a new one. The information about the state $\mathbf{x_{LIN}}(k)$ computed in the nonlinearities compensator is fed back to the dynamic controller, as shown in fig. 6.30.

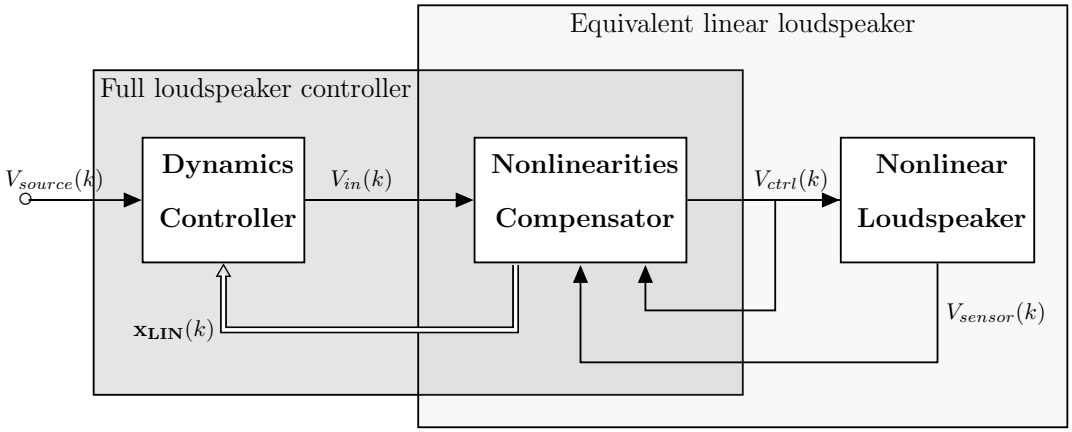

Figure 6.30: Block diagram of the proposed controller with feedback of the equivalent linear loudspeaker state estimate.

6.5 Simulation of the full controller

The proposed loudspeaker controller has been implemented in MATLAB Simulink, combining the dynamics controller displayed in section 6.4 and the nonlinearities compensator displayed in section 6.1.

In the presented simulations, the extended observer of the nonlinearities compensator is implemented with fixed closed loop poles, designed 5 times faster than the nonlinear loudspeaker poles at rest, similarly to the simulations of section 6.3.

To evaluate the performance of the controller, it has been employed to control the nonlinear loudspeaker model, already presented in section 5.2.2.

Four simulations have been performed to evaluate the performance of the controller throughout the working bandwidth $25 - 200Hz$, each one with a different source signal $V_{source}(k)$.

Since it is expected that the dynamics controller amplifies the source signal $V_{source}(k)$ up to $4.83dB$ at $25Hz$, the simulation input signals have been scaled accordingly to avoid exceeding the limits of the current dependency look-up tables.

Preliminary simulations proved that a $V_{source}(k) = +30dBV$ at $25Hz$ would generate currents much larger than the maximum value indexed in the look-up table (13.6A). Accordingly, the simulation input signals have all been scaled down by $5dB$.

The first four simulations employed a sinusoidal input at $+25dBV$, oscillating at $25Hz$, $50Hz$,$100Hz$ and $200Hz$, respectively.

The performance of the controller is evaluated comparing the simulated acceleration of the controlled nonlinear loudspeaker with the simulated accelerations of other two devices: an uncontrolled nonlinear loudspeaker, identical to the controlled one, and an equivalent linear loudspeaker with controlled dynamics. This last device is the reference for the target behavior of the controlled loudspeaker.

The result of each simulation is a set of waveforms: the source signal $V_{source}(k)$, the dynamic control signal $V_{FSF}(k)$, the equivalent linear loudspeaker input signal $V_{in}(k)$, the compensation signal $V_{comp}(k)$, the control signal $V_{ctrl}(k)$, the acceleration of the controlled loudspeaker $a_{CTRL}(k)$, the acceleration of the uncontrolled loudspeaker $a_{NL}(k)$ and the acceleration of the target linear loudspeaker with controlled dynamics $a_{LIN+C}(k)$.

Finally, during a simulation with sinusoidal source signal at $+25dBV$ oscillating at $25Hz$, the controlled and uncontrolled loudspeaker have been periodically linearized, extracting the instantaneous acceleration transfer functions of the two systems. This allows to broadly visualize and evaluate the variations in time to which the two systems are subject due to the nonlinearities.

6.5.1 Time domain measurements

Figures 6.31 to 6.34 show the output acceleration waveforms of the the simulated devices driven with sinusoidal signals at different frequencies.

In contrast to the compensation simulations, the beneficial effects of the designed full control are evident even from the measurements in the time domain.

Again, the effects of the compensation of the nonlinearities can be better appreciated at $25Hz$ and $200Hz$. As already stated, this is due to the specific nature of the considered nonlinearities: the dependencies on the displacement, such as the force factor modulation or the mechanical stiffness variation are more relevant at low frequencies, while the dependency on the current, such as the inductance modulation, becomes relevant at very high frequencies.

The most visible effect is the equalization introduced by the full-state feedback control: the acceleration of the controlled loudspeaker reaches $250\frac{m}{sec^2}$ regardless of the considered frequency. In a real device, this translates to a uniform sound reproduction in the working bandwidth.

Also, the nonlinear controlled loudspeaker perfectly follows the behavior of the ideal, linear loudspeaker with controlled dynamics, proving the effectiveness of the full-state feedback control on the linearized loudspeaker.

The measured source signal V_{source}, the full-state feedback signal V_{FSF}, the compensation signal V_{comp} and the generated control signal V_{ctrl} are shown in figure figs. 6.35 to 6.38. The displayed evolutions of the control signals V_{FSF} and V_{comp} give an idea of the effort required for the control of the dynamics and the compensation of the nonlinearities, respectively.

The most noticeable feature is the large effort required to enforce the designed linear control. This is expected, as the controller must provide the missing dynamics, especially at low frequencies as shown in fig. 6.28. An extreme example of this occur at $25Hz$, where the control signal V_{FSF} exhibits an amplitude equal to the source signal. At $50Hz$ and $200Hz$, the contribution of V_{FSF} is less but still significant, while at $100Hz$ it has very small impact on the control signal.

The compensation signal V_{comp}, as already seen, is generally much lower than the input signal, introducing a small compensation. Again, the only exception is at $25Hz$, where the compensation signal shows a very large peak during the first period of control, and smaller but significant peaks during the rest of the operation.

The first peak is even larger than the one exhibited during the compensation simulation in fig. 6.17. This is due to the fact that the driving signal of the compensation V_{in} is increased by the linear control, forcing the motion of the diaphragm even farther and thus requiring an even larger effort to act against the increasing mechanical stiffness and the decaying force factor.

For the rest of the time, the compensation just slightly corrects the diaphragm motion.

In the considered situations, the control signal V_{ctrl} reaches the $54V$ peak voltage maximum at $25Hz$, that is easily bearable by the considered loudspeaker specimen and by a typical power amplifier. However, the magnitude of the control effort must be taken into account during the design of the controller, avoiding to overdrive both the amplifier and the loudspeaker with an excessive control signal, possibly relaxing the constraints over the frequency response flatness.

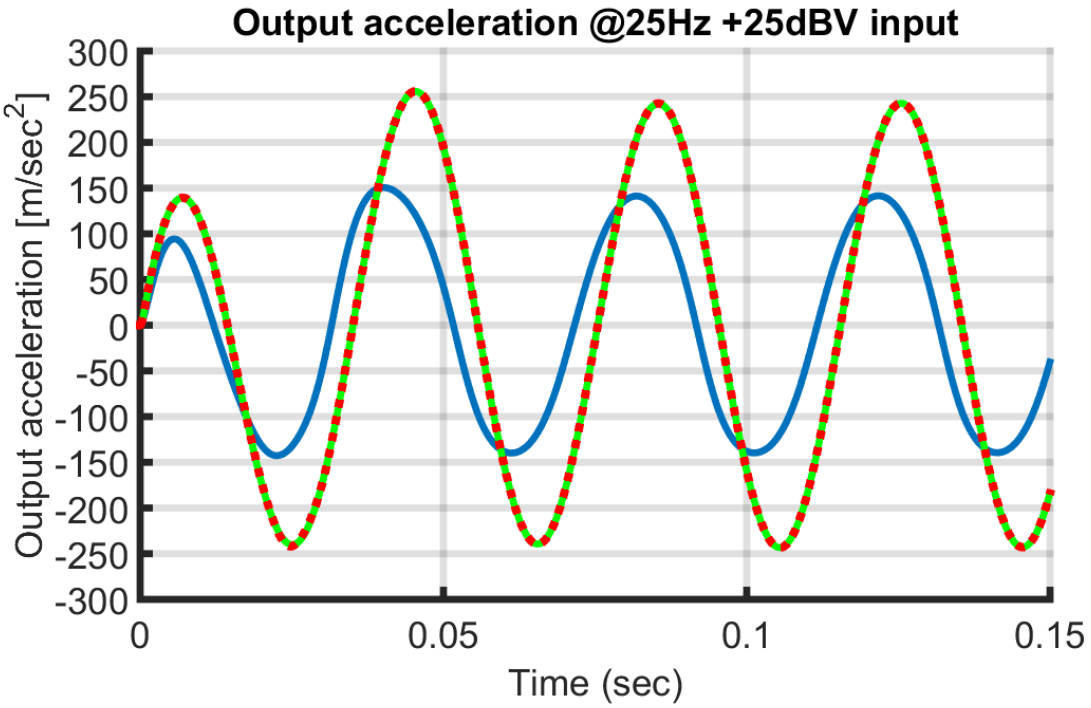

Figure 6.31: Acceleration of the simulated loudspeakers at 25Hz: blue) nonlinear uncontrolled; green) linear with controlled dynamics; dotted red) nonlinear controlled.

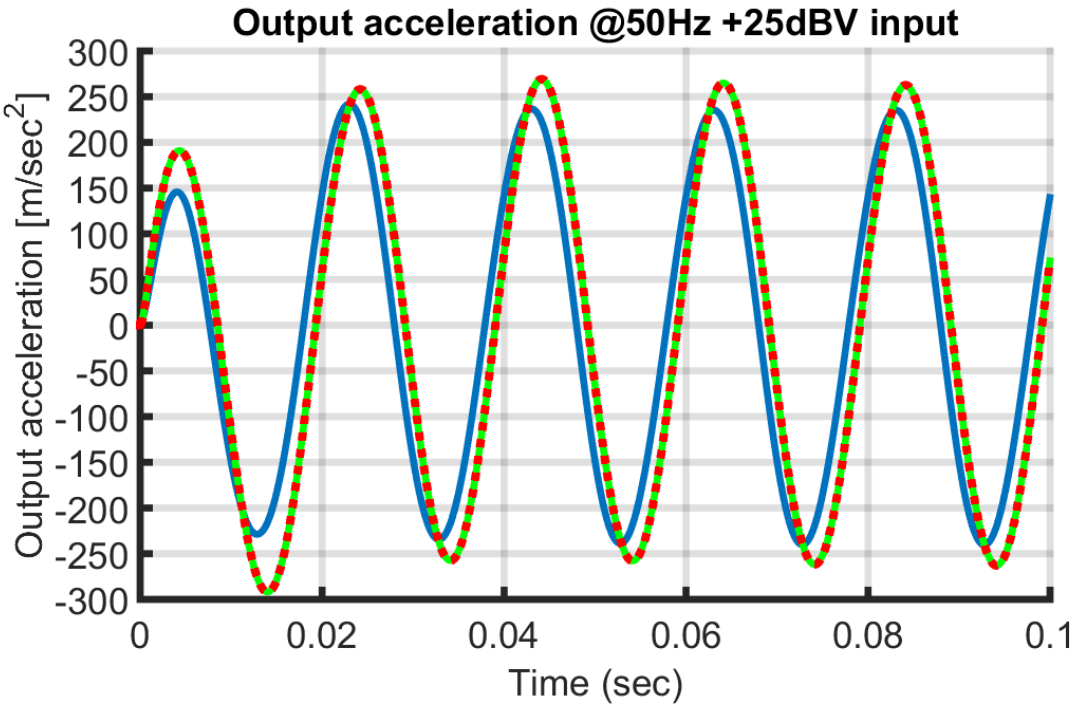

Figure 6.32: Acceleration of the simulated loudspeakers at 50Hz: blue) nonlinear uncontrolled; green) linear with controlled dynamics; dotted red) nonlinear controlled.

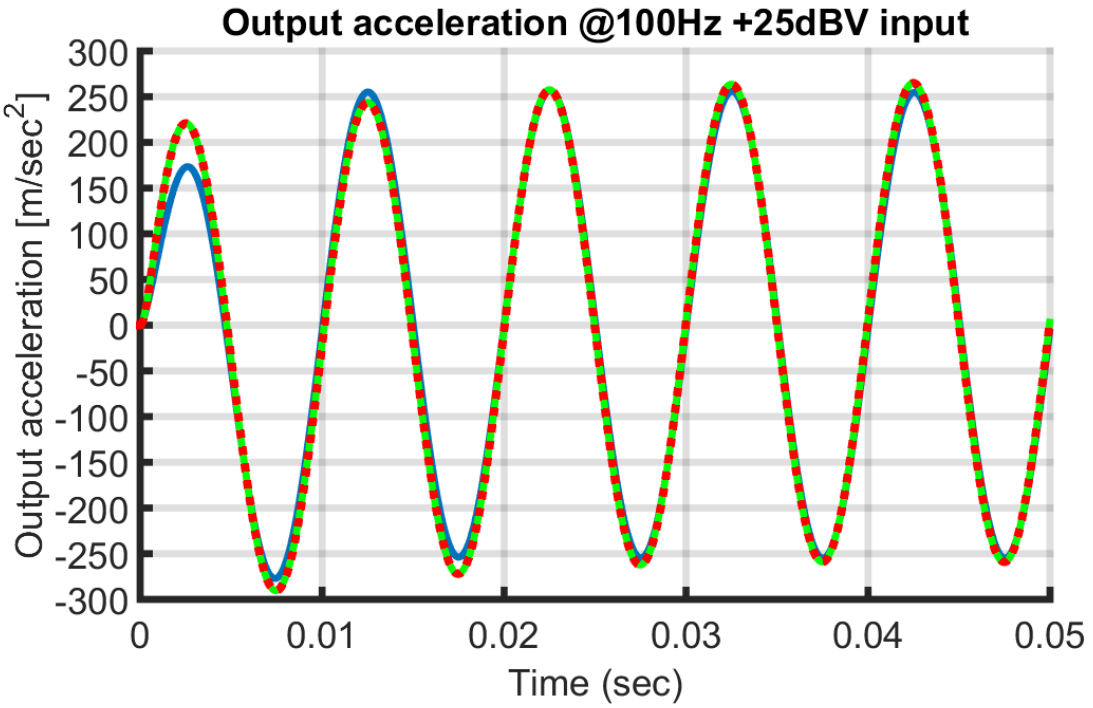

Figure 6.33: Acceleration of the simulated loudspeakers at 100Hz: blue) nonlinear uncontrolled; green) linear with controlled dynamics; dotted red) nonlinear controlled.

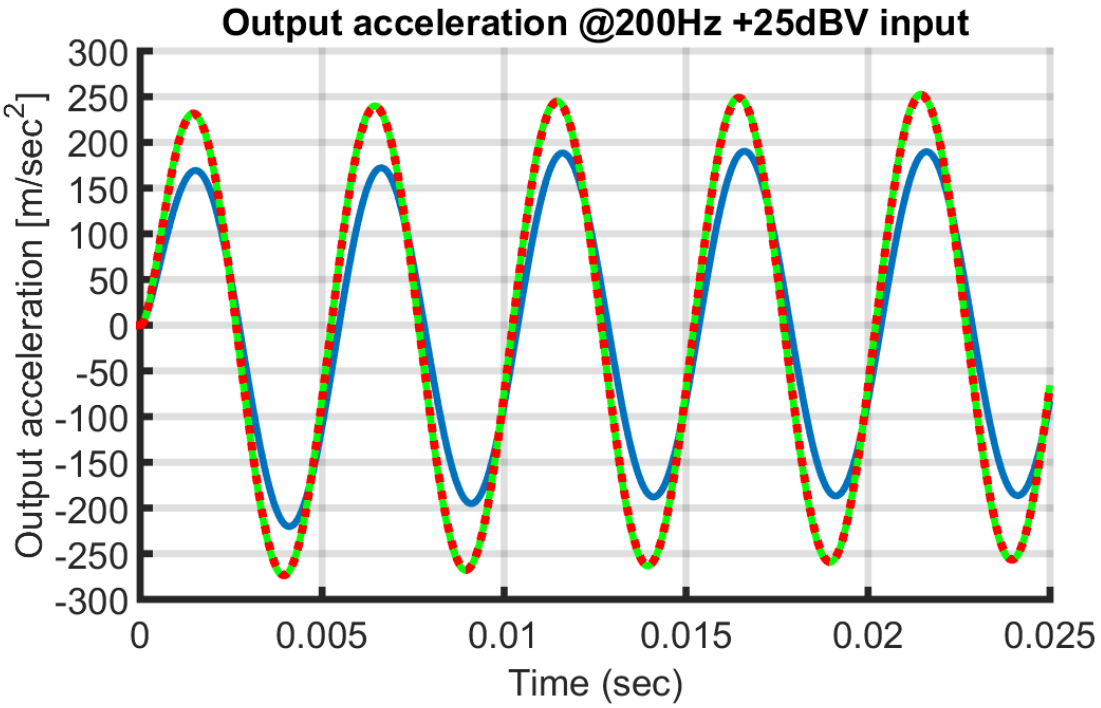

Figure 6.34: Acceleration of the simulated loudspeakers at 200Hz: blue) nonlinear uncontrolled; green) linear with controlled dynamics; dotted red) nonlinear controlled.

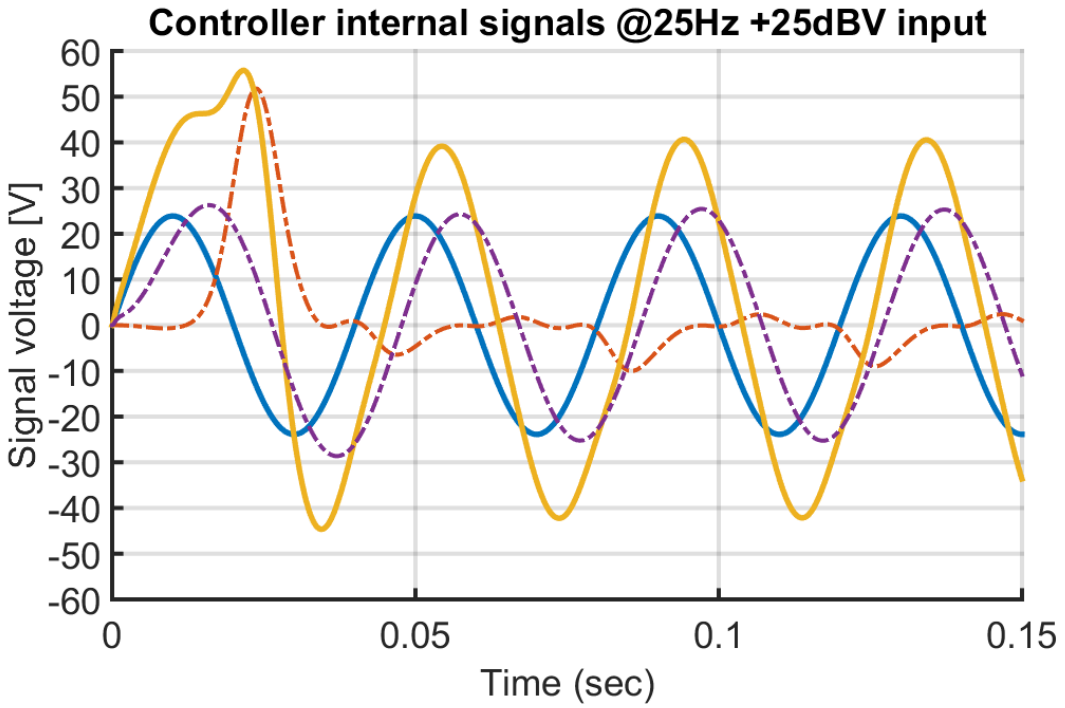

Figure 6.35: Signals of the simulated loudspeakers at 25Hz: blue) source signal V_{source}; yellow) control signal V_{ctrl}; purple dash-dotted) full-state feedback signal V_{FSF}; red dash-dotted) compensation signal V_{comp}.

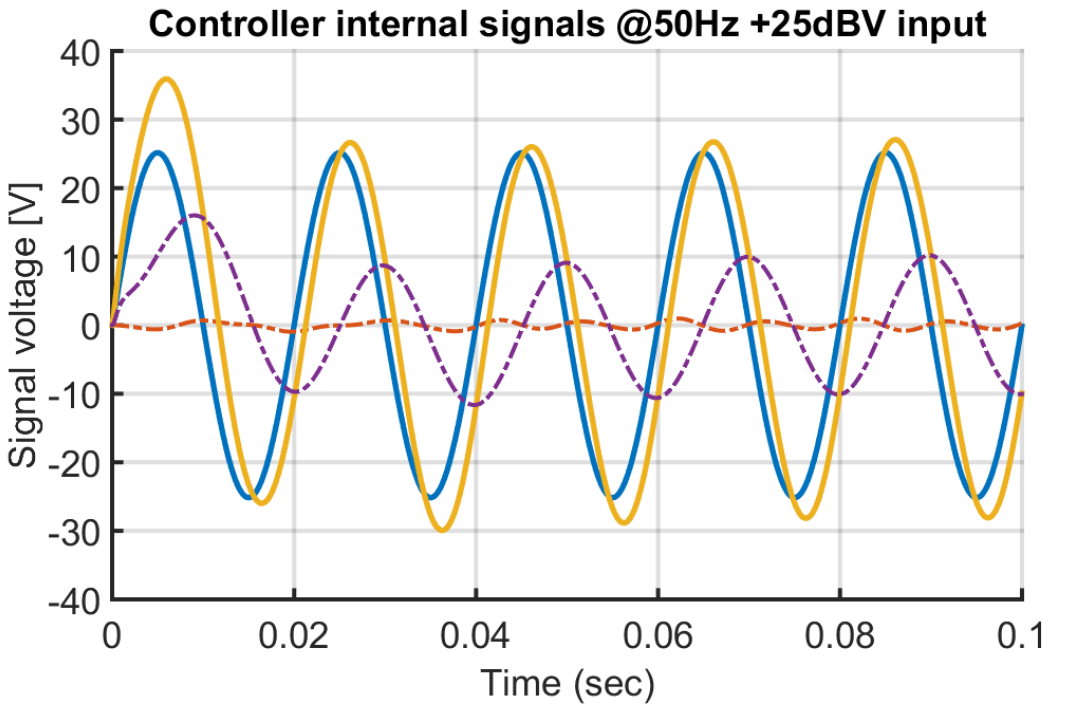

Figure 6.36: Signals of the simulated loudspeakers at 50Hz: blue) source signal V_{source}; yellow) control signal V_{ctrl}; purple dash-dotted) full-state feedback signal V_{FSF}; red dash-dotted) compensation signal V_{comp}.

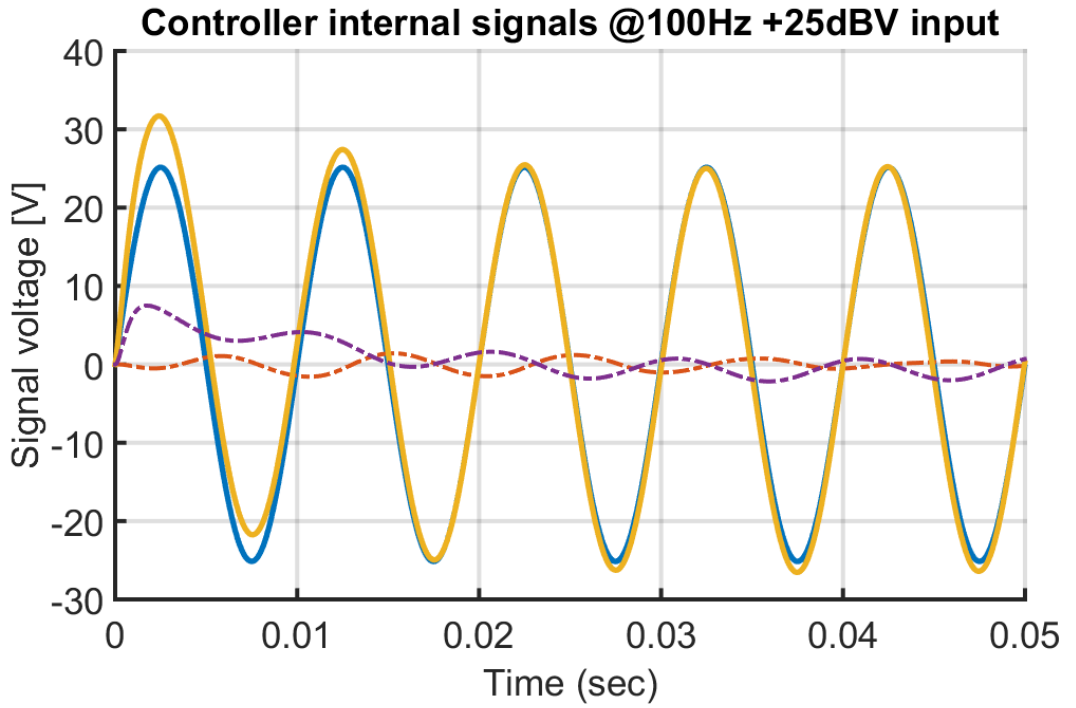

Figure 6.37: Signals of the simulated loudspeakers at 100Hz: blue) source signal V_{source}; yellow) control signal V_{ctrl}; purple dash-dotted) full-state feedback signal V_{FSF}; red dash-dotted) compensation signal V_{comp}.

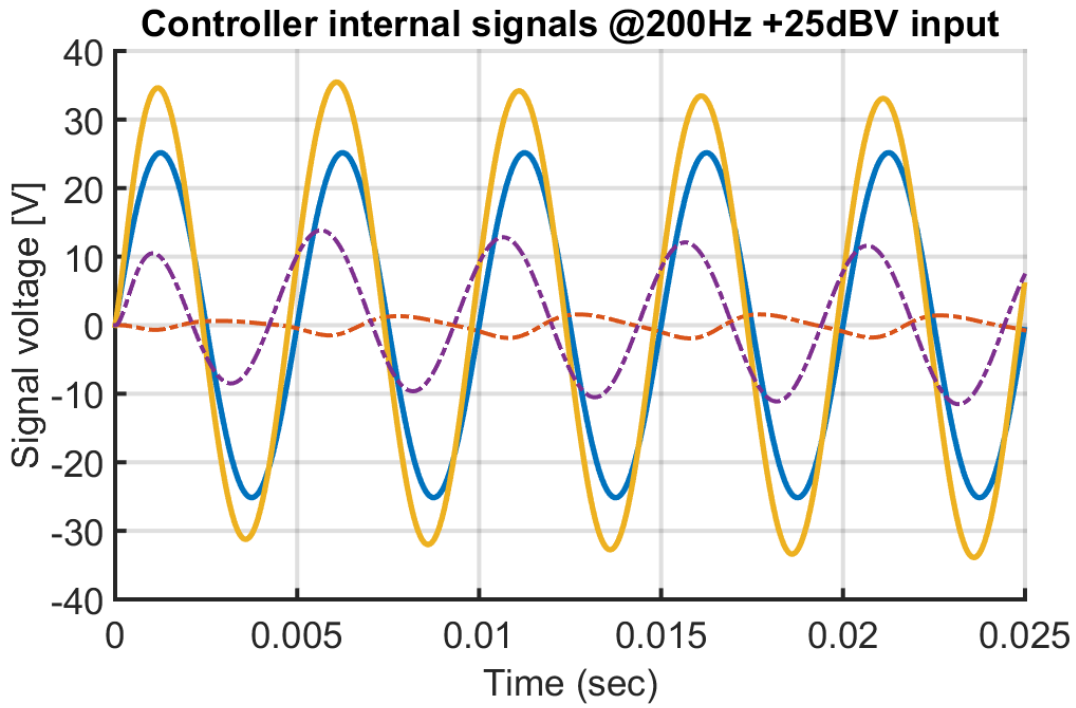

Figure 6.38: Signals of the simulated loudspeakers at 200Hz: blue) source signal V_{source}; yellow) control signal V_{ctrl}; purple dash-dotted) full-state feedback signal V_{FSF}; red dash-dotted) compensation signal V_{comp}.

6.5.2 Frequency domain measurements

The acceleration power spectra, computed from the simulation outputs, are shown in figs. 6.39 to 6.42.

Obviously, the nonlinear uncontrolled loudspeaker exhibits lower harmonics with respect to the measurements performed for the compensator validation, since, being driven with a smaller signal, its nonlinear behaviors are less excited.

However, the full controller achieves, in terms of residual nonlinearities, a performance consistent with those obtained by the sole compensator, displayed in section 6.3.2.

6.5.3 Total Harmonic Distortion

The computed values of the THD relative to the simulated acceleration outputs of the controlled nonlinear loudspeaker and the uncontrolled nonlinear loudspeaker are summarized in table 6.2.

Again, the benefits of the controller are evident: the values of the $THD_{\%}$ exhibited by the controlled loudspeaker are well below any considered threshold for high quality audio.

It is interesting to notice that, even if the controlled loudspeaker reaches higher acceleration values, and thus larger diaphragm displacements, the distortion introduced by the nonlinearities is almost negligible.

The $THD_{\%}$ results are consistent with those obtained by the sole compensator, displayed in section 6.3.3.

	THD nonlinear	THD controlled
$f_0 = 25$ Hz	5.022%	0.027%
$f_0 = 50$ Hz	2.441%	0.018%
$f_0 = 100$ Hz	0.463%	0.064%
$f_0 = 200$ Hz	0.394%	0.102%

Table 6.2: Total Harmonic Distortion of the simulated loudspeakers

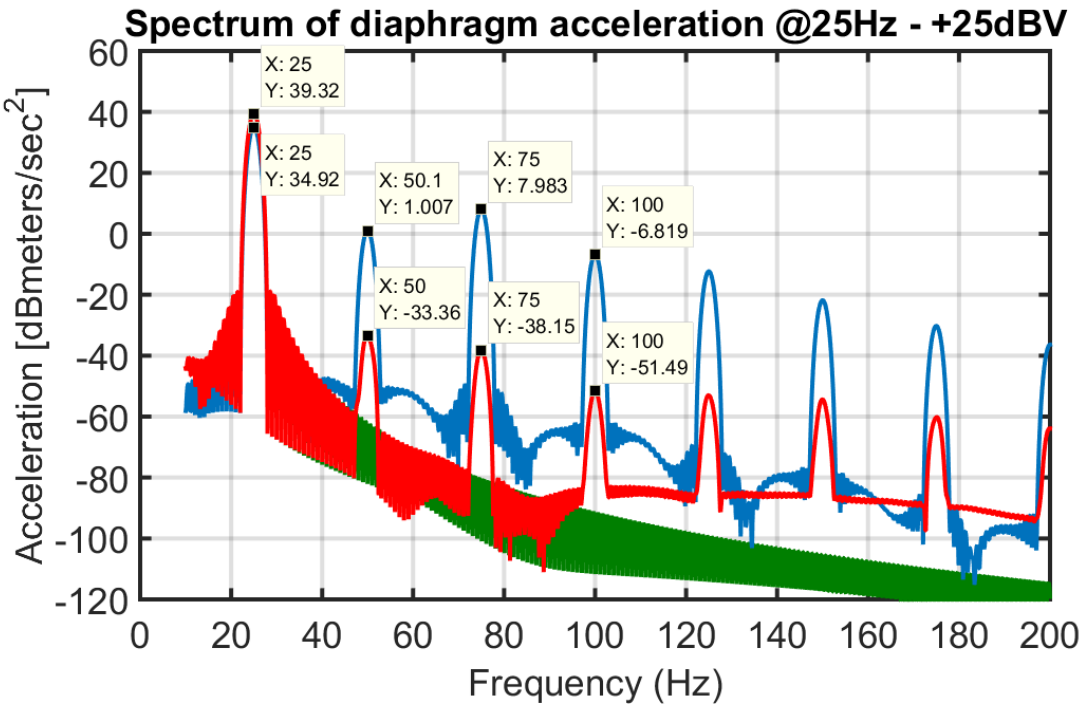

Figure 6.39: Spectra acceleration of the simulated loudspeakers at 25Hz: blue) nonlinear uncontrolled; green) linear with controlled dynamics; red) nonlinear controlled.

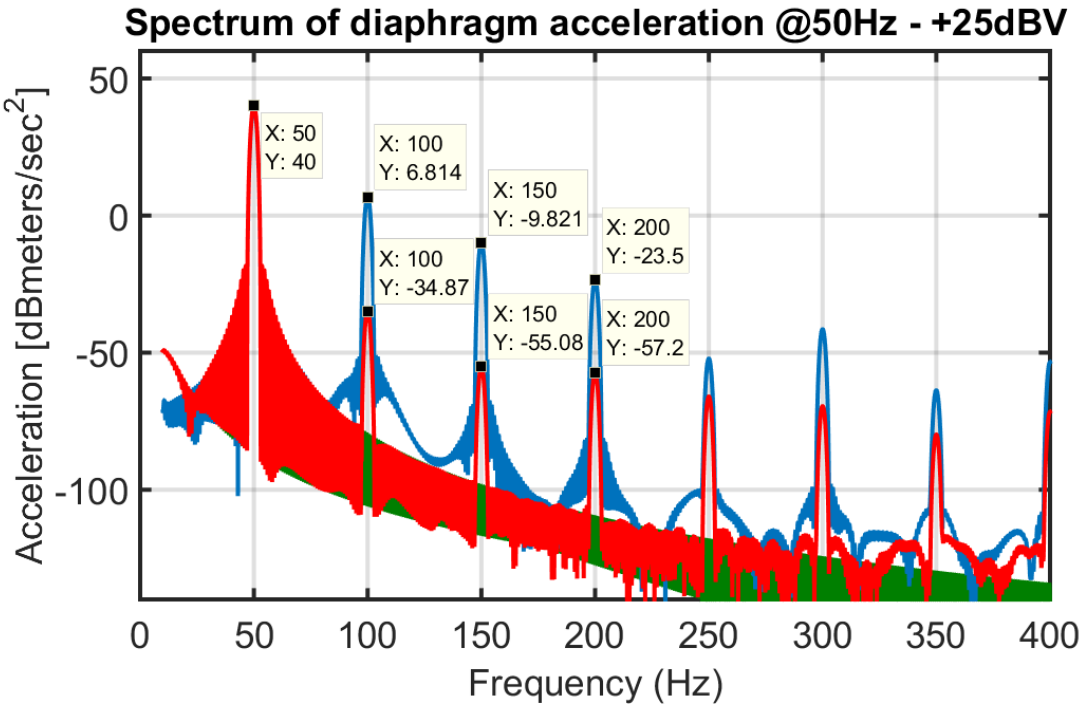

Figure 6.40: Spectra acceleration of the simulated loudspeakers at 50Hz: blue) nonlinear uncontrolled; green) linear with controlled dynamics; red) nonlinear controlled.

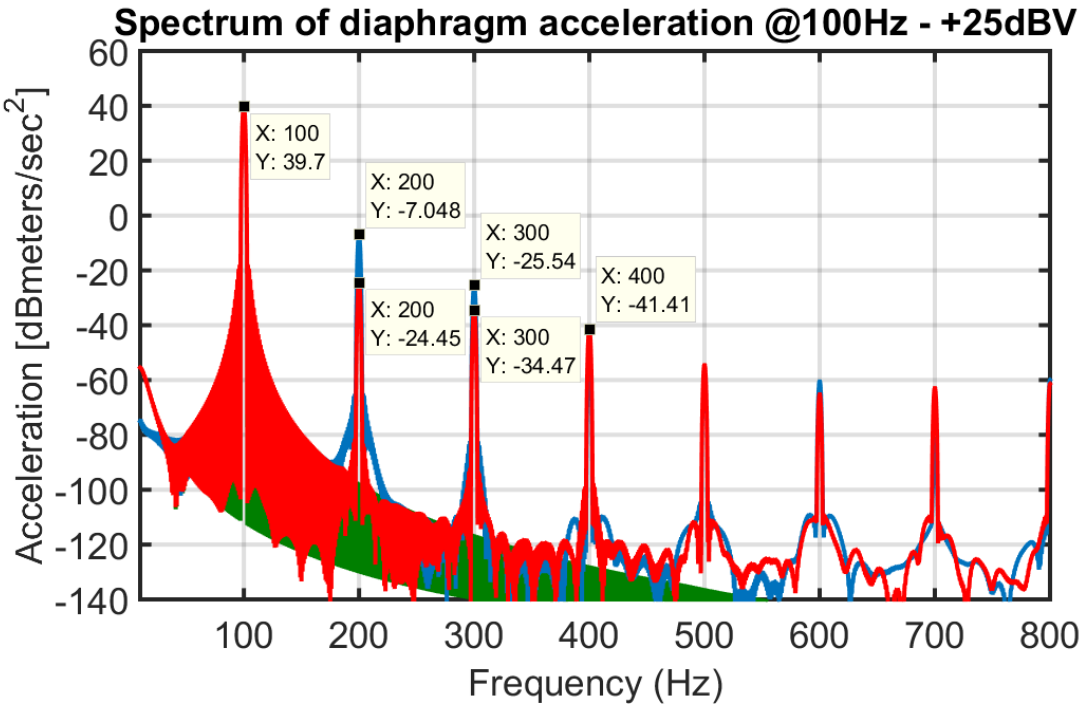

Figure 6.41: Spectra acceleration of the simulated loudspeakers at 100Hz: blue) nonlinear uncontrolled; green) linear with controlled dynamics; red) nonlinear controlled.

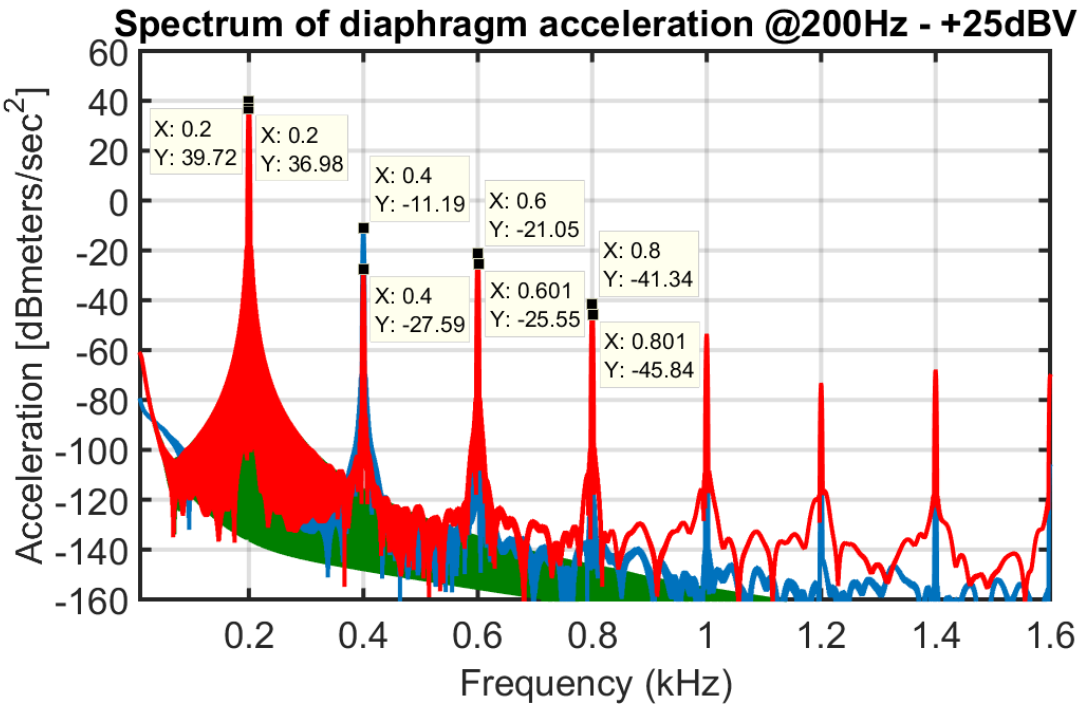

Figure 6.42: Spectra acceleration of the simulated loudspeakers at 200Hz: blue) nonlinear uncontrolled; green) linear with controlled dynamics; red) nonlinear controlled.

6.5.4 Instantaneous transfer functions

Figures 6.43 to 6.47 show the instantaneous transfer functions of the controlled and uncontrolled loudspeaker, obtained through linearization of their respective instantaneous models during the simulations.

The linearizations have been performed with a sampling time of $12.5msec$.

This set of measurements shows the stability of the loudspeaker dynamics enforced by the proposed control with respect to the uncontrolled behavior of the same device.

The uncontrolled loudspeaker, being a strongly nonlinear system, clearly exhibits a time varying instantaneous transfer function. Its peak value oscillate between the $48Hz$ shown at $t = 0.0875sec$ (fig. 6.46) and the $85Hz$ shown at $t = 0.1sec$ (fig. 6.47).

Moreover, variations in the shape of the transfer function and in the maximum exhibited value can be noticed.

Conversely, the controlled loudspeaker exhibits a transfer function that is extremely stable in time, especially in the working bandwidth $25 - 200Hz$, and consistent with the design target shown in fig. 6.28.

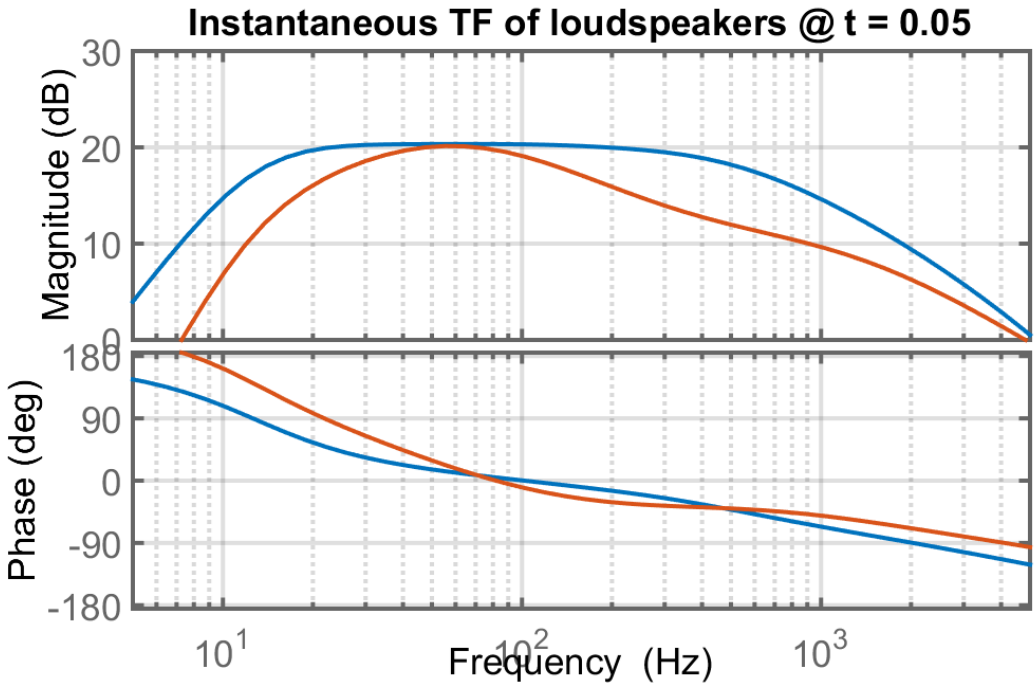

Figure 6.43: Instantaneous transfer function of the loudspeakers at t = 0.05 seconds: blue) nonlinear controlled; red) nonlinear uncontrolled.

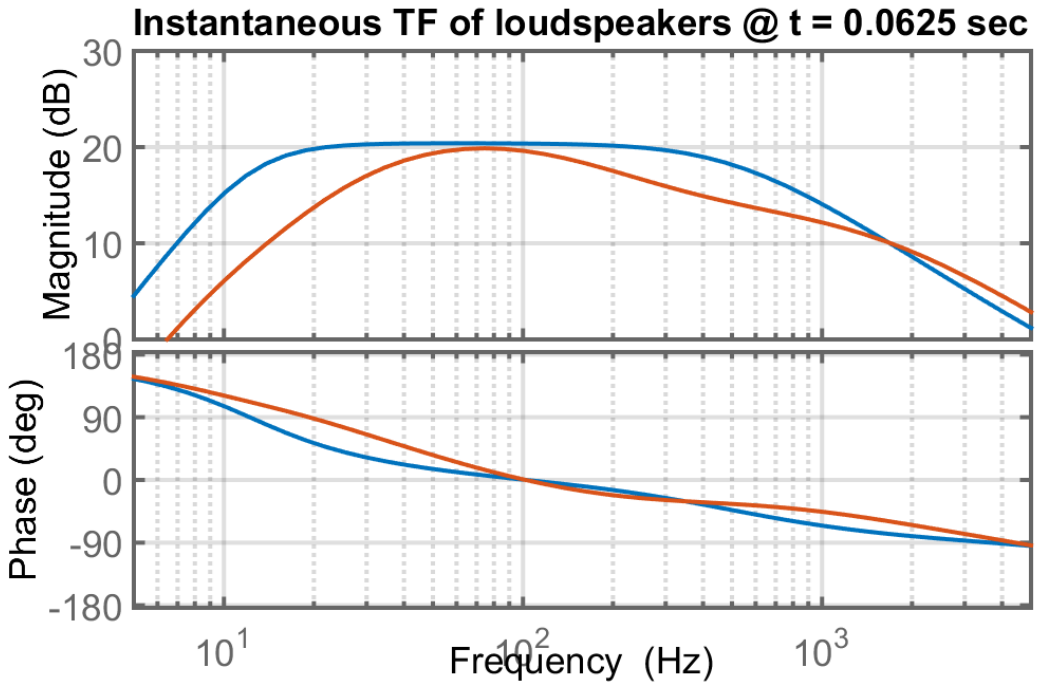

Figure 6.44: Instantaneous transfer function of the loudspeakers at t = 0.0625 seconds: blue) nonlinear controlled; red) nonlinear uncontrolled.

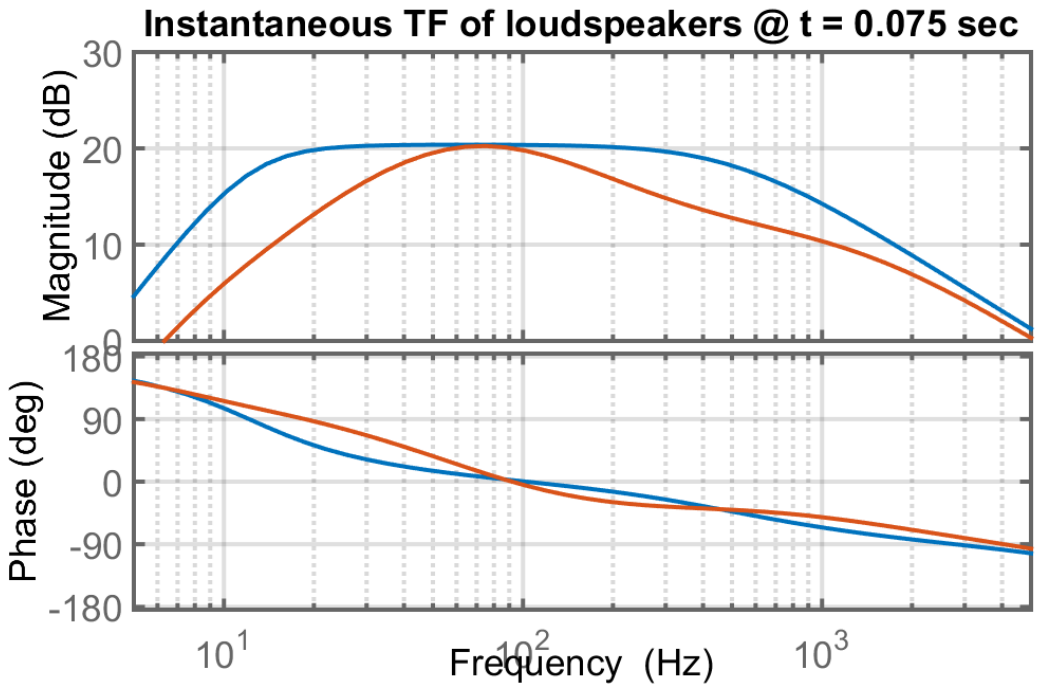

Figure 6.45: Instantaneous transfer function of the loudspeakers at t = 0.075 seconds: blue) nonlinear controlled; red) nonlinear uncontrolled.

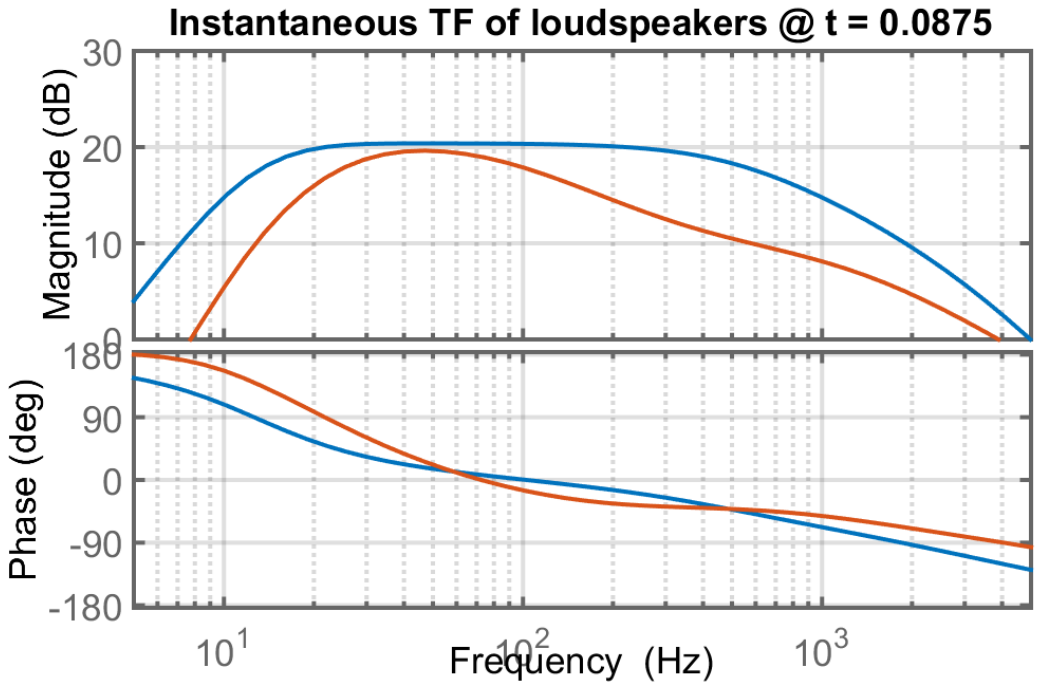

Figure 6.46: Instantaneous transfer function of the loudspeakers at t = 0.0875 seconds: blue) nonlinear controlled; red) nonlinear uncontrolled.

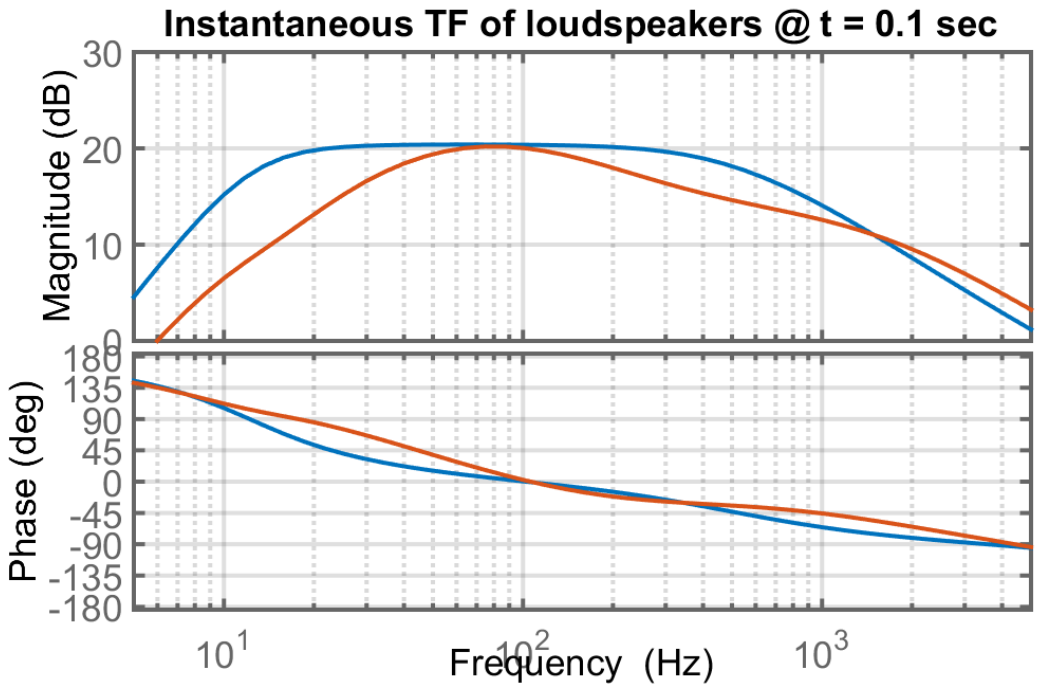

Figure 6.47: Instantaneous transfer function of the loudspeakers at t = 0.1 seconds: blue) nonlinear controlled; red) nonlinear uncontrolled.

6.6 Implementation considerations

In perspective, the presented controller has been developed for an implementation on a typical DSP employed by RCF, to enhance the audio quality of the controlled audio systems.

It is a fact that DSPs necessarily introduce delays due to the analog-to-digital conversion (ADC), required to convert the analog audio signal into the digital domain where it can be processed, and the following digital-to-analog conversion (DAC) required to reconstruct an analog signal from the digital, processed one. Further delay is introduced by the actual digital processing, which implements the developed control technique.

Figure 6.48 shows how these delays are distributed in the developed controller and fig. 6.49 shows the equivalent block diagram of the developed controller, with the delays condensed as input delays.

Feedback control techniques, like the one developed in this thesis, are typically affected by the delay introduced in the feedback loop by the hardware. In fact, a feedback loop delay will provide the observer of the controller with outdated information about the plant. This translates into a degradation of the control performance.

The control of linear systems may easily exploit state prediction techniques to compute a sufficiently good estimate of the plant state from delayed measurements of the plant. For nonlinear systems this is much more complex. For the developed controller it may be possible to introduce a state prediction technique, but the computational load required would make it unfeasible for practical use.

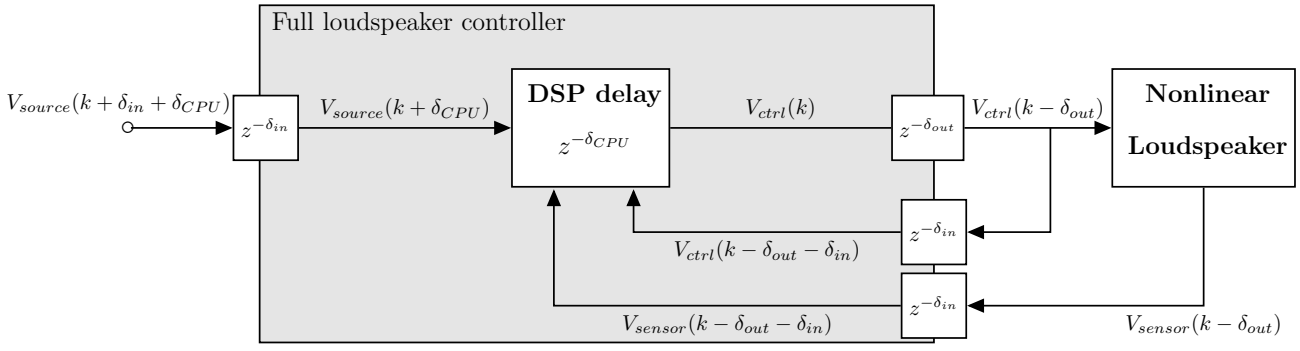

Figure 6.48: Block diagram of the delays present in the controller:
δ_{in}) delay of the ADC;
δ_{CPU}) delay of the digital processing;
δ_{out}) delay of the DAC.

The effects of the introduced delays have been investigated by means of a series of simulations, considering sinusoidal inputs at $+25dBV$, oscillating at $25Hz$, $50Hz$, $100Hz$ and $200Hz$, respectively. For each frequency, the control system has been simulated introducing different values of feedback loop delay, from $0msec$ to $3msec$, and measuring the $THD_{\%}$ of the output acceleration signal as figure of merit of the control performance. For these simulations, the delay introduced on the source signal $V_{source}(k)$ is disregarded, as it only introduces a time shift and thus it does not affect the $THD_{\%}$ results.

Figure 6.51 shows the measured $THD_{\%}$ trends for increasing values of the closed-loop delay achieved by the controller, compared with the $THD_{\%}$ exhibited by the uncontrolled loudspeaker and the 1% $THD_{\%}$ threshold. The performance of the controller shows a quick degradation in the presence of a delay, especially at high frequencies, where the period of the source signal approaches the length of the delay.

At low frequencies it is possible to achieve satisfactory results even with relatively large delays. At $25Hz$ and $50Hz$, the 1% $THD_{\%}$ threshold is reached for delays under $1msec$, while a $1.5msec$ delay allows a 40% reduction of the controlled loudspeaker distortion with respect to an uncontrolled one.

At higher frequencies this is not true anymore. At $100Hz$ the controller effectively achieves a reduction of the $THD_{\%}$ only for delays smaller than $0.7msec$. For greater delays, the controller causes an increase of the $THD_{\%}$, distorting the input signal more than the loudspeaker alone, and exceeding the 1% threshold for delays greater than $1.2msec$.

At $200Hz$ the result are even worse, requiring delays less than $0.2msec$ to achieve the distortion compensation. Also, it has not been possible to complete the simulation batch, since the controller became unstable for delays greater than $1msec$.

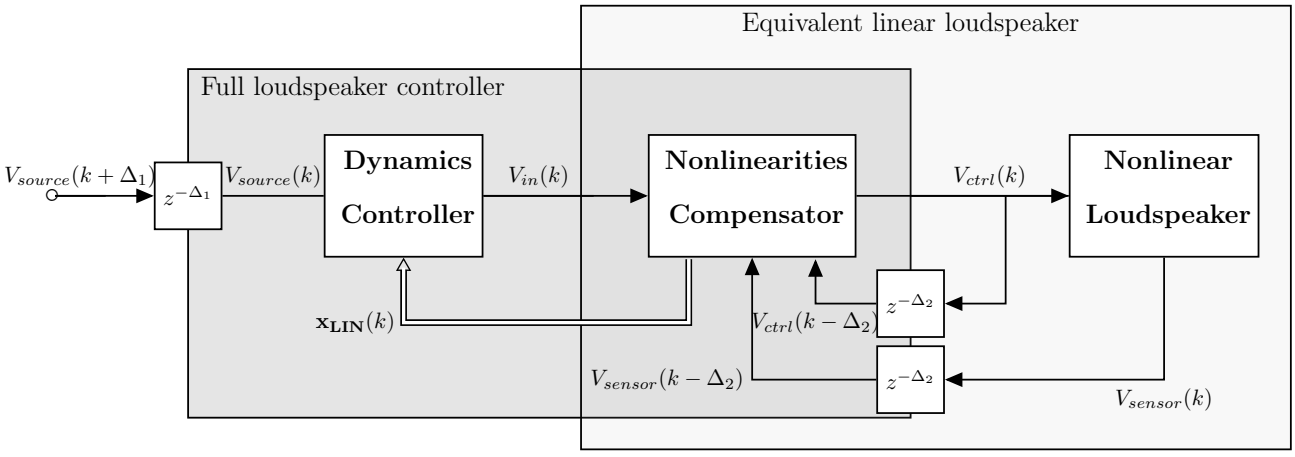

Figure 6.49: Block diagram of the proposed controller with delays introduced by the DSP condensed as input delays: $\Delta_1 = \delta_{in} + \delta_{CPU}$; $\Delta_2 = \delta_{in} + \delta_{CPU} + \delta_{out}$

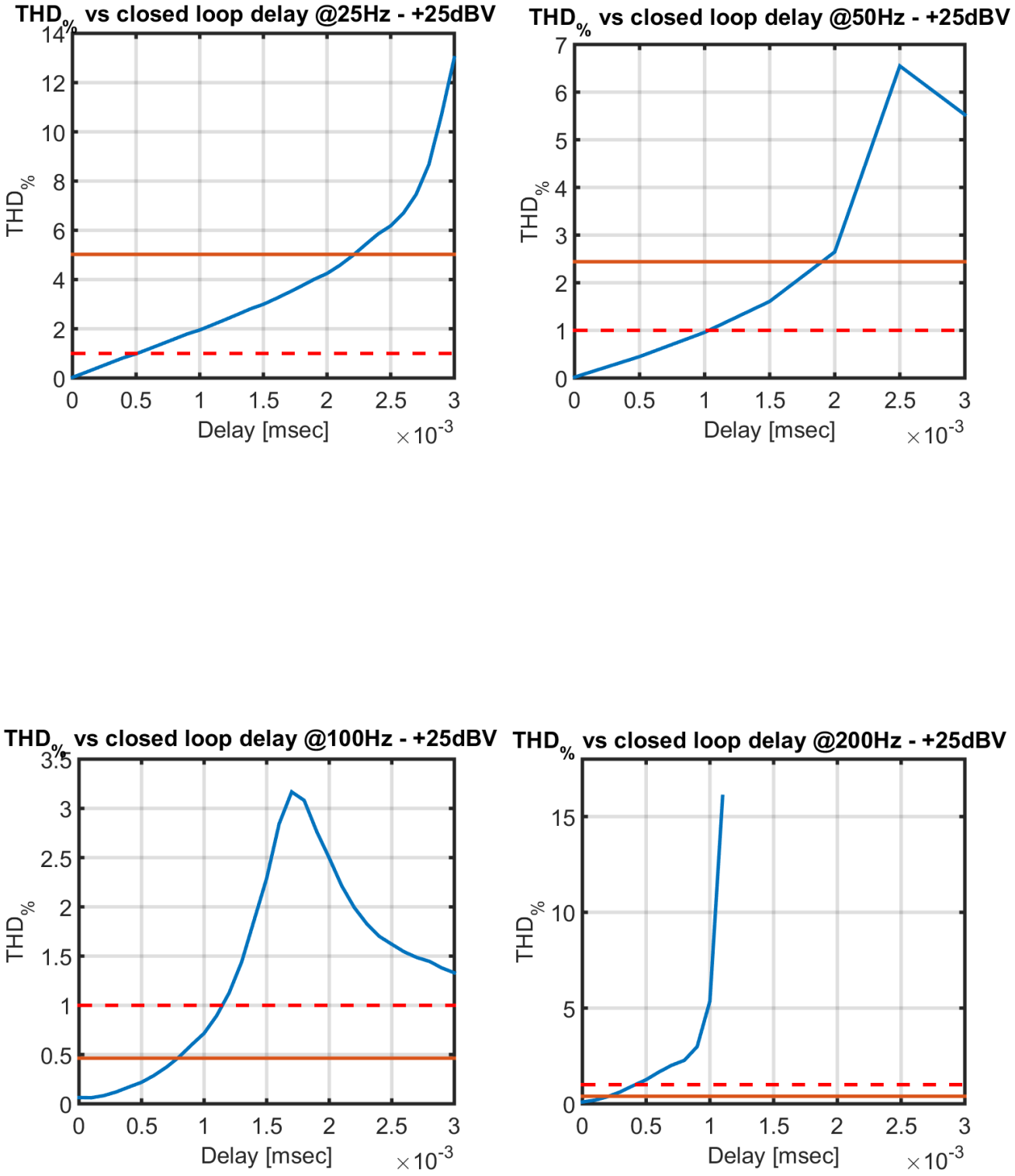

Figure 6.51: Simulated $THD_{\%}$ versus the delay present in the controller closed loop at $25Hz$, $50Hz$, $100Hz$, $200Hz$: blue) controlled loudspeaker; red) uncontrolled loudspeaker; dashed red) 1% THD threshold.

These results indicates that severe constraints on the maximum delay may be introduced by the hardware used for the implementation of a full-range controller. However, the controller can effectively be employed with more relaxed constraints in the lower part of the working bandwidth, even just to partially improve the distortion level.

The DSP employed by RCF for the audio systems on-board processing is a Cirrus Logic CS47024, a 32-bit floating point processor with $147MHz$ base frequency, supporting audio processing at different sample rates, from $192kHz$ to $48kHz$ and equipped with two integrated 32-bit sigma-delta ADC and four audio quality DAC.

The DSP is programmed with a block oriented graphical IDE, named DSP Composer, which allows to implement the required audio process connecting together blocks implementing primitive functions. It is also possible to program customized blocks using a modified version of the C language using a second, textual IDE, named CLIDE. The DSP Composer is also used to automatically convert block diagrams into code, and to program the DSP with the generated code.

Tests performed on the DSP show that the CS47024 introduces, at all the possible sampling frequencies, a fixed time delay $2.8msec$ between the acquisition of the input signals and the output of the computed control signal.

Part of the measured delay is introduced by the ADC and DAC conversions, but most of it is probably introduced during the automatic code generation by the DSP Composer. This information is not found in the documentation, but is very likely that the code is generated to preserve a fixed input-output delay regardless of the computational load.

As can be inferred from fig. 6.51, a delay of $2.8msec$ makes the hardware unsuitable for any possible implementation of the developed controller, since it would increase the distortion level and even lead to instability.

The implementation of the controller is thus left for future work, when a suitable hardware, either a DSP or an FPGA, is available.

Conclusions

This thesis proposes a feedback, model-based technique for the improvement of the audio quality of dynamic loudspeakers provided with a second coil, used as sensor. The control algorithm is developed in discrete-time to enable further implementation on DSP and to be employed for the enhancement of modern audio systems.

The internal structure and the operating principles of a typical dynamic loudspeaker are presented in detail and are exploited for the development of different SS continuous-time models of the transducer. The electromechanical and electroacoustic analogies are used to develop an LTI SS model of the dynamic loudspeaker, valid in the small signals condition, which is later extended by means of state-dependent parameters to develop a nonlinear time-invariant SS model, employed for the characterization of the device in the large signals condition.

The same theoretical framework is used to describe the behavior of the embedded sensor coil and to develop an LTI SS model, valid in the small signals condition, and a nonlinear time-invariant SS model, valid in the large signals condition. The proposed models for the sensor coil establish an improvement with respect to the models already presented in literature.

The parameters and dependency curves required for the characterization of the developed models are estimated from a real loudspeaker specimen. The required parameters are estimated with a grey-box identification process, performed using the Klippel Distortion Analyzer and the dB-Lab software.

The developed models are validated comparing their behavior, simulated in MATLAB Simulink, with the behavior of the loudspeaker specimen. Positive results are obtained from the simulations of the linear models, showing a good match between the simulated an the measured characteristics of the loudspeaker, at least in the considered working bandwidth of the loudspeaker.

Worse results are obtained from the simulations of the nonlinear models, showing an underestimation of the actual nonlinear behavior. This is not to be attributed to errors in the developed nonlinear model, but rather to the drift undergone by the specimen parameters during the time elapsed between the estimation process and the validation measurements. The severe variation of the specimen parameters, mainly the mechanical stiffness, prevents the definition of a sufficiently accurate time-invariant model, suitable for control purposes.

To overcome this limitation, an adaptive technique is required, enabling the periodic and automatic tuning of the model parameters, so that the model can follow the time-varying behavior of the real controlled loudspeaker. The implementation of a model adaptation mechanism is not addressed in this thesis and is left for future work.

For the sake of simplicity, the controller is designed assuming a perfect characterization of the loudspeaker model. The control system is developed employing a feedback architecture, that is preferred over the feedforward one due to its lower sensitivity to model misalignment, and using the sensor coil output voltage as measurement of the system behavior.

The proposed controller addresses both the compensation of the nonlinearities of the controlled loudspeaker, forcing it to exhibit only the underlying LTI part of its nonlinear motional behavior, and the dynamic control of the obtained equivalent linear loudspeaker, enhancing the transducer frequency response. The two functionalities of the controller are separately developed and progressively validated.

The nonlinearities compensation algorithm is designed in continuous-time, exploiting the developed nonlinear models, and implemented in discrete-time using common discretization techniques. The information required for the synthesis of the compensation signal is retrieved by means of an internal model of the controlled loudspeaker and a nonlinear state observer.

The nonlinear state observer is designed as a nonlinear extension of the Luenberger observer, capable of estimating the state of the controlled loudspeaker by approximating its nonlinear behavior with a sequence of locally LTI models, and adapting the feedback gain vector accordingly. Due to its crucial importance, the observer is validated on its own, showing good estimation capabilities and high rejection to initial state errors.The nonlinear observer can be further improved employing more refined nonlinear state estimation techniques, such as the Extended Kalman Filter.

Positive results are also obtained from the simulation of the full nonlinearities compensation algorithm, theoretically achieving $THD_{\%}$ levels below any threshold usually considered for high quality audio reproduction in all the loudspeaker working bandwidth.

The linear dynamic control algorithm is also designed in continuous-time, exploiting the developed linear model of the loudspeaker, and implemented in discrete-time using common discretization techniques. The controller implements a full-state feedback control.

The presented simulations show that the full control action can theoretically achieve the simultaneous compensation of the loudspeaker nonlinearities, obtaining the same $THD_{\%}$ levels exhibited by the sole compensation algorithm, and a perfect control of the exhibited linear dynamics, enforcing a flat frequency response in the considered working bandwidth with a tolerance of $0.2dB$.

However, the designed dynamic control should be considered just as a theoretical example of the proposed controller capabilities. In fact, the design aims at the maximum flatness of the frequency response in the working bandwidth, disregarding the magnitude of the required control effort, which may exceed the working limits of the amplifier or the loudspeaker. For practical purposes, the dynamic control must be designed to match the characteristics of the amplifier and the loudspeaker, possibly relaxing the constraints over the frequency response flatness.

Considering a possible implementation of the proposed controller, the effects of the closed-loop delays introduced by the DSP are simulated. The simulations show that the introduction of a time delay affects the control performance in different ways, depending on the delay length.

For delays smaller than $0.5msec$, the $THD_{\%}$ is kept below the 1% threshold in all the loudspeaker working bandwidth, still achieving a sufficiently good audio quality. For greater time delays, the performance degradation leads to a $THD_{\%}$ exceeding the 1% threshold. However, especially at lower frequencies, the $THD_{\%}$ exhibited by the controlled device is lower compared to an uncontrolled one. Finally, for delays greater than $1msec$, the controller starts to exhibit instability. These results can be used to choose a suitable DSP for the implementation.

The DSPs employed by RCF are characterized by a fixed delay of $2.8msec$, making them unsuitable for an implementation of the proposed controller. Thus, the implementation is left for future work, possibly employing a DSP with delay smaller than $0.5msec$, or even an FPGA with similar or better characteristics.

Bibliography

[Ast08] Karl J. Astorm. *Feedback systems : an introduction for scientists and engineers*. Princeton University Press, Princeton, 2008.

[BBNFS04] Constancio Bortoni, Rosalfonso Bortoni, Sidnei Noceti Filho, and Rui Seara. Real-time voice-coil temperature and cone displacement control of loudspeakers. In *Audio Engineering Society Convention 117*, Oct 2004.

[BDNR05] Delphine Bard, Mauro Del Nobile, and Mario Rossi. Compensation of nonlinearities of horn loudspeakers. In *Audio Engineering Society Convention 119*, Oct 2005.

[Ber86] Leo Beranek. *Acoustics*. Published by the American Institute of Physics for the Acoustical Society of America, New York, N.Y, 1986.

[BSH94] M. A. H. Beerling, Cornelis H. Slump, and Otto E. Hermann. Reduction on nonlinear distortion in loudspeakers with digital motional feedback. In *Audio Engineering Society Convention 96*, Feb 1994.

[Cat85] Johan A. Catrysse. On the design of some feedback circuits for loudspeakers. *J. Audio Eng. Soc*, 33(6):430–435, 1985.

[CCCP81] C-Y Chen, G T-C Chiu, C-C Cheng, and H Peng. Passive voice coil feedback control of closed-box subwoofer systems. *Journal of Mechanical Engineering Science (Part C)*, 214:32–36, 1981.

[Dav06] Don Davis. *Sound system engineering*. Elsevier Focal Press, Amsterdam Boston, 2006.

[DKOB04] Mark Dodd, Wolfgang Klippel, and Jack Oclee-Brown. Voice coil impedance as a function of frequency and displacement. In *Audio Engineering Society Convention 117*, Oct 2004.

[Isi95] Alberto Isidori. *Nonlinear control systems*. Springer, Berlin New York, 1995.

[Kai87] A. J. M. Kaizer. Modeling of the nonlinear response of an electrodynamic loudspeaker by a volterra series expansion. *J. Audio Eng. Soc*, 35(6):421–433, 1987.

[Kal59] R. Kalman. On the general theory of control systems. *Automatic Control, IRE Transactions on*, 4(3):110–110, Dec 1959.

[Kli98] Wolfgang J. Klippel. Adaptive nonlinear control of loudspeaker systems. *J. Audio Eng. Soc*, 46(11):939–954, 1998.

[Kli00] Wolfgang Klippel. Distortion analyzer-a new tool for assessing and improving electrodynamic transducer. In *Audio Engineering Society Convention 108*, Feb 2000.

[Kli03] Wolfgang Klippel. Active compensation of transducer nonlinearities. In *Audio Engineering Society Conference: 23rd International Conference: Signal Processing in Audio Recording and Reproduction*, May 2003.

[Kli04] Wolfgang Klippel. Nonlinear modeling of the heat transfer in loudspeakers. *J. Audio Eng. Soc*, 52(1/2):3–25, 2004.

[Kli05] Wolfgang Klippel. Loudspeaker nonlinearities – causes, parameters, symptoms. In *Audio Engineering Society Convention 119*, Oct 2005.

[KSF+13] Christoph Keplinger, Jeong-Yun Sun, Choon Chiang Foo, Philipp Rothemund, George M. Whitesides, and Zhigang Suo. Stretchable, transparent, ionic conductors. *Science*, 341(6149):984–987, 2013.

[Lea02] W. Marshall Leach, Jr. Loudspeaker voice-coil inductance losses: Circuit models, parameter estimation, and effect on frequency response. *J. Audio Eng. Soc*, 50(6):442–450, 2002.

[MH89] Paul G. Mills and Malcolm J. Hawksford. Distortion reduction in moving-coil loudspeaker systems using current-drive technology. *J. Audio Eng. Soc*, 37(3):129–148, 1989.

[Ols58] H.F. Olson. *Dynamical analogies*. Van Nostrand, 1958.

[Pri96] Jim Primbs. Survey of nonlinear observer design techniques, 1996.

[PSR+13] Gaël Pillonnet, Eric Sturtzer, Timothé Rossignol, Pascal Tournier, and Guy Lemarquand. Distortion improvement in the current coil of a loudspeaker. In *Audio Engineering Society Convention 134*, May 2013.

[RK25] Chester W. Rice and Edward W. Kellogg. Notes on the development of a new type of hornless loud speaker. *American Institute of Electrical Engineers, Transactions of the*, XLIV:461–480, Jan 1925.

[SK01] Ulf Seidel and wolfgang Klippel. Fast and accurate measurement of the linear transducer parameters. In *Audio Engineering Society Convention 110*, May 2001.

[Sma72] Richard H. Small. Direct radiator loudspeaker system analysis. *J. Audio Eng. Soc*, 20(5):383–395, 1972.

[Sma73a] Richard H. Small. Vented-box loudspeaker systems–part 1: Small-signal analysis. *J. Audio Eng. Soc*, 21(5):363–372, 1973.

[Sma73b] Richard H. Small. Vented-box loudspeaker systems-part 2: Large-signal analysis. *J. Audio Eng. Soc*, 21(6):438–444, 1973.

[Sma73c] Richard H. Small. Vented-box loudspeaker systems-part 3: Synthesis. *J. Audio Eng. Soc*, 21(7):549–554, 1973.

[Thi71a] Neville Thiele. Loudspeakers in vented boxes: Part 1. *J. Audio Eng. Soc*, 19(5):382–392, 1971.

[Thi71b] Neville Thiele. Loudspeakers in vented boxes: Part 2. *J. Audio Eng. Soc*, 19(6):471–483, 1971.

[Van89] John Vanderkooy. A model of loudspeaker driver impedance incorporating eddy currents in the pole structure. *J. Audio Eng. Soc*, 37(3):119–128, 1989.

[WB95] Greg Welch and Gary Bishop. An introduction to the kalman filter, 1995.

[Wri89] Julian R. Wright. An empirical model for loudspeaker motor impedance. In *Audio Engineering Society Convention 86*, Mar 1989.

[XCF+08] Lin Xiao, Zhuo Chen, Chen Feng, Liang Liu, Zai-Qiao Bai, Yang Wang, Li Qian, Yuying Zhang, Qunqing Li, Kaili Jiang, and Shoushan Fan. Flexible, stretchable, transparent carbon nanotube thin film loudspeakers. *Nano Letters*, 8(12):4539–4545, 2008. PMID: 18956907.

Acknowledgments

Dire grazie non è niente.
E pur se non c'è maniera altra,
grazie rimane niente.

Allora non dirò niente,
ma vorrei che si sapesse
che in quel niente,
ci son tutte le parole.